TP 15711E

ROBERT ALLAN
Naval Architects & Marine Engineers

Tugboat Underwater Radiated Noise Measurements

Prepared for:
Innovation Centre of Transport Canada
Ottawa, ON Canada

Project 225-034
Revision 3
Document No. RAL02839R-225-034-500
Date: March 9, 2026

Prepared by Robert Allan Ltd.
Naval Architects & Marine Engineers
www.ral.ca

Notices

This report reflects the views of the authors and not necessarily those of the Innovation Centre of Transport Canada.

The Innovation Centre does not endorse products or manufacturers. Trade or manufacturers' names appear in this report only because they are essential to its objectives.

Un sommaire français se trouve avant la table des matières.

Transport Canada / Transports Canada

PUBLICATION DATA FORM

1. Transport Canada Publication No.	2. Project No.	3. Catalogue No.	4. ISBN
TP 15711E	225-034	T29-194/2026E-PDF	978-0-662-35426-0

5. Title and Subtitle	6. Publication Date
Tugboat Underwater Radiated Noise Measurements	June 2026
	7. Performing Organization Document No.: RAL02839R-225-034-500
8. Author(s): Burella, Giorgio; Lee, Waltfred; den Hertog, Vince	9. Transport Canada File No.: T8009-250013
10. Performing Organization Name and Address: Robert Allan Ltd. 400-250 Howe St Vancouver BC V6C 3R8 Canada	11. PWGSC File No.: WS3983439179
	12. PWGSC or Transport Canada Contract No.: CW2413782
13. Sponsoring Agency Name and Address: Transport Canada Place de Ville, Tower C 330 Sparks Street Ottawa, Ontario K1A 0N5	14. Type of Publication and Period Covered: Final technical report
	15. Project Officer: Olivier Maillet Glas

16. Supplementary Notes (Funding programs, titles of related publications, etc.)

This report was funded as part of the Marine RD&D Program

17. Abstract

Robert Allan Ltd. conducted a full-scale study for Transport Canada's Innovation Centre to compare underwater radiated noise (URN) from a modern battery-electric harbour tug and a diesel-mechanical harbour tug of similar size and performance operating in the Port of Vancouver. Sea trials were carried out using a bottom-moored autonomous underwater listening station in ISO 17208-compliant deep-water conditions, with additional onboard noise, vibration, and modal testing to identify dominant noise sources and transmission paths.

The results showed clear differences in URN characteristics between the two propulsion systems. For the diesel-mechanical tug, main engines and azimuth drive gear meshing were the dominant contributors to structure-borne URN, particularly below 1 kHz. In contrast, during battery-only operation, the battery-electric tug did not exhibit a dominant low-frequency machinery source and produced a lower overall URN during stationary and low-speed transit conditions. In these cases, URN was mainly driven by propulsor and gearing-related tonal noise. When gensets were operating, the associated URN increased but remained below diesel-mechanical levels. At higher transit speeds and during bollard pull, cavitation became the dominant URN source for both vessels.

The battery-electric tug achieved source level reductions exceeding 8 dB at transit speeds below 8 knots and 10 dB during loitering, but this advantage decreased at high load, and URN exceeded that of the diesel-mechanical tug by up to 5 dB at full bollard pull. The study also supported Lloyd's Register UWN notation compliance for the battery-electric tug.

18. Key Words	19. Distribution Statement
Underwater Radiated Noise, Sustainable Marine Transportation, Battery-Electric, Harbour and Port Vessel Operations	Digital copy

20. Security Classification (of this publication)	21. Security Classification (of this page)	22. Declassification (date)	23. No. of Pages	24. Price
Unclassified	Unclassified	—	xvii, 60, apps	—

Transports Canada Transport Canada

FORMULE DE DONNÉES POUR PUBLICATION

1. N° de la publication de Transports Canada	2. N° de l'étude	3. N° de catalogue	4. N° de catalogue du destinataire / ISBN
TP 15711E	225-034	T29-194/2026E-PDF	978-0-662-35426-0

5. Titre et sous-titre	6. Date de la publication
Mesure du bruit rayonné sous l'eau d'un bateau remorqueur	Juin 2026
	7. N° de document de l'organisme exécutant RAL02839R-225-034-500

8. Auteur(s)	9. N° de dossier - Transports Canada
Burella, Giorgio; Lee, Waltfred; den Hertog, Vince	T8009-250013

10. Nom et adresse de l'organisme exécutant	11. N° de dossier - TPSGC
Robert Allan Ltd. 400-250 rue Howe Vancouver (Colombie-Britannique) V6C 3R8 Canada	WS5200443588
	12. N° de contrat - TPSGC ou Transports Canada CW2413782

13. Nom et adresse de l'organisme parrain	14. Genre de publication et période visée
Transports Canada Place de Ville, tour C 330, rue Sparks Ottawa (Ontario) K1A 0N5	Rapport technique final
	15. Agent de projet Olivier Maillet Glas

16. Remarques additionnelles (programmes de financement, titres de publications connexes, etc.)

Ce rapport a été financé dans le cadre du programme RDD maritime.

17. Résumé

Robert Allan Ltd. a réalisé une étude à pleine échelle pour le Centre d'innovation de Transports Canada afin de comparer le bruit rayonné sous-marin d'un remorqueur portuaire moderne électrique à batterie et celui d'un remorqueur portuaire diesel-mécanique de taille et de performance similaires opérant dans le port de Vancouver. Des essais en mer ont été effectués à l'aide d'une station d'écoute sous-marine autonome mouillée au fond, dans des conditions d'eaux profondes conformes à la norme ISO 17208. Des essais complémentaires de bruit, de vibration et d'analyse modale à bord ont également été réalisés afin d'identifier les principales sources de bruit et les chemins de transmission. Les résultats ont démontré des différences nettes dans les caractéristiques du bruit entre les deux systèmes de propulsion. Pour le remorqueur diesel-mécanique, les moteurs principaux et l'engrènement des systèmes de propulsion azimutale constituaient les principales sources de bruit structurel rayonné sous l'eau, particulièrement sous 1 kHz. En revanche, lors du fonctionnement uniquement sur batterie, le remorqueur électrique à batterie ne présentait pas de source dominante de bruit mécanique à basse fréquence et produisait un niveau global de bruit inférieur durant les conditions stationnaires et les transits à faible vitesse. Dans ces cas, le bruit était principalement attribuable au bruit tonal lié aux propulseurs et aux engrenages. Lorsque les génératrices étaient en marche, le bruit augmentait, mais demeurait inférieur à celui du remorqueur diesel-mécanique. À des vitesses de transit plus élevées et durant les essais de traction au point fixe, la cavitation devenait la principale source de bruit pour les deux navires. Le remorqueur électrique à batterie a permis des réductions du niveau de source dépassant 8 dB à des vitesses de transit inférieures à 8 nœuds et 10 dB en phase d'attente, mais cet avantage diminuait à forte charge, le bruit dépassant alors celui du remorqueur diesel-mécanique de jusqu'à 5 dB à la traction maximale au point fixe. L'étude a également permis de confirmer la conformité du remorqueur électrique à batterie à la notation UWN de Lloyd's Register.

18. Mots clés	19. Diffusion
Bruit rayonné sous-marin, transport maritime durable, électrique à batterie, exploitation des navires portuaires et de port	Copie numérique

20. Classification de sécurité (de cette publication)	21. Classification de sécurité (de cette page)	22. Déclassification (date)	23. Nombre de pages	24. Prix
Non classifiée	Non classifiée	—	xvii, 60, ann.	—

Acknowledgements

The cooperation of the tug owner, their crew, and the support of the Innovation Centre of Transport Canada, are gratefully acknowledged.

Revision Control Sheet

Prepared by:	Dr. Giorgio Burella, P.Eng. Waltfred Lee, EIT, MASc	**Date**	Feb. 20, 26
Clerical by:	Dionne Addison	**Date**	Mar. 5, 26

Engineer of Record:

Engineers and Geoscientists BC Permit to Practice number 1001019

Rev.	Date	Description	By	Checked	Approved
1	Feb. 20, 26	First issue.	BG/ WL	VdH	VdH
2	March 9, 26	Revised as per TC-IC comments	BG	VdH	VdH
3	March 18, 26	Corrected broken table references, figures	BG	-	-

Confidential

All information contained in or disclosed by this document is proprietary and the exclusive intellectual property of Robert Allan Ltd. This design information is reserved for the exclusive use of the client identified herein. All further use and sales rights attached thereto are exclusively reserved by Robert Allan Ltd., and any reproduction, communication or distribution of this information is prohibited without the prior written consent of Robert Allan Ltd. Absolutely no modifications or alterations to this document may be made by any persons or party without the prior written consent of Robert Allan Ltd.

CERTIFIED ISO 9001
UKAS MANAGEMENT SYSTEMS 001

Executive Summary

Robert Allan Ltd. (RAL) was retained by the Innovation Centre of Transport Canada (TC-IC) to conduct a study to compare the underwater radiated noise (URN) from a modern battery-electric (BE) harbour tug with that from diesel-mechanical (DM) harbour tug with approximately equivalent size and performance. The two tugs used for the study are normally engaged in ship assist operations in the Port of Vancouver. The objective of the study was to characterize and compare URN emissions across representative operating conditions, identify dominant URN sources and transmission mechanisms, and evaluate the potential URN benefits of battery-electric propulsion in environmentally sensitive waters.

Full-scale sea trials were conducted on both vessels using a dedicated bottom-moored underwater listening station (ULS) that was deployed in Indian Arm, a fiord-like inlet that branches northward from Burrard Inlet, within the Vancouver Fraser Port Authority jurisdiction. The location features deep-water and low-traffic conditions, compliant with ISO 17208 requirements. Measurements were performed on October 9, 2025, October 14, 2025, and November 25, 2025, for the BE tug, and on October 16, 2025, and December 15, 2025, for the DM tug. Tested conditions spanned across baseline stationary, straight run (transit), and bollard pull (pushing/pulling at low speeds) operational states, reflecting a typical ship assist duty cycle. Simultaneous onboard noise and vibration measurements and supporting dockside impact modal analysis testing were conducted to investigate mechanisms contributing to URN, including machinery noise generation, structure-borne and airborne noise transmission, and radiation to URN.

Results demonstrate clear differences in URN composition and magnitude between the two tugs. For the diesel-mechanical tug, structure-borne noise generated by the main engines and gear meshing in the azimuthing drives and transmitted through the vessel structure was identified as a dominant contributor to URN across most operating conditions, particularly at frequencies below 1 kHz. In contrast, the battery-electric tug exhibited a fundamentally different noise signature during battery-only operation. The absence of diesel main engines eliminated a major source of low-frequency tonal noise, resulting in lower overall URN levels during baseline stationary and low-speed transit conditions. Under these operating states, URN was primarily driven by propulsor-related noise, including gear meshing within the L-drive and blade-passage-related tonal content. When operating on genset power, increases in structural vibration and URN were observed at frequencies associated with genset rotational speeds; however, these contributions remained lower than those associated with diesel-mechanical main engines.

For both vessels, propeller-related noise increasingly dominated the URN signature as vessel speed and propulsor loading increased. Clear evidence of inception and development of cavitation was observed during higher-speed transit and bollard pull conditions, with cavitation noise becoming the primary contributor to URN at high power. Differences in propeller design and configuration influenced cavitation behaviour and noise characteristics, highlighting the importance of propulsor design in URN performance. URN reduction is not typically a design goal for the propellers in the azimuthing propulsor units supplied for tugs since they are primarily designed to achieve the contractually required bollard pull rating at maximum engine power.

Overall, the battery-electric tug exhibited lower URN levels than the diesel-mechanical tug under the same operating conditions, particularly during low-speed transit and loitering operations that make up a significant portion of typical harbour tug duty cycles. The BE tug showed URN source level reductions exceeding 8 dB for transit speeds below 8 knots and 10 dB during loiters. These findings indicate that battery-electric propulsion offers meaningful URN-reduction benefits. However, during high-speed transits (10 knots) and bollard pull conditions, the URN levels differential between the BE tug and the DM tug was not as high. Differences in URN levels were observed during bollard pull operations when cavitation developed, with the battery-electric tug performing worse than the diesel-mechanical tug, with URN levels increasing by up to 5 dB at full thrust. Although outside the scope of this study, it is worth noting that further URN reduction may be possible with battery-electric tugs, through the application of propulsors that are specifically designed to minimize cavitation and therefore the URN at high loads where propeller noise typically becomes dominant.

The URN measurements collected as part of this study also supported the process for obtaining a Lloyd's Register Underwater Noise (UWN) class notation for the battery-electric tug. The results demonstrated compliance with applicable criteria for both transit and quiet notations within the tested speed ranges, illustrating the suitability of modern battery-electric tugs to meet established underwater noise performance benchmarks.

Sommaire

Robert Allan Ltd. (RAL) a été mandatée par le Centre d'innovation de Transports Canada (CI-TC) pour réaliser une étude visant à comparer le bruit rayonné sous l'eau d'un remorqueur portuaire moderne à propulsion électrique par batteries à celui d'un remorqueur portuaire à propulsion diesel mécanique de taille et de performance approximativement équivalentes. Les deux remorqueurs utilisés pour l'étude sont habituellement engagés dans des opérations d'assistance aux navires dans le port de Vancouver. L'objectif de l'étude était de caractériser et de comparer les émissions de bruit rayonné sous l'eau dans des conditions d'exploitation représentatives, d'identifier les principales sources de bruit et les mécanismes de transmission, et d'évaluer les avantages potentiels de la propulsion électrique par batteries en matière de réduction du bruit dans des eaux écologiquement sensibles.

Des essais en mer à grande échelle ont été réalisés sur les deux navires à l'aide d'une station d'écoute sous-marine dédiée, ancrée au fond marin et déployée dans Indian Arm, un bras de mer de type fjord qui s'étend vers le nord à partir du Burrard Inlet, dans la juridiction de l'Administration portuaire Vancouver Fraser. Le site présente des conditions d'eaux profondes et de faible trafic conformes aux exigences de la norme ISO 17208. Les mesures ont été effectuées les 9 et 14 octobre 2025 ainsi que le 25 novembre 2025 pour le remorqueur à batteries, et les 16 octobre 2025 et 15 décembre 2025 pour le remorqueur mécanique. Les conditions d'essai comprenaient des états de fonctionnement représentatifs, notamment à l'arrêt (condition de référence), en marche rectiligne (transit) et en poussée ou traction au point fixe à faible vitesse, reflétant un cycle de service typique d'assistance aux navires. Des mesures simultanées du bruit et des vibrations à bord, ainsi que des essais d'analyse modale par impact réalisés à quai, ont été effectués afin d'étudier les mécanismes contribuant au bruit rayonné sous l'eau, y compris la génération du bruit par les machines, la transmission par la structure et par voie aérienne, ainsi que le rayonnement vers le milieu aquatique.

Les résultats démontrent des différences claires dans la composition et l'ampleur du bruit entre les deux remorqueurs. Pour le remorqueur diesel mécanique, le bruit transmis par la structure, généré par les moteurs principaux et l'engrènement des engrenages dans les propulseurs azimutaux, puis transmis à travers la structure du navire, a été identifié comme un contributeur dominant au bruit dans la plupart des conditions d'exploitation, en particulier pour les fréquences inférieures à 1 kHz. En revanche, le remorqueur à propulsion électrique par batteries présente une signature acoustique fondamentalement différente lorsqu'il fonctionne en mode batterie seule. L'absence de moteurs diesel principaux élimine une source majeure de bruit tonal à basse fréquence, ce qui se traduit par des niveaux globaux de bruit rayonné sous l'eau plus faibles dans les conditions de référence et lors des déplacements à faible vitesse. Dans ces états de fonctionnement, le bruit est principalement attribuable aux propulseurs, notamment à l'engrènement des engrenages dans les entraînements en L et aux composantes tonales associées au passage des pales. Lorsque le remorqueur fonctionne avec des groupes électrogènes, une augmentation des vibrations structurelles et du bruit est observée à des fréquences correspondant aux vitesses de rotation de ces groupes; toutefois, ces contributions demeurent inférieures à celles associées aux moteurs diesel mécaniques.

Pour les deux navires, le bruit lié aux hélices devient de plus en plus dominant dans la signature du bruit rayonné sous l'eau à mesure que la vitesse du navire et la charge des propulseurs augmentent. Des preuves claires de l'apparition et du développement de la cavitation ont été observées lors des déplacements à vitesse plus élevée et des opérations au point fixe, le bruit de cavitation devenant alors le principal contributeur au bruit à forte puissance. Les différences de conception et de configuration des hélices influencent le comportement de la cavitation et les caractéristiques acoustiques, soulignant l'importance de la conception des propulseurs dans la performance en matière de bruit rayonné sous l'eau. La réduction du bruit n'est généralement pas un objectif de conception pour les hélices des unités de propulsion azimutales destinées aux remorqueurs, celles-ci étant principalement conçues pour atteindre la traction au point fixe contractuelle à la puissance maximale du moteur.

Globalement, le remorqueur à propulsion électrique par batteries a présenté des niveaux de bruit rayonné sous l'eau inférieurs à ceux du remorqueur diesel mécanique dans les mêmes conditions d'exploitation, en particulier lors des déplacements à faible vitesse et des périodes d'attente, qui constituent une part importante du profil d'exploitation typique des remorqueurs portuaires. Le remorqueur électrique à batteries a montré des réductions du niveau de source du bruit dépassant 8 dB pour des vitesses de transit inférieures à 8 nœuds et 10 dB durant les phases d'attente. Ces résultats indiquent que la propulsion électrique par batteries offre des avantages significatifs en matière de réduction du bruit rayonné sous l'eau. Toutefois, lors des déplacements à haute vitesse (10 nœuds) et des opérations au point fixe, l'écart entre les niveaux de bruit rayonné sous l'eau des deux types de remorqueurs est moins marqué. Des différences ont été observées lors des opérations au point fixe lorsque la cavitation se développait; dans ces conditions, le remorqueur à propulsion électrique par batteries a montré des performances moins favorables, avec des niveaux de bruit rayonné sous l'eau pouvant être supérieurs de jusqu'à 5 dB à pleine poussée. Bien que cela dépasse le cadre de cette étude, il convient de noter que des réductions supplémentaires du bruit rayonné sous l'eau pourraient être obtenues avec des remorqueurs à propulsion électrique par batteries grâce à l'utilisation de propulseurs spécifiquement conçus pour minimiser la cavitation et, par conséquent, le bruit rayonné sous l'eau à forte charge, lorsque le bruit des hélices tend à devenir dominant.

Les mesures de bruit rayonné sous l'eau recueillies dans le cadre de cette étude ont également contribué au processus d'obtention d'une notation de classe « Underwater Noise » de Lloyd's Register pour le remorqueur à propulsion électrique par batteries. Les résultats ont démontré la conformité aux critères applicables pour les notations de transit et de faibles émissions sonores dans les plages de vitesses testées, illustrant la capacité des remorqueurs électriques modernes à satisfaire aux normes établies en matière de performance acoustique sous-marine.

Contents

1 Introduction 1

2 Tested Vessels Particulars 3

3 Methodology 7

3.1 Relevant Standards 7

3.2 Measurement Systems 8

3.2.1 Hydrophone Underwater Listening Station (ULS) 8

3.2.2 Noise and Vibration Equipment 11

3.2.3 Vessel Positioning and Status Logging Equipment 12

3.3 Sea Trials 12

3.3.1 Trials Location 12

3.3.2 Trials Weather Conditions 13

3.3.3 Sea Trials Test Description 14

3.3.3.1 Straight Run Tests 14

3.3.3.2 Stationary Measurements 15

3.3.3.3 Background Noise Checks 15

3.3.4 Test Matrix 16

3.3.4.1 Baseline Stationary 16

3.3.4.2 Straight Run 19

3.3.4.3 Bollard Pull 20

3.4 Dockside Tests 22

3.5 Measurements Processing and Analysis 23

3.5.1 URN Postprocessing 23

3.5.2 N&V Postprocessing 23

3.5.3 Data Analyses 24

3.5.3.1 Tonal Analysis 24

3.5.3.2 Structure-borne Noise Contributions from Machinery to Overall URN levels. 27

3.5.3.3 Airborne Noise Contributions to Overall URN levels 29

4 Results 31

4.1 Test Runs Naming Convention 31

4.2 URN Data Results 35

4.2.1 Baseline Stationary 36

4.2.2 Straight Run 38

4.2.3 Bollard Pull 41

4.3 URN Class Notation Process 43

4.4 Vibration Data Results 45

4.4.1 Main Engines Vibration Levels 46

4.4.2 Gensets Vibration Levels 48

4.4.3 Z- and L-Drives Vibration Levels 52

5 Conclusions 56

6 Recommendations 58

References 60

Appendix A. Sea Trials and Dockside Tests Summary

Appendix B. N&V Sensors Positions

Appendix C. URN Narrow-band Data Analysis

Appendix D. *Lv* Narrow-band Data Analysis

Appendix E. Machinery Noise Generation, Transmission, and Radiation

List of Figures

Figure 1: Harbour tugs during ship-assist operations. Four tugs are shown pushing a large cargo vessel, while assisting it to dock on a pier. 1
Figure 2: Battery-electric (BE) schematic propulsion system configuration 3
Figure 3: Diesel-mechanical (DM) schematic propulsion system configuration 4
Figure 4: Schematic arrangements for the L-drive (top) and Z-drive (bottom) configurations. .. 5
Figure 5: Hydrophone station layout and components, courtesy of JASCO Applied Sciences ... 9
Figure 6: Retrieval of the hydrophone station. One of the three AMARs and hydrophones is visible on the left side of the picture. Picture courtesy of JASCO Applied Sciences. 10
Figure 7: Photograph of the Noise and Vibration measurement equipment (from left to right, top to bottom) a high-speed data acquisition system, a laser tachometer, an IEPE high-sensitivity accelerometer, a free-field condenser microphone and a modal hammer . 11
Figure 8: Hydrophone station location with bathymetry and trials site. The figure contains information on the straight run test range waypoints. Image courtesy of JASCO Applied Sciences 13
Figure 9: Beam aspect test course (as shown from the ISO 17208 standard) 15
Figure 10: Impact testing with modal hammer onboard the battery-electric tug 22
Figure 11: Tonal analysis of the straight run at 8 knots for accelerometers installed in the way of the main engine of the DM tug showing (a) vibration levels above the resilient mount, (b) vibration levels below the resilient mount on the main engine support structure, (c) vibration levels at the hull plating in the way of the engine room, and (d) the respective third-octave band spectra. 26
Figure 12: Schematic of the quantities involved in the transmission of structure-borne noise to URN. 28
Figure 13: Picture showing selected MSL source levels spectra for different run types for both BE and DM tugs, where (a) are baseline (BS) runs, (b) are straight travel runs (ST), and (c) are bollard pull runs (BP) 35
Figure 14: MSL spectra in third-octave bands for Baseline Stationary operational states for (a) BE and (b) DM tugs. The 0/1 in the legends represents the on/off of the main engine/motor (M), generators (G) and thruster clutch (C). 37
Figure 15: MSL spectra in third-octave bands for Straight Run operational states for (a) BE and (b) DM tugs. The speed in the legends represents the speed over ground. The figure offers also comparisons of source levels with the LR UWN-T criterion “LR (Transit)” and LR UWN-Q criterion “LR (Quiet)” 39
Figure 16: MSL spectra in third-octave bands for Bollard pull operational states for (a) BE and (b) DM tugs. The percentage in the legends represents the bollard pull loading. 42

Figure 17: Structural vibration levels Lv for DM tug by location and sea trials run as measured in way of the main engine support structure. “top”,“ seating” and “hull” refer to location above the engine mount, the engine foundation and the hull plating, respectively. The bar plots represent the overall broadband levels 46

Figure 18: Structural vibration levels Lv for BE tug by location and sea trials run as measured in way of the genset support structure. “top”,“ seating” and “hull” refer to location above the genset mount, the genset foundation and the hull plating, respectively. The bar plots represent the overall broadband levels. 48

Figure 19: Structural vibration levels Lv for DM tug by location and sea trials run as measured in way of the genset support structure. “top”,“ seating” and “hull” refer to location above the genset mount, the genset foundation and the hull plating, respectively. The bar plots represent the overall broadband levels 50

Figure 20: Structural vibration levels Lv for DM tug by location and sea trials run as measured in way of the Z-drive propulsor. “seating” and “hull” refer to locations at the drive foundation and the hull plating, respectively. The bar plots represent the overall broadband levels 52

Figure 21: Structural vibration levels Lv for DM tug by location and sea trials run as measured in way of the Z-drive propulsor. “seating” and “hull” refer to locations at the drive foundation and the hull plating, respectively. The bar plots represent the overall broadband levels. 54

List of Tables

Table 1: Principal particulars of the case-study vessels 6
Table 2: Hydrophones and Data Acquisition System Main Specifications..... 8
Table 3: Matrix of intended baseline stationary tests for battery-electric and diesel-mechanical tugs. Rows highlighted in grey denote runs that were outlined in [3] but not run during sea trials or differently..... 18
Table 4: Matrix of straight run tests for both battery-electric and diesel-mechanical tugs 19
Table 5: Matrix of intended bollard pull tests for battery-electric and diesel-mechanical tugs . 21
Table 6: Vessel engines, propeller and shafting characteristics 25
Table 7: Straight Travel (ST) run types naming conventions 32
Table 8: Baseline Stationary (BS) run types naming conventions 33
Table 9: Bollard Pull (BP) run types naming conventions 34
Table 10: Broadband MSL levels in dB re 1µPa for baseline (BS) at key frequency ranges. 36
Table 11: Broadband MSL levels in dB re 1µPa for straight travel runs (ST) at key frequency ranges..... 38
Table 12: Broadband MSL levels in dB re 1µPa for bollard pull (BP) at key frequency ranges. 41

Glossary

ABN	Airborne Noise
ADC	Analog-to-Digital Converter
AMAR G4	Autonomous Multichannel Acoustic Recorder Generation 4
ANSI	American National Standards Institute
ASA	Acoustical Society of America
ASD	Azimuthing Stern Drive
BE	Battery-Electric
BP	Bollard Pull
BPF	Propeller Blade Passage Frequency
BS	Baseline Test Runs
CCTV	Closed-Circuit Television
COMEX	Start point of test range for straight runs
CPA	Closest Point of Approach
CTD	Conductivity, Temperature, and Depth
DAQ	Data Acquisition System
DM	Diesel-Mechanical
DWL	Data Window Length
FFT	Fast Fourier Transform
FINEX	End point of test range for straight runs.
GR	Gear Ratio
GSR	Genset Rate
GHG	Greenhouse Gases
GML	Gear Meshing Frequency Lower Gearbox
GMU	Gear Meshing Frequency Upper Gearbox
GNSS	Global Navigation Satellite System
ISO	International Organization for Standardization
IEPE	Integrated Electronics Piezo-Electric
IP	Internet Protocol

JASCO	JASCO Applied Sciences Ltd.
LR	Lloyd's Register
M-DAQ	Maneuvering Data Acquisition System
MER	Main Engine Rate
MOT	Motor Rate
MSL	Monopole Source Level
N&V	Noise and Vibration
RAL	Robert Allan Ltd.
RNL	Radiated Noise Level
SARA	Species at Risk Act
SBN	Structure-Borne Noise
SRKW	Southern Resident Killer Whales
ST	Straight Runs
ST-BATT	Straight Runs on Battery Power
ST-GENS	Straight Runs on Genset Power
TC-IC	Innovation Centre of Transport Canada
TL	Transmission Loss
URN	Underwater Radiated Noise
ULS	Underwater Listening Station
UWN	Underwater Noise and LR Class Notation
VFPA	Vancouver-Fraser Port Authority

1 Introduction

Robert Allan Ltd. (RAL) was contracted by the Innovation Centre of Transport Canada (TC-IC) to conduct a study to compare the Underwater Radiated Noise (URN) from battery electric harbour tugs to that from conventional diesel-mechanical powered harbour tugs.

A push to reduce URN from shipping is of particular interest in southern British Columbia because of concerns about the well-being of the Southern Resident Killer Whales (SRKW). The SRKW are listed as an endangered species in the Species at Risk Act (SARA) in Canada [1]. As tugboat activities overlap with known SRKW habitat areas on Canada's West Coast, it is important to measure and characterize the underwater radiated noise signature of tugs.

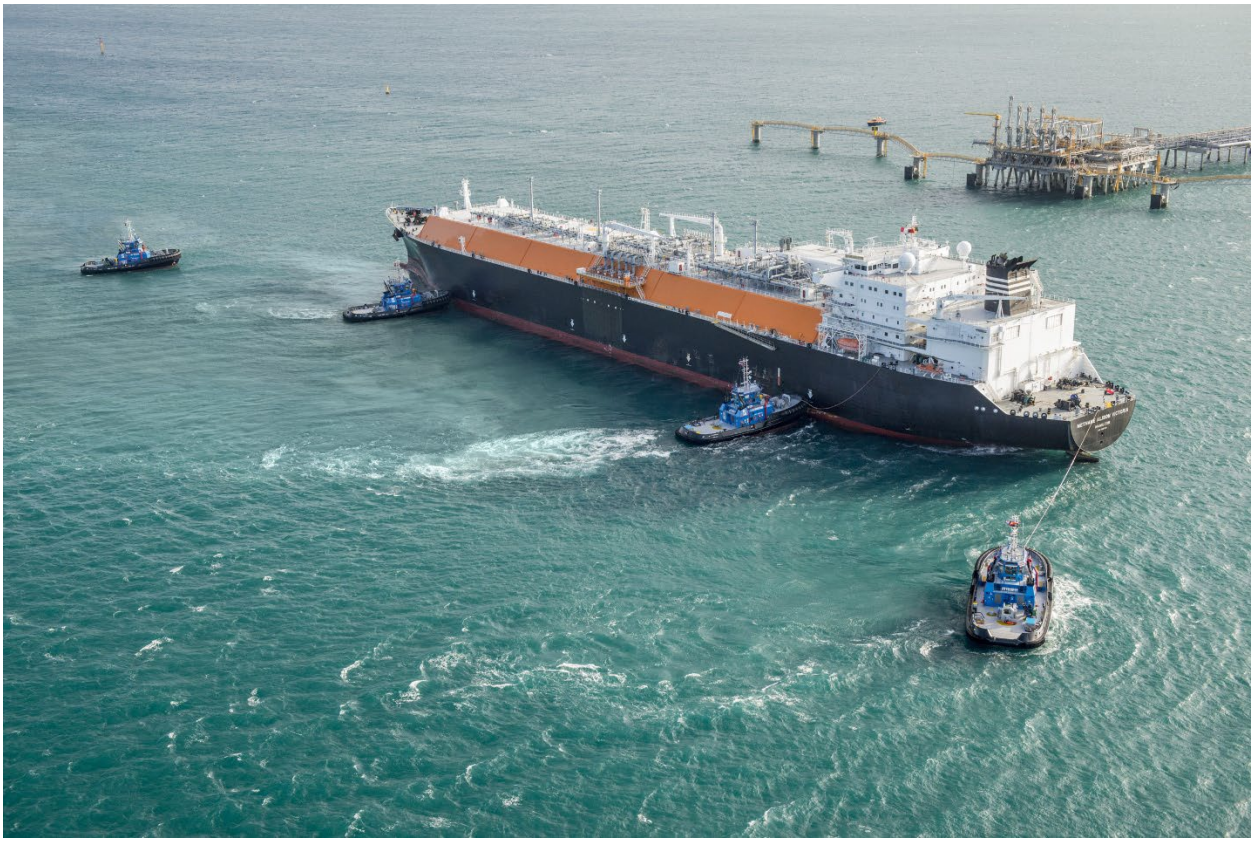


Figure 1: Harbour tugs during ship-assist operations. Four tugs are shown pushing a large cargo vessel, while assisting it to dock on a pier.

Harbour tugs, or equivalently ship-assist tugs, typically assist larger cargo-carrying ships with docking and undocking and executing low speed maneuvers within the confined waters of a port. Figure 1 shows a picture of a typical ship-assist operation where harbour tugs are assisting a larger

vessel into docking. They operate over duty cycles that are made up of several operational states that include loitering, transit, and pushing/pulling at low speeds (generally referred to as bollard pull). Recognizing this, the URN characterization must consider not only the different URN emissions associated with each operational states, but also the time the tug operates in each state.

The application of battery-electric tugs has been identified as a potential pathway to reduce the overall URN impact of tug operations. In addition, battery-electric tugs have been recognized to be an effective means to reduce greenhouse gases (GHG) [2].

Battery-electric propulsion is expected to reduce URN generated by machinery by removing the diesel main engines. Another major source of underwater noise is propellers, for which URN reduction is not typically a design goal; rather, the focus is on achieving the contractually required bollard pull.

The study supported a URN measurement program through the deployment of a dedicated, temporary Underwater Listening Station (ULS) in Indian Arm, British Columbia, where it operated continuously for seven (7) weeks. The ULS was designed, deployed, managed, and retrieved by JASCO Applied Sciences Ltd (JASCO) who also provided post-processing of the URN data. The test matrix included measurements at all the major operational states within a typical harbour tug duty cycle. Simultaneously, noise and vibration (N&V) data was collected on major propulsive equipment and on the hull using specialized accelerometer and microphone instrumentation. Dockside testing was also conducted to characterize the transmission of structure-borne noise from machinery to the hull (which subsequently radiates noise underwater). Tests were conducted in agreement with the TC-IC-approved URN Measurements Test Plan [3], and procedures and methodologies are outlined in this report.

Measurements were performed on October 9, 2025, October 14, 2025, and November 25, 2025, for the BE tug, and on October 16, 2025, and December 15, 2025, for the DM tug. From the analysis, the following insights were gained:

- General characteristics of the URN signature of modern ship-assist tugs operating in the Port of Vancouver, and how they vary between different typical operational states
- Composition of noise sources that contribute to the overall URN signature
- How the URN of a battery-electric tug compares to that of a conventional diesel-mechanical tug

In addition, valuable lessons were learned from the process of pursuing a marine classification society notation (Lloyd's Register UWN notation) for the battery-electric tug.

2 Tested Vessels Particulars

Two tugs, one battery-electric (BE) and one diesel-mechanical (DM), were identified as suitable for the testing. Both vessels are modern Azimuthing Stern Drive (ASD) twin propulsor tugs with two steerable nozzled propellers at the stern to provide maneuverability and the ability to push/pull in any direction. These tugs have a bollard pull of 70 tonnes and a length overall of ~23 m, which is representative of modern ship-assist tugs operating in the Salish Sea and in and around the Port of Vancouver. Typical modern ship-assist tugs are ASD tugs between 23 m and 29 m in length and have bollard pull ratings between 60 and 80 tonnes.

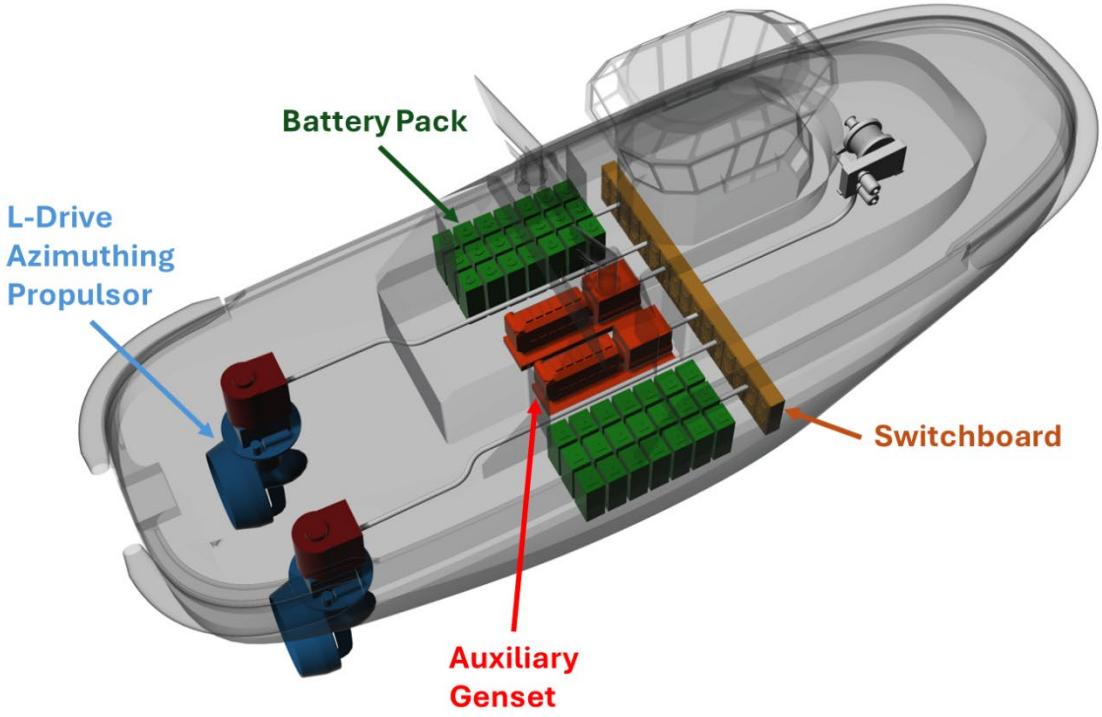


Figure 2: Battery-electric (BE) schematic propulsion system configuration

BE tugs utilize large battery packs to power the vessel during ship-assist operations. Propulsion is provided by azimuthing L-drive propulsors, with electric propulsion motors mounted vertically on top. An L-drive consists of a vertically oriented shaft that runs down from inside the vessel, through the hull and propulsor appendage, and then turns 90° degrees via a bevel gear to drive a horizontally oriented propeller shaft. This results in the “L-shaped” mechanical power flow from

prime mover to propeller. In addition to powering the propulsors, the batteries also supply other electrical loads on board. Auxiliary electric generators (if installed) are typically used to extend range and charge batteries when shore-based charging is unavailable. Figure 2 shows a schematic of a typical propulsion system arrangement of BE tugs with major propulsion equipment.

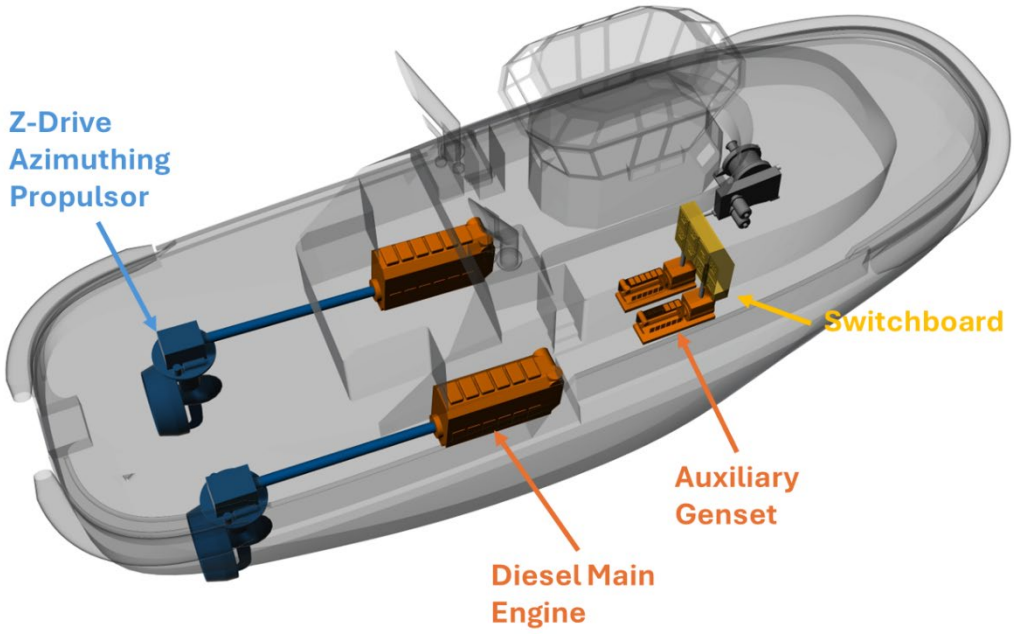


Figure 3: Diesel-mechanical (DM) schematic propulsion system configuration

DM tugs typically have a pair have high-speed marine diesel main engines. Steel or composite shafts transmit power from the engines to the Z-drives. A Z-drive consists of a horizontally oriented input shaft inside the vessel that turns 90° degrees via a bevel gear into a vertical shaft through the hull and then turns another 90° degrees via gearing to drive a horizontally oriented propeller shaft within the propulsor appendage. This results in a characteristic “Z-shaped” power flow between the prime mover and the propeller. Separate diesel gensets provide power for electrical ship loads. Figure 3 shows a schematic of the propulsive system arrangement of DM tugs with major propulsion equipment.

Figure 4 shows the schematic drawing of the typical shafting arrangement of L-drive and Z-drive propulsors.

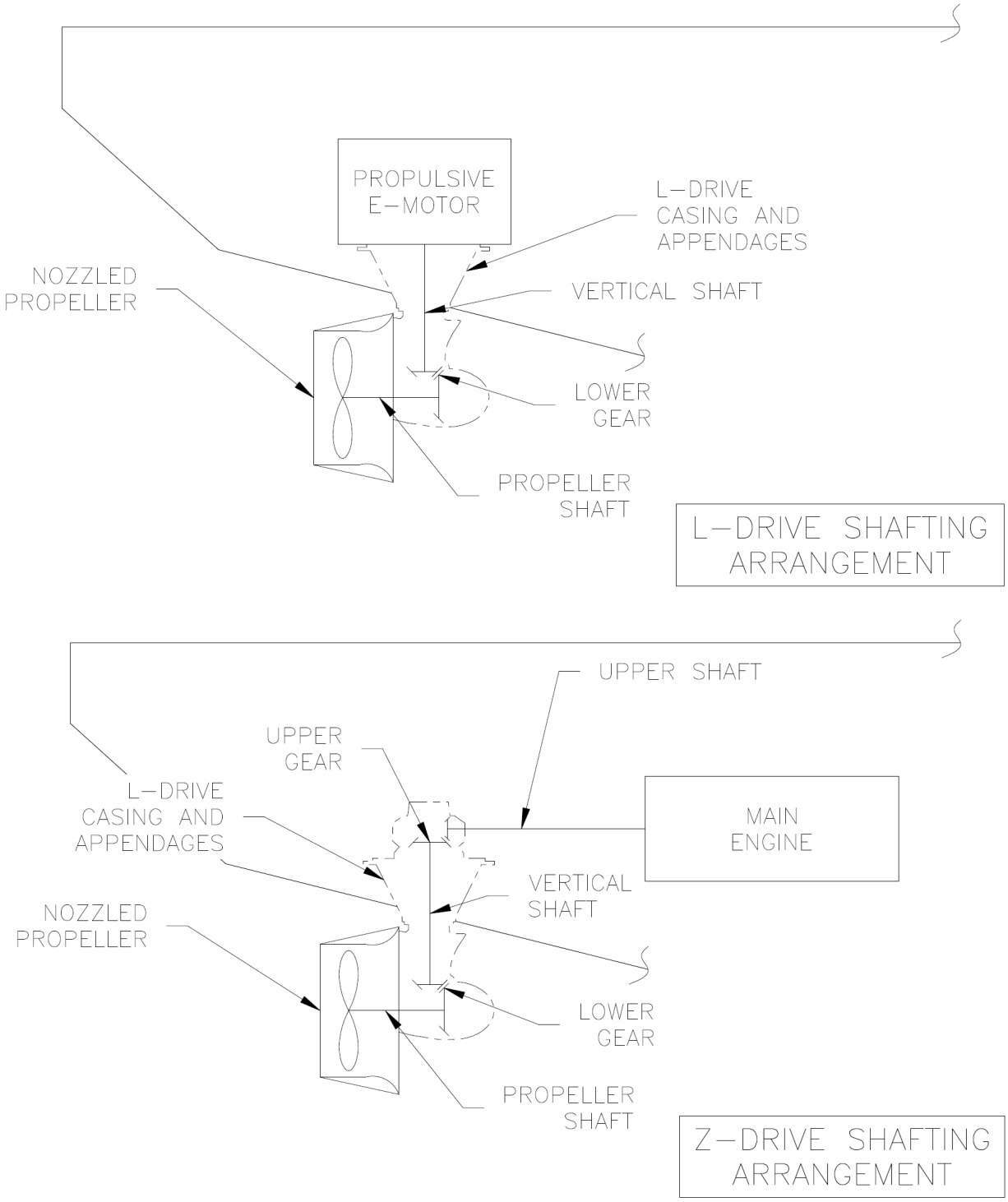


Figure 4: Schematic arrangements for the L-drive (top) and Z-drive (bottom) configurations

Main engines (on the DM tug) and gensets (on both tugs) are resiliently mounted on rubber mounts that effectively isolate engine vibration from the vessel's structure. The Z-drive and L-drive unit are rigidly mounted to the vessel structure, either by welded or bolted connections. Both Z-drive and L-drive units are equipped with speed-reduction and power-transmission gears.

The principal particulars for the two vessels are given in Table 1.

Table 1: Principal particulars of the case-study vessels

Vessel's Type	**Battery-Electric Tug (BE)**	**Diesel-Mechanical Tug (DM)**
Length Overall (m**)**	23.4	22.2
Moulded Breadth (m**)**	11.9	11.4
Moulded depth (m**)**	4.9	4.4
Bollard Pull (tonnes**)**	70	70
Maximum Speed (knots**)**	~13	~12
Transit Speed, Typical (knots**)**	8	8
Propulsion Prime Movers	2 x 2100 kW electric motors, hard-mounted	2 x 1902 kW diesel main engines, resiliently mounted
Gensets	2 x 940 ekW range-extender gensets, resiliently mounted	2 x 80 ekW auxiliary gensets, resiliently mounted on skids
Thrusters	2 x azimuthing stern L-drives with fixed pitch nozzled 4-bladed propellers, 2700 mm diameter	2 x azimuthing stern Z-drives with fixed pitch nozzled 3-bladed propellers, 2800 mm diameter

Since the two tugs have similar hull dimensions, installed propulsive power and approximately the same displacement, measured differences in URN can be attributed primarily to the differing noise and vibration characteristics of their powering systems, rather than factors related size, resistance, power or propeller/nozzle design.

3 Methodology

The study relied on data collection from full-scale sea trials on the vessels identified in Section 2. The data was subsequently post-processed and analyzed to obtain metrics relevant to this study. The following sections report the methodology utilized to collect, post-process and analyze the data. In particular:

- Section 3.1 lists the applicable standards used for the measurements and processing
- Section 3.2 describes the measurement equipment used for the URN and N&V data acquisition
- Section 3.3 describes methodologies for the sea trials
- Section 3.4 describes methodologies for the dockside trials
- Section 3.5 describes the data processing and analysis procedures

3.1 Relevant Standards

The following standards were applicable for the measurements of URN and onboard noise and vibration:

- The ISO 17208 series outlines materials and methodologies for characterizing the underwater noise source levels of sea-going vessels. This methodology is the basis for all underwater noise measurements on the two vessels
- LR-SR-ADP-016 outlines the procedures and methodologies to obtain an underwater noise notation from Lloyd's Register. The guidelines explicitly refer to ISO 17208 for the methodology and procedures for obtaining source levels for sea-going vessels
- ISO 20283 outlines the general procedures to measure structural vibration onboard vessels. The measurement of structural vibration is carried out in general conformance with this standard, with particular care taken in the installation of accelerometers to cover a suitable frequency range
- ISO 2923 outlines methodologies for measuring airborne noise onboard ships. In general, onboard airborne noise measurements are conducted in general accordance with this standard
- ISO 7626 outlines methodologies for the experimental determination of the mechanical mobility of mechanical structures. Impact testing to determine structure-borne noise transmission characteristics is carried out in general accordance with this standard

3.2 Measurement Systems

3.2.1 Hydrophone Underwater Listening Station (ULS)

The measurement system was composed of a bottom-moored vertical array of three (3) Autonomous Multichannel Acoustic Recorder (AMAR) G4 recorders connected to three (3) GeoSpectrum M-36 hydrophones. The hydrophones were located at 27 m, 58 m and 100 m below mean sea level. These depths correspond to depression angles of 15°, 30°, and 45° degrees, with a closest point of approach (CPA) of 100 m.

Table 2 presents the main specifications of the hydrophone and data acquisition system. Figure 5 shows the configuration at deployment and the main specifications of the recording system.

Table 2: Hydrophones and Data Acquisition System Main Specifications

Hydrophone name	GeoSpectrum M-36
Number of hydrophones	3
Directionality	Omni-directional
Sensitivity	-175 dB re /µV
Uncertainty	Less than 3 dB

Recorder name	AMAR G4
ADC converter	24 bits
Sampling rate	256k samples per second

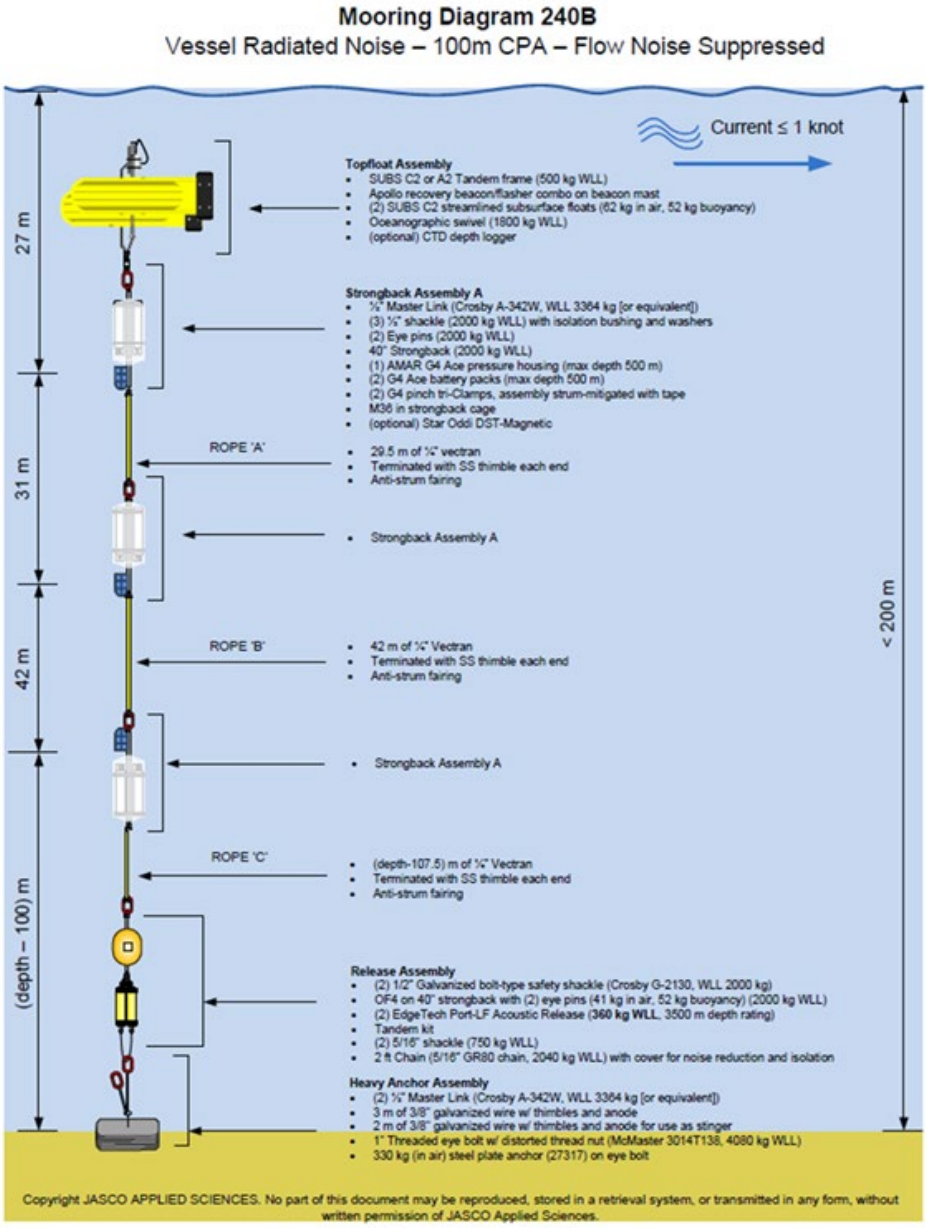


Figure 5: Hydrophone station layout and components, courtesy of JASCO Applied Sciences

The AMAR recorder's sampling rate ensured that the measurements covered the frequency range from 10 Hz to 125,000 Hz. The hydrophones were mounted inside a cage surrounded by yellow fabric flow shields above the AMAR. The flow shields reduce noise from ocean currents on the hydrophone. A conductivity, temperature, and depth (CTD) profiler was used to determine the sound speed profile during deployment and before commencing trials.

The longitude and latitude position of the ULS were recorded at the time of deployment. Tilt and depth sensors were attached to each hydrophone on the mooring system to measure their position and depth during trials.

The hydrophones were deployed and retrieved under JASCO's supervision from a chartered vessel.

Figure 6 shows the retrieval of the station after the deployment.



Figure 6: Retrieval of the hydrophone station. One of the three AMARs and hydrophones is visible on the left side of the picture. Picture courtesy of JASCO Applied Sciences.

The listening station was deployed for seven (7) weeks, from September 29, 2025, to November 19, 2025.

3.2.2 Noise and Vibration Equipment

The data acquisition system for onboard and vibration, shown in Figure 7, consisted of the following:

- Eight (8) analog and digital channel high-speed data acquisition system (DAQ), Dewesoft DEWE 43-A, to allow for the collection of simultaneous noise, vibration and shaft speed data with on-the-fly data processing software. The DAQ acquired signals with a sampling rate of 100 kHz. It uses a 24-bit analog-to-digital converter (ADC) to maximize the signal dynamic range
- Eight (8) Integrated Electronics Piezo-Electric (IEPE) PCB 352C33 high-sensitivity accelerometers to capture structure-borne sound from machinery to hull plating
- Two (2) free-field IEPE pre-amplified PCB 378B02 condenser microphones to capture airborne sound levels in the machinery spaces
- One (1) digital laser Monarch ROLS-W TTL tachometer to measure the shaft speed synchronously. As no shafting is present on the battery-electric tug, this was only installed on the diesel-mechanical tug. However, propeller speed on the BE tug was recorded with the setup described in Section 3.2.3
- One (1) Integrated Electronics Piezo-Electric (IEPE) low impedance modal hammer Kistler 9726A20000 for impact testing during the dockside trials



Figure 7: Photograph of the Noise and Vibration measurement equipment (from left to right, top to bottom) a high-speed data acquisition system, a laser tachometer, an IEPE high-sensitivity accelerometer, a free-field condenser microphone and a modal hammer

3.2.3 Vessel Positioning and Status Logging Equipment

To record the relative distance from ULS to the vessel, the tugs were equipped with a Global Navigation Satellite System (GNSS) compass and M-DAQ provided by RAL. The GNSS compass provided speed over ground and the vessel's position relative to the vessel reference point, as defined in the ISO 17208 standard.

Additionally, RAL utilized several Internet Protocol (IP) Closed-Circuit Television (CCTV) cameras in the wheelhouse to monitor and record the thruster's motor power, throttle, and azimuth angle.

3.3 Sea Trials

The goal of sea trials was to collect URN data and noise and vibration measurements to identify the key sources of noise and their contributions to the overall URN signature of the vessels. URN was recorded with the three hydrophones on the ULS, while simultaneously capturing N&V data on board. Appendix B contains the locations of the accelerometers and microphone at sea trials for the BE and DM vessels.

3.3.1 Trials Location

The measurement test site was located in Indian Arm, a fiord-like inlet that branches northward from Burrard Inlet. Indian Arm is within the jurisdiction of the VFPA. Permitting with the VFPA was obtained to deploy the ULS and conduct sea trials. The permitting requirements included: a) ensuring that the work was done in a professional manner; b) abiding by local and federal regulations; c) conducting work within permitted time slots, d) informing the port authority of sea trials ahead of time, and; e) informing the Canadian Coast Guard of sea trials activities so that a Navigational Warning could be published to inform the marine community of potential hazards. During permitting and upon the VFPA's request, the Tsleil-Waututh Nation was consulted and informed of the activities planned in their traditional territory.

Figure 8 shows the site and the local bathymetry. The deployment location of the ULS was approximately:

- Latitude: 49° 25.3554' N Longitude: 122° 52.2360' W

The area was selected for its ideal location for acoustic measurements. The site is sheltered with little fetch for wind to form waves. Furthermore, marine traffic in Indian Arm primarily consists of recreational boating. There is generally little traffic at the trial location because of its relatively remote location near the northern end of Indian Arm. There are no industrial sources of underwater noise in the area.

The average water depth below mean sea level is ~165 metres at the ULS. The water depth below the keels of the tugs to be tested was greater than 150 metres. Therefore, the arrangement complied with deep-water and far-field conditions as specified in the ISO 17028 standard [4].

3.3.2 Trials Weather Conditions

The tests were conducted with the following maximum weather conditions:

- Maximum wind speed of 13.6 knots
- Maximum Sea State 3 (1.22 metre significant wave height)
- No rain or snow
- Minimal tidal currents

The trials on both vessels were conducted within these weather and environmental conditions.

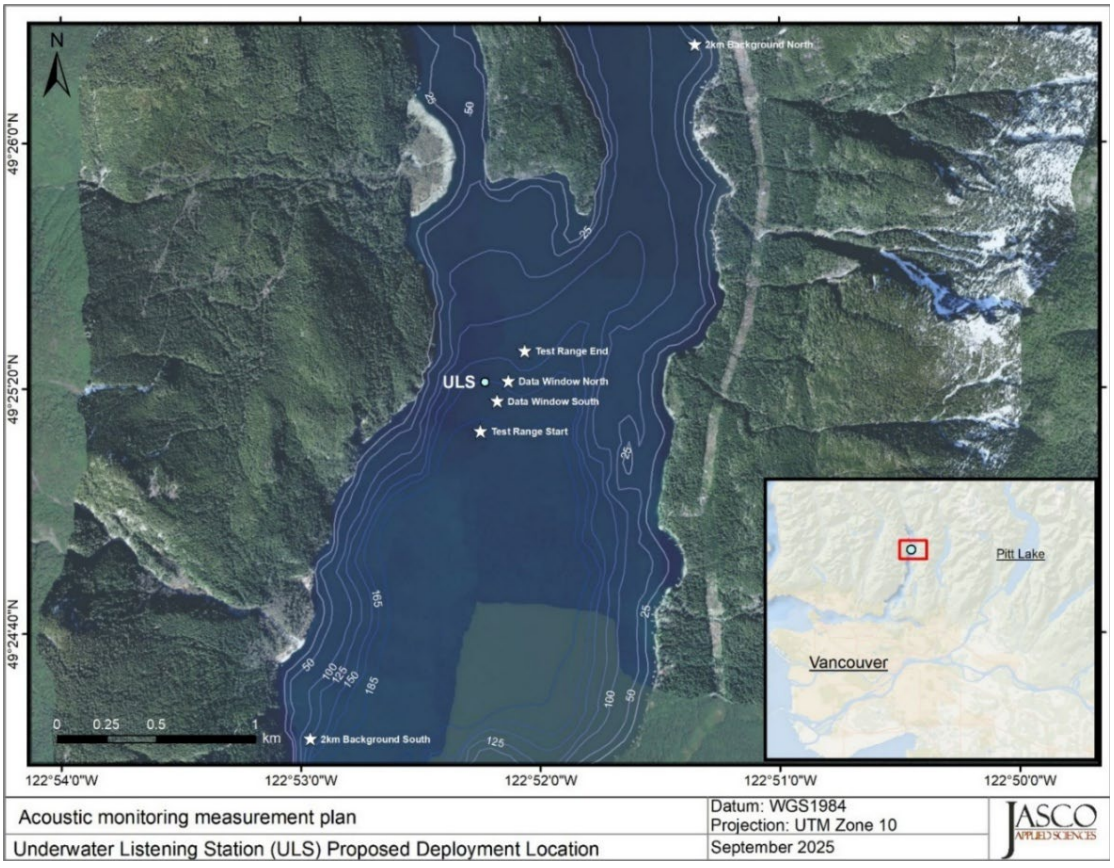


Figure 8: Hydrophone station location with bathymetry and trials site. The figure contains information on the straight run test range waypoints. Image courtesy of JASCO Applied Sciences

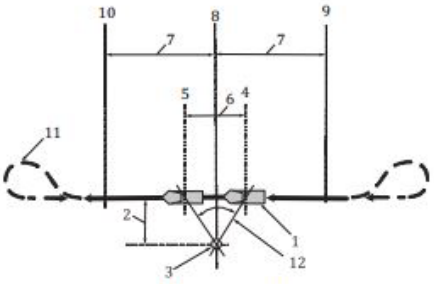
3.3.3 Sea Trials Test Description

3.3.3.1 Straight Run Tests

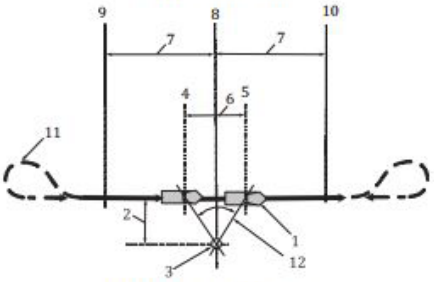
During the test, the vessel sailed over a straight-line course, passing alongside the ULS with the closest point of approach (CPA) at the required distance of 100 metres. During the passages alongside the ULS, the vessel port and starboard beam aspect is alternatively presented, for a minimum of two passages on each aspect.

The data window length (DWL), which is centered at the CPA, defines the range where data collected are usable for processing. Within the DWL, the vessel maintained a steady operating condition by ensuring the propeller rotation rate remained constant from the point at which the set speed was reached, prior to entering the DWL.

The DWL is contained within the Test Range, which is set to four times the DWL and bounded by the COMEX and FINEX points. This is an area where the vessel maintains a stable course and speed before entering and after exiting the DWL, and it defines the beginning and end of one test run. Additional information on testing procedures for straight runs is contained in the URN Measurements Test Plan [3]. An example test course, the waypoints defining the test range and data windows are shown in Figure 9.



a) Port approach



b) Starboard approach

Key

1	ship under test	7	2 × DWL
2	distance, dCPA, at closest point of approach (CPA)	8	CPA point
3	hydrophone(s)	9	COMEX
4	start data	10	FINEX
5	end data	11	Williamson curve
6	DWL	12	±30° (total = 60°)

NOTE 1 $l_{DW} = 2d_{CPA}\tan(30°)$, where d_{CPA} = 100 m or one overall ship length, whichever is the greater.

NOTE 2 $t_{DWP} = \left(\frac{l_{DW}}{v}\right)$, where v is the ship's speed, in m/s.

Figure 9: Beam aspect test course (as shown from the ISO 17208 standard)

3.3.3.2 Stationary Measurements

The vessel was kept stationary at the CPA position for at least two minutes in the intended operational state. The test was repeated with the vessel presenting both starboard and port beam aspects to the listening station.

3.3.3.3 Background Noise Checks

During the trials, the vessel moved to the background noise position 2 km away from the ULS (either north or south) to perform a background noise measurement. Background checks were performed at the beginning and end of day, and when significant changes in environmental conditions were noted. This measurement was necessary to ensure a sufficient signal-to-noise ratio is achieved during data post-processing.

3.3.4 Test Matrix

The test runs were designed to represent typical operational states that comprise the tugs' ship assist duty cycle. These conditions are identified in three main categories:

- Straight run (ST), representing transits at various speeds
- Baseline stationary (BS), utilized to gather insight from URN composition of machinery and also the URN signature during tug loiters
- Bollard pull (BP), intended to simulate bollard pull conditions, and representative of ship-assist operations when the tug is required to provide push or pull to the assisted vessel during docking/undocking operations

3.3.4.1 Baseline Stationary

These measurements were intended to provide insights into the relative contributions of main engines, the gensets, the propeller and the shaft gearing to the overall underwater noise levels. With this in mind, measurements started with as many systems as possible shut down, and then systems were brought online one by one in a controlled, systematic manner.

Table 3 shows the planned number and type of tests, according to the procedure outlined in Section 3.3.3.2.

Changes to the tug baseline stationary testing were necessary due to the technical difficulties encountered with certain test runs in the test matrix. In particular:

- BE tests e), f), were not run, as normal operations on the BE tug with genset power are always run with both gensets on. Past tests on similar tugs have shown that the changes between one to two gensets online usually correspond to a ~3 dB increase in noise levels as the sound power from the gensets emitted underwater doubles
- BE tests g) and h) were run, but with 2 gensets on
- DM tests a) and b) were not run as the Chief Engineer deemed it not safe to have both propulsion engines shut off at sea while at sea in close proximity to shore. However, during dockside trials it was possible to collect the N&V data from this condition
- DM test c) and d) were not run as intended. Under those tests, the Z-drive clutch is supposed to be completely disengaged. However, due to a misadjustment in the clutch wheelhouse controls that could not be corrected during the testing, the clutch could not be fully disengaged. This resulted in a slow rotation of the propeller during the testing, which did not significantly contribute to the overall URN signature.

These changes to the planned test plan did not have a significant impact on the overall results.

Table 3: Matrix of intended baseline stationary tests for battery-electric and diesel-mechanical tugs. Rows highlighted in grey denote runs that were outlined in [3] but not run during sea trials or differently.

BATTERY-ELECTRIC (BE) TUG			
Run #	**Tug Motors**	**Tug Course WRT Hydrophone**	**Tug Gensets**
0	Background	-	Background
a	off	port	off
b	off	starboard	off
c	min rpm	port	off
d	min rpm	starboard	off
e	off	port	running - 1 Genset
f	off	starboard	running - 1 Genset
g	min rpm	port	running - 1 Genset
h	min rpm	starboard	running - 1 Genset
i	off	port	running - 2 Gensets
j	off	starboard	running - 2 Gensets

DIESEL-MECHANICAL (DM) TUG			
Run #	**Tug Engines**	**Tug Course WRT Hydrophone**	**Tug Z-Drives**
0	Background		Background
a	off	port	de-clutched
b	off	starboard	de-clutched
c	idle	port	de-clutched
d	idle	starboard	de-clutched
e	idle	port	clutched
f	idle	starboard	clutched

3.3.4.2 Straight Run

Straight run tests were conducted from 6 knots to 10 knots. This range reflects the speeds at which tugs might travel during transit in a harbour setting or from one port to another.

The BE tug operated in one of two power modes: battery power only, or genset power only (where all electric and propulsive loads are supplied by the generators). For the battery-electric tug, data collected during battery-powered runs served as the basis for obtaining the Lloyd's Register UWN notation [5]. Since the LR standard for conducting sea trials is equivalent to ISO 17208, the URN measurements made during straight runs could also be used as the basis for the LR UWN notation.

Table 4 shows the planned number and type of tests, according to the procedure outlined in Section 3.3.3.1.

Table 4: Matrix of straight run tests for both battery-electric and diesel-mechanical tugs

Run # (*)	**Tug Speed [**knots**]**	**Tug Course WRT Hydrophone**
a-1	6 knots	passing abeam stbd
a-2		passing abeam port
a-3		passing abeam stbd
a-4		passing abeam port
b-1	7 knots	passing abeam stbd
b-2		passing abeam port
b-3		passing abeam stbd
b-4		passing abeam port
c-1	8 knots	passing abeam stbd
c-2		passing abeam port
c-3		passing abeam stbd
c-4		passing abeam port
d-1	9 knots	passing abeam stbd
d-2		passing abeam port
d-3		passing abeam stbd
d-4		passing abeam port
e-1	10 knots	passing abeam stbd
e-2		passing abeam port
e-3		passing abeam stbd
e-4		passing abeam port
Notes: (*) Battery-electric repeated tests, on genset power only		

3.3.4.3 Bollard Pull

Bollard-pull conditions were tested using a stationary test. As there was no opportunity to tether the tug towlines to a shore bollard for a traditional bollard pull test at the trials location, the two stern thrusters were azimuthed to oppose each other, both pushing inboard, so that the net effect was that the vessel remained stationary under full power, or as near stationary as practically achievable by the tug master. Although this is not a like-for-like substitute for a true bollard pull situation, previous URN testing on tugs showed noise levels and noise-spectrum composition consistent with bollard pull conditions in that the propellers are highly loaded and experience consistent cavitation, and the main engines are at maximum revolutions, delivering nearly full-rated power.

For tests with the battery-electric tugs operating in genset-only power mode, a reduced set of runs was conducted since the gensets are designed to provide only up to ~50% of the maximum installed propulsive power.

Table 5 shows the planned number and type of tests, according to the procedure outlined in Section 3.3.3.2.

Table 5: Matrix of intended bollard pull tests for battery-electric and diesel-mechanical tugs

BATTERY-ELECTRIC (BE) TUG		
Run #	**Mains or Motor Power**	**Tug End Facing Hydrophone**
0	Background Noise	away
a	20% Max power	port aspect
b	20% Max power	starboard aspect
c	50% Max power	starboard aspect
d	50% Max power	port aspect
e	75% Max power	starboard aspect
f	75% Max power	port aspect
g	100% Max power	port aspect
h	100% Max power	starboard aspect
i	20% Max power - 1 Genset	starboard aspect
j	20% Max power - 1 Genset	port aspect
k	~50% Max power - 2 Gensets	port aspect
l	~50% Max power - 2 Gensets	starboard aspect

DIESEL-MECHANICAL (DM) TUG		
Run #	**Mains or Motor Power**	**Tug End Facing Hydrophone**
0	Background Noise	away
a	20% Max power	port aspect
b	20% Max power	starboard aspect
c	50% Max power	starboard aspect
d	50% Max power	port aspect
e	75% Max power	starboard aspect
f	75% Max power	port aspect
g	100% Max power	port aspect
h	100% Max power	starboard aspect

3.4 Dockside Tests



Figure 10: Impact testing with modal hammer onboard the battery-electric tug

The primary goal of the dockside trials was to establish the mechanical mobility functions that quantify how structure-borne noise is transmitted from machinery items to the hull plating, subsequently radiated as underwater noise.

Mechanical mobility is evaluated by impact testing with a "modal hammer," with simultaneous measurement of the impact response using accelerometers. Figure 10 shows an example of impact testing performed on a marine genset. A modal hammer (held in the right hand of the person in Figure 10) was used to excite the supporting structure of the main propulsive equipment. Simultaneously, response data is collected from several accelerometers attached to the supporting structure and hull plating below. This data is then processed by specialized post-processing software that works out the mechanical mobilities. These mobilities can then be used to model the structural response at the hull plating and calculate the radiated noise due to structure-borne sound transmitted from main propulsive machinery items.

Vibrational responses were collected normal to the structure, as bending of plates is primarily responsible for the radiation of noise. The DAQ software, DewesoftX, acquired the data and processed the mobilities on the fly during testing.

Appendix B shows the locations of the accelerometers and hammer impact positions at sea trials for the BE and DM vessels. The mechanical mobility functions were collected and evaluated for the battery-electric and diesel-mechanical tugs, as summarised in Appendix A.

3.5 Measurements Processing and Analysis

The following section outlines the procedures followed for postprocessing raw measurements into URN and N&V spectral data, as well as methodologies for analyzing the data to evaluate noise and source composition.

3.5.1 URN Postprocessing

The software used for post-processing URN was ShipSound™, a component of JASCO's custom vessel noise measurement system, PortListen®. ShipSound performs semi-automated data processing and calculates the sound monopole source level (MSL) at 1 m of the vessel's acoustic reference point in 1/3-octave frequency bands from 10 Hz to 128 kHz. The software also provides 1 Hz radiated noise levels (RNL) power spectral density for each pass in the frequency range from 10 Hz to 128 kHz.

The procedure used to process the underwater radiated noise data was compliant with the methodologies listed in ISO 17208-2 for obtaining averaged MSL and RNL levels in third-octave band spectrum form.

MSL and RNL are forms of source levels that can be used to directly compare one vessel with another.

3.5.2 N&V Postprocessing

DewesoftX software was used to obtain Fast Fourier Transforms (FFT) of the measured noise and vibration signals. FFT can be used to obtain narrow-band spectra with a resolution of 1.53 Hz and a maximum frequency of 50 kHz. The signals were also converted to third-octave bands spectra. The spectra are provided over the range of 10 Hz to 5 kHz, where most of the machinery noise power is concentrated.

In this report, only structural velocity levels L_v are reported extensively, as it is known that noise generated by onboard machinery is mainly transmitted via the structure-borne noise path, that is, through structural vibration that propagate to the wetted hull plating and are radiated as underwater noise. Therefore, structural vibrations are of interest for a better understanding of the composition of URN sources, their noise generation, and their transmission. The airborne sound pressure levels L_p are only used for the analysis shown in Section 3.5.3.3.

3.5.3 Data Analyses

3.5.3.1 Tonal Analysis

When a sound has a distinct component at given frequencies, it is said to exhibit tonal content. Tonal sound and noise occur when machinery produces excitations at a base or fundamental frequency and multiples of the base frequency, referred to as higher-order harmonics. Tonal noise can be transmitted to the structure as vibration, to the interior spaces as airborne sound and into the water through structure-borne vibrations and be discernible in the noise emissions from vessels. Tonal content is a dominant contributor to the overall noise generated by machinery.

Rotating machinery on the vessel, such as engines, propellers, and reduction and transmission gears, produces tonal noise. The first-order harmonic (or fundamental) corresponds to the rotation rate of machinery, and the higher-order harmonics are multiples of this fundamental frequency. The fundamental frequencies of interest are the main engine rate (MER), the generator set rate (GSR), motor rate (MOT), the propeller blade passing frequency (BPF), and the gear meshing frequencies of the azimuthing thrusters' upper gearbox (GMU) and lower gearbox (GML). The rates are defined in Equations (1), (2) and (3) below.

$$MER_n = n\,\frac{RPM_{ME}}{120}, \quad GSR_n = n\,\frac{RPM_{GS}}{120}, \quad MOT_n = n\,\frac{RPM_{MOT}}{60} \tag{1}$$

$$BPF_n = n\,p_{blade}\,\frac{RPM_{ME,MOT}}{60\,GR} \tag{2}$$

$$GML_n = n\,t_L\,\frac{RPM_{ME}}{60\,GR},\; GMU_n = n\,t_U\,\frac{RPM_{ME}}{60} \tag{3}$$

Where RPM is the rotation rate in revolutions per minute of the relevant machinery, n is the n^{th} harmonic, p_{blade} is the number of propeller blades, GR is the reduction gear ratio between the main engine shaft and the propeller shaft, t_L and t_U are the number of teeth in the lower gear crown and the pinion of the upper gear within the azimuthing thrusters, respectively. The characteristics of the engines, propeller and shaft gearing of each vessel are summarized in Table 6. Harmonics generated by other sources, such as compressors, pumps and fans, were not examined in this study, as they generally produce lower vibration levels than the machinery listed above.

Table 6: Vessel engines, propeller and shafting characteristics

Vessel	p_{blade}	GR	t_L	t_U
Battery Electric Tug	4	2.929	41	-
Diesel-Mechanical Tug	3	8.441	41	17

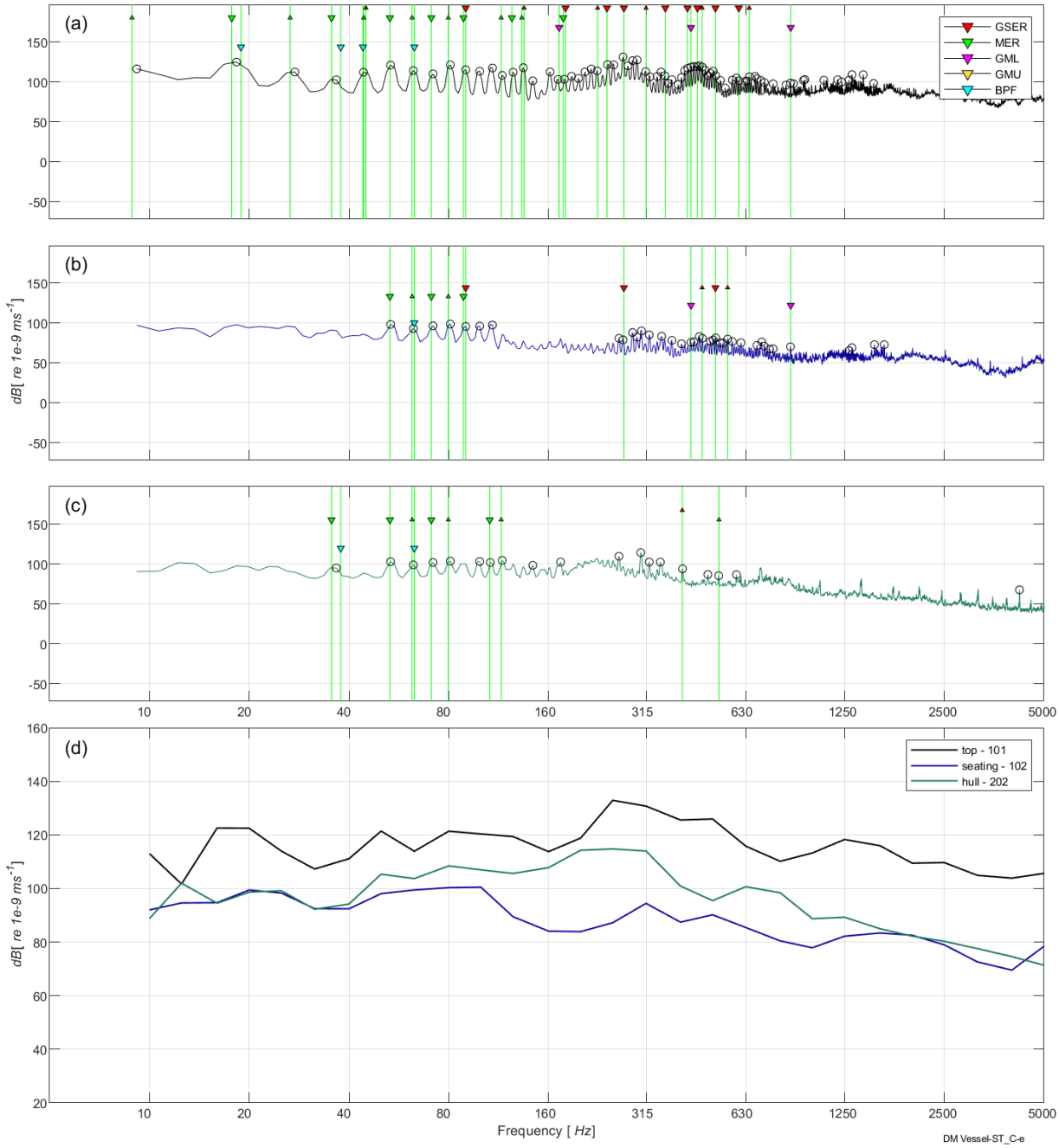


Figure 11: Tonal analysis of the straight run at 8 knots for accelerometers installed in the way of the main engine of the DM tug showing (a) vibration levels above the resilient mount, (b) vibration levels below the resilient mount on the main engine support structure, (c) vibration levels at the hull plating in the way of the engine room, and (d) the respective third-octave band spectra.

Narrow-band data has higher frequency resolution than the third-octave band spectrum. The increase in resolution allows the detailed characterization of noise signatures. A tonal composition analysis of the narrow-band spectra was performed by overlaying the harmonics onto the spectrum. In this way, the composition of the noise source can be associated with a specific operational state tested at sea trials.

The narrow-band spectra for both structural velocity levels L_v and *RNL* were analyzed. As an example, the narrow-band L_v spectrum and its respective third-octave band plot for one selected run for the DM tug are shown in Figure 11. The harmonics of relevant machinery are included in the upper portion of the sub-plot (marked ▼ for harmonics of integer orders and ← for harmonics of half-orders, where applicable). The open circles on the narrow-band spectrum curves correspond to spectral peaks. The spectral peaks are automatically detected when they stack higher than the neighbouring spectral lines by more than 6 dB. If any machinery harmonic lies within 1 Hz of an identified tone, a vertical line is drawn from the harmonic marker, denoting the likely source.

3.5.3.2 Structure-borne Noise Contributions from Machinery to Overall URN levels.

Structure-borne noise contributions to URN for a given piece of machinery can be computed using the collected data and quantities related to structure-borne noise source levels and transmission.

Mobility functions collected during dockside trials were used to calculate structure-borne noise transmission loss (TL). A transmission loss is a function that describes how velocity levels are attenuated by the structure between a source and a receiver point. Equation (4) can be used to calculate the transmission loss as the difference in structure-borne velocity level between two points A and B on a structure.

$$\begin{aligned} TL_{SBN,\ A\to B}(f) &= 20\log_{10}\left(\frac{|V_A(f)|}{|V_B(f)|}\right) \\ &= 20\log_{10}\left(\frac{|V_A(f)|}{|F_A(f)|}\right) + 20\log_{10}\left(\frac{|F_A(f)|}{|V_B(f)|}\right) \\ &= 20\log_{10}(|Y_{A\to A}(f)|) - 20\log_{10}(|Y_{A\to B}(f)|) \end{aligned} \tag{4}$$

where $|V_A(f)|$, and $|F_A(f)|$ are the magnitudes of velocity and force levels spectra, respectively at point A, $|V_B(f)|$, and $|F_B(f)|$ are the velocity and force levels spectra magnitudes, respectively at point B, $|Y_{A\to A}(f)|$ is the direct point mobility function magnitude of point A and $|Y_{A\to B}(f)|$ is the transfer mobility function magnitude of point A to B. The TL is expressed in dB. $TL_{SBN,\ A\to B}(f)$ will also be referred to $TL_{SBN}(f)$ in this report. The (f) symbol denotes that all quantities are a function of frequency. The mobility used here is the third-octave band mobility functions obtained as per the procedure in the Section 3.4.

Radiated noise levels and hull structural velocities collected during sea trials can be correlated using the structure's radiation efficiency. Radiation efficiency (σ) is a measure of how effectively a wetted plate converts structure-borne vibrations into radiated sound in an acoustic field, as shown in Equation (5).

$$\sigma(f) \sim \frac{W_{ac}(f)}{\langle v^2(f) \rangle} \tag{5}$$

The radiation efficiency is proportional to the ratio of the effective radiated power (W_{ac}) and the mean-square normal structural velocity $\langle v(f)^2 \rangle$. Therefore, vibration levels, represented by the mean velocity levels L_v, which is the dB counterpart of $\langle v(f)^2 \rangle$, can be correlated to the radiated noise levels RNL, which serves as a proxy for radiated URN power W_{ac}, as measured by hydrophones.

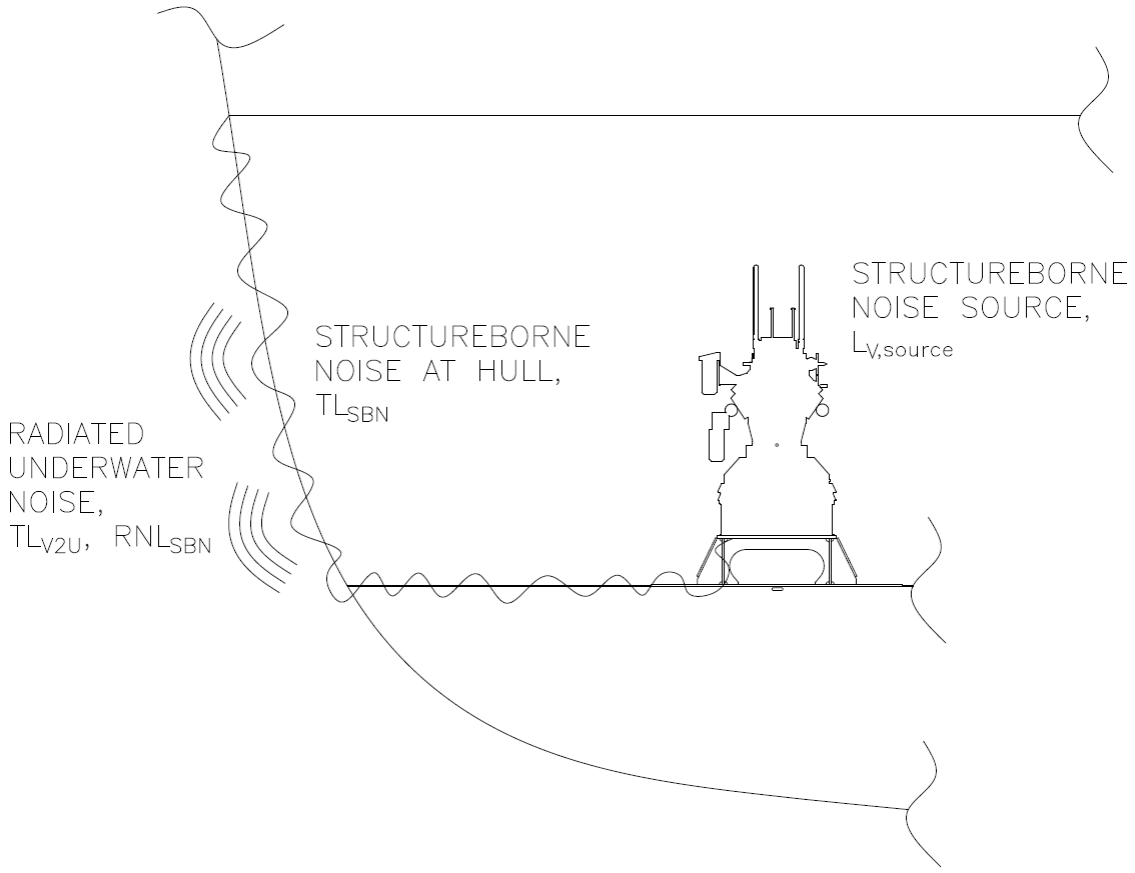


Figure 12: Schematic of the quantities involved in the transmission of structure-borne noise to URN.

Data from trials were used to obtain the transmission loss of structural velocity to underwater noise TL_{V2U} defined in Equation (6).

$$TL_{V2U}(f) = RNL(f) - L_v(f) \tag{6}$$

This was calculated using the available narrow-band spectra of structural velocities to obtain $L_v(f)$ and $RNL(f)$ at frequencies that correlated with specific machinery, as identified using the methodology in the Section 3.5.3.1. The collected narrow-band $TL_{V2U}(f)$ datapoints from the measurements, which map a function of frequency, were then band-averaged over third-octave bands and reported in dB units.

The concept of transmission from a structure-borne noise source to URN is illustrated in Figure 12. The calculation of $RNL_{SBN}(f)$ levels due to structure-borne noise from a given machinery can be obtained by using Equation (7).

$$RNL_{SBN}(f) = L_{V,source}(f) - TL_{SBN}(f) - TL_{V2U}(f) \tag{7}$$

The equation uses the velocity levels at the source ($L_{V,source}$), and the transmission losses from source to hull (TL_{SBN}) and from velocity levels at hull to RNL (TL_{V2U}). $RNL_{SBN}(f)$ is a function of frequency and is calculated in third-octave bands.

Once RNL_{SBN} is calculated, it can be directly compared with the *RNL* levels measured during sea trials, thereby helping quantify the contribution of machinery noise to URN. Although this analysis is presented only for *RNL* levels, it can give insight into the relative composition of structure-borne noise contribution to the overall radiated levels.

Results for this analysis are reported in Appendix E, and they complement the discussions of Section 4.

3.5.3.3 Airborne Noise Contributions to Overall URN levels

Airborne noise contribution to the overall MSL levels can be computed using the formula in Equation (8).

$$MSL_{ABN}(f) = L_p(f) - TL_{ABN}(f) + 10\log_{10}(S) + const \tag{8}$$

Where $TL_{ABN}(f)$ is the transmission loss of air-to-water noise for a typical tug hull structure, available to RAL through previous work, $L_p(f)$ is the airborne sound pressure level inside the vessel's machinery room, S is the surface area of the wetted boundary plate between the water and the interior acoustic space, and $const$ is a constant that takes into account the conversion from L_p to MSL.

Results for this analysis are reported in Appendix E, and they complement the discussions of Section 4.

4 Results

This section contains results from the URN, noise and vibration and data analysis. The section is organized in the following way:

- Section 4.1 shows the naming conventions adopted for the test runs results presented in this Section
- Section 0 presents and discusses the results of the measured underwater noise in terms of source levels. The discussion is restricted to third-octave band spectra. For more information on the narrow-band analysis, please refer to Appendix C
- Section 4.3 discussed lessons learned from the process to get a URN class notation
- Section 4.4 presents and discusses results on noise and vibration data collected during sea trials simultaneously with URN. Also in this case, the discussion is focusing on third-octave band data, with more information available on the narrow-band data in Appendix D

The analysis of the noise generation and transmission from the main propulsive machinery items to URN contained in Appendix E complements the analysis provided in this section.

4.1 Test Runs Naming Convention

In this section, the results are referred to as run types. The test runs presented here were averaged across operationally similar test runs presented in the test matrix in Section 3.3.4. A summary of run types with reference to the tests shown in the test matrix is provided in Appendix A for clarity, along with the vessel's state during trials, including propeller, main engine (or motor), and genset speeds.

Table 9 on the following pages summarize the run types.

Table 7: Straight Travel (ST) run types naming conventions

BE Tug		
Run ID	Speed Over Ground (knots)	Power Source
BE ST-BATT-I	6	Battery
BE ST-BATT-II	7	Battery
BE ST-BATT-III	8	Battery
BE ST-BATT-IV	9	Battery
BE ST-BATT-V	10	Battery
BE ST-GENS-I	6	2x Gensets
BE ST-GENS-II	7	2x Gensets
BE ST-GENS-III	8	2x Gensets
BE ST-GENS-IV	9	2x Gensets
BE ST-GENS-V	10	2x Gensets
DM Tug		
Run ID	Speed Over Ground (knots)	
DM ST-I	6	
DM ST-II	7	
DM ST-III	8	
DM ST-V	9	
DM ST-V	10	

Table 8: Baseline Stationary (BS) run types naming conventions

BE Tug		
Run ID	Speed Over Ground (knots)	Description
BE BS-I	0	Motor Off, Gensets Off
BE BS-II	0	Motor On, Gensets Off
BE BS-III	0	Motor Off, 2x Gensets On
BE BS-IV	0	Motor On, 2x Gensets On
DM Tug		
Run ID	Speed Over Ground (knots)	Description
DM BS-I	Not run at sea trials, only N&V	Genset On, Engine off
DM BS-II	0	Genset On, Engine Idle, Z-drives almost clutch-off
DM BS-III	0	Genset On, Engine Idle, Z-drives clutched-in

Table 9: Bollard Pull (BP) run types naming conventions

BE Tug		
Run ID	Bollard Pull (% of max)	Power Source
BE BP-I	20	Battery
BE BP-II	50	Battery
BE BP-III	75	Battery
BE BP-IV	100	Battery
BE BP-V	20	2x Gensets
BE BP-VI	50	2x Gensets

DM Tug	
Run ID	Bollard Pull (% of max)
BE BP-I	20
BE BP-II	50
BE BP-III	75
BE BP-IV	100

4.2 URN Data Results

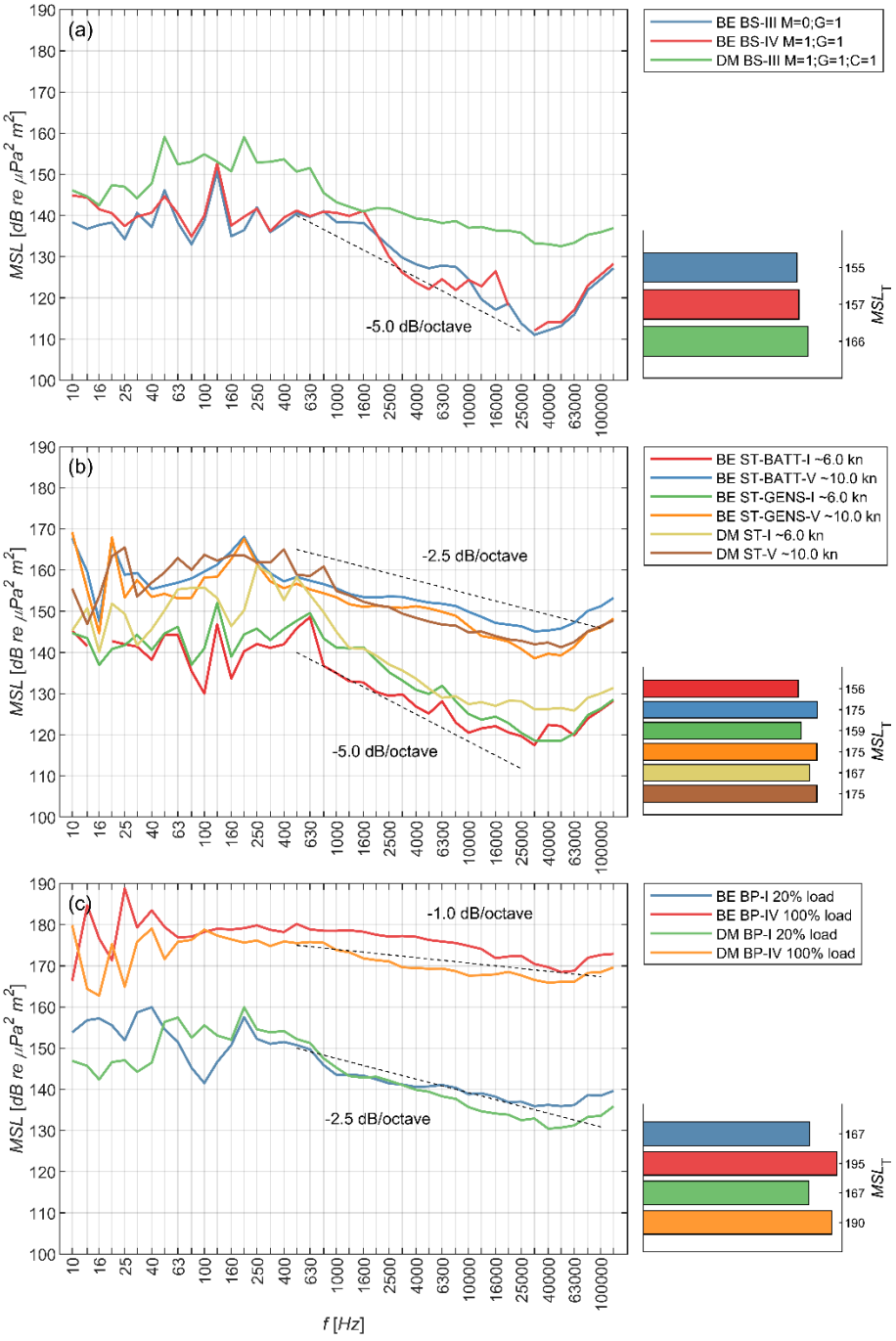


Figure 13: Picture showing selected *MSL* source levels spectra for different run types for both BE and DM tugs, where (a) are baseline (BS) runs, (b) are straight travel runs (ST), and (c) are bollard pull runs (BP)

The URN of the BE and DM tugs across the different operational states in the test matrix are compared and discussed in this section. Selected third-octave band MSL, derived from Section 3.5.1, for the baseline stationary, straight runs and bollard pull operational states are shown in Figure 13. This figure is intended to provide a quick comparison between MSL levels across the tested conditions and for both tugs. A more in-depth analysis for the runs and comparison between vessels are provided in the sections below for baseline (BS), straight travel (ST) and bollard pull (BP) runs, respectively.

The bar chart at the bottom left of each sub-plot shows the total broadband MSL_T level for each operational state, providing a quantitative comparison across the test matrix. Data points with poor signal-to-noise ratios relative to background noise were invalidated and omitted during JASCO's measurement data quality check [6].

The discussion on the URN results is supplemented by the analysis performed in Appendix C, which shows in detail the correlation between tonal features and the main noise sources in the narrow-band spectra.

4.2.1 Baseline Stationary

Table 10: Broadband MSL levels in dB re 1μPa for baseline (BS) at key frequency ranges.

BE Tug				
	BE BS-I	BE BS-II	BE BS-III	BE BS-IV
10 Hz - 100 Hz	148	169	150	152
100 Hz - 1000 Hz	141	142	153	154
1000 Hz - 10000 Hz	136	143	145	146
> 10000 Hz	130	132	131	133

DM Tug		
	DM BS-II	DM BS-III
10 Hz - 100 Hz	159	162
100 Hz - 1000 Hz	154	164
1000 Hz - 10000 Hz	138	151
> 10000 Hz	129	146

Figure 14(a) and (b) show the baseline stationary URN measurements results for both BE tug and DM tug, respectively. Table 10 shows broadband MSL levels at key frequencies for baseline runs. The BE tug is quietest, during BE BS-I, when both generator set and motor are off, with total noise levels below 150 dB. During BE BS-II, with the motor on at minimum rpm (~40 rpm), tonal components in the noise spectra increase significantly at low-frequency bands (up to 40 Hz, associated with blade passage frequencies and gear mesh from the thrusters) and mid frequency bands (1 kHz < f < 1600 Hz, associated with motor noise). During BE BS-III, with both the generator sets operating, but with the motor off, distinct spectral peaks appear at 125 Hz, associated with the generators' diesel engines. Additionally, an increase in levels at mid-to-high frequency

bands is observed, up to 20000 Hz that is also associated with the gensets.

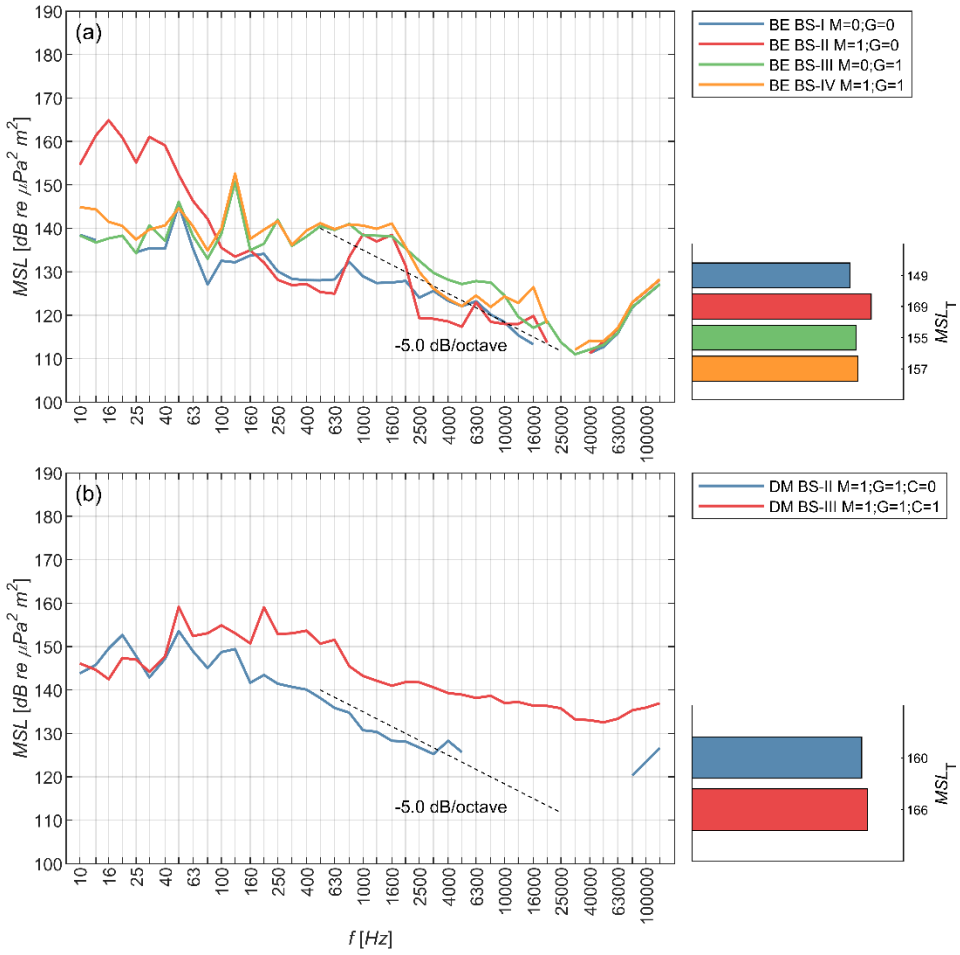


Figure 14: *MSL* spectra in third-octave bands for Baseline Stationary operational states for (a) BE and (b) DM tugs. The 0/1 in the legends represents the on/off of the main engine/motor (M), generators (G) and thruster clutch (C).

Interestingly, when both the motor and generator sets are on, and the propeller is rotating at minimum rpm (BE BS-IV), the low-frequency broadband levels are lower than those in the BE BS-II battery mode condition. The spectral features in the mid- to high-frequency bands match between BE BS-IV and BE BS-II, except for the specific spectral peaks due to the gensets. This suggests that the significant increase in low-frequency noise observed in BE BS-II is likely due to some noise source in the environment that was present temporarily. The increase in mid-frequency (~1250 Hz) broadband components observed in both BE BS-IV and BE BS-II, whenever the propeller is turning, is likely due to machinery noise from the motor coming online.

During baseline measurements, the DE tug's main engines (running at idle speed, 650 rpm) and auxiliary generator sets (running at 1800 rpm) were always operating to ensure maneuvering safety

and electrical power supply. However, going from a lightly clutched-in propeller (DM BS-II, where the propeller was rotating at 26 rpm) to a fully clutched-in propeller (DM BS-III, where the propeller was rotating at 78 rpm) led to an increase of 6 dB in MSL_T (Figure 14(b)), characterized by several distinct spectral peaks at low- and mid-frequencies that are associated with blade passing frequencies and lower gear meshing, accompanied by an increase in broadband components in mid- and high-frequency bands that may be attributed to propeller noise.

4.2.2 Straight Run

Table 11: Broadband MSL levels in dB re $1\mu Pa$ for straight travel runs (ST) at key frequency ranges.

	BE Tug									
	BE ST-BATT-I	BE ST-BATT-II	BE ST-BATT-III	BE ST-BATT-IV	BE ST-BATT-V	BE ST-GENS-I	BE ST-GENS-II	BE ST-GENS-III	BE ST-GENS-IV	BE ST-GENS-V
10 Hz - 100 Hz	152	158	166	175	172	153	160	158	172	172
100 Hz - 1000 Hz	153	155	161	167	172	157	157	160	163	171
1000 Hz - 10000 Hz	141	144	154	158	163	147	148	152	156	161
> 10000 Hz	134	136	146	150	159	134	136	140	145	154

	DM Tug				
	DM ST-I	DM ST-II	DM ST-III	DM ST-IV	DM ST-V
10 Hz - 100 Hz	161	162	165	166	170
100 Hz - 1000 Hz	166	168	168	170	172
1000 Hz - 10000 Hz	149	151	156	158	161
> 10000 Hz	139	142	145	150	155

Table 11 shows broadband MSL levels at key frequencies for straight travel runs. The BE tug is quietest when travelling at 6 knots in battery mode (BE ST-BATT-I), achieving MSL_T of 156 dB, as shown in Figure 15 (a). At speeds below 8 knots, the main sources of noise are gear-mesh noise from the propulsor and blade-passage frequency noise from the propeller, and genset noise when operating under genset power. As travel speed reaches 8 knots (BE ST-BATT-II/ BE ST-GENS-II), the total noise level increases, with discernible changes in the spectral signature, comprising a progressively defined spectral peak at 200 Hz and a broadband hump centred around 6300 Hz. These changes in noise signature are true for both battery and generator mode, where the signature becomes more pronounced with increasing speeds. These divergence in peak and broadband features on the spectra likely indicates the inception of cavitation as suggested by literature [7][8]. The spectral peak at 200 Hz may be attributed to the combination of tip vortex cavitation, sheet cavities and/or propeller singing, which intensifies with increasing propeller rpm [9][10]. The broadband hump in the mid- to high-frequency bands can be associated with broadband cavitation noise and bubble noise, reflected in the change in the logarithmic decay trend from -5 dB/octave (when cavitation is non-present) to -2.5 dB/octave (following cavitation inception) [11].

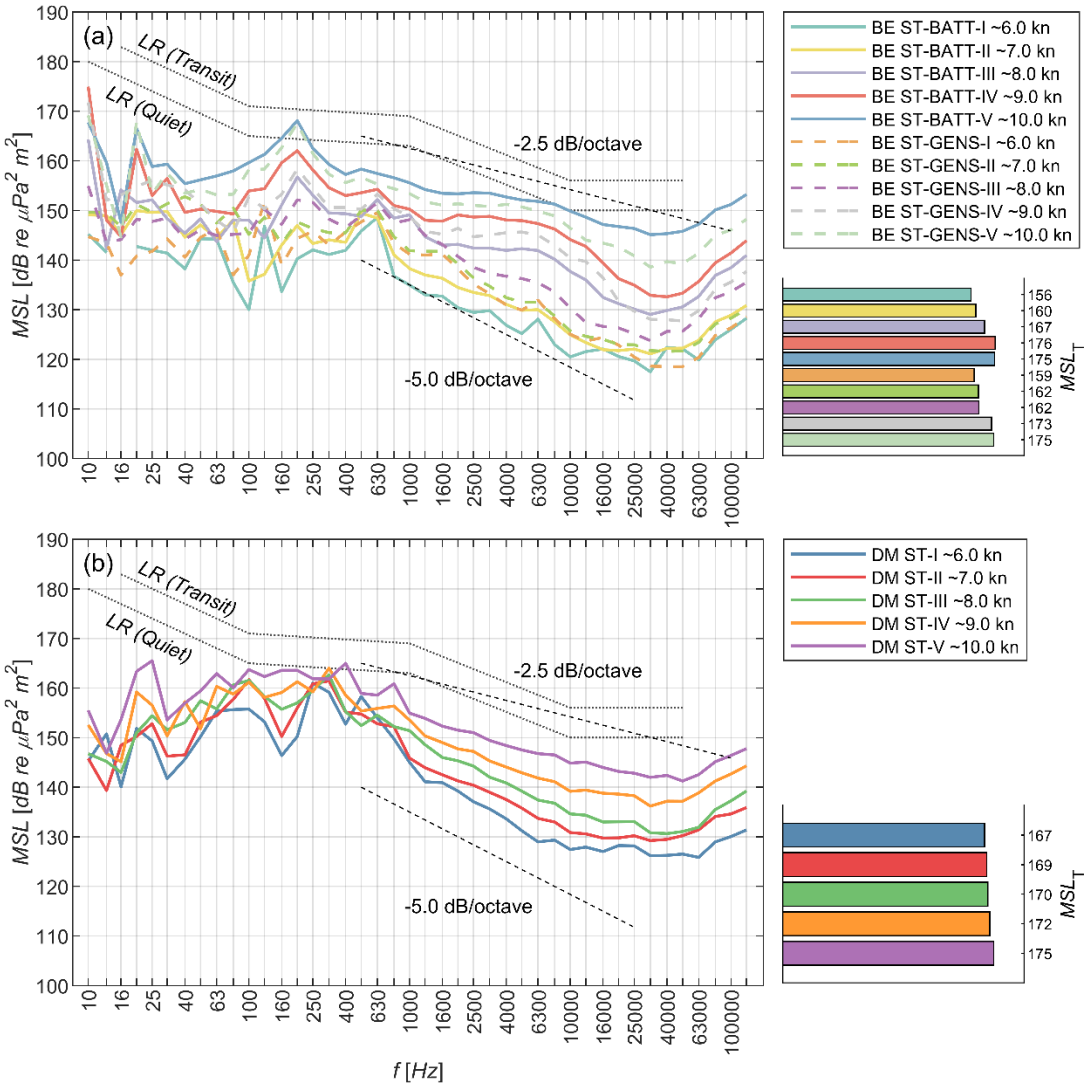


Figure 15: *MSL* spectra in third-octave bands for Straight Run operational states for (a) BE and (b) DM tugs. The speed in the legends represents the speed over ground. The figure offers also comparisons of source levels with the LR UWN-T criterion "LR (Transit)" and LR UWN-Q criterion "LR (Quiet)"

Higher noise levels across the spectra are observed for battery mode travelling at speeds of 8 knots and beyond, when compared to the generator mode. This behaviour is likely due to slightly harsher weather conditions during the battery mode trials, resulting in generally higher motor speeds by approximately 20 rpm (see Appendix A for details on sea trials motor speed conditions). If the rotational speeds had been similar during the two test days, the measured levels would be expected to be more closely aligned.

The DM tug shows noise level increasing uniformly as travel speed increases (Figure 15 (b)). At

low speeds below 8 knots, noise levels in the low- to mid-frequency bands are primarily contributed by a mixture of machinery and propeller noise. As speed increases above 8 knots, broadband content and more pronounced blade passage frequency tonals suggest that the propeller and likely onset of cavitation become the dominant source of URN. At high-frequency bands, the broadband noise exhibits a similar change in the logarithmic decay trend from -5 dB/octave to -2.5 dB/octave with increasing speeds, while no broadband hump was observed, in contrast to that seen for the BE tug (Figure 15 (a)). This observation highlights the influence of propeller selection and design, such as the number and size of propeller blades (Table 6), on cavitation noise. In this case, the 4-bladed 2.7 m propeller on the BE tug seems to be more prone to cavitation during transit, when compared to the three-bladed 2.8 m propeller from the DM tug.

Overall, the BE tug operating in both battery and generator mode, is consistently quieter than the DM tug at each transit speed, except at notable frequencies, such as 200 Hz, where the BE tugs generate more URN than the DM tug. These differences are due to the differences in propeller design that lead to different URN signature and cavitation inception characteristics as a function of propeller loading.

Both tugs satisfy the Lloyd's Register's UWN notation requirements, meeting UWN-Q (quiet) up to 9 knots and UWN-T (transit) up to 10 knots [5]. The UWN-T criterion was met by both tugs with a sizable margin at 10 knots (>2 dB). The UWN-Q criterion was met by both tug at 9 knots within a 2 dB margin for the BE tug, and within a 1 dB margin for the DM tug, due to the presence of tonal noise from machinery. Notably, the BE tug source levels would have met the UWN-Q criteria at 10 knots if it were not for the presence of the 200Hz peak, which exceeds the quiet criteria by 4 dB. Likewise, the DM tug source levels would have met the UWN-Q criteria at 10 knots if it were not for a 400Hz peak that exceeds the criteria by 2 dB.

4.2.3 Bollard Pull

Table 12: Broadband MSL levels in dB re $1\mu Pa$ for bollard pull (BP) at key frequency ranges.

BE Tug						
	BE BP-I	BE BP-II	BE BP-III	BE BP-IV	BE BP-V	BE BP-VI
10 Hz - 100 Hz	166	180	186	192	160	180
100 Hz - 1000 Hz	162	180	184	189	160	179
1000 Hz - 10000 Hz	152	172	182	187	152	172
> 10000 Hz	148	170	180	182	145	171

DM Tug				
	DM BP-I	DM BP-II	DM BP-III	DM BP-IV
10 Hz - 100 Hz	162	169	183	185
100 Hz - 1000 Hz	165	174	184	186
1000 Hz - 10000 Hz	152	161	177	181
> 10000 Hz	144	154	171	178

Table 12 shows broadband MSL levels at key frequencies for bollard pull runs. In Figure 16(a), the BE tug exhibits low noise level at low frequency bands ($\leq$ 160 Hz) during 20% load (BE BP-I & BE BP-V), where motor and generator noise are the main contributors. The URN radiated during battery mode again exhibits higher noise levels than the one radiated on generator mode at this load, likely attributed to environmental noise, similarly to what was seen in baseline stationary operations (Section 4.2.1).

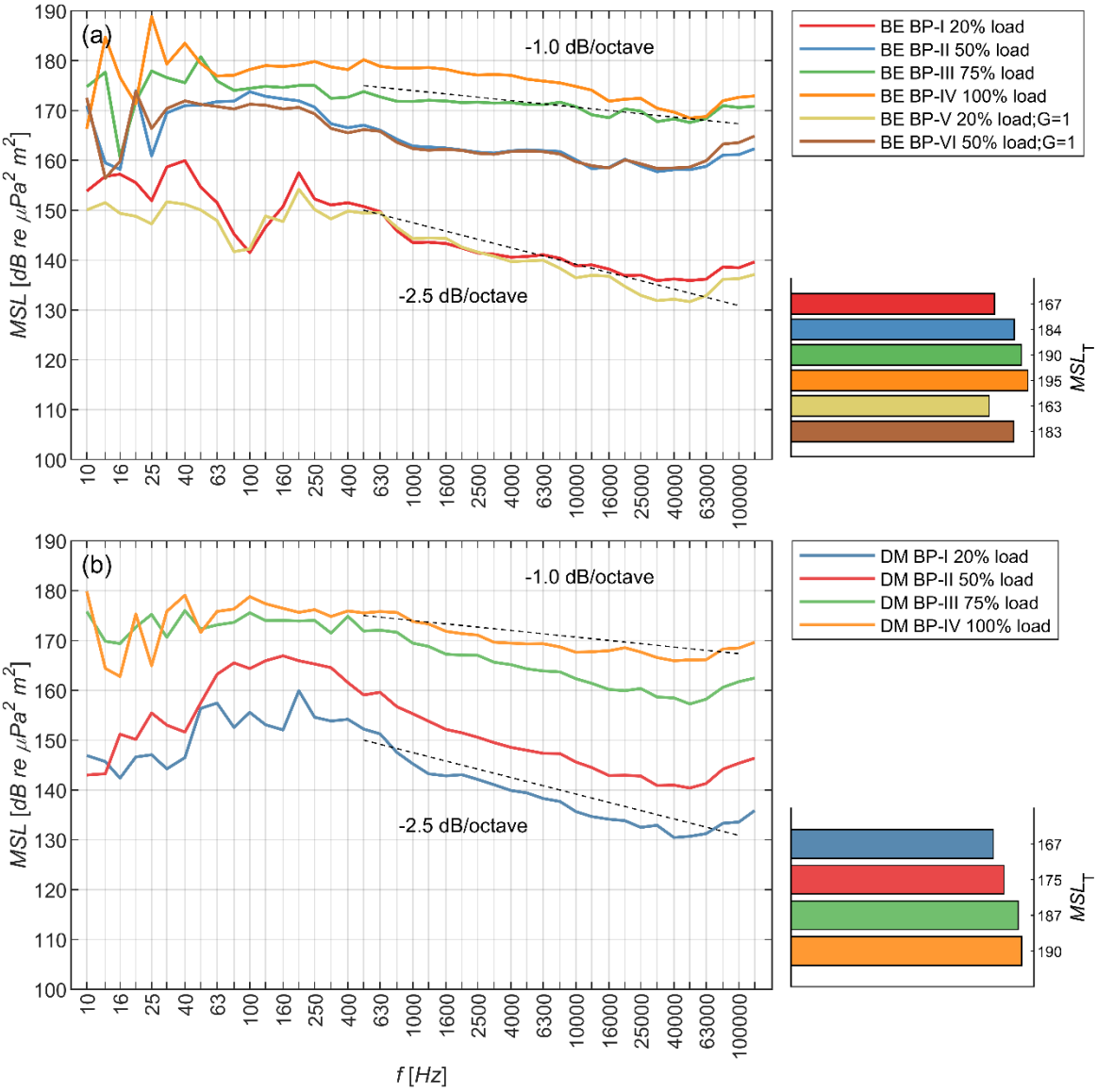


Figure 16: *MSL* spectra in third-octave bands for Bollard pull operational states for (a) BE and (b) DM tugs. The percentage in the legends represents the bollard pull loading.

On the other hand, the DM tug shows higher noise levels at low frequency bands (≤ 160 Hz) during 20% load, with contributions from main engines, generator set and additionally propeller blade passage frequency noise (Figure 16(b)). This suggests that differences in propeller construction, such as the number of propeller blades and slightly larger diameter of the DM tug propellers (Table 6), influence noise differently under bollard pull operating conditions. In this case, the 3-bladed propeller on the DM tug seems to be noisier at low load bollard pull due to the presence of both strong tonal content from the propeller, gear meshing from the propulsors and main engines.

As loading increases from 20% to 50%, a distinct transition in the noise spectra is observed for both BE and DM tugs, where a broadband hump component centered around 100~160 Hz is formed, likely the inception of cavitation [7][8]. In the low frequency bands, propeller noise from blade passage frequency starts to dominate over the motor/engine components.

Finally, at peak loading conditions of approximately 75% to 100%, the total noise level, MSL_T produced by both BE and DM tugs increases with engine/motor power. The noise spectra show the onset of fully developed cavitation across the frequency bands. Noise levels in the low-frequency bands are mainly dominated by blade passing related cavitation, and mid- to high-frequency bands dominated by broadband cavitation and bubble noise. The logarithmic decay trend for both tugs' changes from -2.5 dB/octave at 20% load to approximately -1 dB/octave at 100% load. The BE tug produces the highest MSL_T at 195 dB at 100% load (BE and DM BP-IV).

4.3 URN Class Notation Process

Part of the measurements collected in this work supported obtaining a notation from a classification society that certifies the battery-electric tug's URN emissions performance. The process for obtaining and the lessons learned from this experience are summarized below. In this case, the specific example is obtaining the LR-UWN notation from Lloyd's Register. Other classes follow a similar process.

Class notations generally involve collecting URN data from sea trials according to a standard and comparing URN levels to a criteria curve. Each set of criteria curves is generally associated with a specific notation. These notations are in addition to the one class normally grants to a vessel to certify adherence to its design and operational standards.

The standards used for URN data collection roughly adhere with ISO 17032 [4] or ANSI/ASA S12.64-2009 [12]. These standards require precision, which requires a high level of sophistication in the measurement setup and equipment.

The process begins by contacting the marine classification society. Class societies will usually provide a guideline that outlines the process for pursuing the URN notation, step by step.

Firstly, the class requires that the measurements either be collected by them or by a certified service supplier. In this case, JASCO had to go through LR's approval process to become a service supplier. It is important to identify a service supplier early in the process, but this might be challenging in some areas where access to a qualified underwater noise measurement provider is not readily available.

The owner, service supplier, and class then agree on the type of notation to pursue. Usually, different class societies offer several notations that correspond to specific criteria designed around

operational needs and scenarios. For instance, LR offers transit-type notation, which certifies that noise is below a certain criteria curve for a given transit speed agreed upon by the class and owner. Usually, a second-tier criterion is offered for quiet operations, which certifies the transit speed at which the vessel can meet a more stringent criterion for URN emissions. In this case, the owner decided to apply for both regular (UWN-L(T)) and quiet (UWN-L(Q)) transit speeds.

A measurement plan or protocol must be provided, including information on the vessel particulars, the sea trials location, the measurement systems, the sea trials operation, and the post-processing procedures. The measurement plan in this case was prepared by RAL and JASCO with the owner's input and was reviewed and approved by LR. This measurement plan was similar to the one provided for this work to TC-IC [3], and presented in the section 3 of this report, with a deeper focus on the post-processing procedures to obtain the source levels. Once the plan is approved, the sea trials can commence.

Once the measurements are concluded, a measurement report must be provided to the class illustrating procedures and results. The report, in particular, provides details on the measured source levels at different speeds for straight run tests and a comparison with relevant URN notation criteria, similar to what is shown on Figure 15 in Section 4.2.2 of this report. It also proposes which class notations are to be awarded to the vessel. At the time of writing this report, the measurement report has been submitted pending class approval. Once the class reviews and approves the report, the notation is assigned to the vessel.

There are generally a few challenges associated with these types of sea trials, which include the following:

- The choice of sea trials locations suitable for acoustic ranging, which might entail meeting depth or vessel traffic requirements for low environmental noise
- URN measurement equipment deployment must be planned well ahead of trials. Depending on the equipment type, permits may be required from the relevant authorities to deploy it
- The logistics and time constraints associated with the sea trials (which usually involve a full day out), especially with already operational vessels. Sea trials maneuvers usually require repeated turns and the vessel passing over the acoustic range several times. Fortunately, since most harbour tugs are highly maneuverable, they can execute maneuvers quickly
- Weather, sea state and vessel traffic dependencies. Sea trials might be postponed due to unacceptable weather. It is important to choose a weather window or time of the year that maximizes the chance of successful trials. During trials, vessel traffic in the area needs to be monitored to allow for clean runs without exterior noise contamination
- Cost might be prohibitive for operators. Unless access to existing stations or outside financial support is provided, the cost of the ULS deployment is currently prohibitive for most tug owners.

4.4 Vibration Data Results

This section presents the results and discussion of the vibration data collected during sea trials. The main purpose of the data collection was to evaluate the structural vibration responses to establish the mechanisms of transmission of onboard noise sources that manifest in underwater noise.

The discussion is centred on third-octave spectra presented in locations in the way of the main propulsive machinery items (main engines, Z- and L-drive propulsors, and gensets), on the hull, at the support structure, and above resilient mounts (where applicable). The location of the accelerometers during sea trials is available in Appendix B.

In this section, a broad discussion of the spectral composition is presented based on tonal content of the spectra, and a more in-depth analysis is provided in Appendix D.

4.4.1 Main Engines Vibration Levels



Figure 17: Structural vibration levels L_v for DM tug by location and sea trials run as measured in way of the main engine support structure. "top"," seating" and "hull" refer to location above the engine mount, the engine foundation and the hull plating, respectively. The bar plots represent the overall broadband levels

Figure 17 shows the Structural vibration levels L_v spectra for DM tug by location and run type. This result is shown only for the DM tug, as the battery-electric counterpart does not have a diesel main engine. The results show the following:

- Velocity levels at the engine above the mount ("engine top" on Figure 17) can be treated as the input vibrational source levels, i.e. the amount of vibration that is input on the structure by the engine. These spectra show large contributions from main engine tones throughout the frequency range. The main engine source content is mainly concentrated in the 10 Hz~630 Hz range. Vibration levels at the source increase with the engine speed (as shown in progressions from DM BP-I to DM BP-IV, and DM ST-I to DM ST-V)

- Structural velocity levels at the engine foundation seating structure ("engine seating" on Figure 17), i.e. the structure where the engine sits on resilient mounts, is effectively reduced by the presence of rubber mounts, particularly in the 160 Hz~630 Hz range where most of the main engine source vibrational energy is concentrated. The main engine's tonal content remains dominant in the velocity levels at this location

- Structural velocity levels on the hull ("engine hull" on Figure 17, whose measurement locations were close to the propulsors) show higher levels than at the engine foundation, due to the combination of vibration from different sources, such as gear meshing, and propeller blade pass frequencies. Tonal analysis revealed that the structural velocity levels associated with engine tones are of similar magnitude to those measured on the engine foundation, suggesting little reduction in vibration levels between the structure in the way of the engine and the hull. As such, the engine foundation and resilient mounting are responsible for most of the structural vibration reduction from the main engine. Tonal content from the main engine is particularly dominant in the frequency range <100 Hz. As vibration at the hull is responsible for structure-borne noise radiation underwater, URN from engine-generated structure-borne noise is predominant below 100 Hz

4.4.2 Gensets Vibration Levels



Figure 18: Structural vibration levels L_v for BE tug by location and sea trials run as measured in way of the genset support structure. "top"," seating" and "hull" refer to location above the genset mount, the genset foundation and the hull plating, respectively. The bar plots represent the overall broadband levels.

Figure 18 shows the structure velocity levels L_v spectra as measured during sea trials, by run type and by measurement location, for the BE tug. The results show the following:

- It is possible to see the effect on structural velocity levels in test runs performed on battery power only and on genset power. For reference, see Figure 15: 1) BE BP-V and BE BP-VI, gensets running and their counterparts on battery mode, BE BP-I and BE BP-II; 2) BE BS-III and BE BS-IV, with gensets running and their counterparts on battery mode, BE BS-I and BE BS-II, and 3) BE ST-GENS with gensets running versus BE ST-BATT runs on battery mode. This leads to an increase between 5 and 10 dB in velocity levels seen at locations on the genset foundation and hull plating below the genset ("genset seating" and "genset hull" on Figure 18, respectively). The above mount measurements ("genset top" on Figure 18) shows a drop in velocity levels in battery mode, as the gensets are shut off

- Opposed to the main engine-generated source levels, the genset source velocity levels ("genset top" on Figure 18) do not vary from run to run when on genset power. As expected, source levels of internal combustion engines do not vary extensively with load but rather depend on the prime mover speed. The tonal analysis shows that tonal content does not vary between runs, as it is associated with the constant genset speed throughout the runs in genset mode. The presence of rubber mounts effectively decreases structural velocity levels throughout the frequency range on the structural foundation of the gensets ("genset seating" on Figure 18), especially in the frequency range 40 Hz and up, effectively reducing the vibrational power input from the genset in the structure by ~20 dB. At genset seating, the tonal analysis shows that tones associated with the gensets are predominant. At low frequencies (<50 Hz), it is possible to identify tonal content associated with the propeller blade passage frequency on the seatings

- Structural velocity levels on the hull plating below the genset structure ("genset hull" on Figure 18) do not significantly decrease relative to the levels measured on the genset support structure, and, in fact, they are increased (~5 dB). The increase is due to the presence of other sources, namely, propeller blade passage frequency pressure pulses, as observed in the tonal analysis. Genset tonal content is still predominant, especially above 100 Hz



Figure 19: Structural vibration levels L_v for DM tug by location and sea trials run as measured in way of the genset support structure. "top"," seating" and "hull" refer to location above the genset mount, the genset foundation and the hull plating, respectively. The bar plots represent the overall broadband levels

Figure 19 shows the structural vibration levels L_v spectra for the DM tug in the way of the auxiliary genset support structure. Similar to what is seen on the L_v for the BE tug, the following is observed:

- Genset structural velocity source levels ("genset top" on Figure 19) does not vary between run, and similarly to the BE tug gensets, the source levels are independent of loading, but only a function of engine speed. As the gensets' prime movers always rotate at 1800 rpm, source levels are constant between runs

- The structural velocities measured below the auxiliary genset on the DM tug ("genset seating" on Figure 19) is effectively reduced by ~20 dB. The signature is heavily dominated by genset tonal signatures and does not vary significantly from run to run

- The hull plating structural velocities signature ("genset hull" on Figure 19) does not show significant genset tonal content, suggesting that genset structure-borne noise transmitted to the hull is masked by other, more dominant sources, such as the main engines, Z-drive gear meshing and propeller blade passage frequency. The only case in which genset-generated structural velocity levels are dominant is DM BS-I, where the main engines are shut down. This leads to a decrease in L_v of ~20 dB between a loiter with main engines on and a loiter with main engines shut down (see DM BS-I compared to DM BS-II). The DM BS-I condition was not run during sea trials, but it is expected that the URN radiated in this condition will be ~20 dB lower than the DM BS-II condition. As most loiters will be run at a condition similar to DM BS-III, genset noise on DM tugs is not a dominant source during loiters. Also, as genset noise is masked by other onboard sources at hull locations, in general, it is not a dominant source of URN noise on DM tugs

4.4.3 Z- and L-Drives Vibration Levels

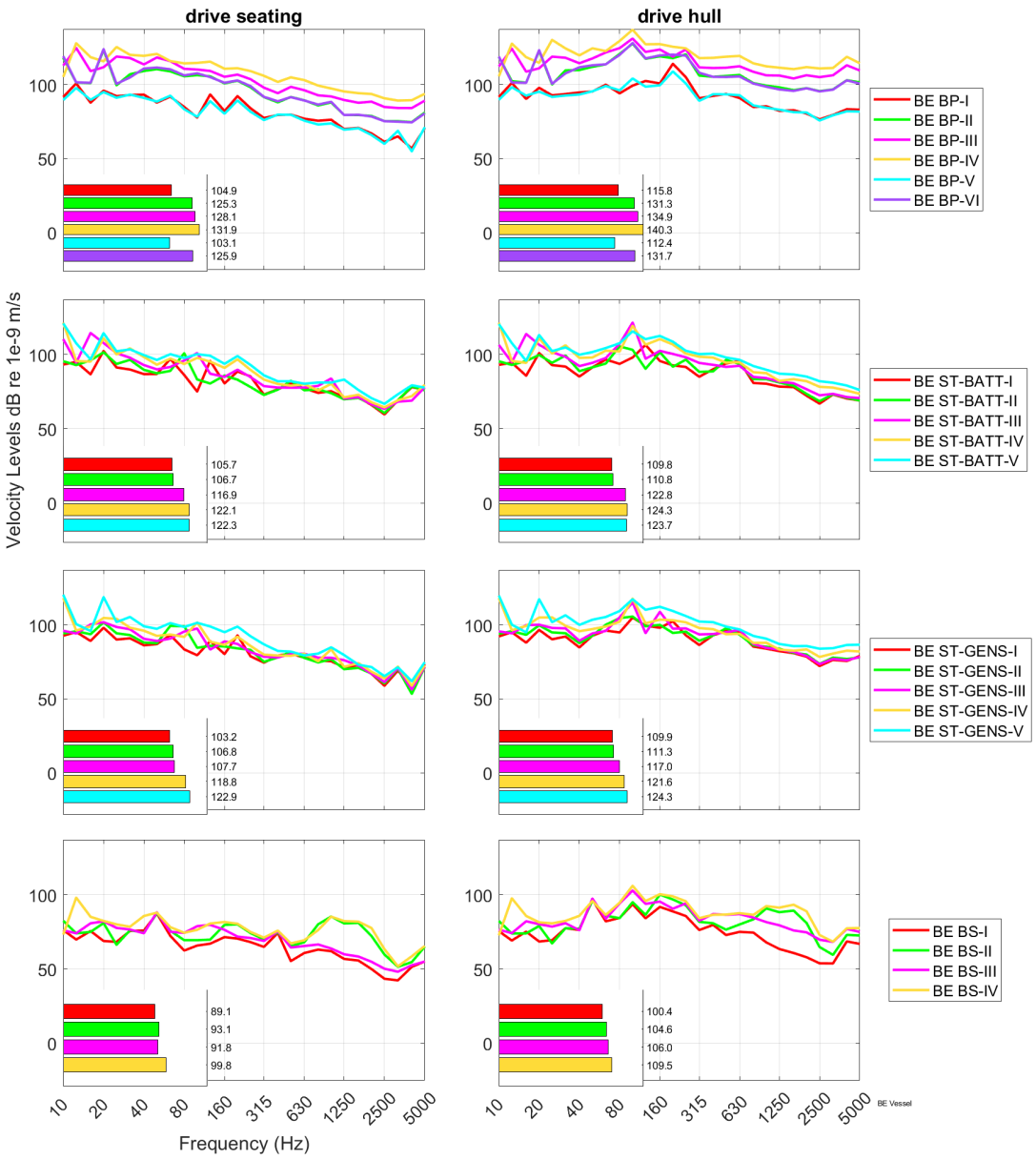


Figure 20: Structural vibration levels L_v for DM tug by location and sea trials run as measured in way of the Z-drive propulsor. "seating" and "hull" refer to locations at the drive foundation and the hull plating, respectively. The bar plots represent the overall broadband levels

Figure 20 shows the structural vibration levels L_v spectra for the BE tug by location and run type as measured in the way of the L-drive propulsor support structure. The results show the following:

- There are virtually no differences in L_v signatures between the runs on genset power and the runs on battery power for locations in the way of the propulsor support structure. For reference see in Figure 20: 1) BE BP-V and BE BP-VI, gensets running and their counterparts on battery mode, BE BP-I and BE BP-II; 2) BE BS-III and BE BS-IV, with gensets running and their counterparts on battery mode, BE BS-I and BE BS-II, and 3) BE ST-GENS with gensets running versus BE ST-BATT runs on battery mode. Genset tonal signature is present at hull location ("drive hull" on Figure 20) but is not contributing majorly to the overall velocity levels

- Structural velocity levels at the supporting structure of the drive, where the propulsor is hard-mounted to the structure, show the presence of a strong tonal signature from gear meshing from the L-drive lower reduction gear and blade passage frequency pressure pulses, in frequencies <150 Hz. There is little reduction of structural velocity levels between the foundation ("drive foundation" on Figure 20) and hull plating below ("drive hull" on Figure 20)

- For baseline measurements (BS), the signatures of the runs with motor on (BE BS-II and BE BS-IV), when compared with the motor off (BE BS-I and BE BS-III), show an increase in the ~630 to 1250Hz, similar to what is seen in the URN signature shown in Section 0. This spectral feature is likely due to the motor coming online. Similarly, the L_v spectra show a feature centred around 630Hz on low-speed ST-runs (BE ST-I to BE ST-III), which also appears on the respective URN signature, as seen on Section 4.2.2, with a suspected source from the motor and variable-frequency drive system. These mid-frequency features are not noticeable during the BP runs at low power (BE BP-I), as they are masked by broadband vibration generated by the propeller



Figure 21: Structural vibration levels L_v for DM tug by location and sea trials run as measured in way of the Z-drive propulsor. "seating" and "hull" refer to locations at the drive foundation and the hull plating, respectively. The bar plots represent the overall broadband levels.

Figure 21 shows the third-octave L_v spectra measured on the DM tug in the way of the Z-drive propulsor support structure, by location and runs. The behaviour of the vibration composition is similar to that found on the BE tug. Specifically, the following was found:

- Structural velocity levels at the supporting structure of the drive, where the propulsor is hard-mounted to the structure, show a strong tonal signature from gear meshing in the Z-drive upper and lower reduction gears and propeller blade passage frequency pressure pulses, in frequencies <150 Hz

- There is little reduction of structural velocity levels associated with gear meshing between the foundation ("drive foundation" on Figure 21) and hull plating below ("drive hull" on Figure 21). Overall the L_v spectra at hull locations show higher levels than at the support structure of the propulsor, due to the presence of strong engine tonal content, especially in the frequencies < 315 Hz across all runs
- As engine and propeller power go up (as in high-speed ST and high-power BP runs), tonal content starts to be masked by more broadband features, likely due to the strong influence of hydrodynamic loading from the propellers and the onset of cavitation.

5 Conclusions

This study has provided a detailed comparison of underwater radiated noise (URN) from a modern battery-electric (BE) harbour tug and a comparable diesel-mechanical (DM) tug, based on full-scale sea trials, onboard noise and vibration measurements, and supporting dockside testing. The results highlight the differences in URN signatures identified through measurements designed to cover the range of operations carried out by harbour tugs.

- **URN Advantages of Battery-Electric Propulsion:**

  The BE tug consistently achieved lower noise levels during baseline stationary, transit and low power bollard pull operational states, which make up a large portion of typical tug duty cycles (~75% of the time). The reduction exceeded 8 dB at low transit speeds below and at 8 knots, while showing similar URN levels at higher speeds. During loiters, the URN reductions between the BE tug and its DM counterpart exceeded 10 dB. This reduction in URN is especially relevant in environmentally sensitive port areas, where prolonged low-speed (< 8 knots) and loitering operations can contribute significantly to cumulative underwater noise exposure. At bollard pull, however, where cavitation patterns dominate the URN radiation, the BE tug was performing worse (5 dB higher levels) than its DM tug counterpart.

- **Composition of Noise and Differences Between DM and BE Tugs:**

  The composition of URN was shown to depend strongly on propulsion system type (electric or diesel-mechanical) and operational state. For the diesel-mechanical tug, structure-borne noise generated by the main engines and transmitted through the vessel structure was a significant contributor to the overall URN signature across baseline stationary, straight run, and low-power bollard pull operational states. Distinct tonal components associated with engine firing rates (below 100 Hz), gear meshing frequencies (between 100 Hz and 630 Hz), and propeller blade passage frequencies (below 50 Hz) were consistently observed in both structural vibration and underwater noise measurements. Resilient mounting of the main engines and gensets provided effective attenuation at the machinery foundations, in excess of 20 dB. Overall, significant URN contributions from machinery are observed, particularly below 1 kHz.

  In contrast, the battery-electric tug exhibited a substantially different noise composition. During battery-only operation, the absence of diesel main engines eliminated a major source of low-frequency tonal structure-borne noise. Under these conditions, URN was primarily driven by propulsor noise, including gear meshing within the L-drive (at frequencies below 400 Hz) and tonal noise generated at blade passage frequency (below 50 Hz). When operating on genset power, increases in structural vibration and URN were observed at frequencies associated with genset rotational speeds (50 Hz to 630 Hz); however, these contributions remained lower than those associated with the diesel-mechanical main engines.

Across straight run and bollard pull conditions, propeller-related noise increasingly dominated the URN signature for both vessels as speed and load increased, with clear evidence of cavitation inception and development at higher power operating points. Differences in the cavitation behaviour can be attributed to the difference in propeller design, where there is a slightly different diameter between the two vessels (the DM tug has a 100 mm larger propeller diameter when compared to the BE counterpart), a three-bladed propeller (DM tug) versus a four-bladed propeller (BE tug), different blade pitch and skew distributions and different nozzle cross-section geometries. Despite these differences, the BE tug generally exhibited lower overall URN levels than the DM tug for equivalent transit speeds and operational states, particularly at low to moderate power, owing to the generally lower radiated noise from propulsive machinery.

URN measurements in support of a Lloyd's Register Underwater Noise (UWN) class notation for the battery-electric tug were completed successfully. The measured URN levels met the applicable criteria for both transit and quiet notations across the tested speed ranges. Results indicate that the diesel-mechanical tug could also be assigned such notations.

The class notation process highlighted the importance of early coordination with the classification society, the use of an approved service supplier, and the development of a detailed measurement plan aligned with ISO 17208 requirements. There are still significant challenges to obtaining a URN notation, namely, high costs and the availability of appropriate testing locations. Overall, this work demonstrates that modern battery-electric tugs are well-positioned to meet stringent URN performance criteria and that standardized class notations provide a robust framework for benchmarking and potentially incentivizing quieter vessel designs.

6 Recommendations

Based on the findings of this study and the insights gained from full-scale sea trials, onboard noise and vibration measurements, and supporting analyses, the following recommendations are proposed to guide future work aimed at improving the understanding and mitigation of underwater radiated noise (URN) from harbour tugs.

Changes to Conduction of Sea Trials

One issue encountered during sea trials concerns the repeatability of trials held on different days. Results show differences in a few runs held on different days, due to higher power required to reach a given speed over water from higher winds and wave conditions, or from the presence of unwanted environmental noise. The selected ULS configuration, which is fully autonomous, does not allow for data download or verification immediately after the sea trials. If such an arrangement were possible, the data could have been quality-checked, and perhaps a decision could have been made to re-run trials. Even more so, the ability to have a system with on-the-fly URN reading could be even more beneficial, so that a decision to re-run certain conditions could be made right on the water. Future deployments could explore such possibilities.

Continued Collection of High-Quality, Systematic URN Data

It is recommended that efforts continue toward the systematic collection of high-quality URN data from harbour tugs across a broad range of vessel types, propulsion configurations, and operational profiles. Expanding the dataset beyond single case studies will improve statistical robustness and enable more reliable comparisons between propulsion technologies, propulsor designs, and operating conditions. In particular, repeated measurements under controlled and well-documented environmental conditions would support the development of representative URN baselines for harbour tug operations. Such datasets would also facilitate refinement of empirical relationships between vessel speed, propulsor loading, machinery state, and resulting URN levels, supporting both regulatory and design-stage decision-making.

As URN measurements done using ISO 17208 align with data collection methodologies required by major classification societies to grant a URN notation, these efforts might also serve as a way for more tug operators to access URN notation for harbour tugs.

Data collected might also serve as the baseline required to develop URN management plans for ship-assist operators and port authorities, in line with the International Maritime Organization (IMO) Revised Guidelines for the Reduction of Underwater Radiated Noise from Shipping to Address Adverse Impacts on Marine Life [13].

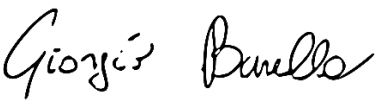
Reduction of URN from Nozzled Tug Propellers

Given that propeller-related noise and cavitation were identified as dominant contributors to URN at higher speeds and loads, exploring possibilities to reduce URN from the type of commercially available azimuthing propulsors installed on ASD harbour tugs is strongly recommended. The propellers used in these units are generally pitched and otherwise designed to provide a rated bollard pull at maximum power, with the major design goal to achieve the contractually required thrust at zero speed. Cavitation generation is a secondary consideration, even though it is a major contributor to URN. Future work should prioritize investigation into propeller and nozzle design features that influence cavitation inception, tonal content, and broadband noise generation, particularly under bollard pull and high-load conditions. Design optimization studies, supported by targeted model-scale testing and numerical studies, could explore alternative blade geometries, nozzle profiles, and clearance arrangements to reduce hydrodynamic noise while analyzing trade-offs with the required thrust performance and propulsive efficiency. In parallel, operational guidance on propeller loading and azimuthing strategies could provide practical noise-reduction benefits in the short term.

Development and Use of Live URN Information

The development and integration of live or near-real-time URN information systems is recommended as a next step toward operational noise management. The real-time information could be provided by means of pre-computed or measured source levels, or by integrating live measurements of propulsors' speed and vibration onboard to obtain a source level. Providing operators with real-time feedback on URN emissions during typical harbour operations could enable informed operational adjustments, such as speed management or power-setting optimization, particularly in environmentally sensitive areas. Live URN information would also support adaptive operational strategies during loitering, transit, and ship-assist activities, helping to reduce cumulative underwater noise exposure without compromising safety or operational effectiveness.

for Robert Allan Ltd.





Dr. Giorgio Burella, P.Eng.
Project Manager

Waltfred Lee, EIT
Mechanical Engineer

BG/WL:da

References

[1] *Species at Risk Act*, S.C. 2002, c. 29, Canada.

[2] Burella, G. and Den Hertog, V., *The Benefits of Adopting a Battery Electric Powertrain: The Case of the ElectRA 2300 SX,* November 2022, GreenShip Conference, Vancouver.

[3] Burella G., *Measurements Test Plan Report*, Robert Allan Ltd. document # RAL02704R-225-034-500, Revision R4.

[4] International Standards Organization (ISO), *ISO 17208 Standard Series - Underwater Acoustics,* 2016.

[5] Lloyd's Register (LR), *LR-SR-ADP-016 Underwater Radiated Noise from Ships*, May 2025.

[6] Wladichuk, J. and Li, Z., *Tugboat Underwater Radiated Noise Measurements*, JASCO Applied Sciences Ltd. Document # 04225.

[7] Serkan Turkmen et al., *On-board measurement techniques to quantify underwater radiated noise level*, AMT'15, September 2015.

[8] Cheolsoo Park et al., *Noise Localization Method for Model Tests in a Large Cavitation Tunnel Using a Hydrophone Array*, Remote Sens. 2016, 8(3), 195.

[9] D. McIntyre et al., *Experimental measurements and numerical simulations of underwater radiated noise from a model-scale propeller in uniform inflow*, Ocean Engineering, vol. 255, p. 111409, 2022.

[10] Lee, W., *Systematic Underwater Radiated Noise Measurement. Report 1 – Harbour Tug Operational Conditions and its Underwater Radiated Noise*, Robert Allan Ltd. document # RAL02280R-221-039-500, Revision R1.

[11] D. McIntyre et al., *Influence of propellers and operating conditions on underwater radiated noise from coastal ferry vessels*, Ocean Engineering, vol. 232, p. 109075, 2021.

[12] American National Standards Institute (ANSI), *ANSI/ASA S12.64-2009 Quantities and Procedures for Description and Measurement of Underwater Sound from Ships,* 2009.

[13] International Maritime Organization (IMO), *Revised Guidelines for the Reduction of Underwater Radiated Noise from Shipping to Address Adverse Impacts on Marine Life,* MEPC.1/Circ.906, August 2023

Appendix A. Sea Trials and Dockside Tests Summary

This appendix shows the as-run measurement matrix summary of all trials, with information on the state of main propulsive equipment. Table B-1, B-2, B-3, B-4, B-5 and B-6 show the tests run during sea trials, including relevant test conditions. In these tables, column "Run #" directly references the run numbers identified in the test matrix in Section 3.3.4. Tables B-7 and B-8 show the impact test matrix for modal hammer and acceleration response positions performed during dockside trials. These locations can be identified in the sketches in Appendix B.

Table B-1: Summary of runs for the Baseline Stationary (BS) conditions for BE tug

BE Tug								
Run #	Run Type	Speed Over Ground (knots)	Motor Speed (rpm)		Propeller Speed (rpm)		Genset Speed (rpm)	
			Port	Starboard	Port	Starboard	Aft	Fwd
a	BE BS-I	0	0	0	0	0	0	0
b			0	0	0	0	0	0
c	BE BS-II	0	60	60	20	20	0	0
d			60	60	20	20	0	0
g	BE BS-III	0	0	0	0	0	1800	1800
h			0	0	0	0	1800	1800
i	BE BS-IV	0	60	60	20	20	1800	1800
j			60	60	20	20	1800	1800

Table B-2: Summary of runs for the Baseline Stationary (BS) conditions for DM tug

DM Tug							
Run #	Run Type	Speed Over Ground (knots)	Main Engine Speed (rpm)		Propeller Speed (rpm)		Aux Genset Speed (rpm)
			Port	Starboard	Port	Starboard	
a	DM BS-I	Not run at sea trials, Only N&V data	0	0	0	0	1800
b			0	0	0	0	1800
c	DM BS-II	0	650	650	26	26	1800
d			650	650	26	26	1800
e	DM BS-III	0	650	650	78	78	1800
f			650	650	78	78	1800

Table B-3: Summary of runs for the Straight Run (ST) conditions for BE tug

			BE Tug			
Run #	Run Type	Speed Over Ground (knots)	Motor Speed (rpm)		Genset Speed (rpm)	
			Port	Starboard	Aft	Fwd
a-1-batt	BE ST-BATT-I	6	276	270	0	0
a-2-batt			284	284	0	0
a-3-batt			257	270	0	0
a-4-batt			274	272	0	0
b-1-batt	BE ST-BATT-II	7	319	322	0	0
b-2-batt			318	318	0	0
b-3-batt			329	331	0	0
b-4-batt			314	293	0	0
c-1-batt	BE ST-BATT-III	8	364	359	0	0
c-2-batt			388	384	0	0
c-3-batt			371	377	0	0
c-4-batt			383	384	0	0
d-1-batt	BE ST-BATT-IV	9	414	430	0	0
d-2-batt			436	431	0	0
d-3-batt			409	412	0	0
d-4-batt			428	432	0	0
e-1-batt	BE ST-BATT-V	10	465	478	0	0
e-2-batt			455	455	0	0
e-3-batt			477	490	0	0
e-4-batt			494	456	0	0
a-1-gens	BE ST-GENS-I	6	263	269	0	0
a-2-gens			263	265	0	0
a-3-gens			263	267	0	0
a-4-gens			270	268	0	0
b-1-gens	BE ST-GENS-II	7	309	284	0	0
b-2-gens			328	310	0	0
b-3-gens			308	312	0	0
b-4-gens			315	320	0	0
c-1-gens	BE ST-GENS-III	8	349	352	0	0
c-2-gens			356	365	0	0
c-3-gens			369	366	0	0
c-4-gens			364	377	0	0

BE Tug						
Run #	Run Type	Speed Over Ground (knots)	Motor Speed (rpm)		Genset Speed (rpm)	
			Port	Starboard	Aft	Fwd
d-1-gens	BE ST-GENS-IV	9	394	407	0	0
d-2-gens			419	409	0	0
d-3-gens			396	404	0	0
d-4-gens			411	419	0	0
e-1-gens	BE ST-GENS-V	10	450	450	0	0
e-2-gens			462	453	0	0
e-3-gens			452	452	0	0
e-4-gens			461	463	0	0

Table B-4: Summary of runs for the Straight Run (ST) conditions for DM tug

DM Tug					
Run #	Run Type	Speed Over Ground (knots)	Main Engine Speed (rpm)		Aux Genset Speed (rpm)
			Port	Starboard	
a-1	DM ST-I	6	797	803	1800
a-2			797	797	1800
a-3			797	797	1800
a-4			797	797	1800
b-1	DM ST-II	7	903	902	1800
b-2			908	920	1800
b-3			908	921	1800
b-4			904	916	1800
c-1	DM ST-III	8	1079	1073	1800
c-2			1073	1075	1800
c-3			1079	1070	1800
c-4			1069	1070	1800
d-1	DM ST-IV	9	1190	1192	1800
d-2			1190	1190	1800
d-3			1194	1184	1800
d-4			1190	1190	1800
e-1	DM ST-V	10	1329	1330	1800
e-2			1330	1340	1800
e-3			1335	1335	1800

DM Tug					
Run #	Run Type	Speed Over Ground (knots)	Main Engine Speed (rpm)		Aux Genset Speed (rpm)
			Port	Starboard	
e-4			1336	1370	1800

Table B-5: Summary of runs for the Bollard Pull (BP) conditions for BE tug

BE Tug						
Run #	Run Type	Bollard Pull (% of max)	Motor Speed (rpm)		Genset Speed (rpm)	
			Port	Starboard	Aft	Fwd
a	BE BP-I	20	263	270	0	0
b			265	267	0	0
c	BE BP-II	50	453	439	0	0
d			434	438	0	0
e	BE BP-III	75	519	518	0	0
f			504	513	0	0
g	BE BP-IV	100	593	614	0	0
h			591	603	0	0
i	BE BP-V	20	255	257	1800	1800
j			255	263	1800	1800
k	BE BP-VI	50	404	460	1800	1800
l			435	455	1800	1800

Table B-6: Summary of runs for the Bollard Pull (BP) conditions for DM tug

DM Tug					
Run #	Run Type	Bollard Pull (% of max)	Main Engine Speed (rpm)		Aux Genset Speed (rpm)
			Port	Starboard	
a	DM BP-I	20	685	685	1800
b			685	682	1800
c	DM BP-II	50	1000	1000	1800
d			1006	1006	1800
e	DM BP-III	75	1555	1555	1800
f			1555	1555	1800
g	DM BP-IV	100	1720	1720	1800
h			1712	1746	1800

Table B-4: Positions for hammer impact and structural responses for the battery-electric (BE) tug at dockside trials. See Appendix B for details on the positions.

BATTERY ELECTRIC TUG				BATTERY ELECTRIC TUG			
Machinery Item: Genset				**Machinery Item: L-drive**			
Hammer impact positions		Response Structure positions		Hammer impact positions		Response Structure positions	
ID	Description	ID	Description	ID	Description	ID	Description
H1Z+	Port Genset, Port Side, Above Aft Mount	R1Z+	Port Genset, Port Side, Above Aft Mount	H1Z+	Port L-drive – Forward	R1Z+	Port L-drive – Aft
		R2Z+	Port Genset, Port Side, Below Aft Mount			R2Z+	Port L-drive – Stbd
H2Z+	Port Genset, Port Side, Below Aft Mount	R3Z+	Port Side, Below Genset Seating, Hull Position # 1	H2Z+	Port L-drive – Starboard	R3Z+	Port L-drive – Forward
		R4Z+	Port Side, Genset Seating Top Plate, Between Mounts			R4Z+	Port L-drive – Port
		R5Z+	Port Genset, Port Side, Above Aft Mount	H3Z+	Port L-drive – Aft	R5Z+	Hull Position #1
H3Z+	Port Genset, Port Side, Above Forward Mount	R6Z+	Port Genset, Port Side, Below Aft Mount			R6Z+	Hull Position #2
		R7Z+	Port Side, Below Genset Seating, Hull Position # 2	H4Z+	Port L-drive – Port	R7Z+	Hull Position #3

Table B-5: Positions for hammer impact and structural responses on the diesel-mechanical (DM) tug at dockside trials. See Appendix B for details on the positions.

DIESEL MECHANICAL TUG			
Machinery Item: Main Engine			
Hammer impact positions		Response Structure positions	
ID	Description	ID	Description
H1Z+	Port Main Engine, Above Mount Aft	R1Z+	Port Main Engine, Above Aft Mount
		R2Z+	Port Main Engine, Below Aft Mount
H2Z+	Port Main Engine, Below Mount Aft	R3Z+	Hull Position #1, in way of Z-drive
		R4Z+	Port Main Engine, Above Forward Mount
H3Z+	Port Main Engine, Above Forward Mount	R5Z+	Port Main Engine, Below Forward Mount
		R6Z+	Hull Position #2, in way of Main Engine
H4Z+	Port Main Engine, Below Forward Mount	R7Z+	Hull Position #3, in way of Z-drive

DIESEL MECHANICAL TUG			
Machinery Item: Z-Drive			
Hammer impact positions		Response Structure positions	
ID	Description	ID	Description
H1Z+	Starboard Z-drive – Starboard	R1Z+	Starboard Z-drive – Starboard
		R2Z+	Starboard Z-drive – Aft
H2Z+	Starboard Z-drive – Aft	R3Z+	Hull Position #1, in way of Z-drive
		R4Z+	Starboard Z-drive – Port
H3Z+	Starboard Z-drive – Port	R5Z+	Starboard Z-drive – Forward
		R6Z+	Hull Position #3, in way of Main Engine
H4Z+	Starboard Z-drive – Forward	R7Z+	Hull Position #3, in way of Z-drive

(continues next page…)

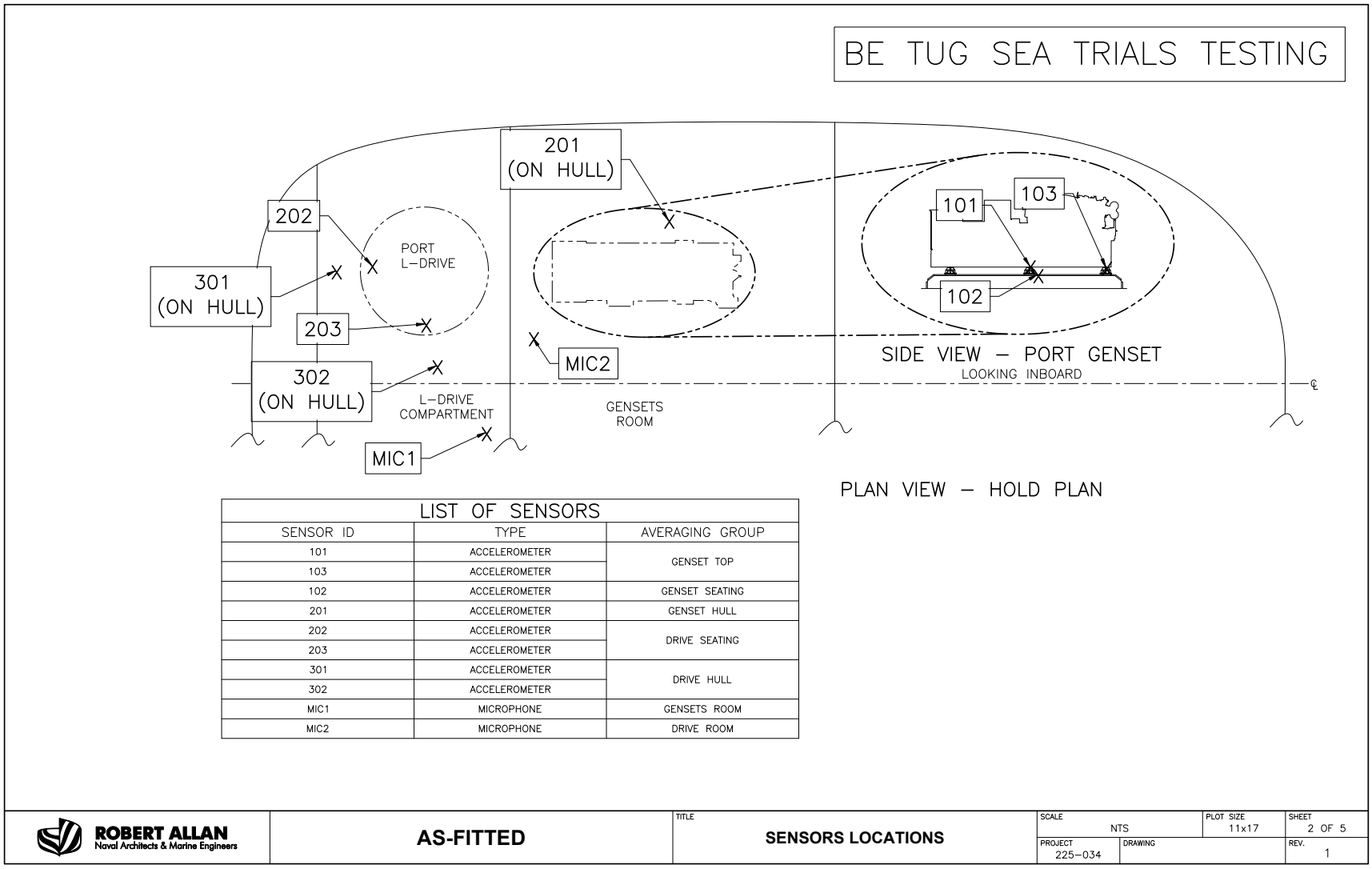
DIESEL MECHANICAL TUG			
Machinery Item: Genset			
Hammer impact positions		Response Structure positions	
ID	Description	ID	Description
H1Z+	Port Genset – Tank Top Forward	R1Z+	Port Genset, Above Forward Mount,
		R2Z+	Port Genset, On Skid, forward
		R3Z+	Hull Position #1, in way of Z-drive
		R4Z+	Port Genset, On Tank Top, forward
H2Z+	Port Genset – Tank Top Aft	R5Z+	Port Genset, On Tank Top, Aft
		R6Z+	Hull Position #3, in way of Main Engine
		R7Z+	Hull Position #3, in way of Z-drive

Appendix B. N&V Sensors Positions

This appendix shows the accelerometer and microphone positions during the sea trials. The following is shown in the figures below:

- For the BE tug, Figure B-1 shows the sea trials sensors positions and B-2 shown the dockside sensors positions.
- For the DM tug, Figure B-3 shows the sea trials sensors positions and B-4 shown the dockside sensors positions.

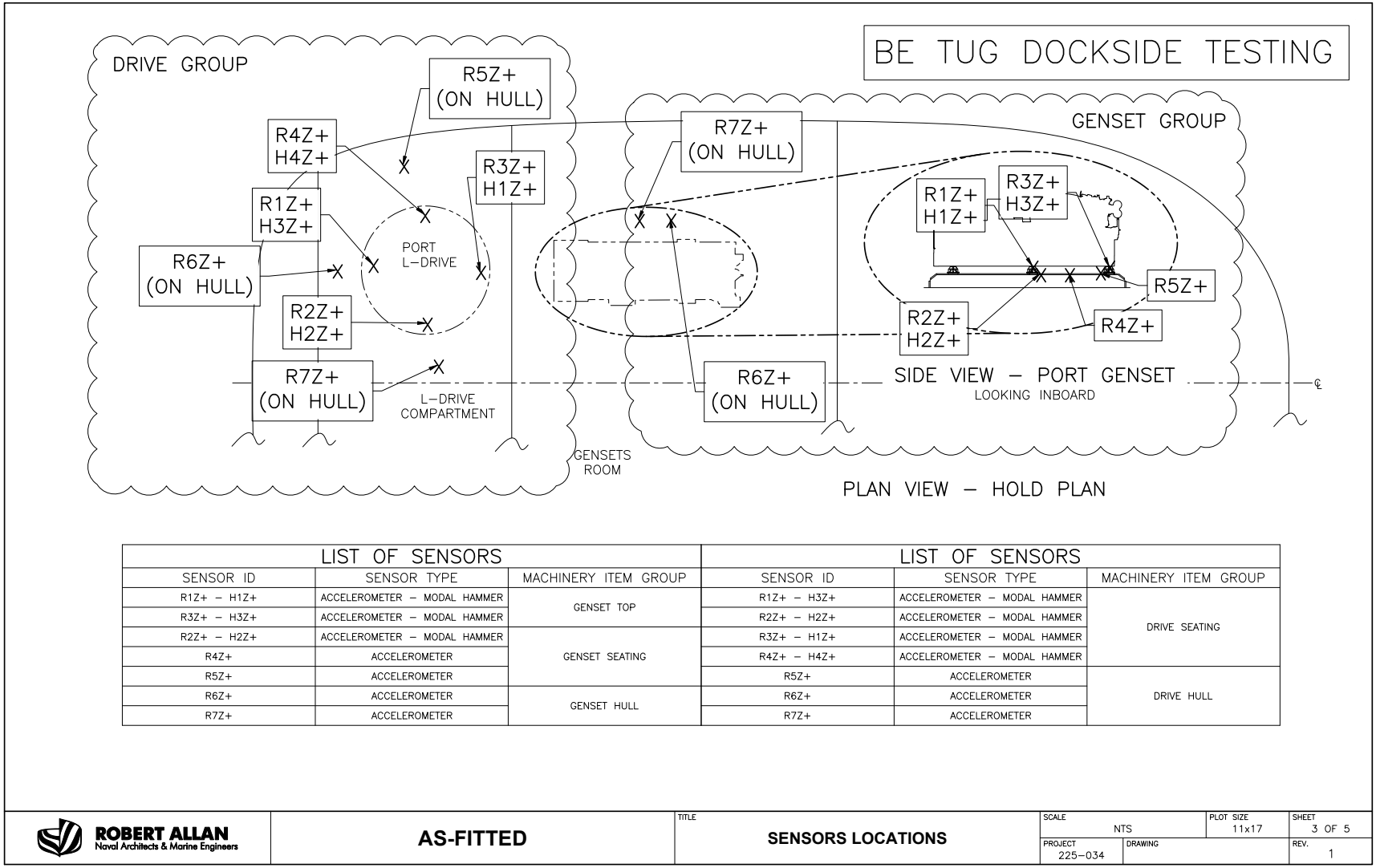
See overleaf for the images.



LIST OF SENSORS

SENSOR ID	TYPE	AVERAGING GROUP
101	ACCELEROMETER	GENSET TOP
103	ACCELEROMETER	
102	ACCELEROMETER	GENSET SEATING
201	ACCELEROMETER	GENSET HULL
202	ACCELEROMETER	DRIVE SEATING
203	ACCELEROMETER	
301	ACCELEROMETER	DRIVE HULL
302	ACCELEROMETER	
MIC1	MICROPHONE	GENSETS ROOM
MIC2	MICROPHONE	DRIVE ROOM

Figure B-1: N&V sensors positions during sea trials - BE tug



LIST OF SENSORS		
SENSOR ID	SENSOR TYPE	MACHINERY ITEM GROUP
R1Z+ - H1Z+	ACCELEROMETER - MODAL HAMMER	GENSET TOP
R3Z+ - H3Z+	ACCELEROMETER - MODAL HAMMER	
R2Z+ - H2Z+	ACCELEROMETER - MODAL HAMMER	GENSET SEATING
R4Z+	ACCELEROMETER	
R5Z+	ACCELEROMETER	
R6Z+	ACCELEROMETER	GENSET HULL
R7Z+	ACCELEROMETER	

LIST OF SENSORS		
SENSOR ID	SENSOR TYPE	MACHINERY ITEM GROUP
R1Z+ - H3Z+	ACCELEROMETER - MODAL HAMMER	DRIVE SEATING
R2Z+ - H2Z+	ACCELEROMETER - MODAL HAMMER	
R3Z+ - H1Z+	ACCELEROMETER - MODAL HAMMER	
R4Z+ - H4Z+	ACCELEROMETER - MODAL HAMMER	
R5Z+	ACCELEROMETER	DRIVE HULL
R6Z+	ACCELEROMETER	
R7Z+	ACCELEROMETER	

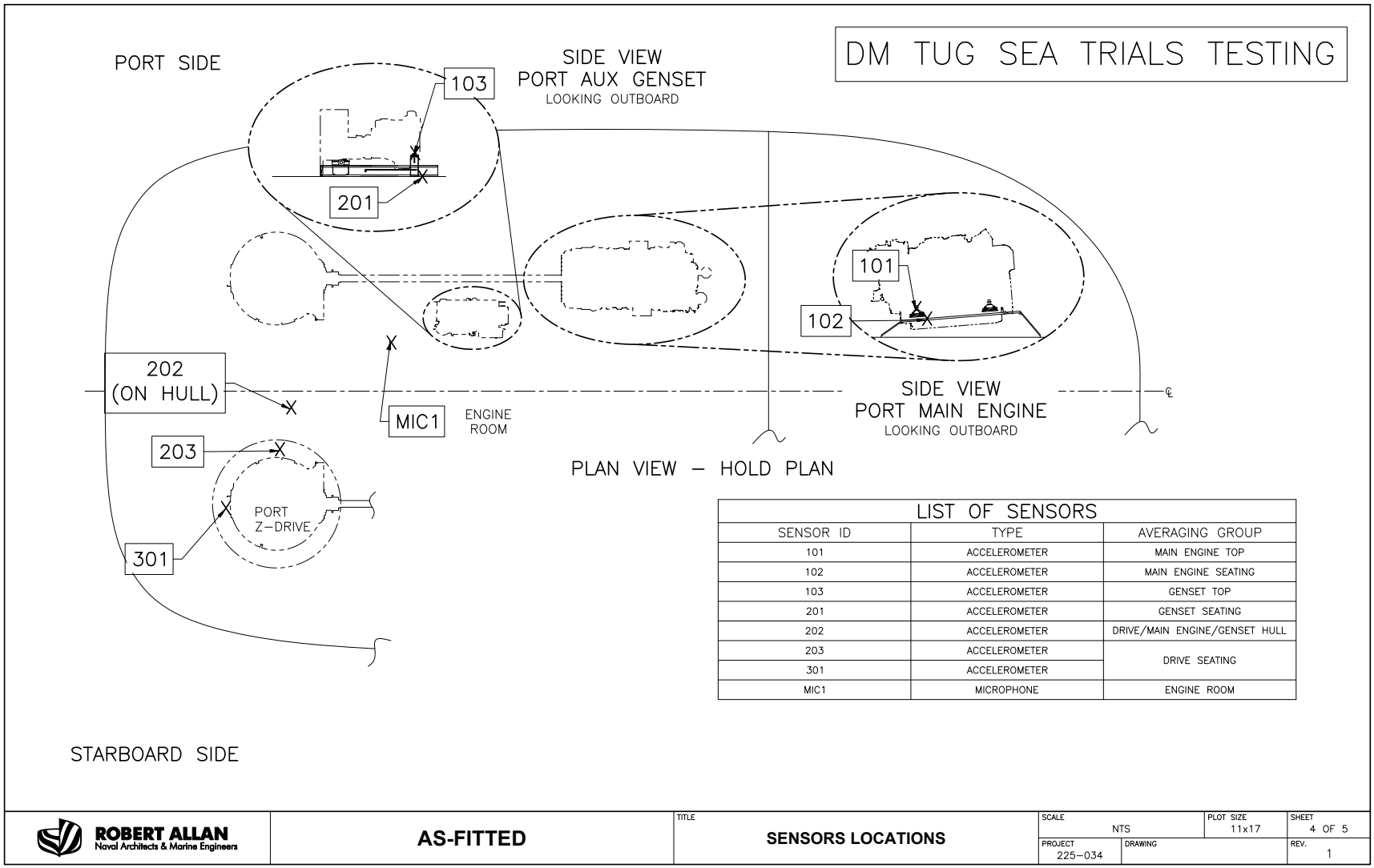
ROBERT ALLAN
Naval Architects & Marine Engineers

AS-FITTED

TITLE: SENSORS LOCATIONS

SCALE: NTS | PLOT SIZE: 11x17 | SHEET: 3 OF 5
PROJECT: 225-034 | DRAWING: | REV.: 1

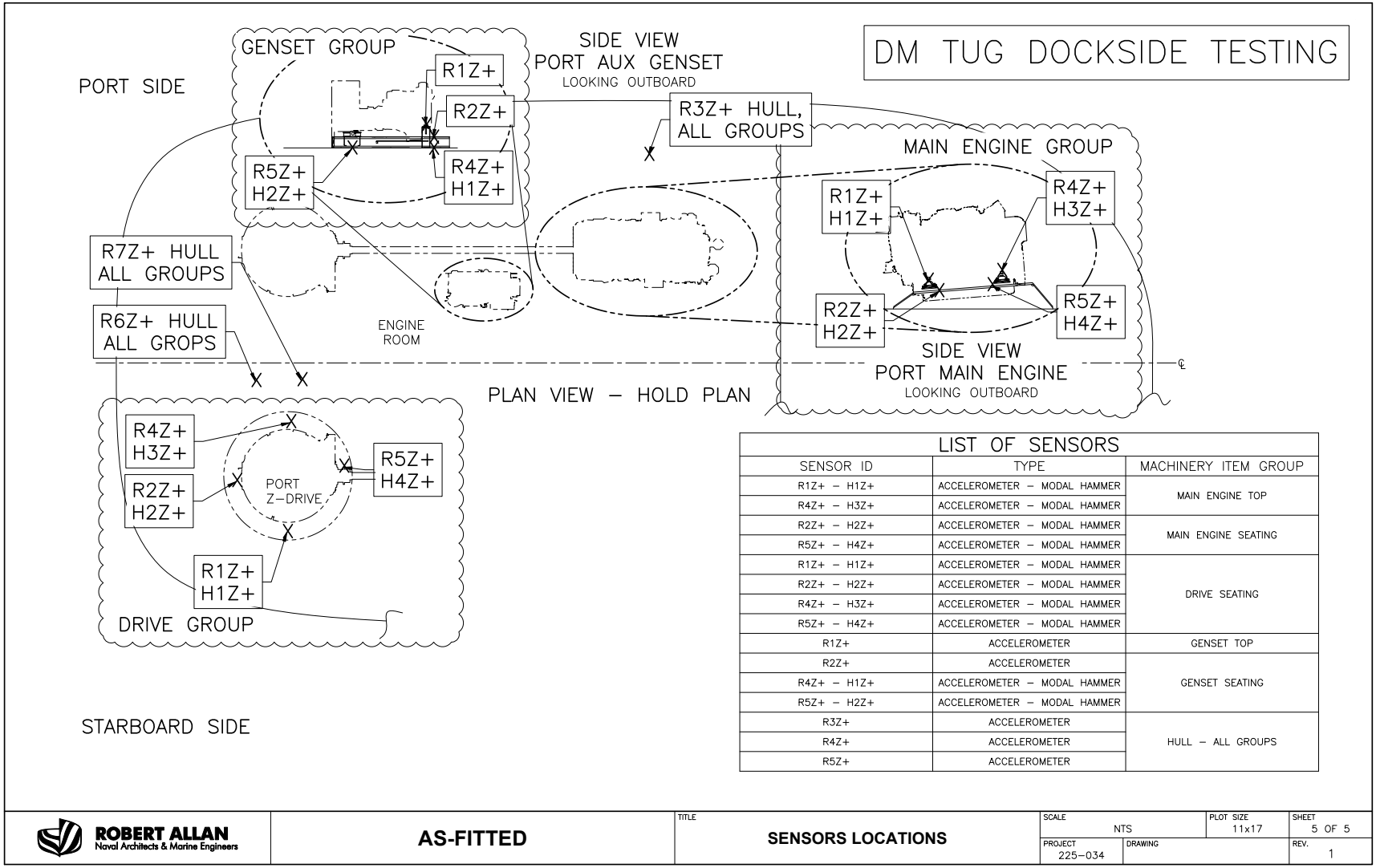
Figure B-2: N&V sensors positions during dockside testing - BE tug



LIST OF SENSORS

SENSOR ID	TYPE	AVERAGING GROUP
101	ACCELEROMETER	MAIN ENGINE TOP
102	ACCELEROMETER	MAIN ENGINE SEATING
103	ACCELEROMETER	GENSET TOP
201	ACCELEROMETER	GENSET SEATING
202	ACCELEROMETER	DRIVE/MAIN ENGINE/GENSET HULL
203	ACCELEROMETER	DRIVE SEATING
301	ACCELEROMETER	
MIC1	MICROPHONE	ENGINE ROOM

Figure B-3: N&V sensors positions during sea trials - DM tug



LIST OF SENSORS		
SENSOR ID	TYPE	MACHINERY ITEM GROUP
R1Z+ – H1Z+	ACCELEROMETER – MODAL HAMMER	MAIN ENGINE TOP
R4Z+ – H3Z+	ACCELEROMETER – MODAL HAMMER	
R2Z+ – H2Z+	ACCELEROMETER – MODAL HAMMER	MAIN ENGINE SEATING
R5Z+ – H4Z+	ACCELEROMETER – MODAL HAMMER	
R1Z+ – H1Z+	ACCELEROMETER – MODAL HAMMER	DRIVE SEATING
R2Z+ – H2Z+	ACCELEROMETER – MODAL HAMMER	
R4Z+ – H3Z+	ACCELEROMETER – MODAL HAMMER	
R5Z+ – H4Z+	ACCELEROMETER – MODAL HAMMER	
R1Z+	ACCELEROMETER	GENSET TOP
R2Z+	ACCELEROMETER	GENSET SEATING
R4Z+ – H1Z+	ACCELEROMETER – MODAL HAMMER	
R5Z+ – H2Z+	ACCELEROMETER – MODAL HAMMER	
R3Z+	ACCELEROMETER	HULL – ALL GROUPS
R4Z+	ACCELEROMETER	
R5Z+	ACCELEROMETER	

ROBERT ALLAN
Naval Architects & Marine Engineers

AS-FITTED

TITLE: SENSORS LOCATIONS

SCALE: NTS | PLOT SIZE: 11x17 | SHEET: 5 OF 5
PROJECT: 225–034 | DRAWING: | REV.: 1

Figure B-4: N&V sensors positions during dockside testing - DM tug

Appendix C. URN Narrowband Data Analysis

The following figures show the narrow-band spectra of the *RNL* levels and respective third-octave band spectra, for all run types performed on the vessels at sea trials. The figures show the tonal analysis outlined in Section 2.5.3.1 of this report. Table C-1 provides a a list of figures by run types and by vessel.

Table C-1: Summary of runs and figures in the tonal analysis

Vessel	Run Type	Fig.	Page
BE Vessel	Baseline Stationary (BS)	C-1	C-2
BE Vessel	Straight Run On Battery (ST-BATT)	C-2	C-3
BE Vessel	Straight Run On Gensets (ST-GENS)	C-3	C-4
BE Vessel	Bollard Pull (BP)	C-4	C-5
DM Vessel	Baseline Stationary (BS)	C-5	C-6
DM Vessel	Straight Travel (ST)	C-6	C-7
DM Vessel	Bollard Pull (BP)	C-7	C-8

C.1 BE Vessel

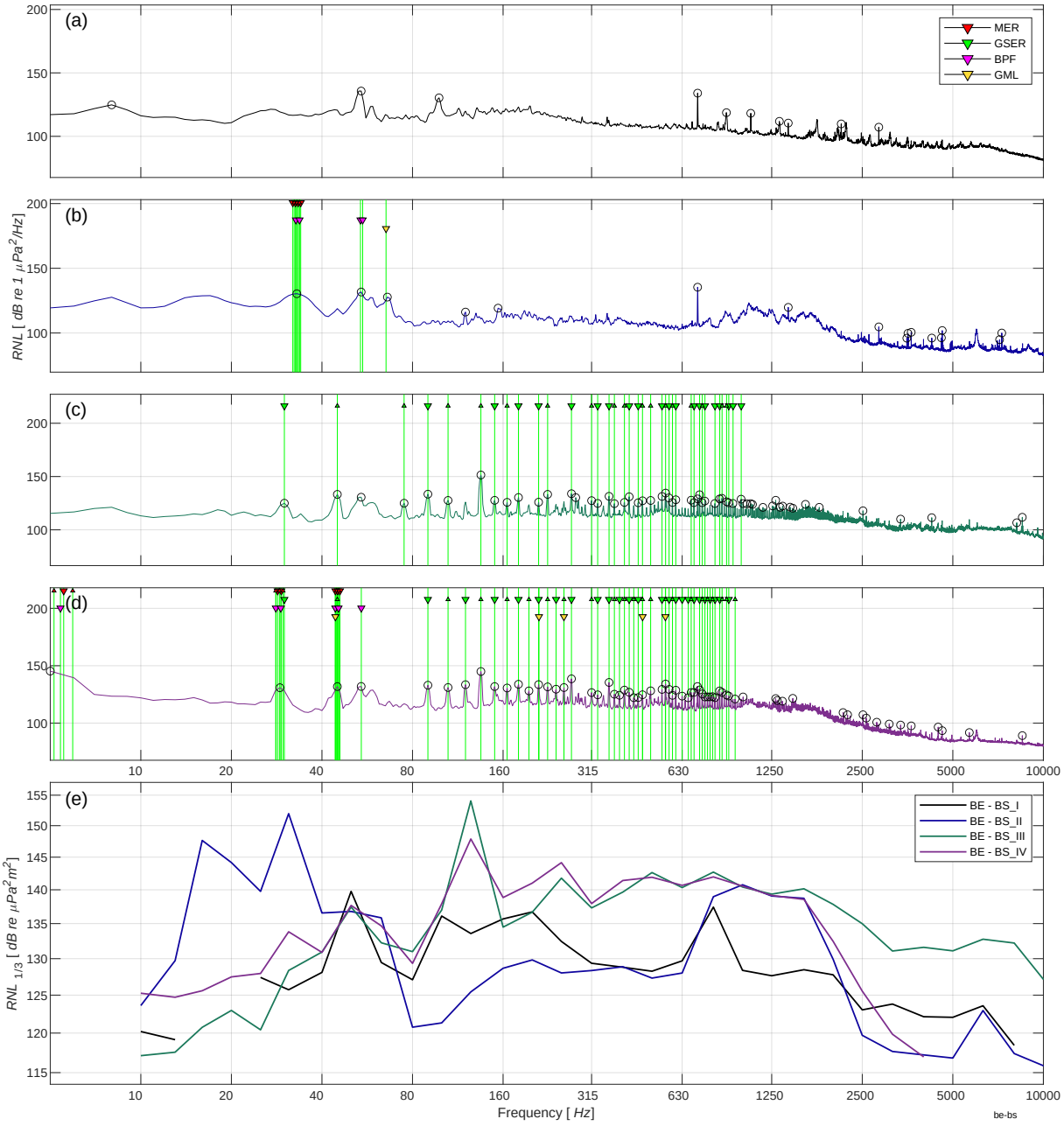


Figure C-1: RNL narrow-band spectra for (a) BE BS-I, (b) BE BS-II, (c) BE BS-III, (d) BE BS-IV and the respective (e) third-octave band spectra.

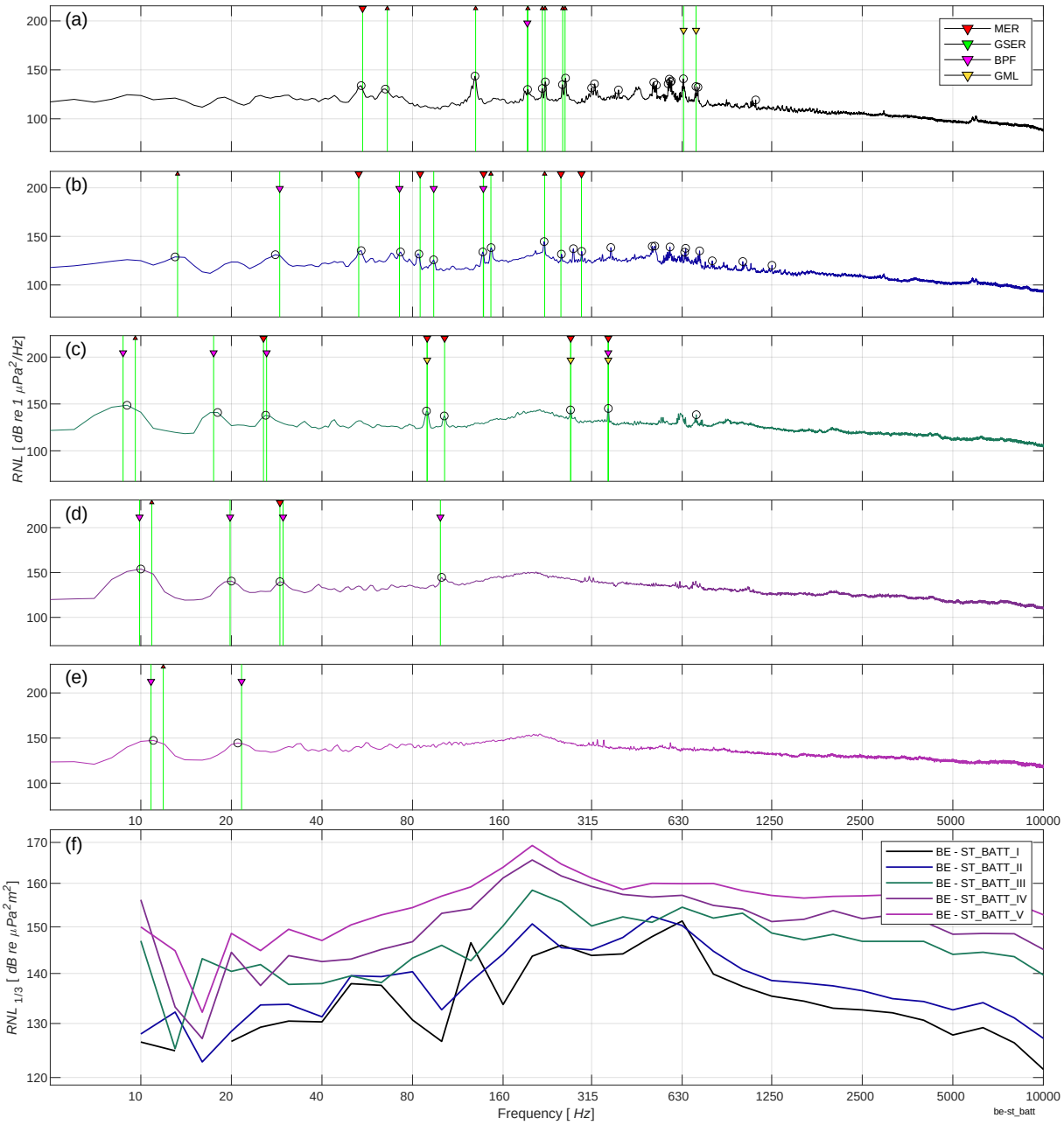


Figure C-2: RNL narrow-band spectra for (a) BE ST-BATT-I, (b) BE ST-BATT-II, (c) BE ST-BATT-III, (d) BE ST-BATT-IV, (e) BE ST-BATT-V and the respective (f) third-octave band spectra.

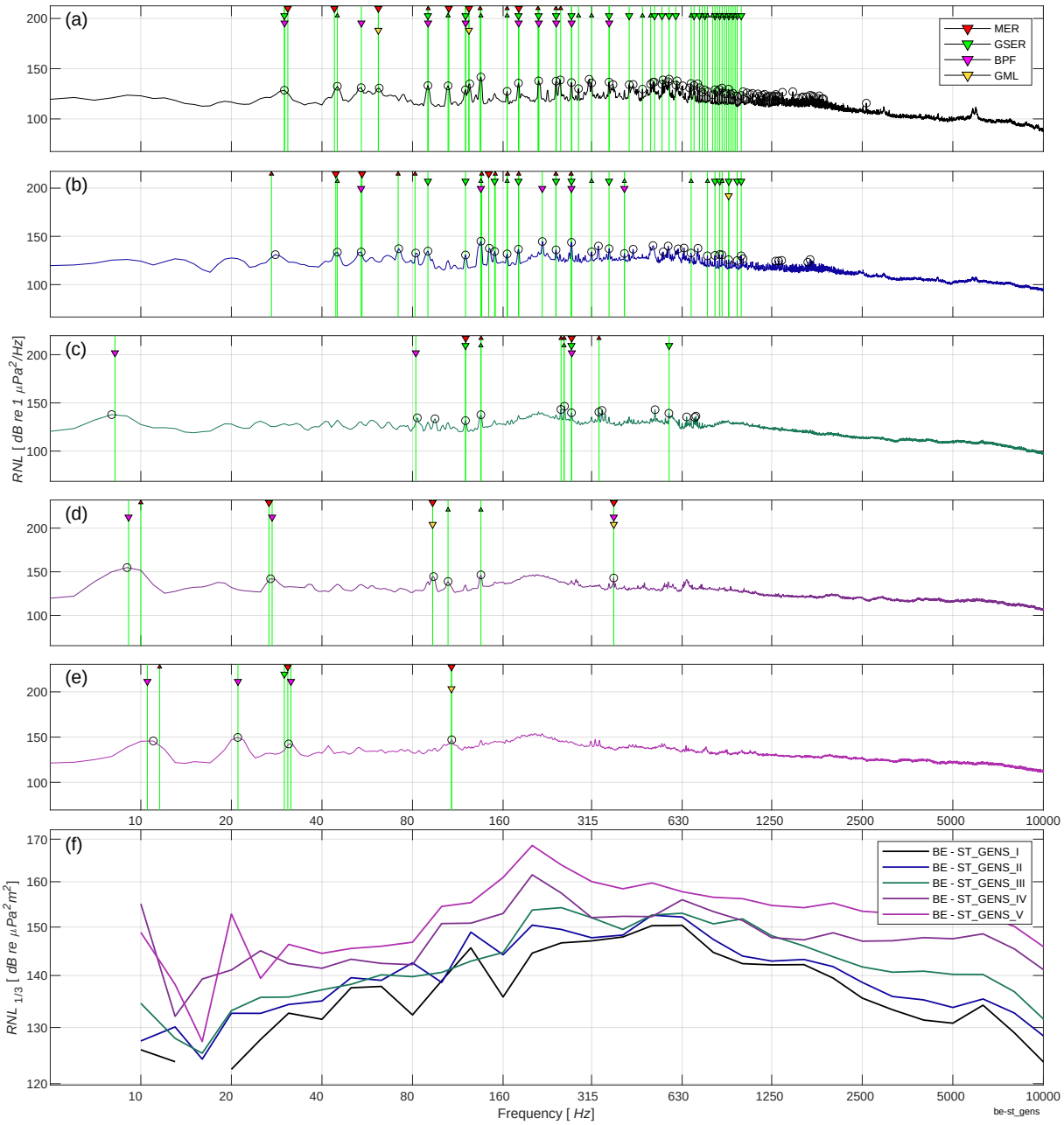


Figure C-3: RNL narrow-band spectra for (a) BE ST-GENS-I, (b) BE ST-GENS-II, (c) BE ST-GENS-III, (d) BE ST-GENS-IV, (e) BE ST-GENS-V and the respective (f) third-octave band spectra.

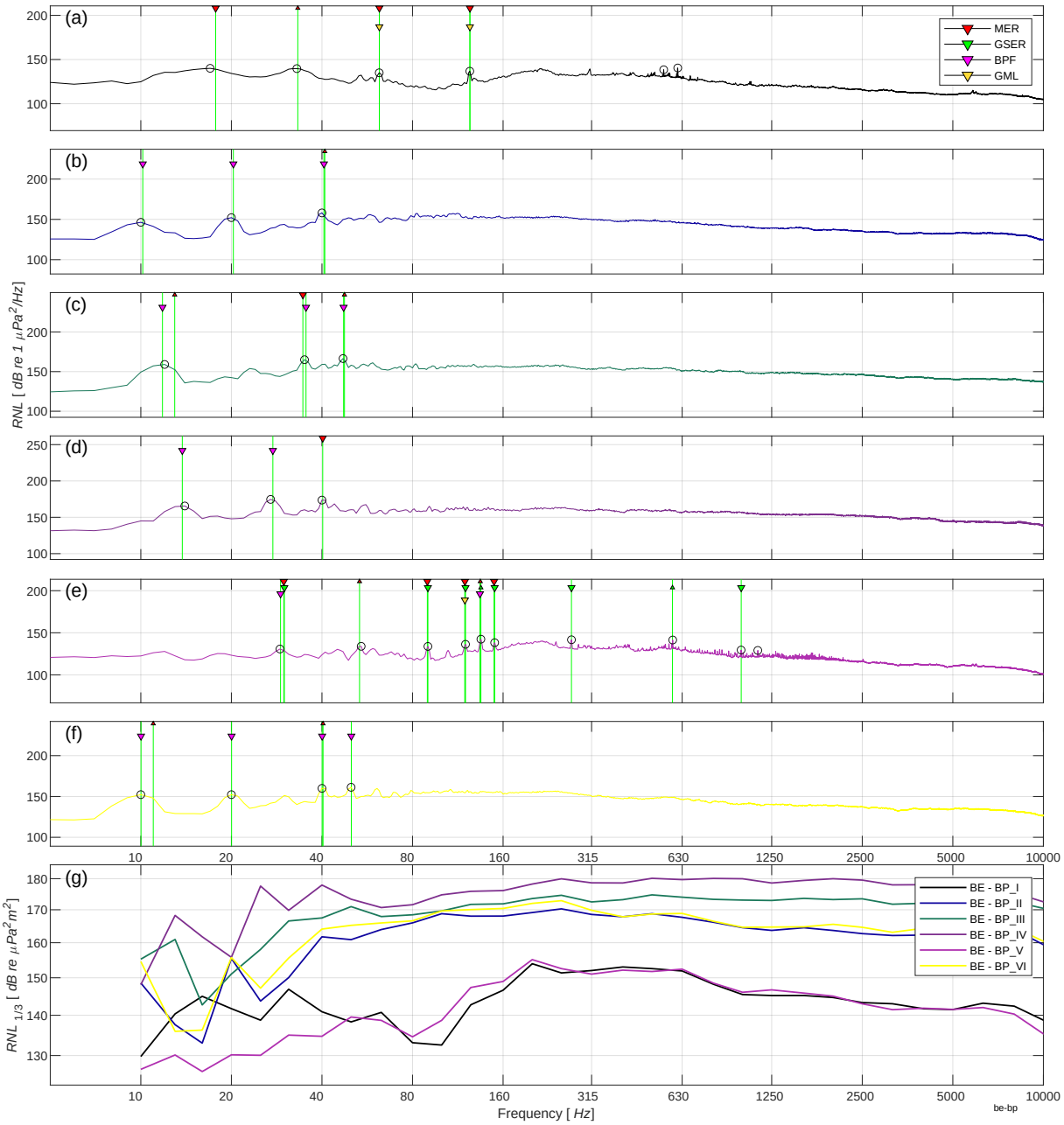


Figure C-4: RNL narrow-band spectra for (a) BE BP-I, (b) BE BP-II, (c) BE BP-III, (d) BE BP-IV, (e) BE BP-V, (f) BE BP-VI and the respective (g) third-octave band spectra.

C.2 DM Vessel

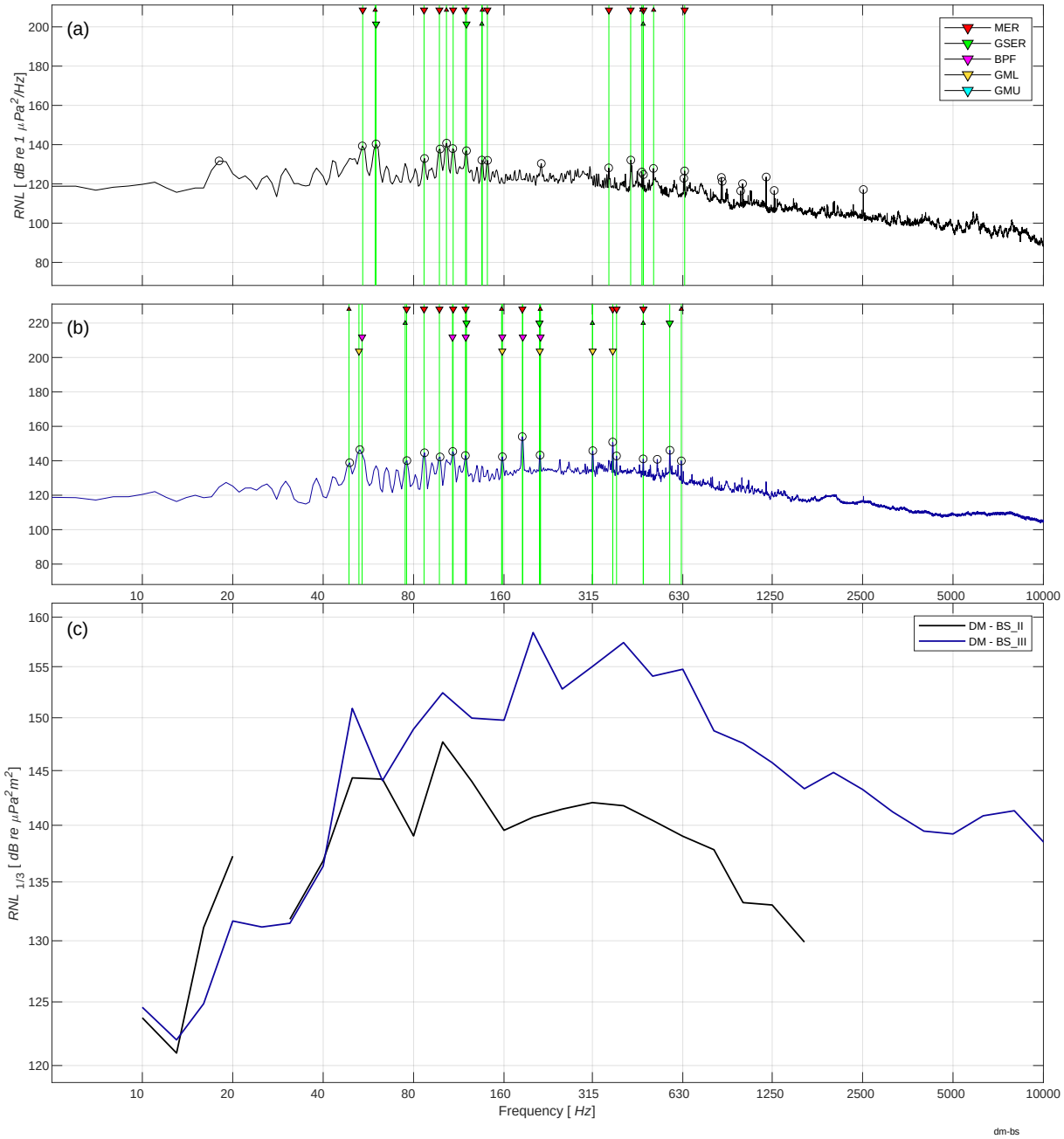


Figure C-5: RNL narrow-band spectra for (a) DM BS-II, (b) DM BS-III and the respective (c) third-octave band spectra.

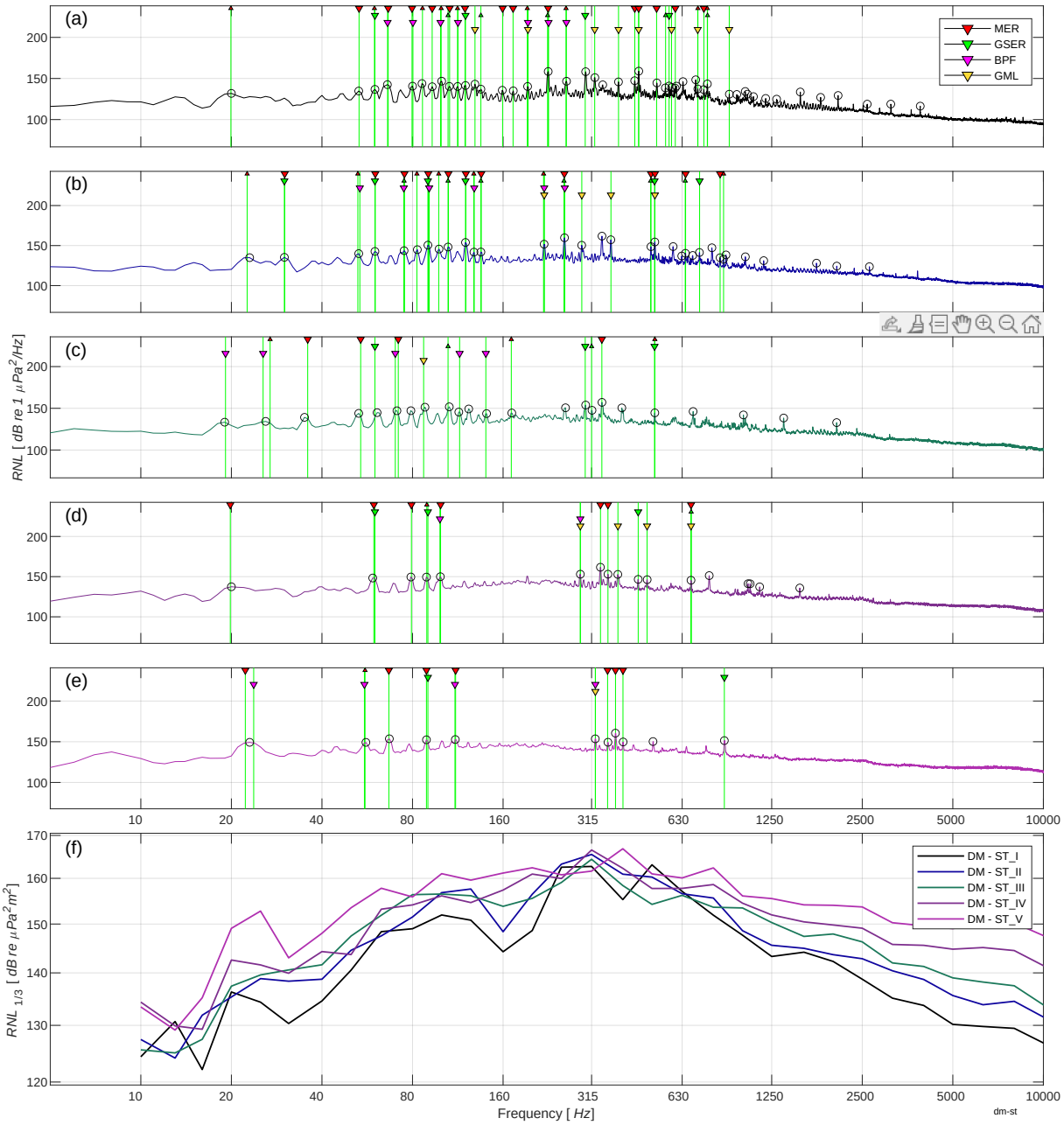


Figure C-6: RNL narrow-band spectra for (a) DM ST-I, (b) DM ST-II, (c) DM ST-III, (d) DM ST-IV, (e) DM ST-V and the respective (f) third-octave band spectra.

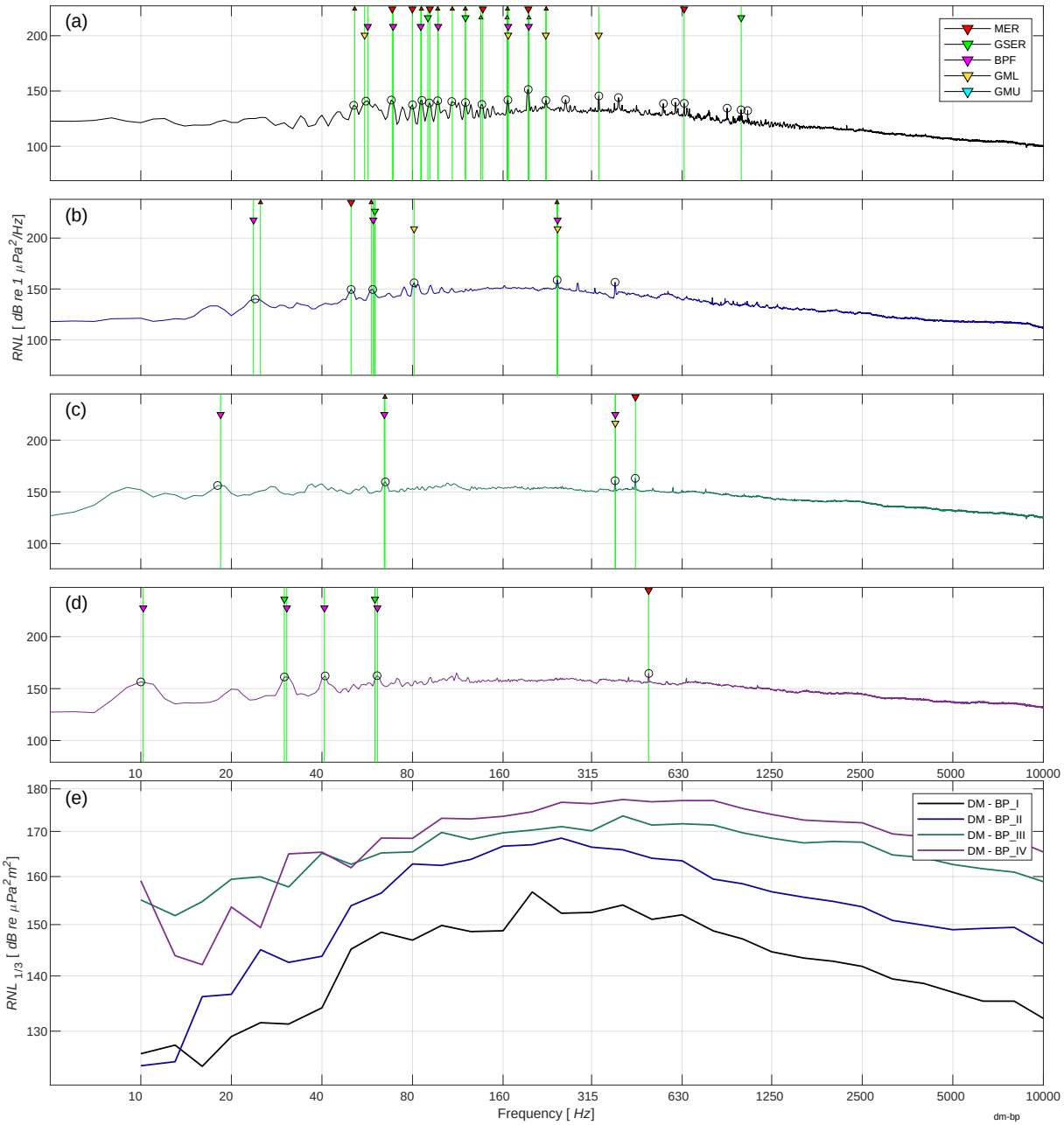


Figure C-7: RNL narrow-band spectra for (a) DM BP-I, (b) DM BP-II, (c) DM BP-III, (d) DM BP-IV and the respective (e) third-octave band spectra.

Appendix D. L_v Narrowband Data Analysis

The following figures show the narrow-band spectra of the structural velocity levels L_v and respective third-octave band spectra, for all run types performed on the vessels at sea trials. The figures show the tonal analysis outlined in Section 2.5.3.1 of this report. Table D-1 provides a a list of figures by run types and by vessel.

Table D-1: Summary of runs and figures in the tonal analysis

Vessel	Run Type	Description	Measurement Position	Fig.	Page
BE Vessel	BS-I	Baseline Motor Off Battery	Drive Structure	D-1	D-4
BE Vessel	BS-II	Baseline Motor Min Battery	Drive Structure	D-2	D-5
BE Vessel	BS-III	Baseline Motor Off 2x Genset	Drive Structure	D-3	D-6
BE Vessel	BS-IV	Baseline Motor Min 2x Genset	Drive Structure	D-4	D-7
BE Vessel	ST-BATT-I	Straight Run 6 kts Battery	Drive Structure	D-5	D-8
BE Vessel	ST-BATT-II	Straight Run 7 kts Battery	Drive Structure	D-6	D-9
BE Vessel	ST-BATT-III	Straight Run 8 kts Battery	Drive Structure	D-7	D-10
BE Vessel	ST-BATT-IV	Straight Run 9 kts Battery	Drive Structure	D-8	D-11
BE Vessel	ST-BATT-V	Straight Run 10 kts Battery	Drive Structure	D-9	D-12
BE Vessel	ST-GENS-I	Straight Run 6 kts 2x Gensets	Drive Structure	D-10	D-13
BE Vessel	ST-GENS-II	Straight Run 7 kts 2x Gensets	Drive Structure	D-11	D-14
BE Vessel	ST-GENS-III	Straight Run 8 kts 2x Gensets	Drive Structure	D-12	D-15
BE Vessel	ST-GENS-IV	Straight Run 9 kts 2x Gensets	Drive Structure	D-13	D-16
BE Vessel	ST-GENS-V	Straight Run 10 kts 2x Gensets	Drive Structure	D-14	D-17
BE Vessel	BP-I	Bollard Pull 20% Power Battery	Drive Structure	D-15	D-18
BE Vessel	BP-II	Bollard Pull 55% Power Battery	Drive Structure	D-16	D-19
BE Vessel	BP-III	Bollard Pull 75% Power Battery	Drive Structure	D-17	D-20
BE Vessel	BP-IV	Bollard Pull 100% Power Battery	Drive Structure	D-18	D-21
BE Vessel	BP-V	Bollard Pull 20% Power 2x Genset	Drive Structure	D-19	D-22
BE Vessel	BP-VI	Bollard Pull 55% Power 2x Genset	Drive Structure	D-20	D-23
BE Vessel	BS-I	Baseline Motor Off Battery	Genset Structure	D-21	D-24
BE Vessel	BS-II	Baseline Motor Min Battery	Genset Structure	D-22	D-25
BE Vessel	BS-III	Baseline Motor Off 2x Genset	Genset Structure	D-23	D-26
BE Vessel	BS-IV	Baseline Motor Min 2x Genset	Genset Structure	D-24	D-27
BE Vessel	ST-BATT-I	Straight Run 6 kts Battery	Genset Structure	D-25	D-28
BE Vessel	ST-BATT-II	Straight Run 7 kts Battery	Genset Structure	D-26	D-29
BE Vessel	ST-BATT-III	Straight Run 8 kts Battery	Genset Structure	D-27	D-30
BE Vessel	ST-BATT-IV	Straight Run 9 kts Battery	Genset Structure	D-28	D-31
BE Vessel	ST-BATT-V	Straight Run 10 kts Battery	Genset Structure	D-29	D-32
BE Vessel	ST-GENS-I	Straight Run 6 kts 2x Gensets	Genset Structure	D-30	D-33
BE Vessel	ST-GENS-II	Straight Run 7 kts 2x Gensets	Genset Structure	D-31	D-34
BE Vessel	ST-GENS-III	Straight Run 8 kts 2x Gensets	Genset Structure	D-32	D-35
BE Vessel	ST-GENS-IV	Straight Run 9 kts 2x Gensets	Genset Structure	D-33	D-36

Vessel	Run Type	Description	Measurement Position	Fig.	Page
BE Vessel	ST-GENS-V	Straight Run 10 kts 2x Gensets	Genset Structure	D-34	D-37
BE Vessel	BP-I	Bollard Pull 20% Power Battery	Genset Structure	D-35	D-38
BE Vessel	BP-II	Bollard Pull 55% Power Battery	Genset Structure	D-36	D-39
BE Vessel	BP-III	Bollard Pull 75% Power Battery	Genset Structure	D-37	D-40
BE Vessel	BP-IV	Bollard Pull 100% Power Battery	Genset Structure	D-38	D-41
BE Vessel	BP-V	Bollard Pull 20% Power 2x Genset	Genset Structure	D-39	D-42
BE Vessel	BP-VI	Bollard Pull 55% Power 2x Genset	Genset Structure	D-40	D-43
DM Vessel	BS-II	Baseline ME Idle, Clutch off, 2x Gensets On	Engine Structure	D-41	D-44
DM Vessel	BS-III	Baseline ME Idle, Clutch on, 2x Gensets On	Engine Structure	D-42	D-45
DM Vessel	ST-I	Straight Run 6 kts	Engine Structure	D-43	D-46
DM Vessel	ST-II	Straight Run 7 kts	Engine Structure	D-44	D-47
DM Vessel	ST-III	Straight Run 8 kts	Engine Structure	D-45	D-48
DM Vessel	ST-IV	Straight Run 9 kts	Engine Structure	D-46	D-49
DM Vessel	ST-V	Straight Run 10 kts	Engine Structure	D-47	D-50
DM Vessel	BP-I	Bollard Pull 20% Power	Engine Structure	D-48	D-51
DM Vessel	BP-II	Bollard Pull 55% Power	Engine Structure	D-49	D-52
DM Vessel	BP-III	Bollard Pull 75% Power	Engine Structure	D-50	D-53
DM Vessel	BP-IV	Bollard Pull 100% Power	Engine Structure	D-51	D-54
DM Vessel	BS-I	Baseline ME Off, Clutch off, 1x Gensets On	Drive Structure	D-52	D-55
DM Vessel	BS-II	Baseline ME Idle, Clutch off, 2x Gensets On	Drive Structure	D-53	D-56
DM Vessel	BS-III	Baseline ME Idle, Clutch on, 2x Gensets On	Drive Structure	D-54	D-57
DM Vessel	ST-I	Straight Run 6 kts	Drive Structure	D-55	D-58
DM Vessel	ST-II	Straight Run 7 kts	Drive Structure	D-56	D-59
DM Vessel	ST-III	Straight Run 8 kts	Drive Structure	D-57	D-60
DM Vessel	ST-IV	Straight Run 9 kts	Drive Structure	D-58	D-61
DM Vessel	ST-V	Straight Run 10 kts	Drive Structure	D-59	D-62
DM Vessel	BP-I	Bollard Pull 20% Power	Drive Structure	D-60	D-63
DM Vessel	BP-II	Bollard Pull 55% Power	Drive Structure	D-61	D-64
DM Vessel	BP-III	Bollard Pull 75% Power	Drive Structure	D-62	D-65
DM Vessel	BP-IV	Bollard Pull 100% Power	Drive Structure	D-63	D-66
DM Vessel	BS-I	Baseline ME Off, Clutch off, 1x Gensets On	Genset Structure	D-64	D-67
DM Vessel	BS-II	Baseline ME Idle, Clutch off, 2x Gensets On	Genset Structure	D-65	D-68
DM Vessel	BS-III	Baseline ME Idle, Clutch on, 2x Gensets On	Genset Structure	D-66	D-69
DM Vessel	ST-I	Straight Run 6 kts	Genset Structure	D-67	D-70

Vessel	Run Type	Description	Measurement Position	Fig.	Page
DM Vessel	ST-II	Straight Run 7 kts	Genset Structure	D-68	D-71
DM Vessel	ST-III	Straight Run 8 kts	Genset Structure	D-69	D-72
DM Vessel	ST-IV	Straight Run 9 kts	Genset Structure	D-70	D-73
DM Vessel	ST-V	Straight Run 10 kts	Genset Structure	D-71	D-74
DM Vessel	BP-I	Bollard Pull 20% Power	Genset Structure	D-72	D-75
DM Vessel	BP-II	Bollard Pull 55% Power	Genset Structure	D-73	D-76
DM Vessel	BP-III	Bollard Pull 75% Power	Genset Structure	D-74	D-77
DM Vessel	BP-IV	Bollard Pull 100% Power	Genset Structure	D-75	D-78

D.1 BE Vessel - Structure-borne Noise - Drive Structure - Baseline Stationary (BS)

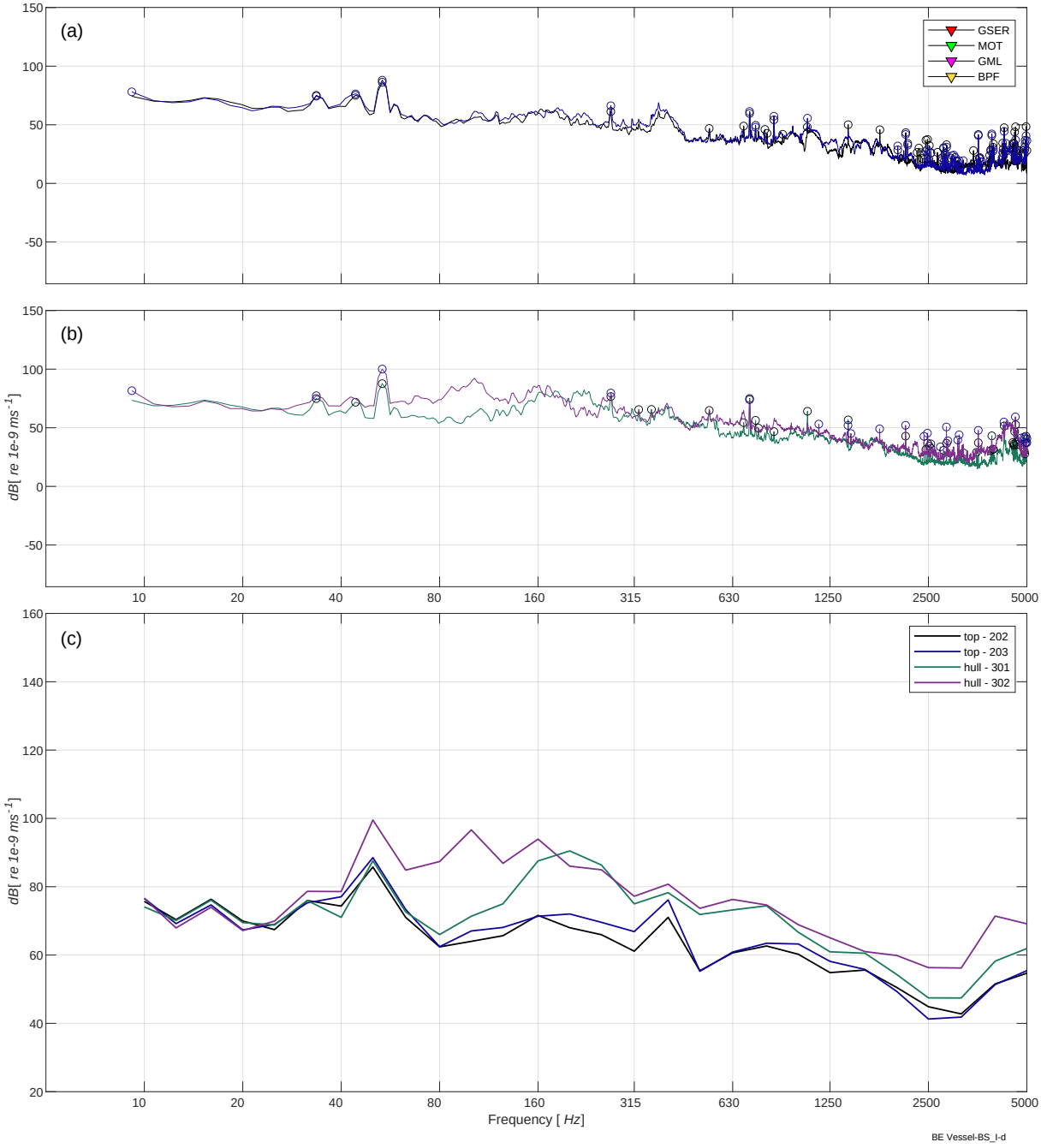


Figure D-1: Structural velocity narrow-band spectra (a) on the seating, (b) on the hull and the respective (c) third-octave band spectra. Run: BE BS-I - Drive Structure

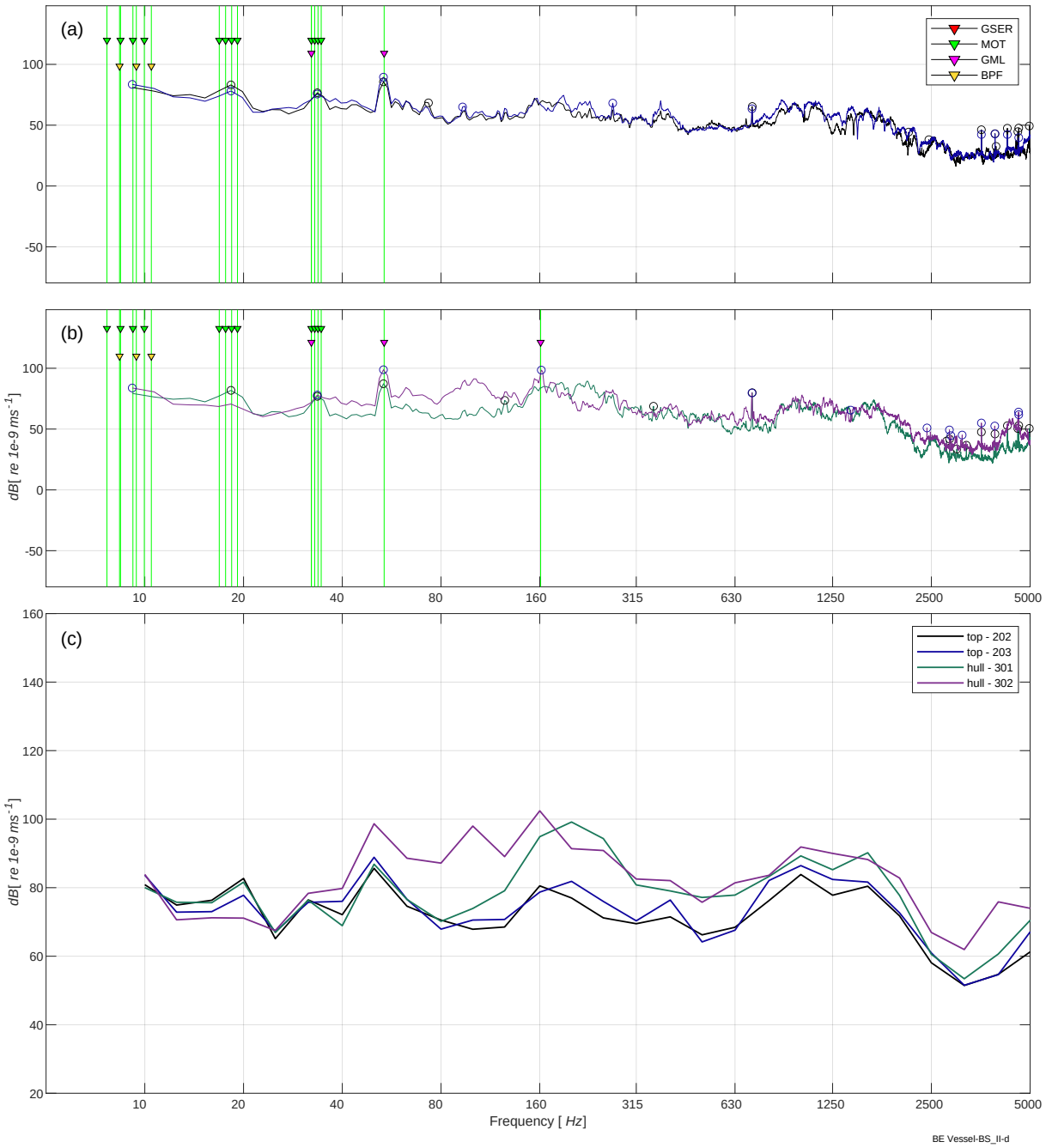


Figure D-2: Structural velocity narrow-band spectra (a) on the seating, (b) on the hull and the respective (c) third-octave band spectra. Run: BE BS-II - Drive Structure

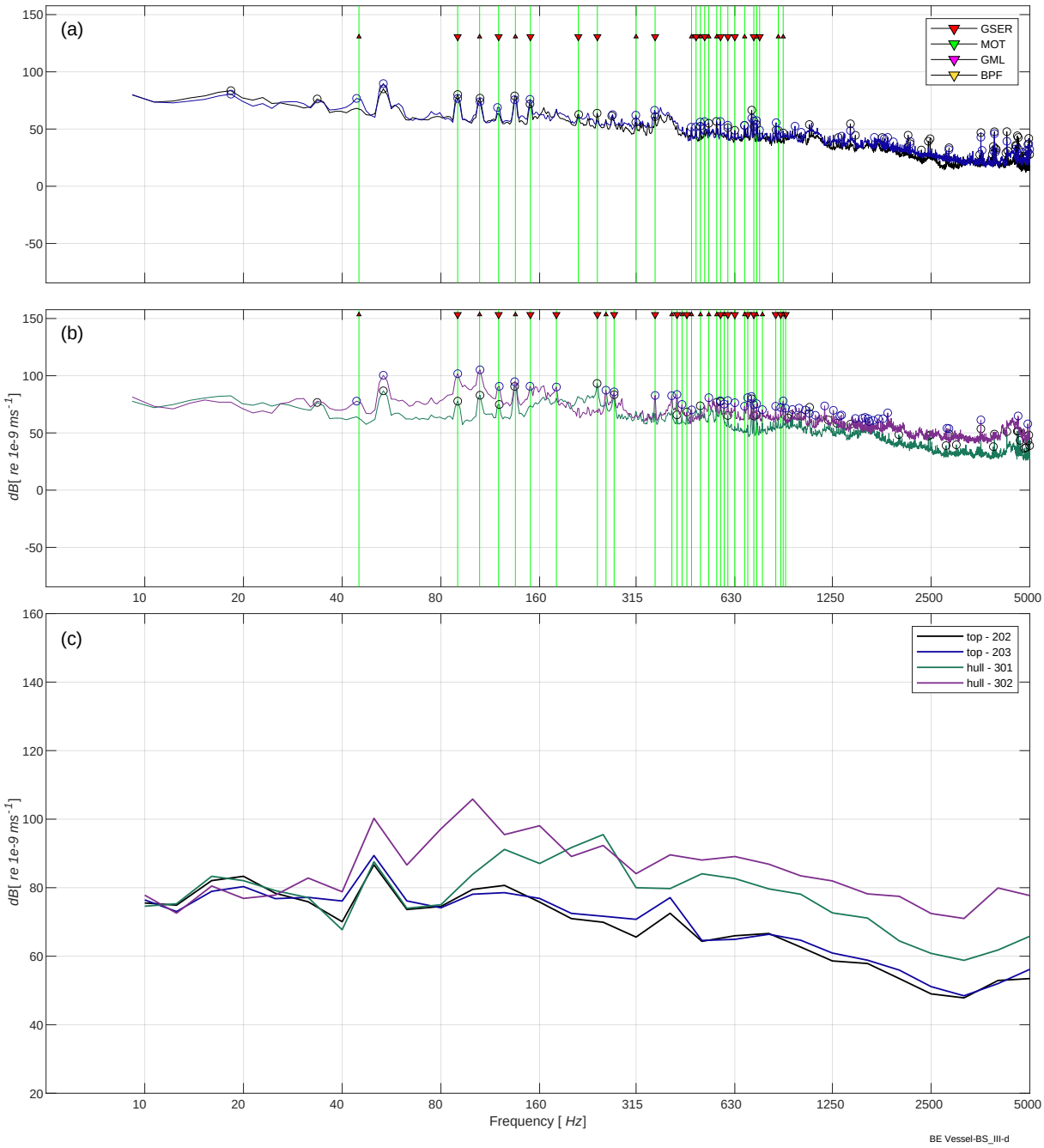


Figure D-3: Structural velocity narrow-band spectra (a) on the seating, (b) on the hull and the respective (c) third-octave band spectra. Run: BE BS-III - Drive Structure

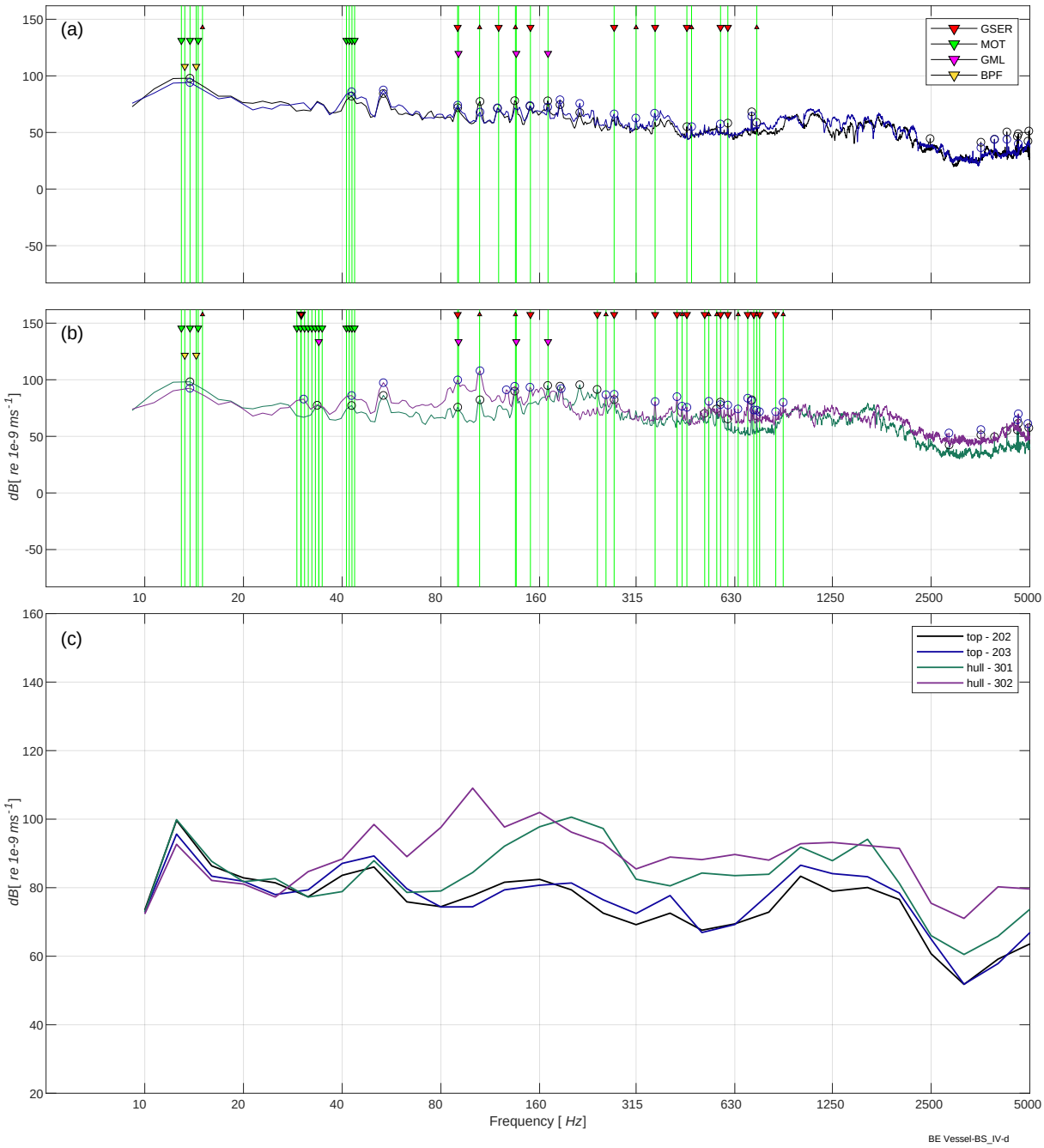


Figure D-4: Structural velocity narrow-band spectra (a) on the seating, (b) on the hull and the respective (c) third-octave band spectra. Run: BE BS-IV - Drive Structure

D.2 BE Vessel - Structure-borne Noise - Drive Structure - Straight Run On Battery (ST-BATT)

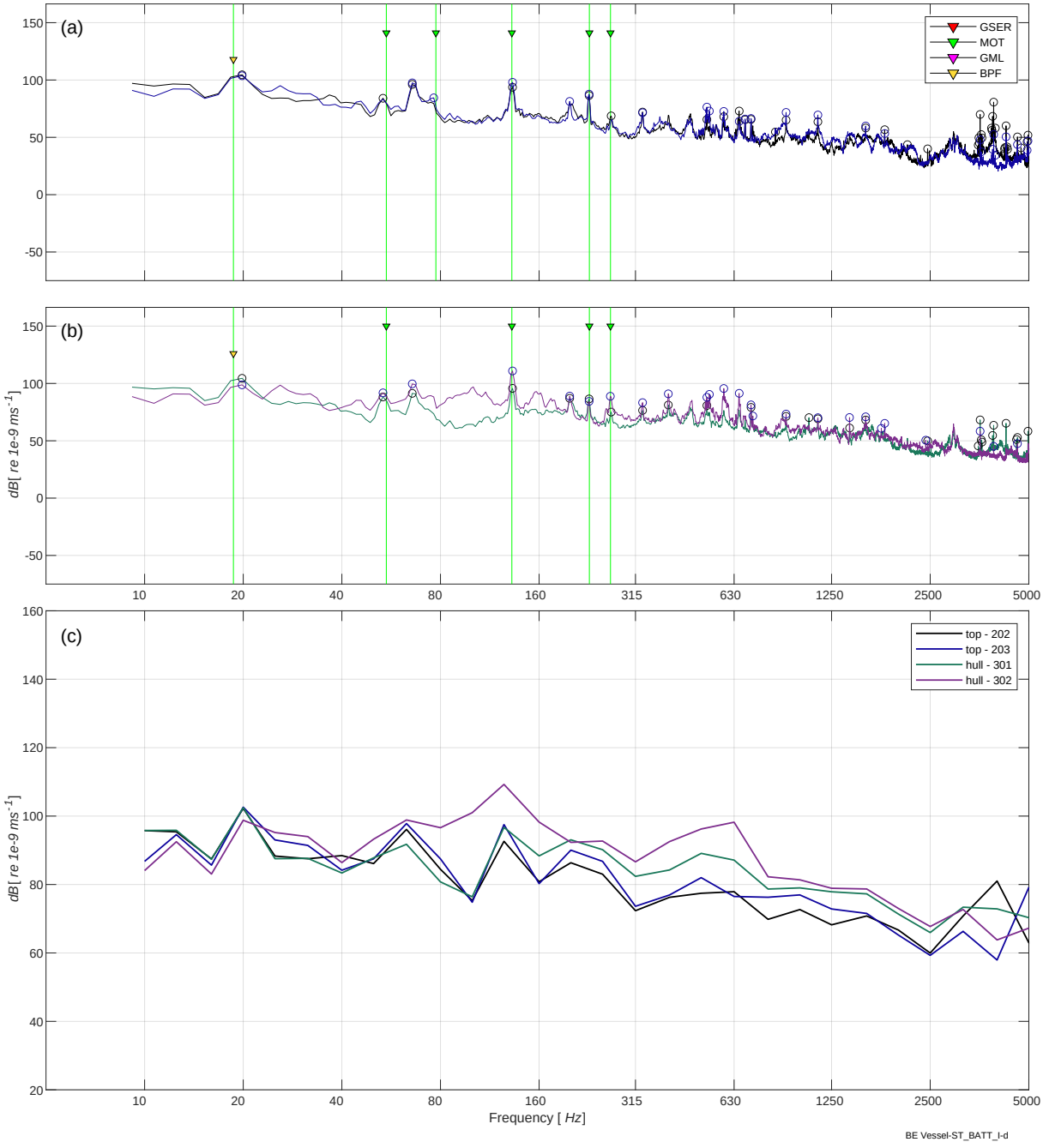


Figure D-5: Structural velocity narrow-band spectra (a) on the seating, (b) on the hull and the respective (c) third-octave band spectra. Run: BE ST-BATT-I - Drive Structure

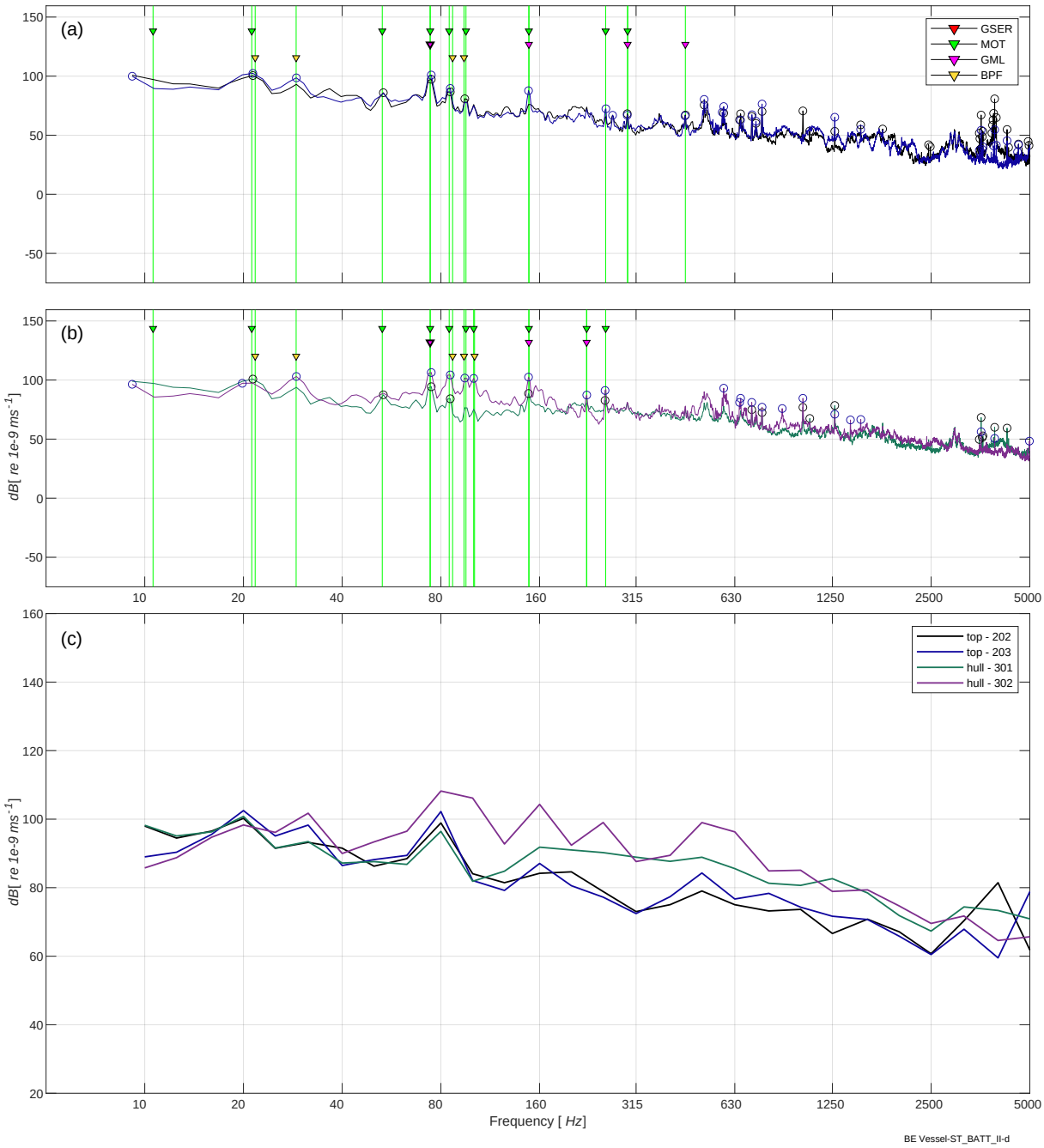


Figure D-6: Structural velocity narrow-band spectra (a) on the seating, (b) on the hull and the respective (c) third-octave band spectra. Run: BE ST-BATT-II - Drive Structure

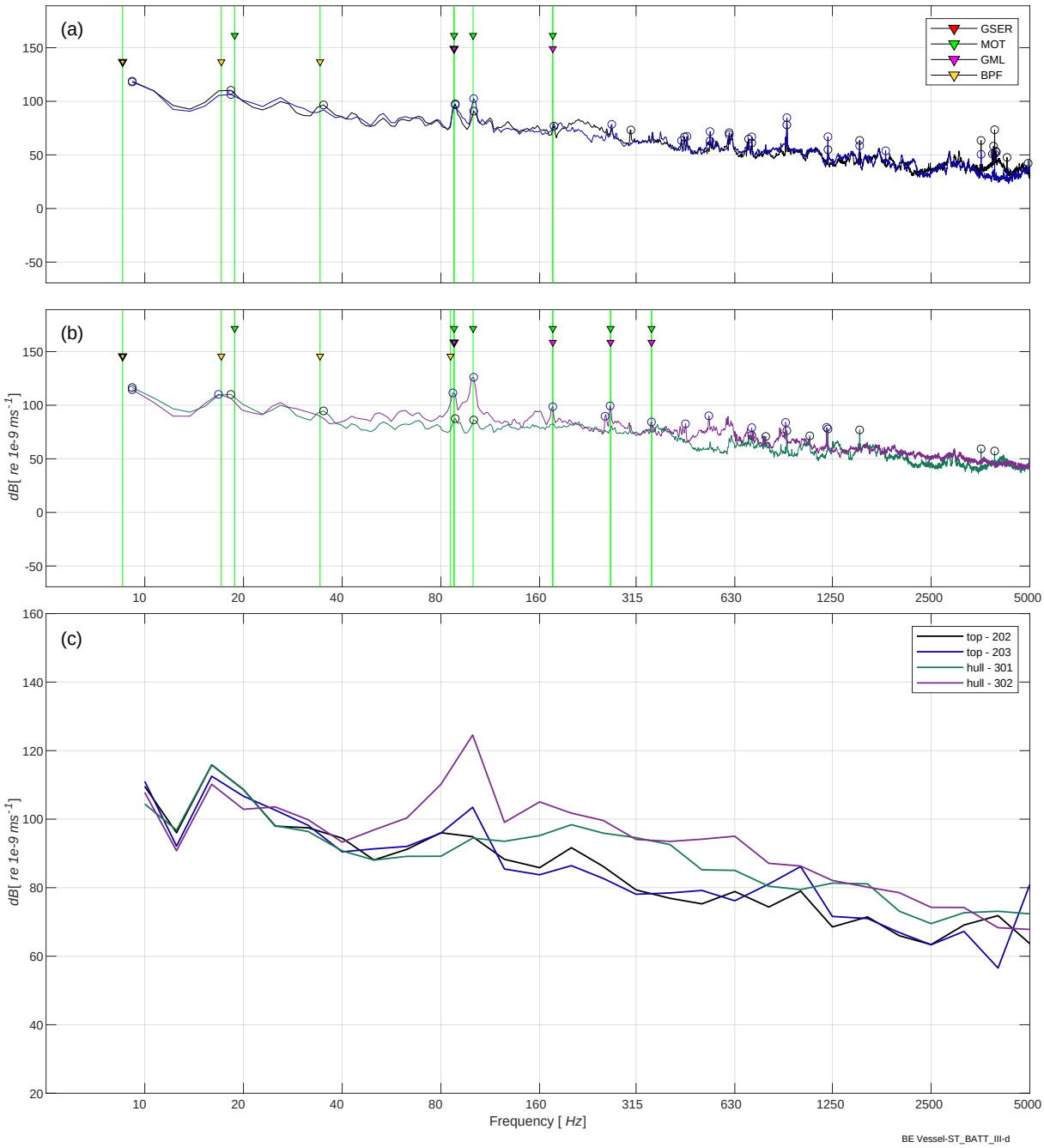


Figure D-7: Structural velocity narrow-band spectra (a) on the seating, (b) on the hull and the respective (c) third-octave band spectra. Run: BE ST-BATT-III - Drive Structure

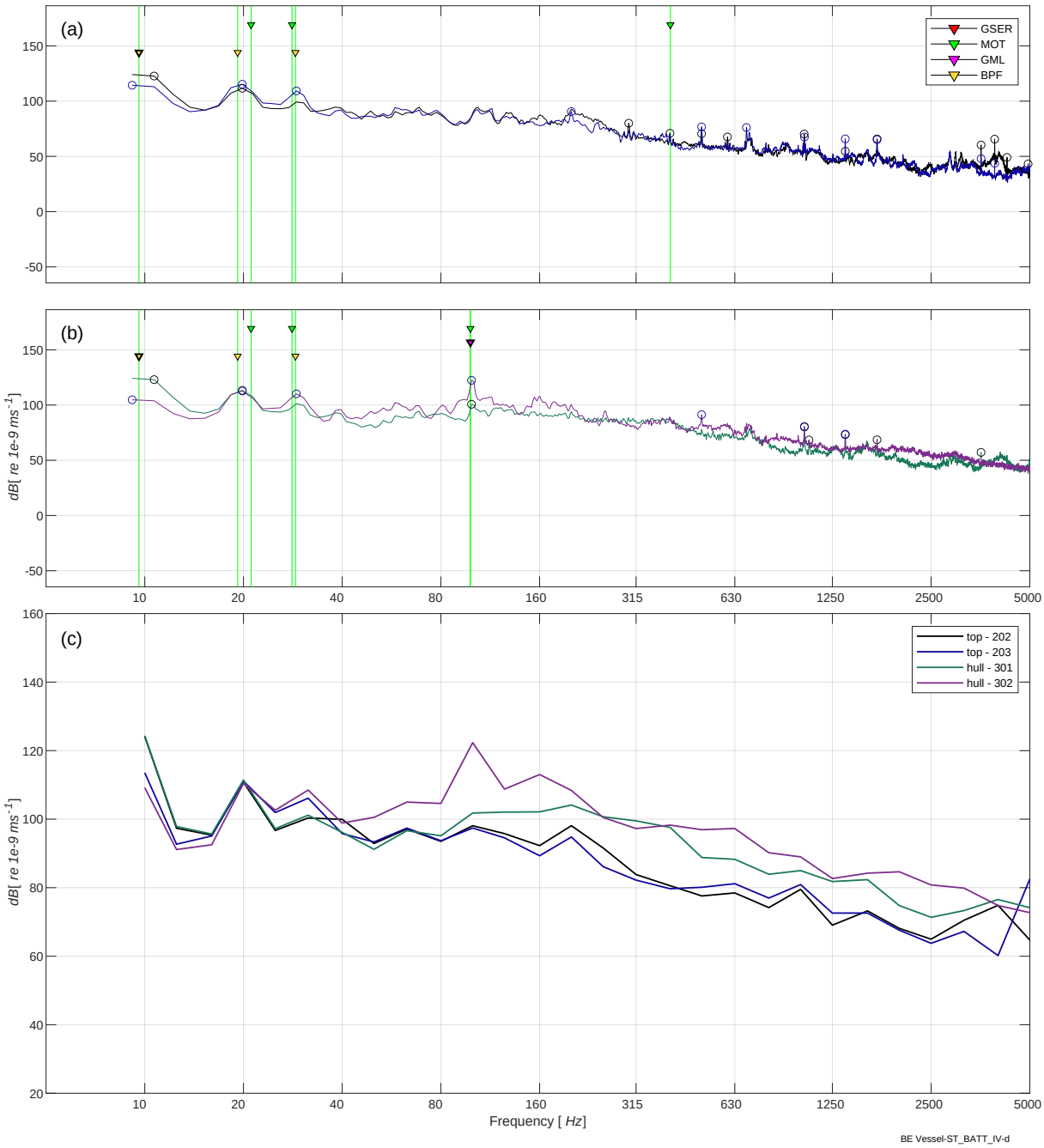


Figure D-8: Structural velocity narrow-band spectra (a) on the seating, (b) on the hull and the respective (c) third-octave band spectra. Run: BE ST-BATT-IV - Drive Structure

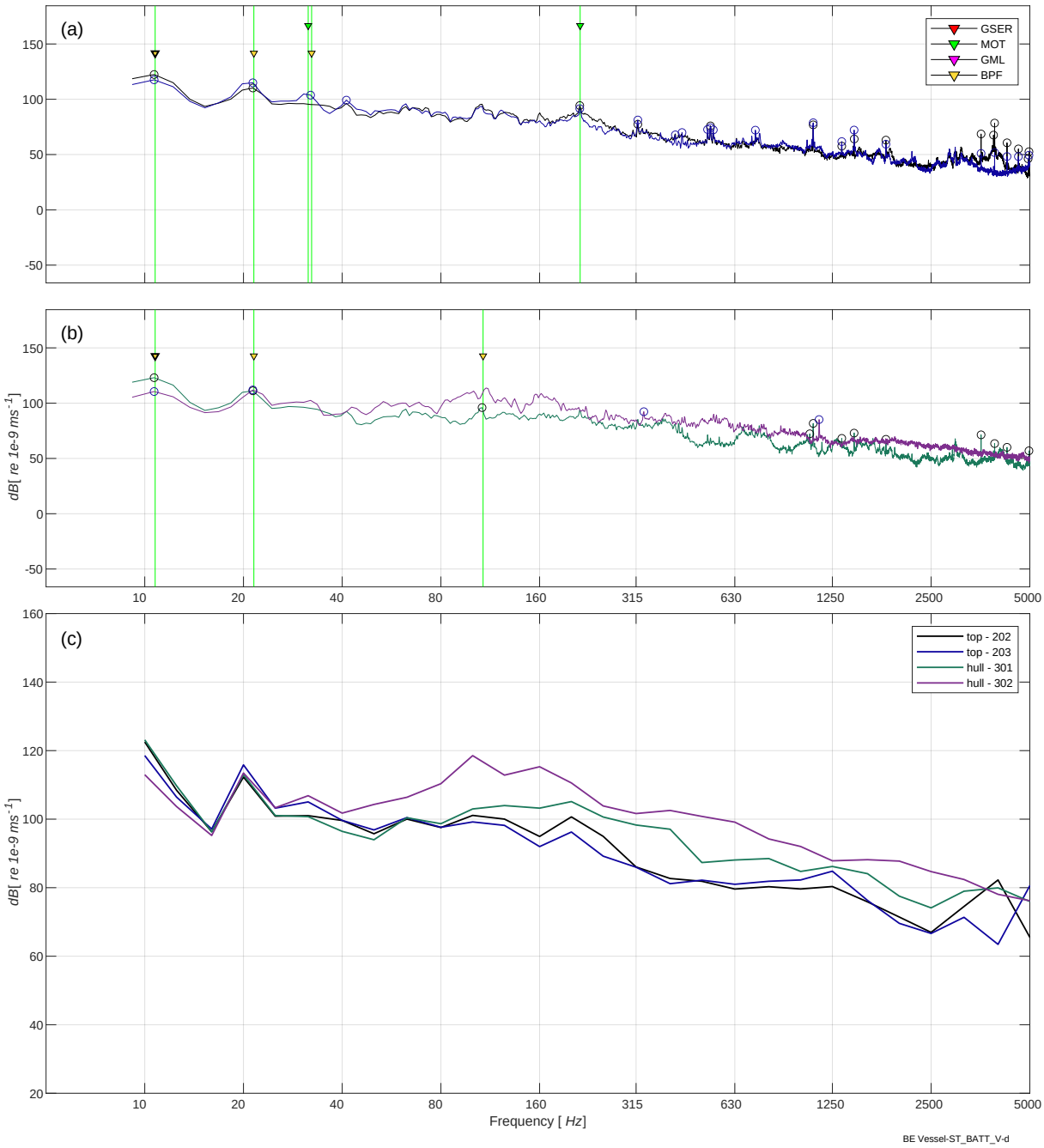


Figure D-9: Structural velocity narrow-band spectra (a) on the seating, (b) on the hull and the respective (c) third-octave band spectra. Run: BE ST-BATT-V - Drive Structure

D.3 BE Vessel - Structure-borne Noise - Drive Structure - Straight Run On Gensets (ST-GENS)

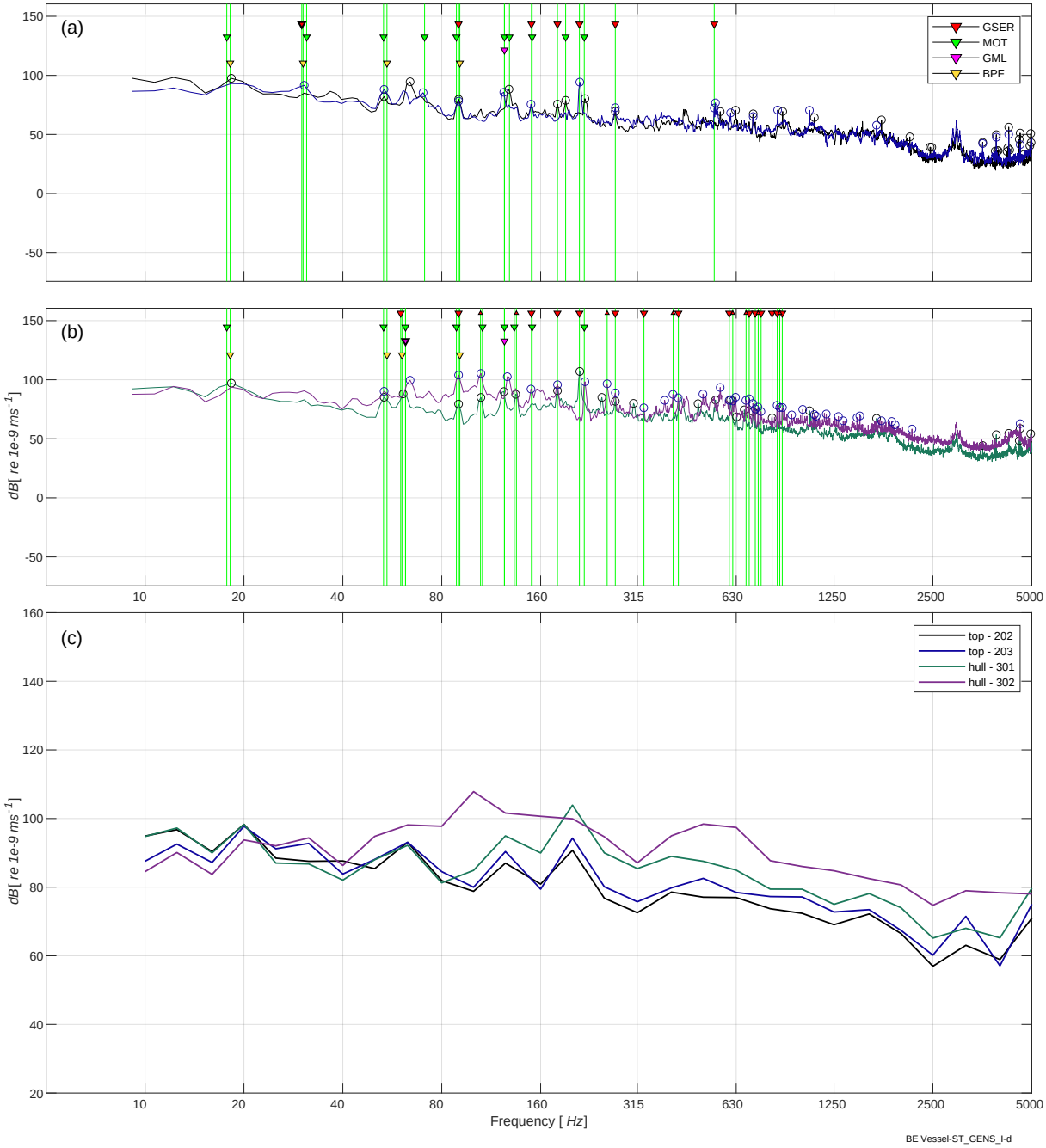


Figure D-10: Structural velocity narrow-band spectra (a) on the seating, (b) on the hull and the respective (c) third-octave band spectra. Run: BE ST-GENS-I - Drive Structure

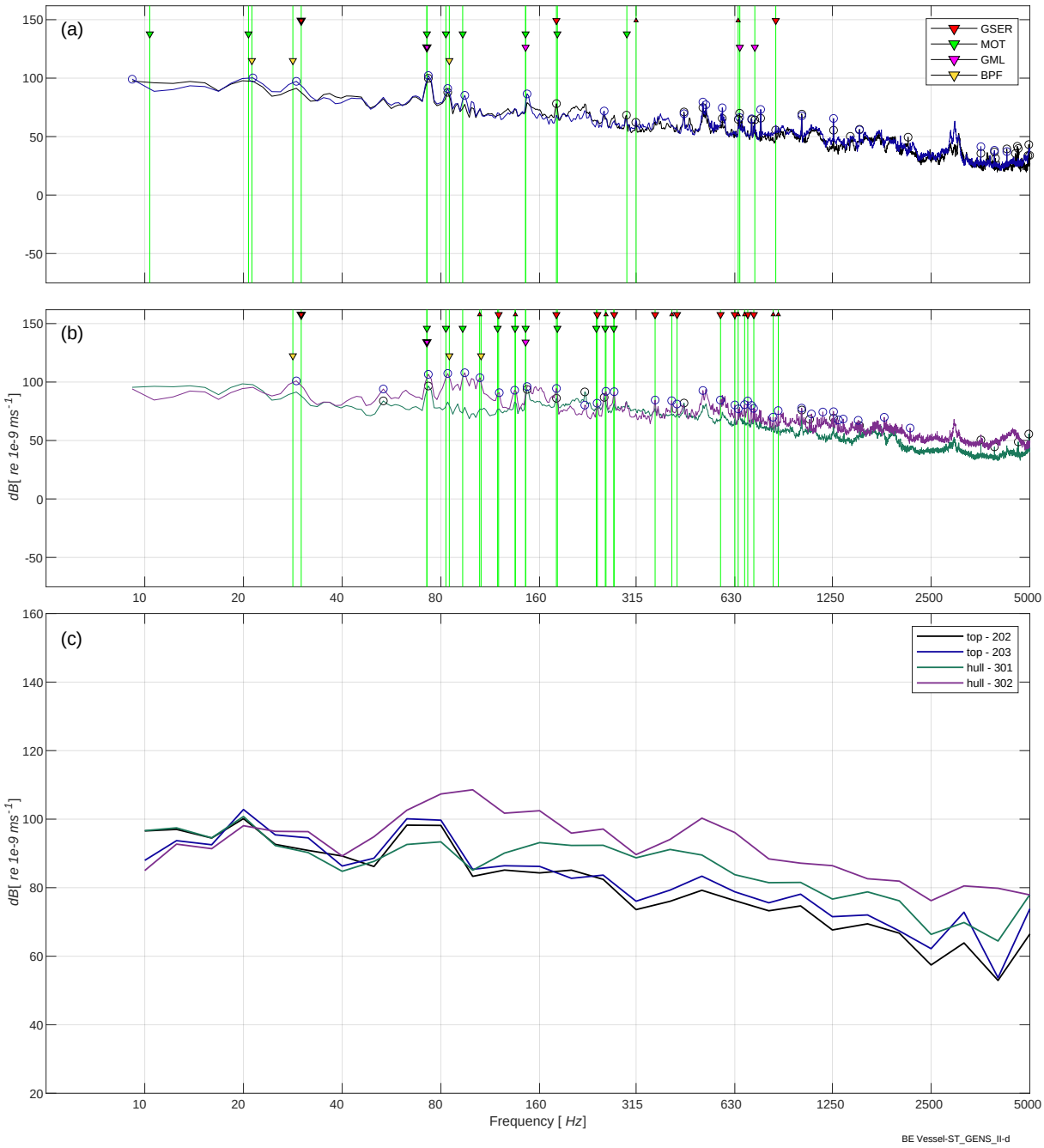


Figure D-11: Structural velocity narrow-band spectra (a) on the seating, (b) on the hull and the respective (c) third-octave band spectra. Run: BE ST-GENS-II - Drive Structure

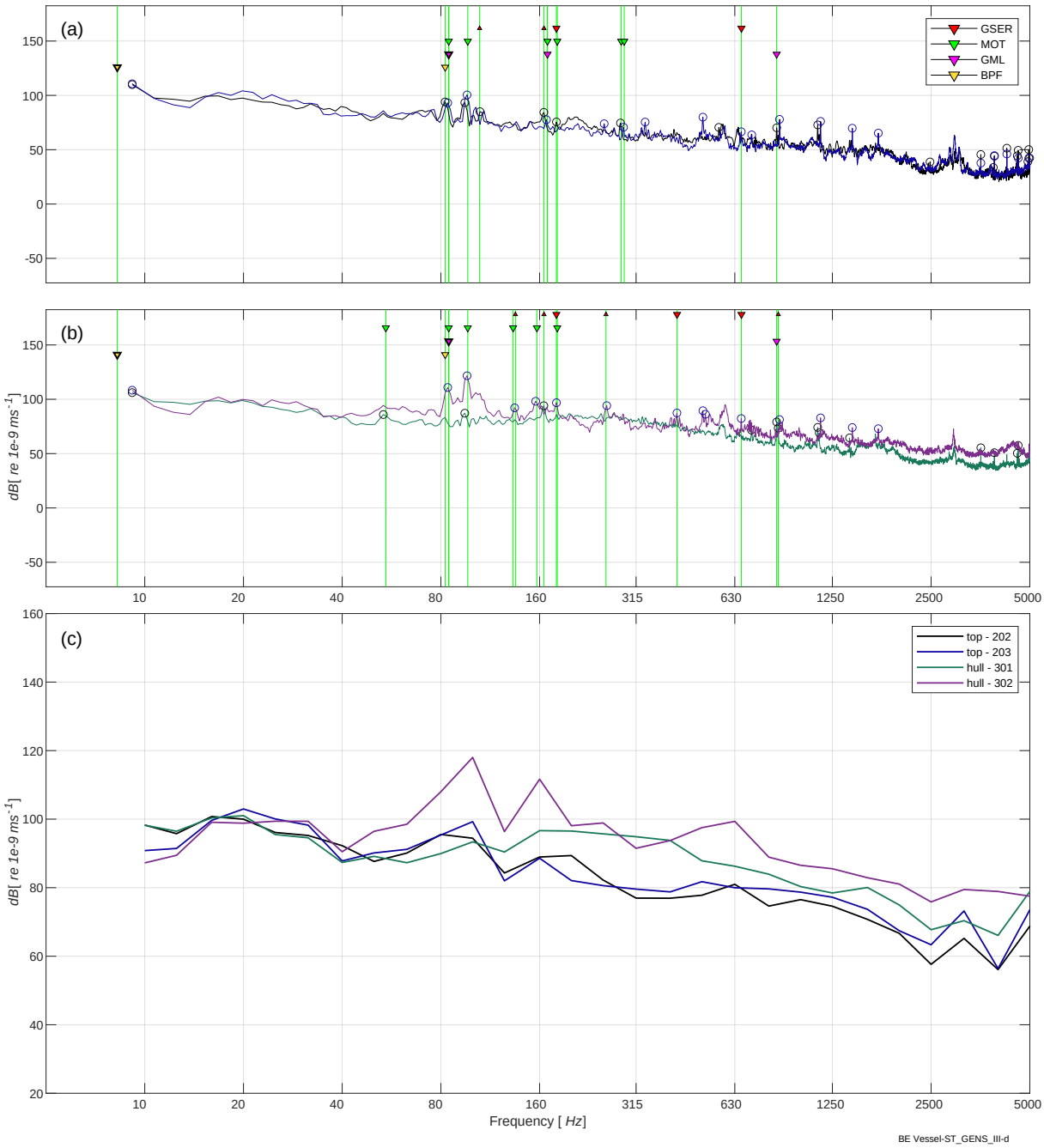


Figure D-12: Structural velocity narrow-band spectra (a) on the seating, (b) on the hull and the respective (c) third-octave band spectra. Run: BE ST-GENS-III - Drive Structure

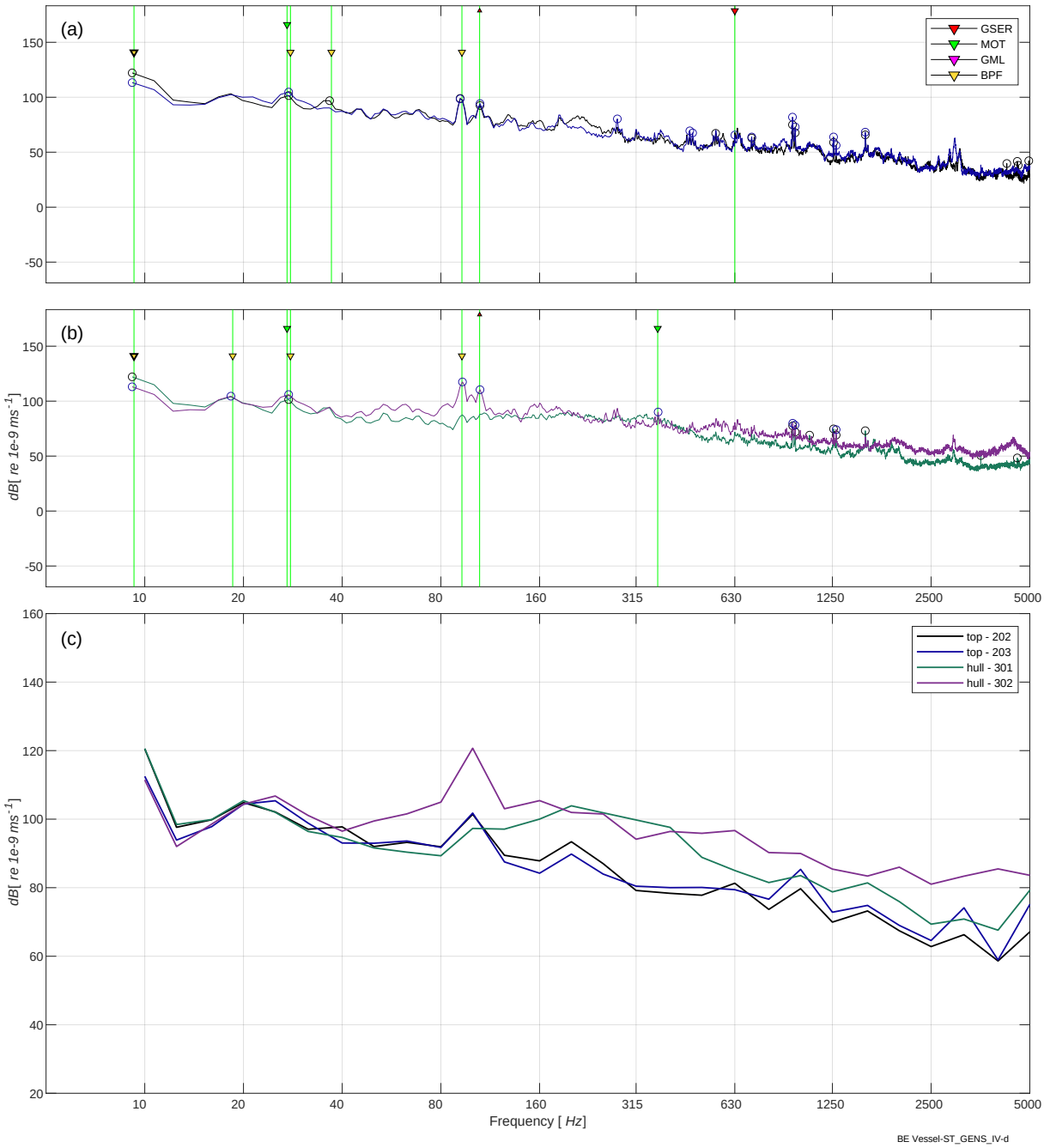


Figure D-13: Structural velocity narrow-band spectra (a) on the seating, (b) on the hull and the respective (c) third-octave band spectra. Run: BE ST-GENS-IV - Drive Structure

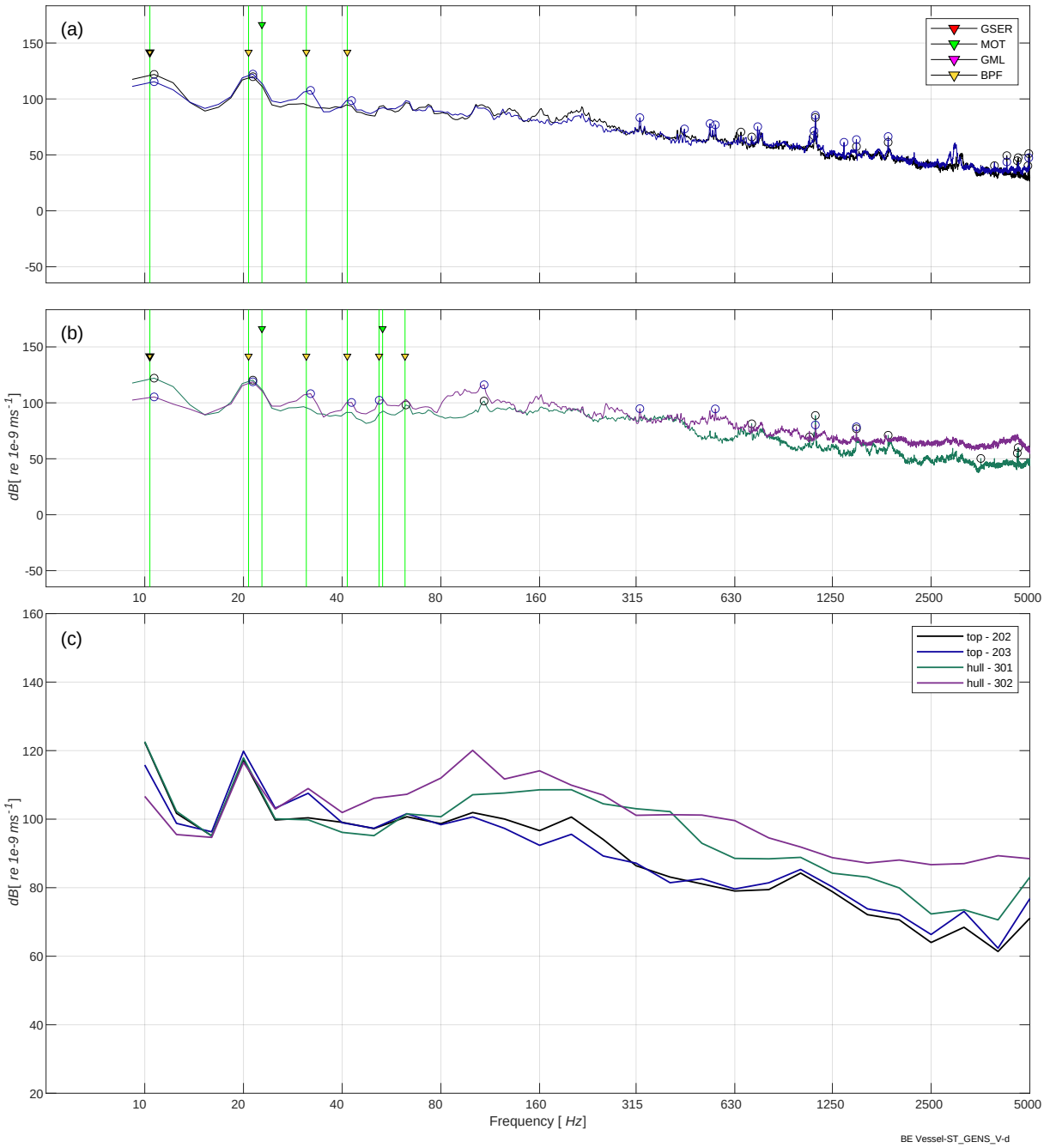


Figure D-14: Structural velocity narrow-band spectra (a) on the seating, (b) on the hull and the respective (c) third-octave band spectra. Run: BE ST-GENS-V - Drive Structure

D.4 BE Vessel - Structure-borne Noise - Drive Structure - Bollard Pull (BP)

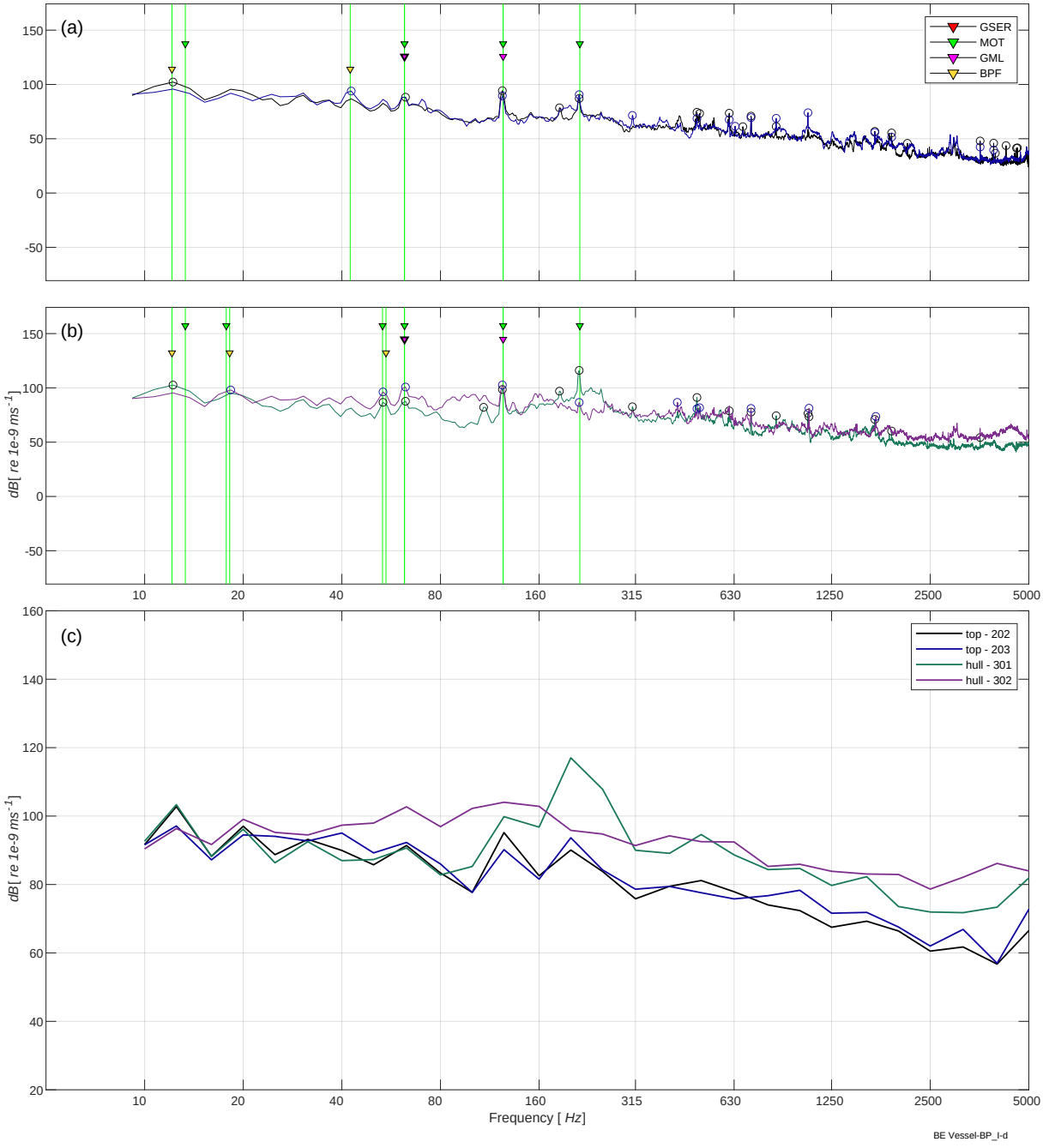


Figure D-15: Structural velocity narrow-band spectra (a) on the seating, (b) on the hull and the respective (c) third-octave band spectra. Run: BE BP-I - Drive Structure

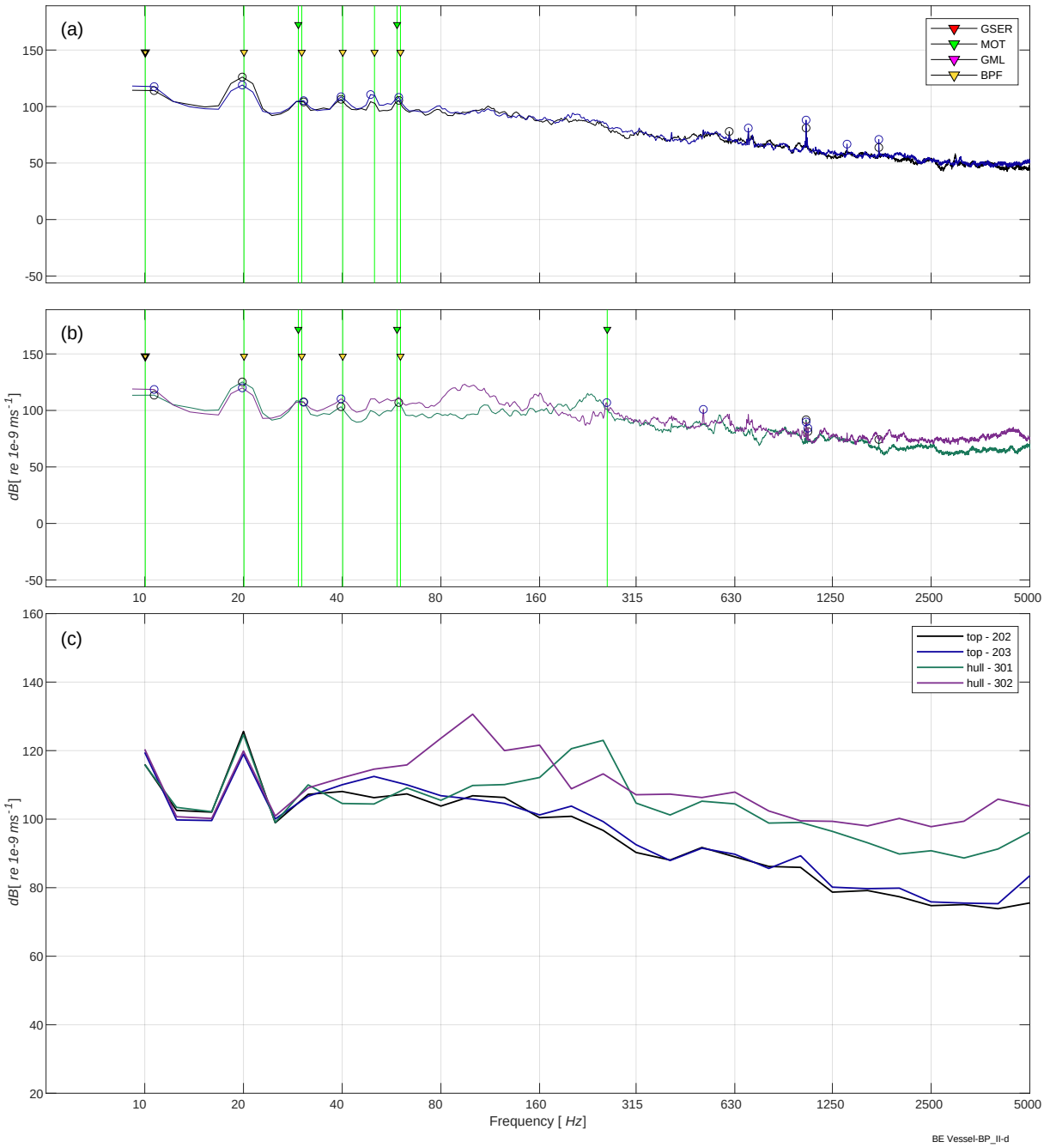


Figure D-16: Structural velocity narrow-band spectra (a) on the seating, (b) on the hull and the respective (c) third-octave band spectra. Run: BE BP-II - Drive Structure

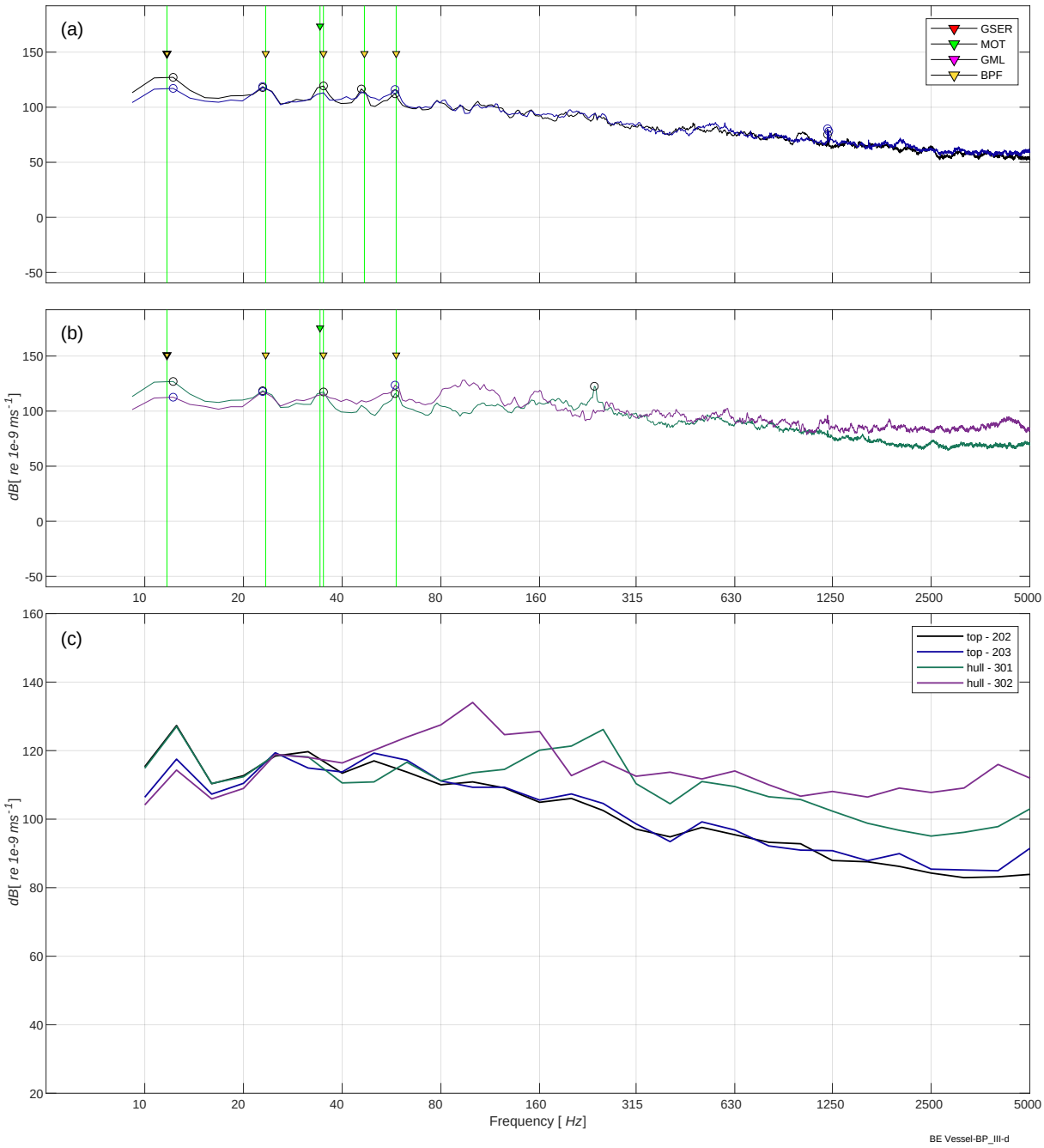


Figure D-17: Structural velocity narrow-band spectra (a) on the seating, (b) on the hull and the respective (c) third-octave band spectra. Run: BE BP-III - Drive Structure

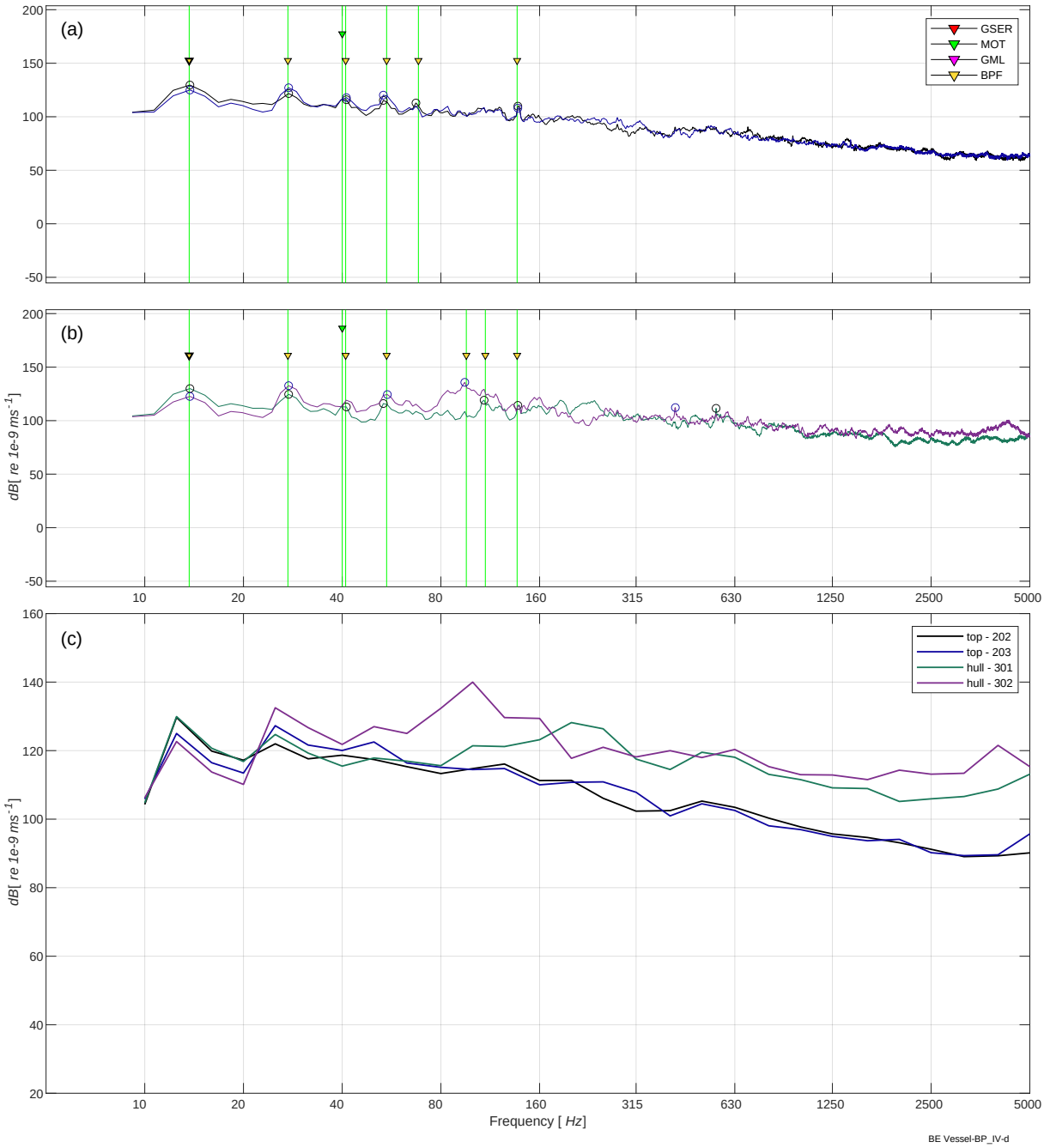


Figure D-18: Structural velocity narrow-band spectra (a) on the seating, (b) on the hull and the respective (c) third-octave band spectra. Run: BE BP-IV - Drive Structure

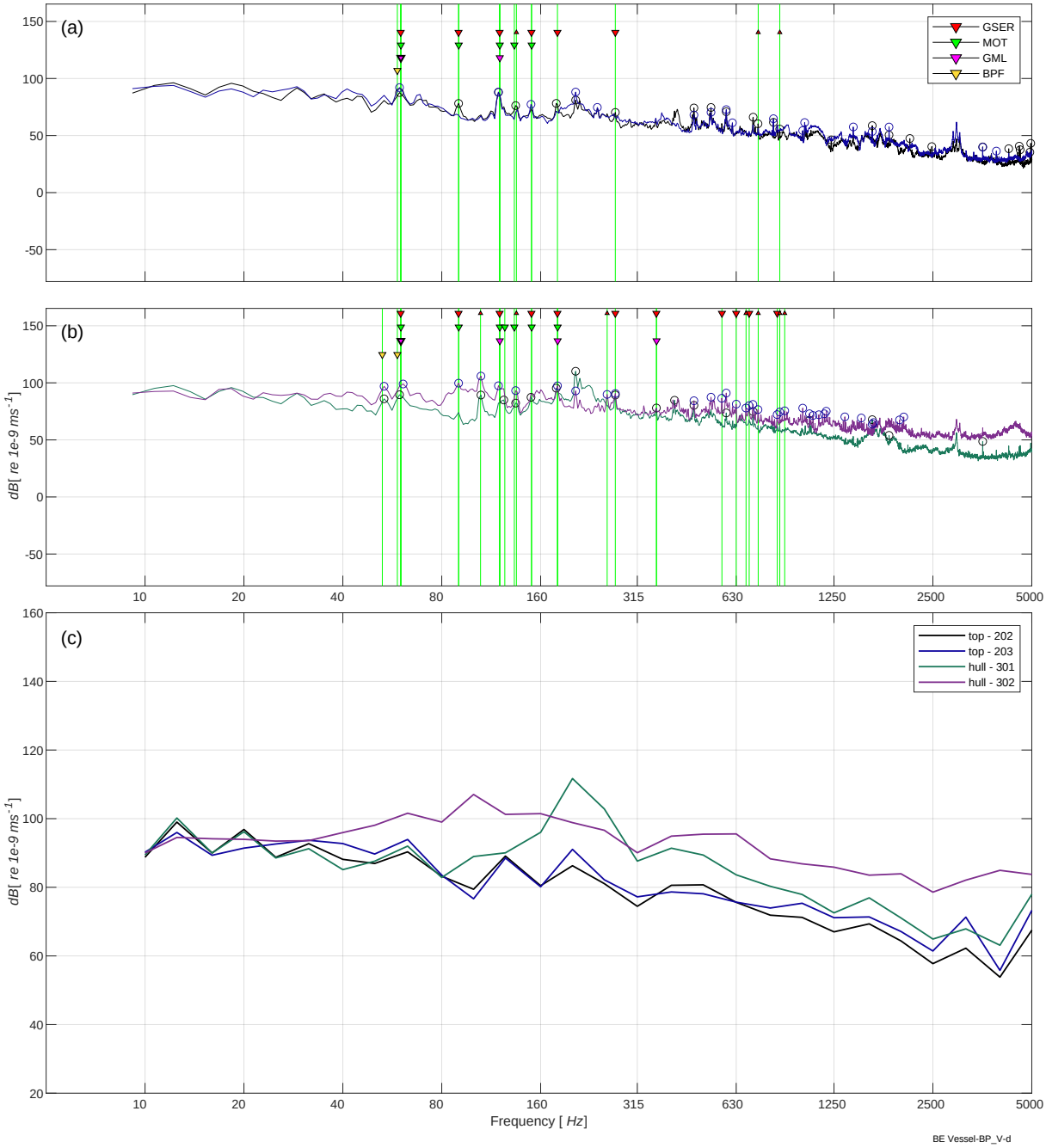


Figure D-19: Structural velocity narrow-band spectra (a) on the seating, (b) on the hull and the respective (c) third-octave band spectra. Run: BE BP-V - Drive Structure

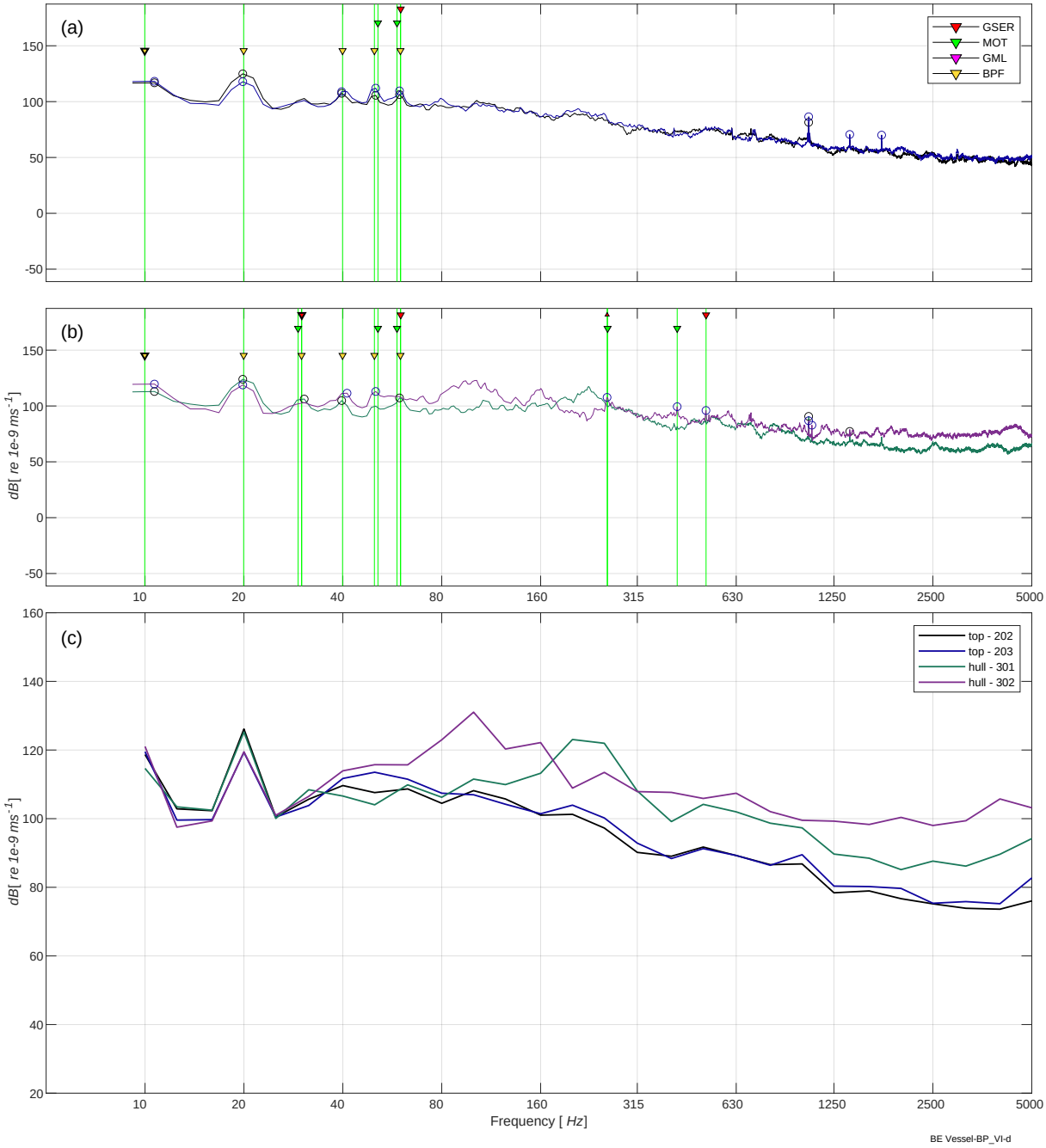


Figure D-20: Structural velocity narrow-band spectra (a) on the seating, (b) on the hull and the respective (c) third-octave band spectra. Run: BE BP-VI - Drive Structure

D.5 BE Vessel - Structure-borne Noise - Genset Structure - Baseline Stationary (BS)

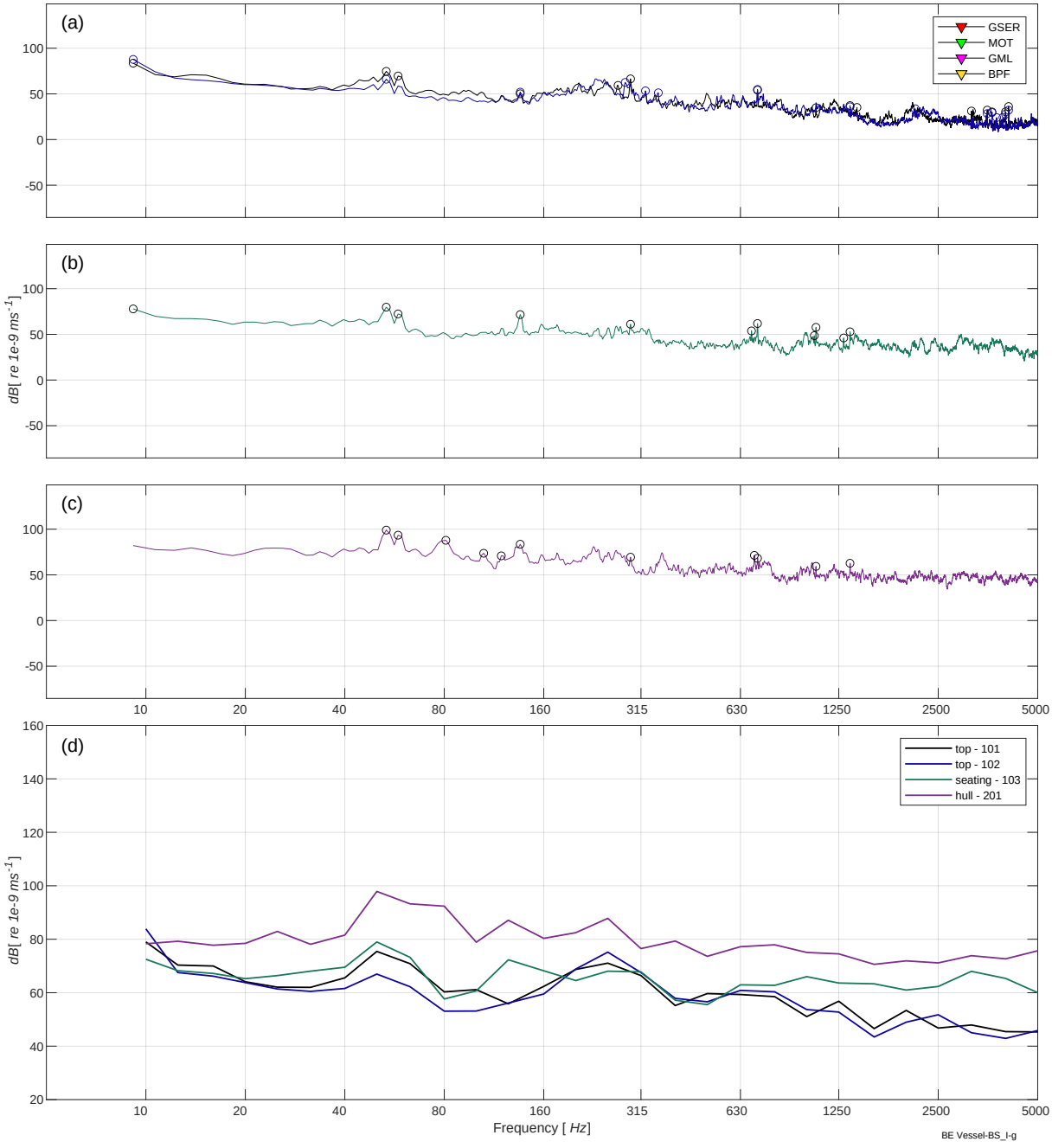


Figure D-21: Structural velocity narrow-band spectra (a) above the resilient mount, (b) on the seating, (c) on the hull and the respective (d) third-octave band spectra. Run: BE BS-I - Genset Structure

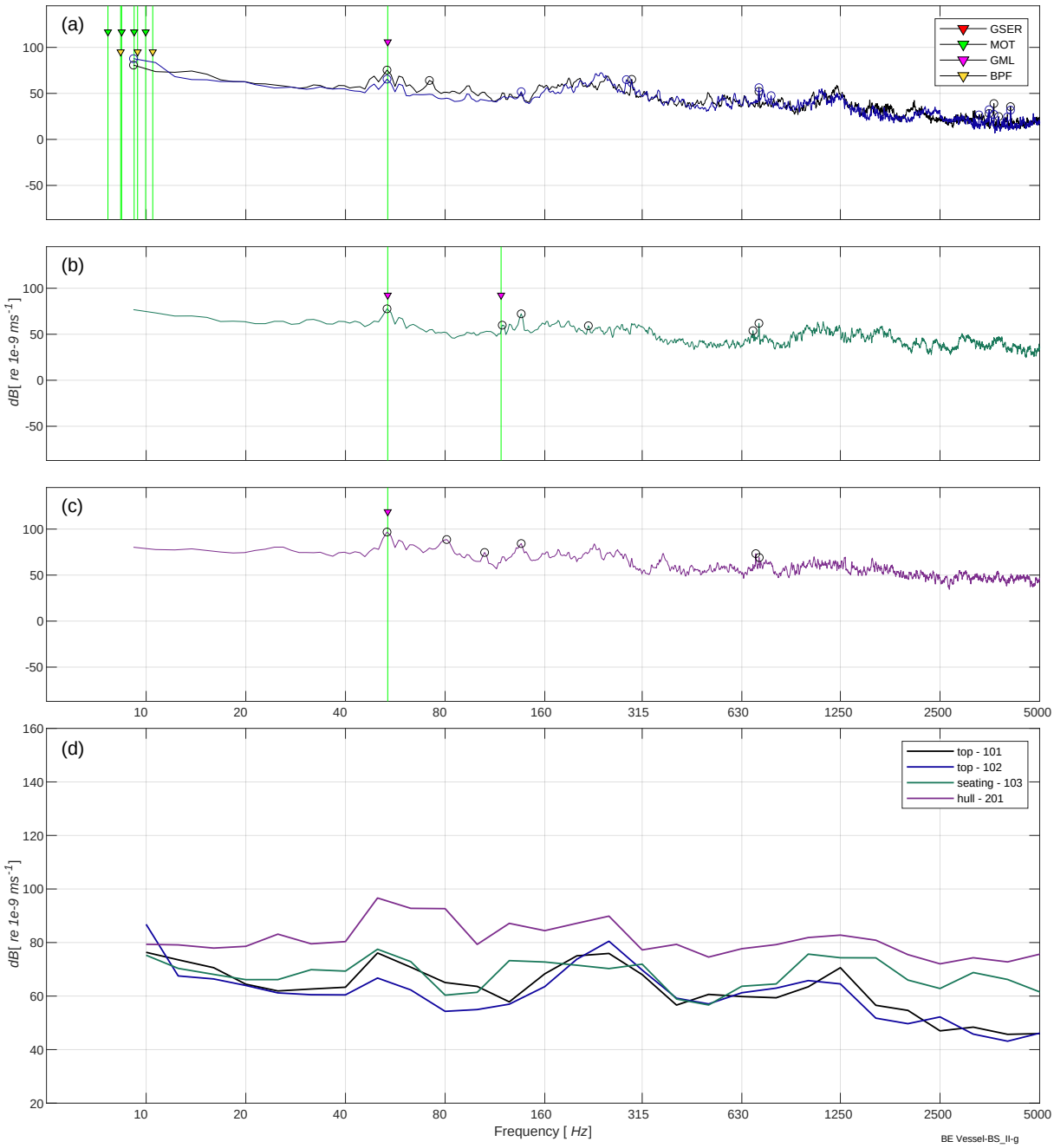


Figure D-22: Structural velocity narrow-band spectra (a) above the resilient mount, (b) on the seating, (c) on the hull and the respective (d) third-octave band spectra. Run: BE BS-II - Genset Structure

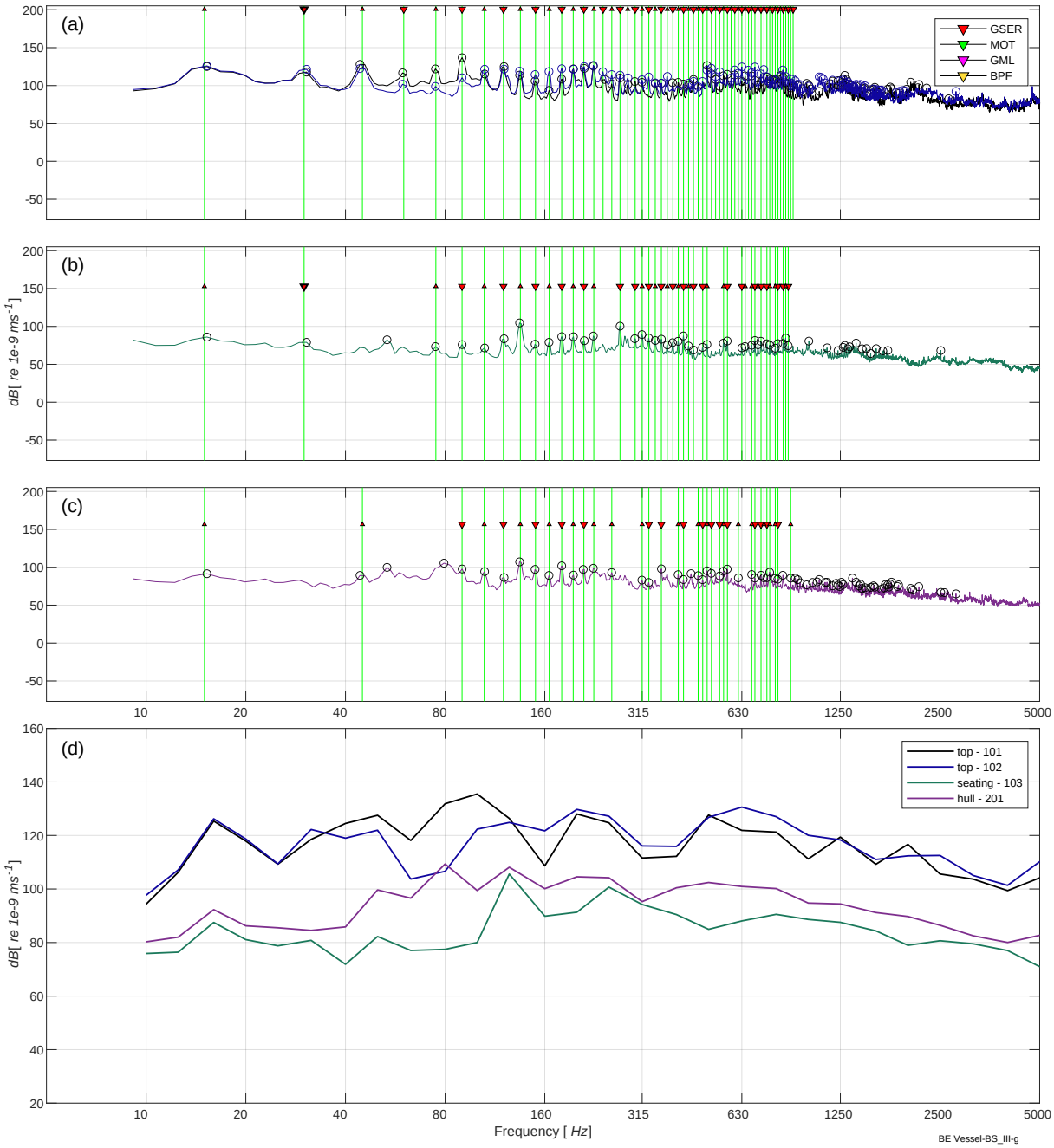


Figure D-23: Structural velocity narrow-band spectra (a) above the resilient mount, (b) on the seating, (c) on the hull and the respective (d) third-octave band spectra. Run: BE BS-III - Genset Structure

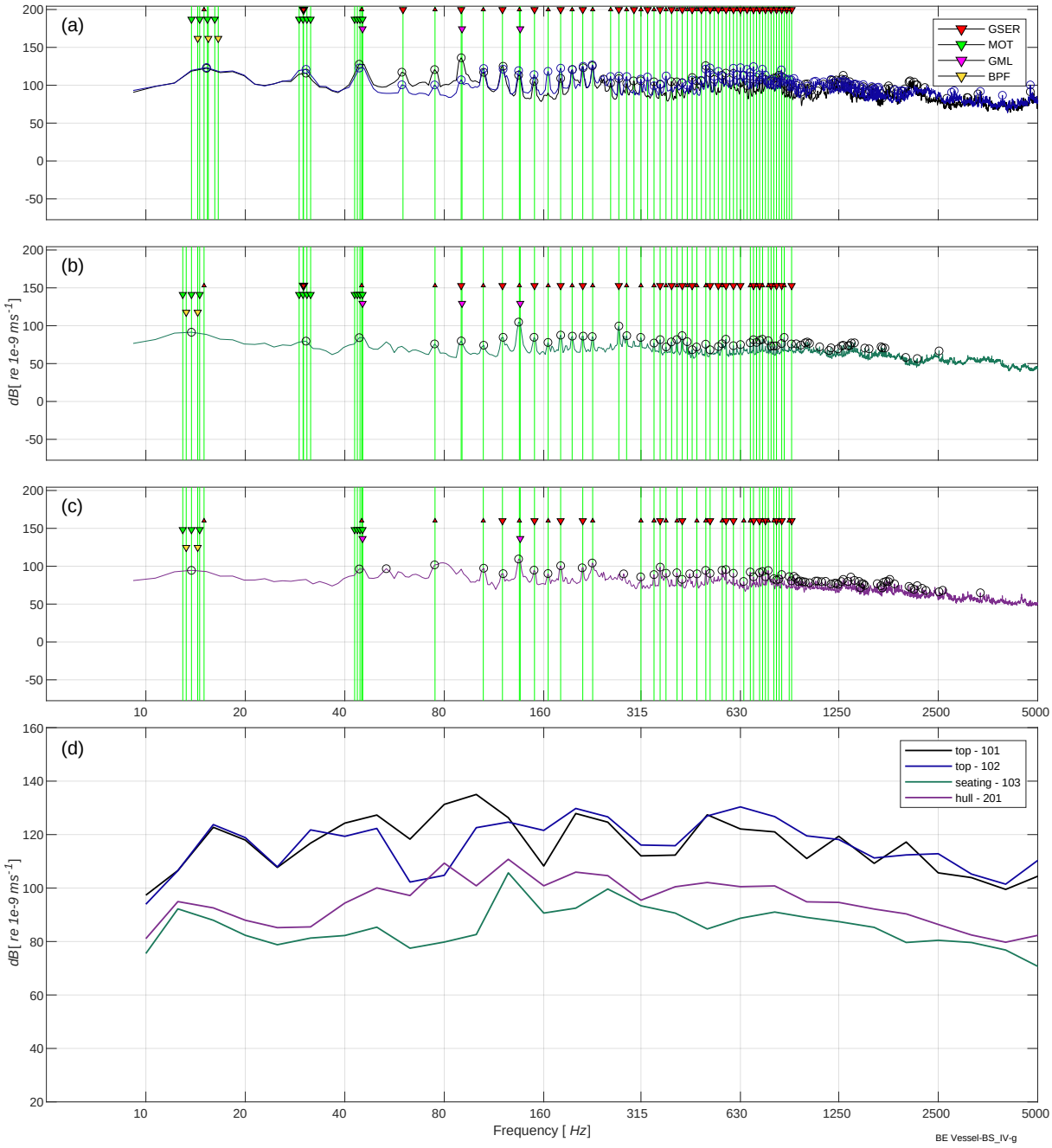


Figure D-24: Structural velocity narrow-band spectra (a) above the resilient mount, (b) on the seating, (c) on the hull and the respective (d) third-octave band spectra. Run: BE BS-IV - Genset Structure

D.6 BE Vessel - Structure-borne Noise - Genset Structure - Straight Run On Battery (ST-BATT)

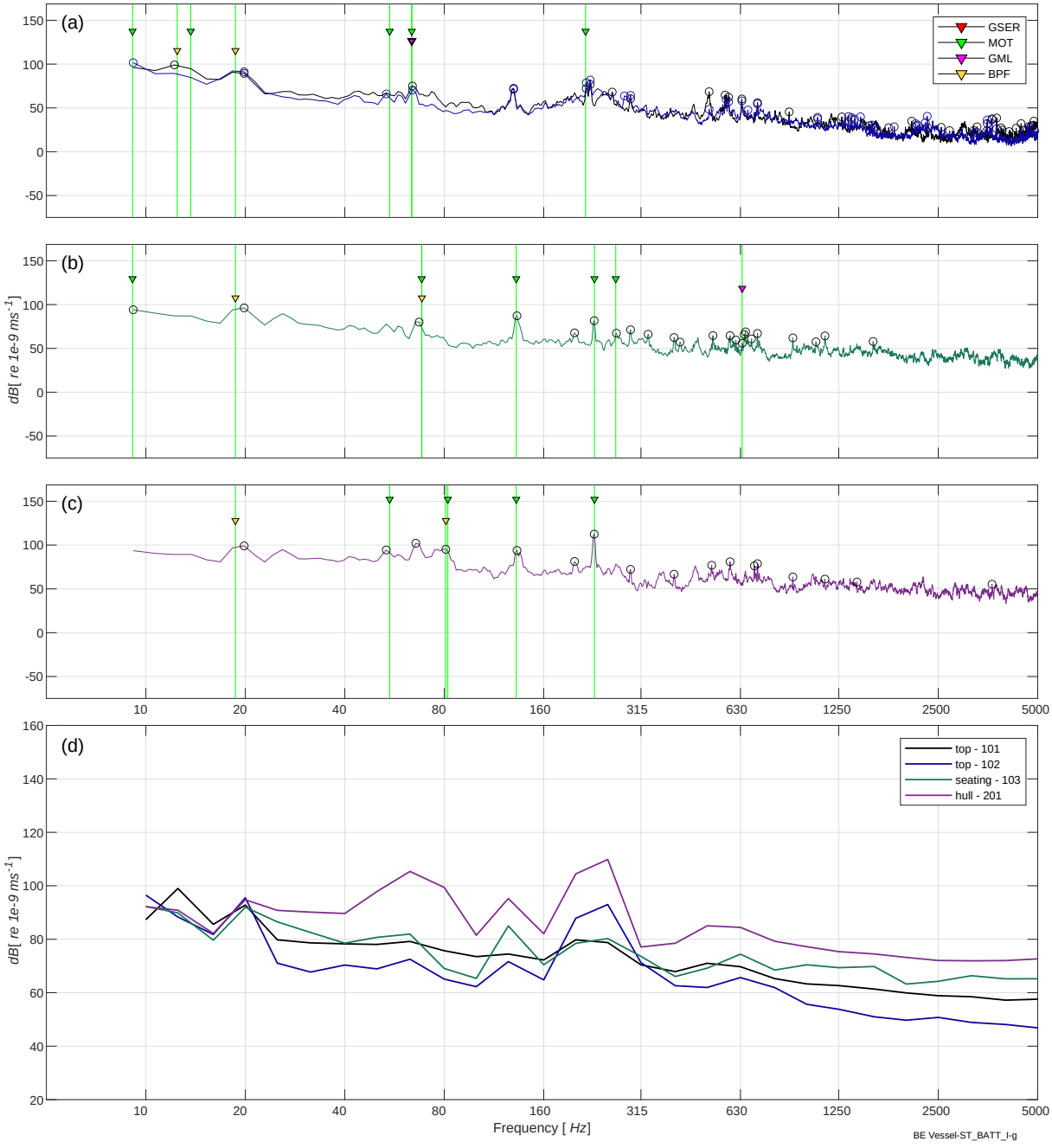


Figure D-25: Structural velocity narrow-band spectra (a) above the resilient mount, (b) on the seating, (c) on the hull and the respective (d) third-octave band spectra. Run: BE ST-BATT-I - Genset Structure

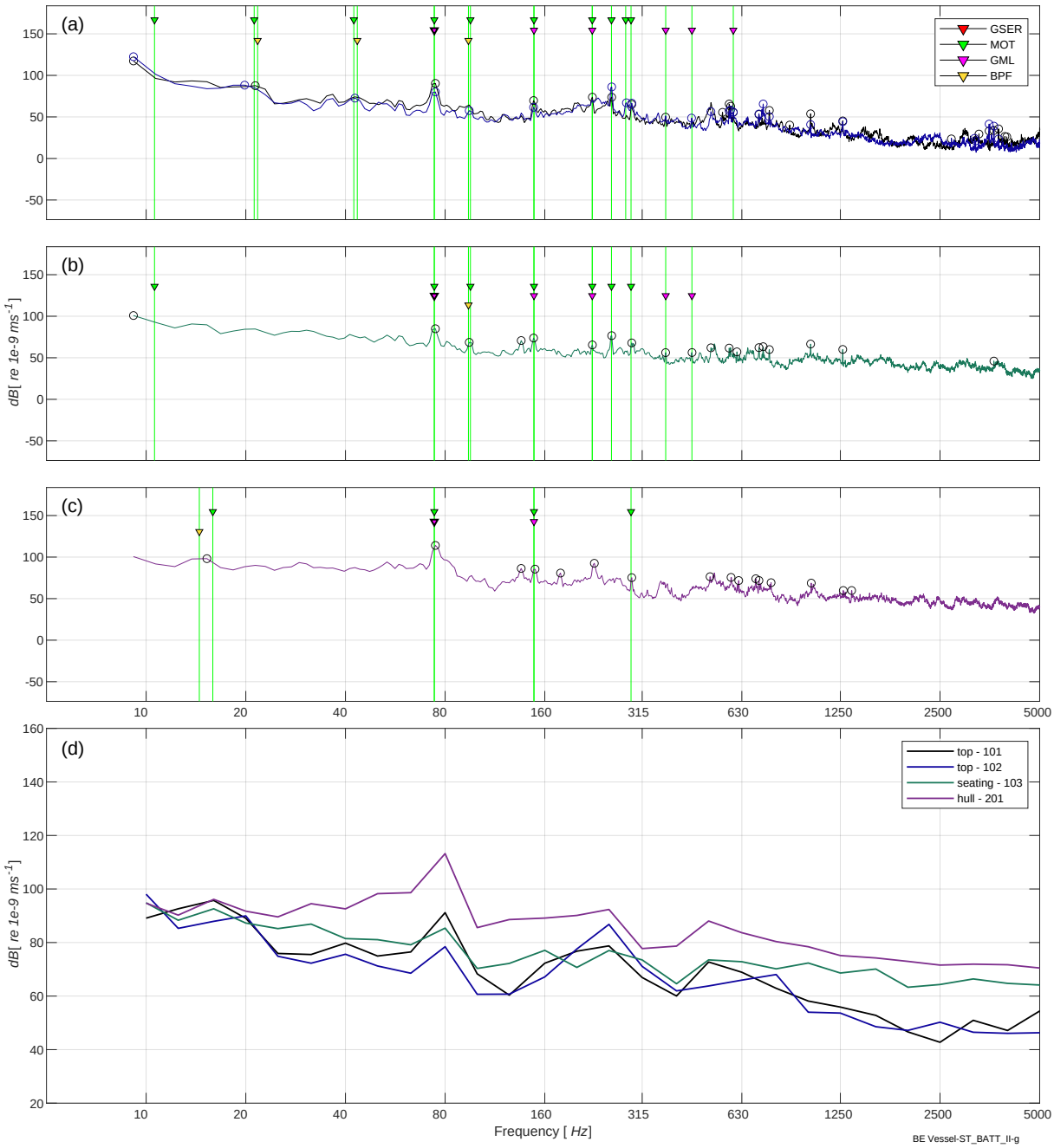


Figure D-26: Structural velocity narrow-band spectra (a) above the resilient mount, (b) on the seating, (c) on the hull and the respective (d) third-octave band spectra. Run: BE ST-BATT-II - Genset Structure

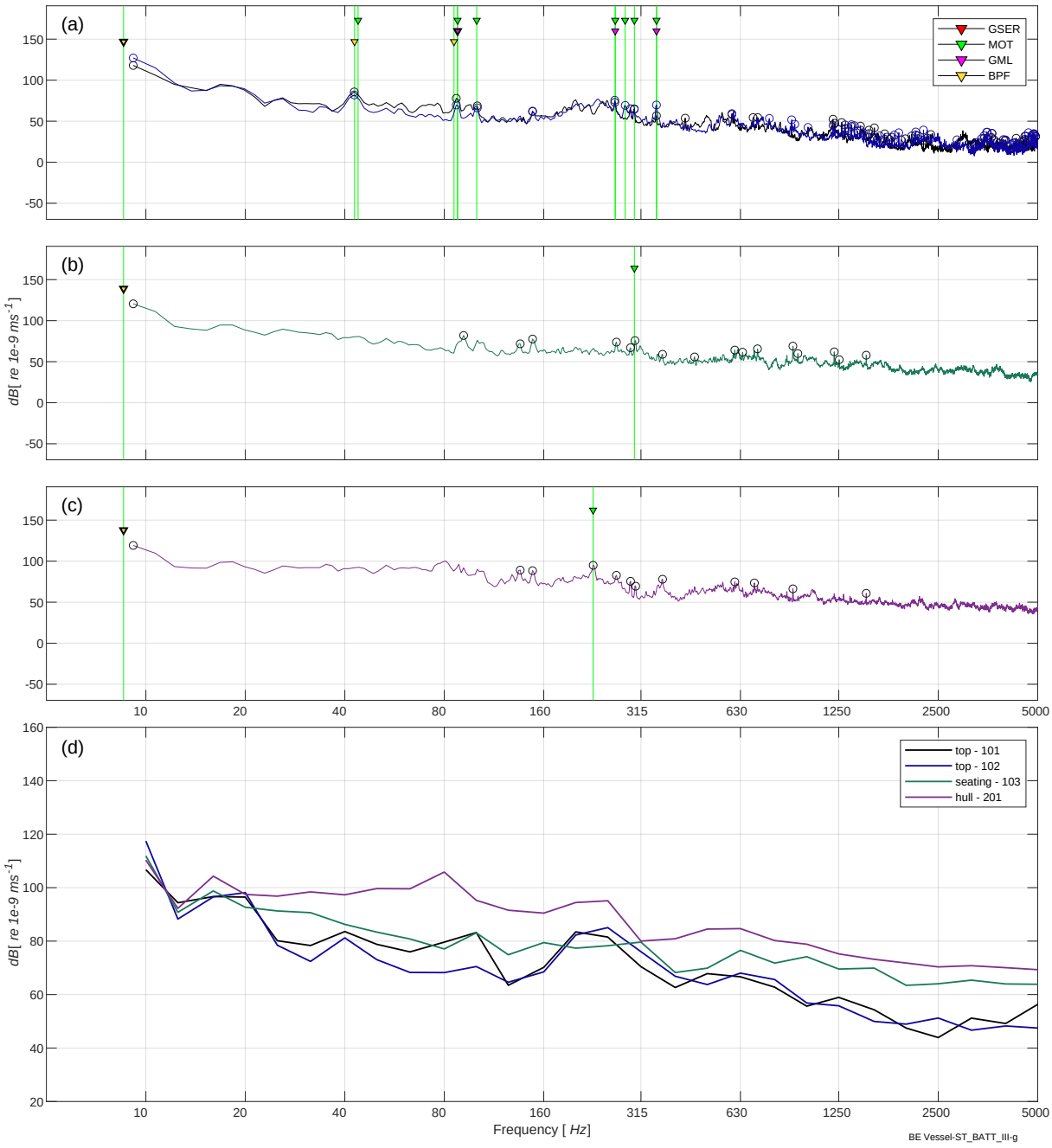


Figure D-27: Structural velocity narrow-band spectra (a) above the resilient mount, (b) on the seating, (c) on the hull and the respective (d) third-octave band spectra. Run: BE ST-BATT-III - Genset Structure

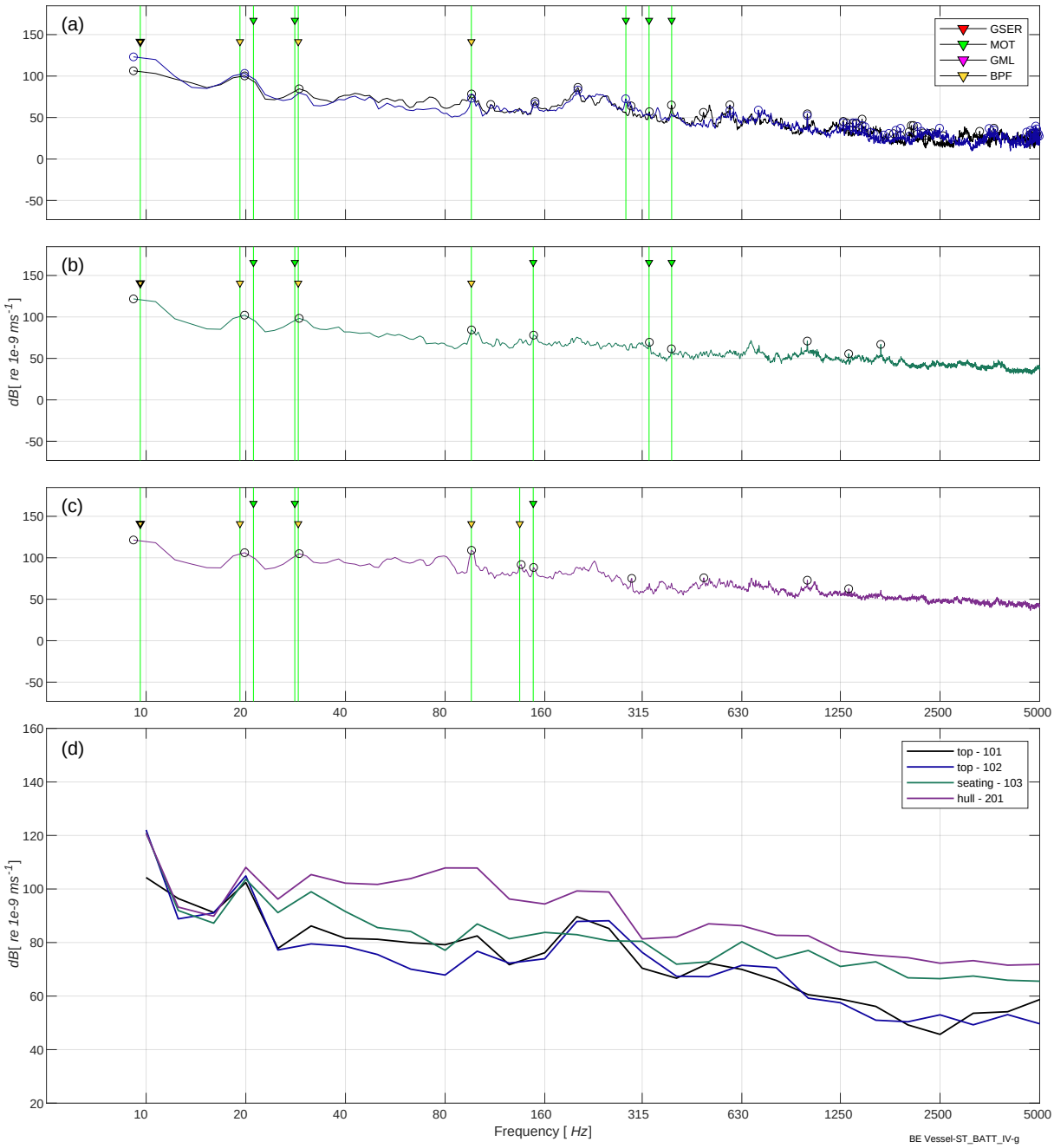


Figure D-28: Structural velocity narrow-band spectra (a) above the resilient mount, (b) on the seating, (c) on the hull and the respective (d) third-octave band spectra. Run: BE ST-BATT-IV - Genset Structure

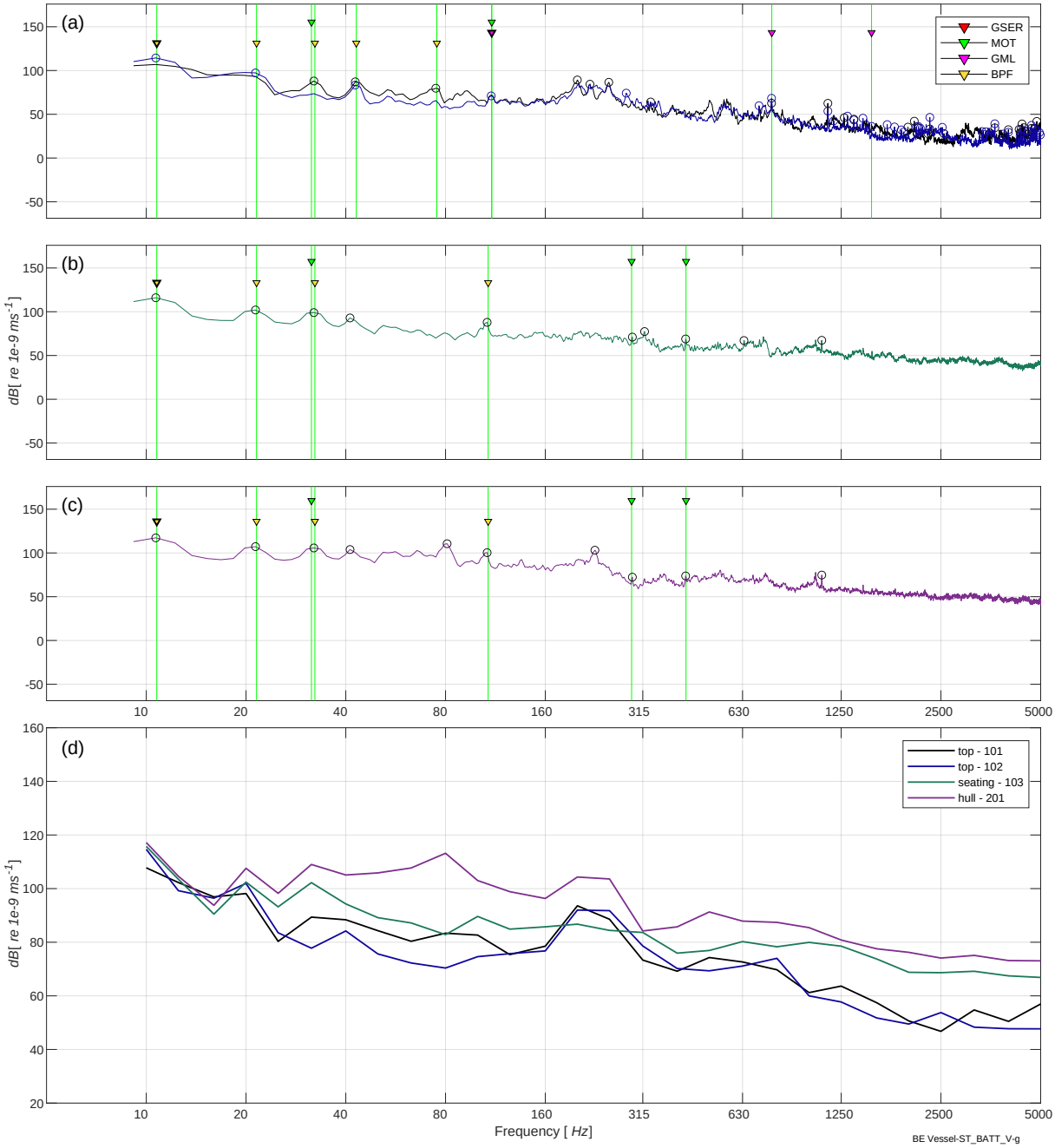


Figure D-29: Structural velocity narrow-band spectra (a) above the resilient mount, (b) on the seating, (c) on the hull and the respective (d) third-octave band spectra. Run: BE ST-BATT-V - Genset Structure

D.7 BE Vessel - Structure-borne Noise - Genset Structure - Straight Run On Gensets (ST-GENS)

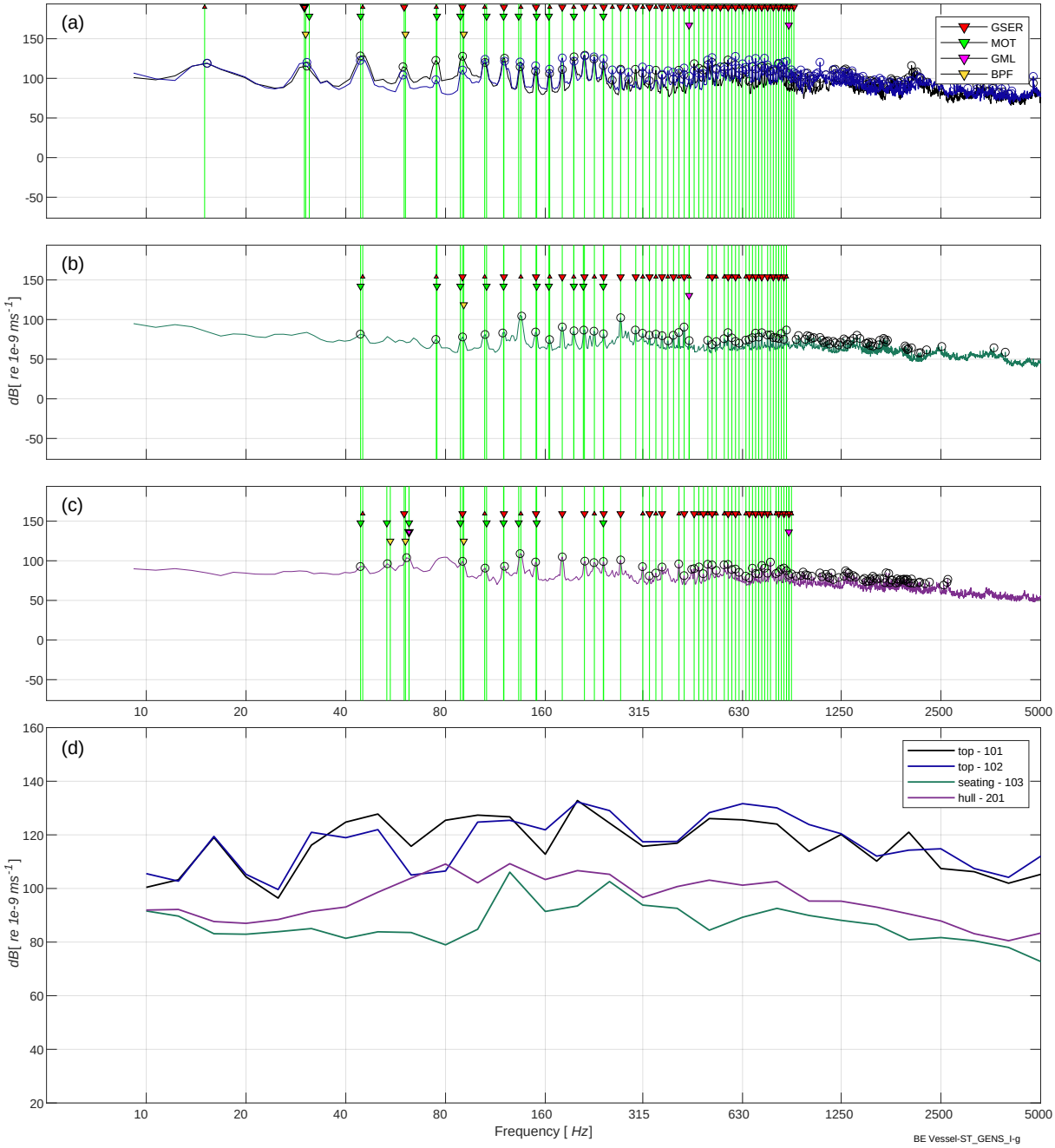


Figure D-30: Structural velocity narrow-band spectra (a) above the resilient mount, (b) on the seating, (c) on the hull and the respective (d) third-octave band spectra. Run: BE ST-GENS-I - Genset Structure

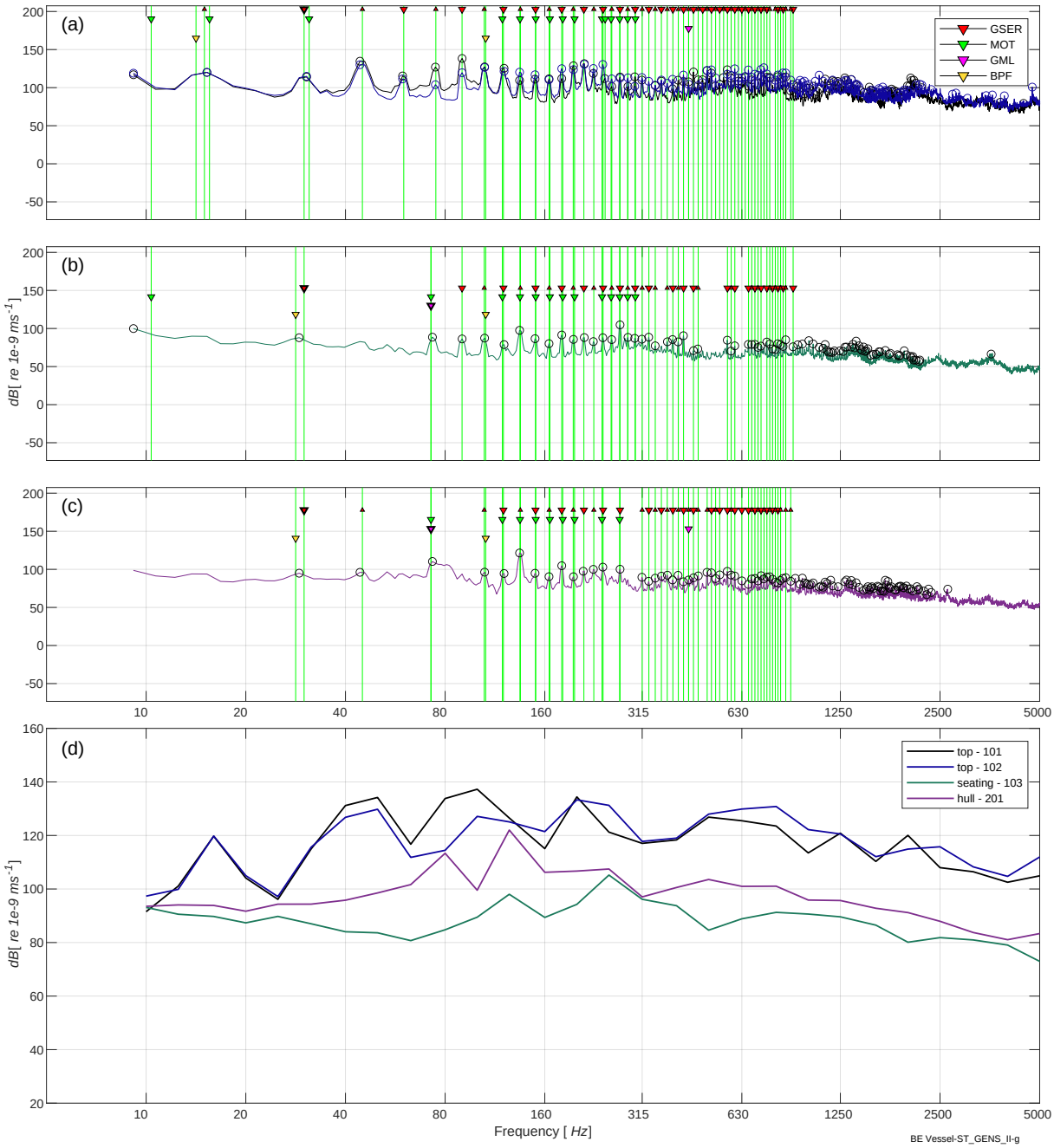


Figure D-31: Structural velocity narrow-band spectra (a) above the resilient mount, (b) on the seating, (c) on the hull and the respective (d) third-octave band spectra. Run: BE ST-GENS-II - Genset Structure

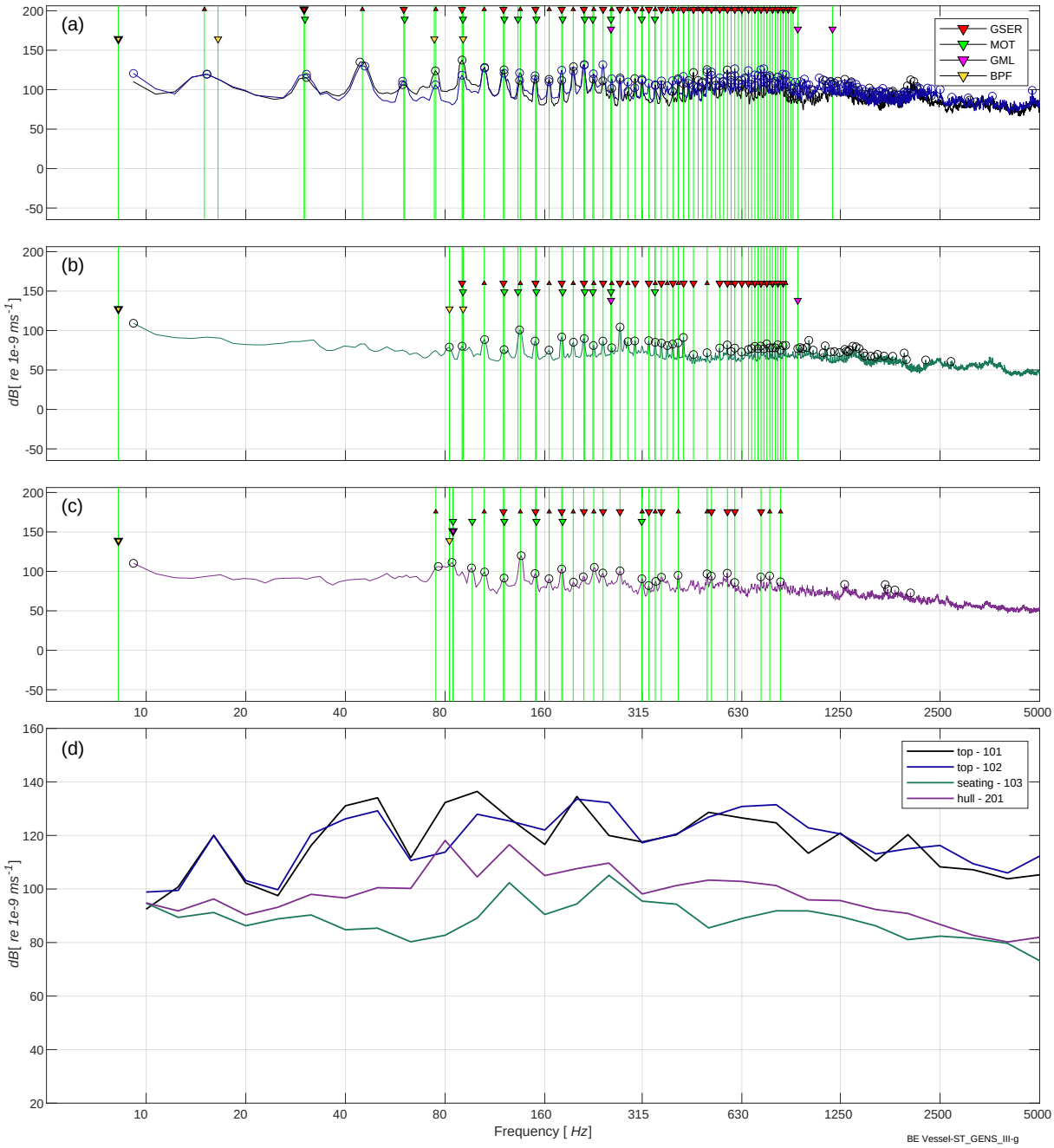


Figure D-32: Structural velocity narrow-band spectra (a) above the resilient mount, (b) on the seating, (c) on the hull and the respective (d) third-octave band spectra. Run: BE ST-GENS-III - Genset Structure

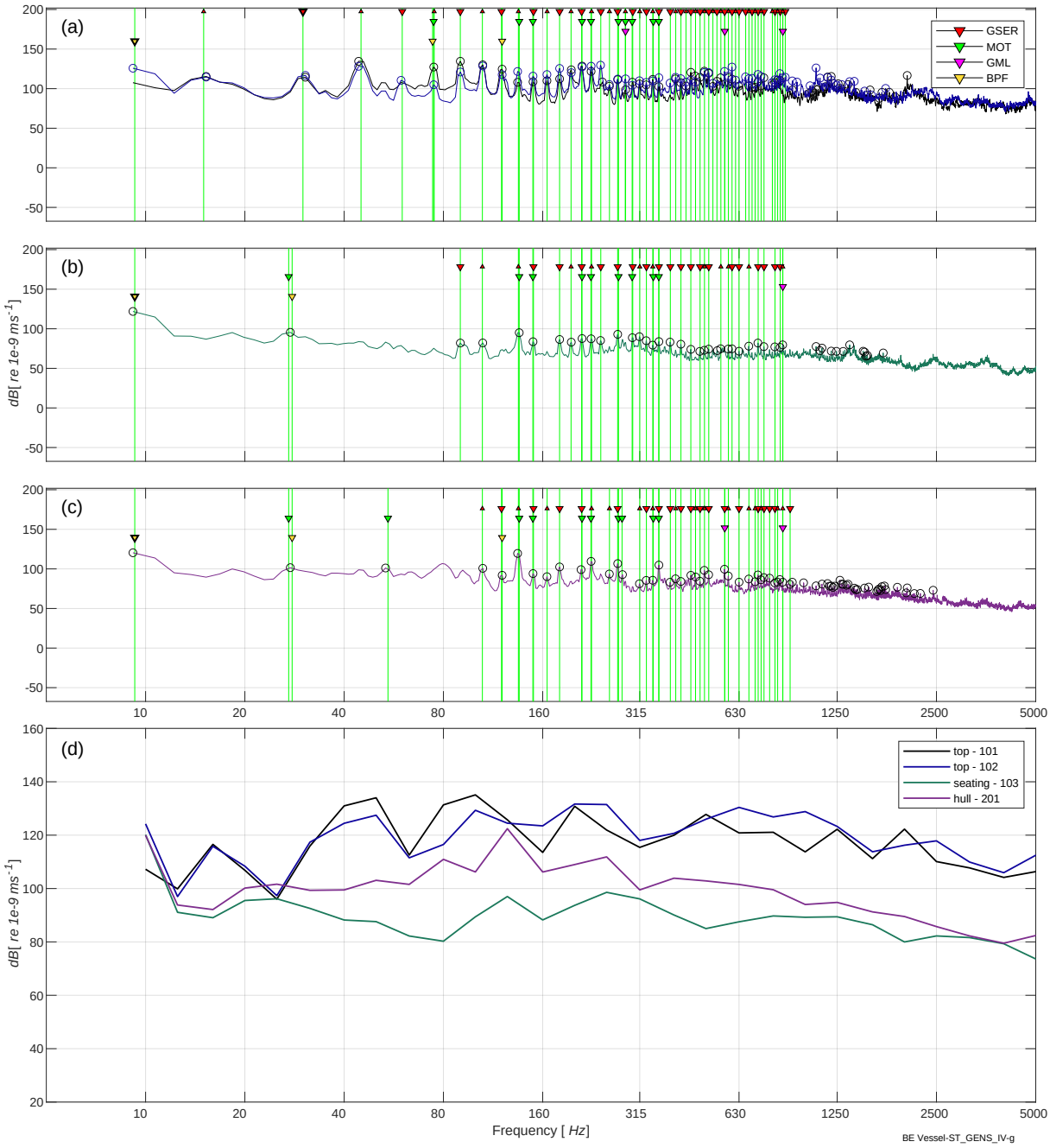


Figure D-33: Structural velocity narrow-band spectra (a) above the resilient mount, (b) on the seating, (c) on the hull and the respective (d) third-octave band spectra. Run: BE ST-GENS-IV - Genset Structure

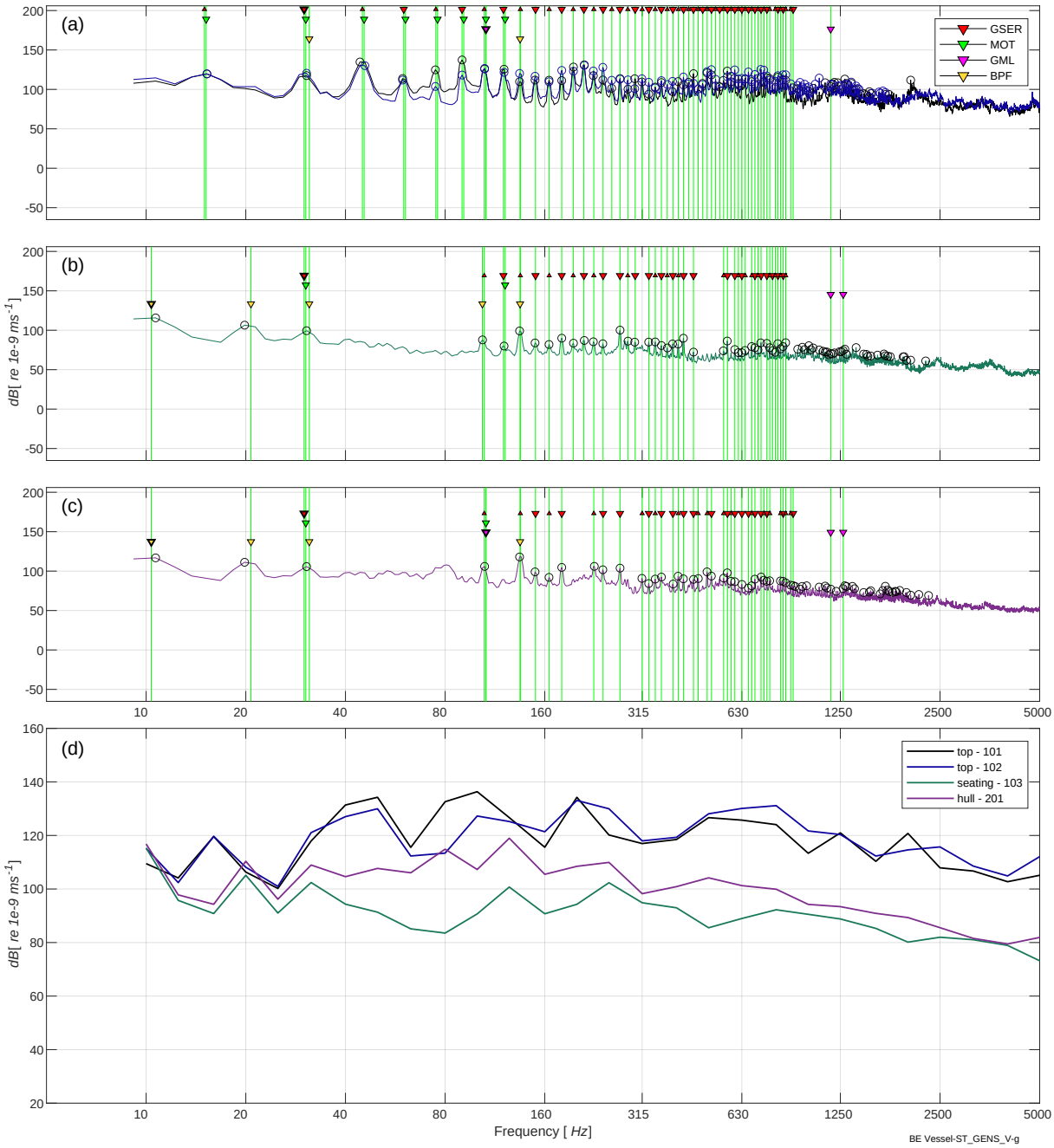


Figure D-34: Structural velocity narrow-band spectra (a) above the resilient mount, (b) on the seating, (c) on the hull and the respective (d) third-octave band spectra. Run: BE ST-GENS-V - Genset Structure

D.8 BE Vessel - Structure-borne Noise - Genset Structure - Bollard Pull (BP)

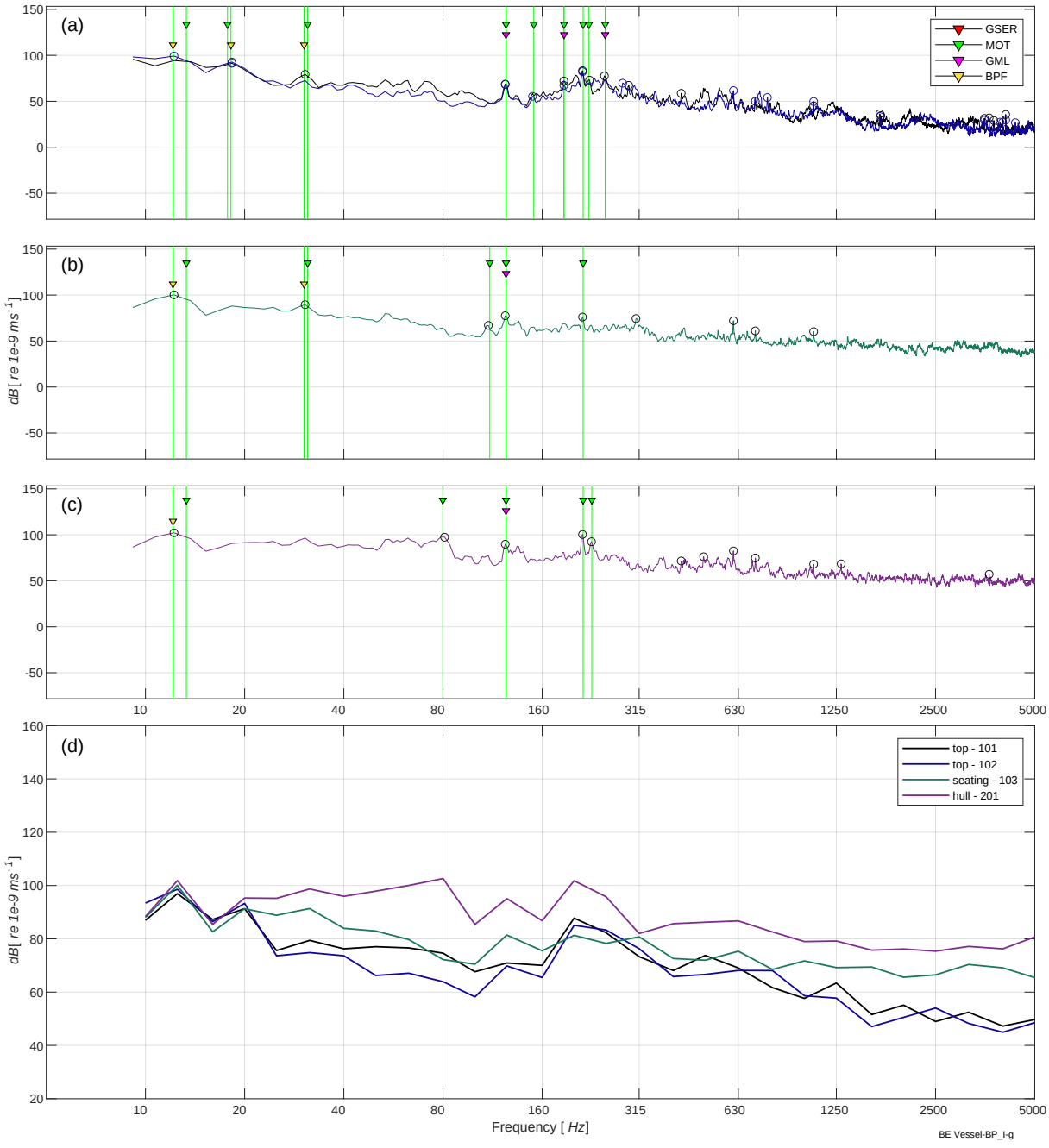


Figure D-35: Structural velocity narrow-band spectra (a) above the resilient mount, (b) on the seating, (c) on the hull and the respective (d) third-octave band spectra. Run: BE BP-I - Genset Structure

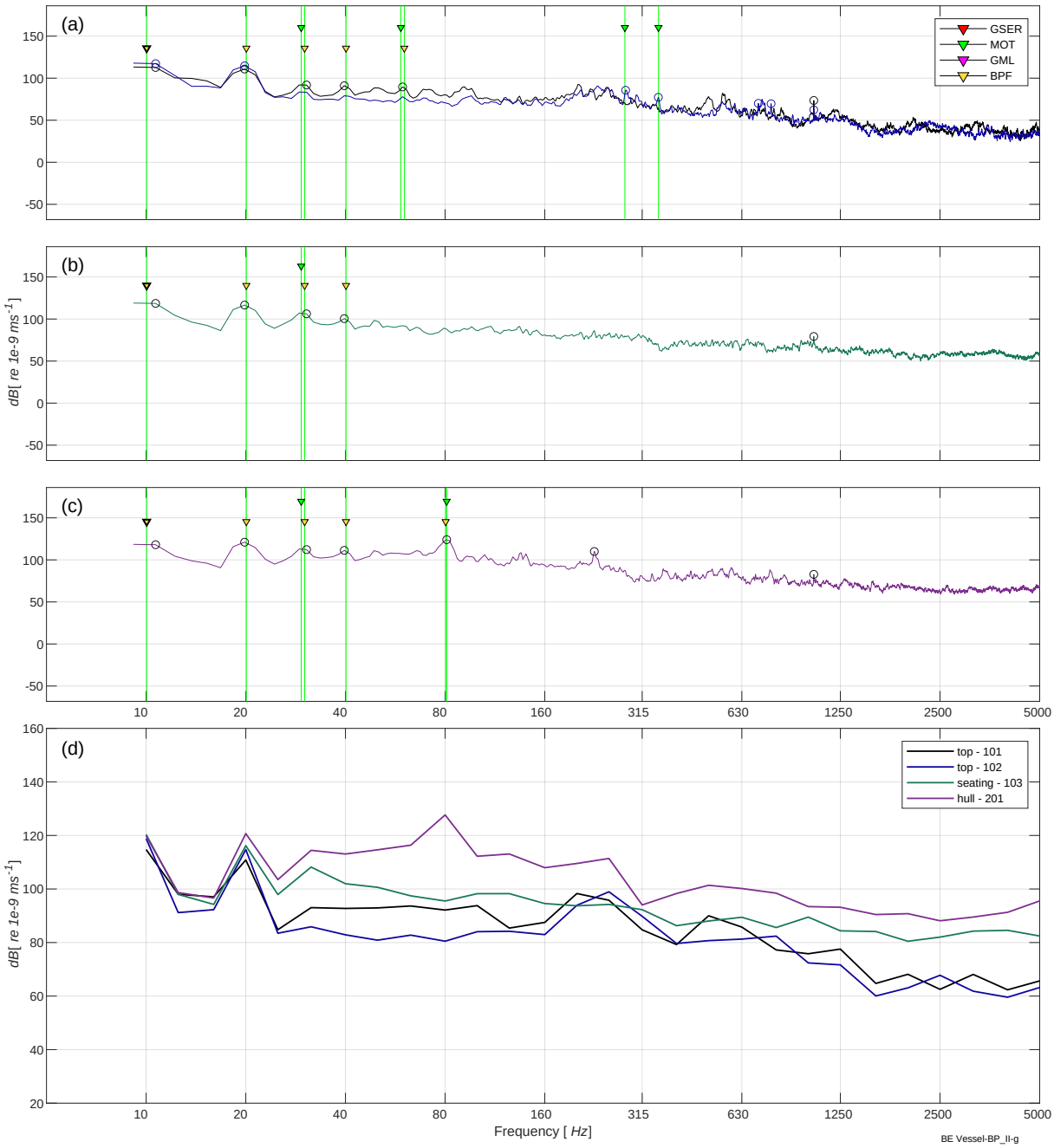


Figure D-36: Structural velocity narrow-band spectra (a) above the resilient mount, (b) on the seating, (c) on the hull and the respective (d) third-octave band spectra. Run: BE BP-II - Genset Structure

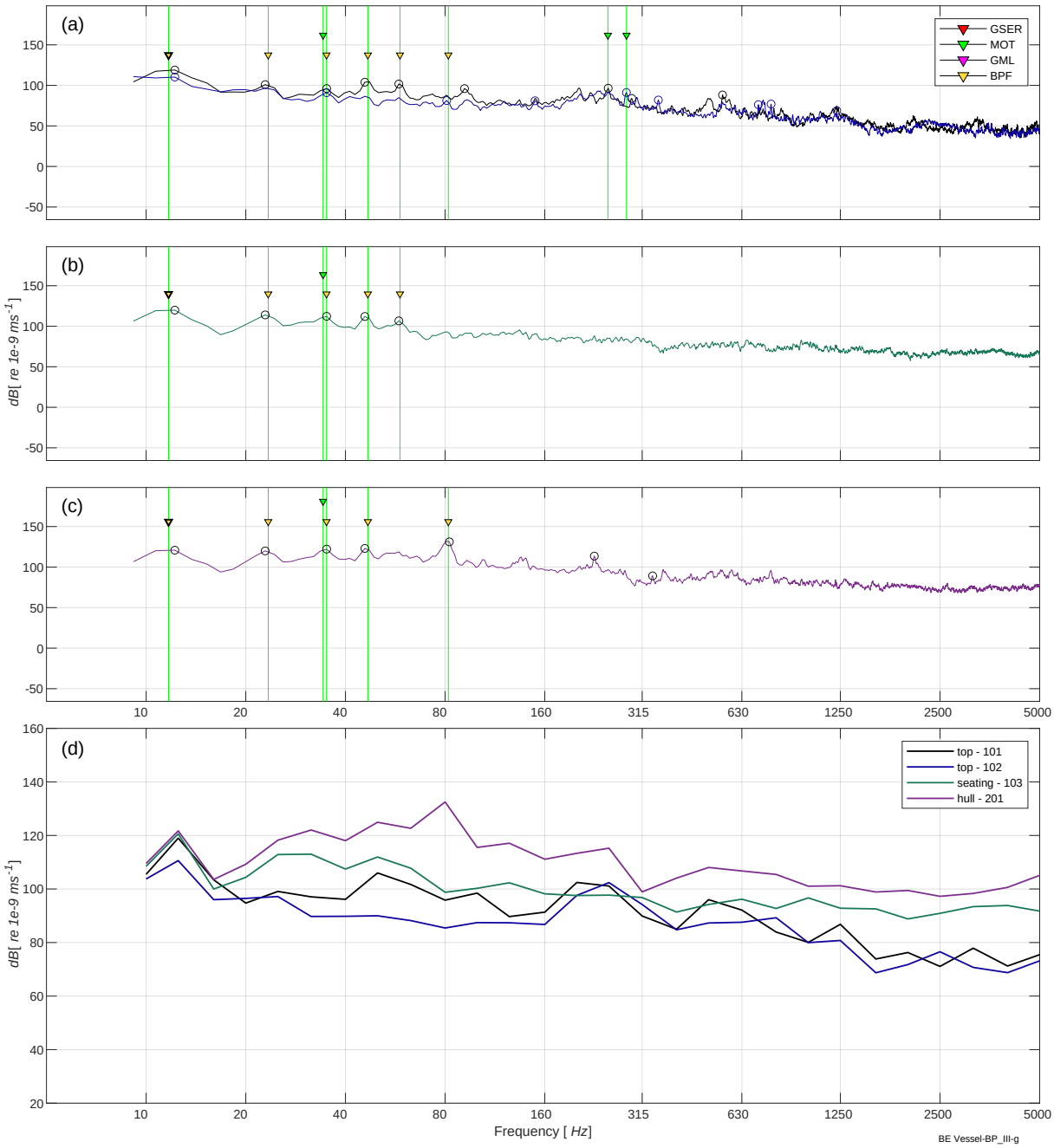


Figure D-37: Structural velocity narrow-band spectra (a) above the resilient mount, (b) on the seating, (c) on the hull and the respective (d) third-octave band spectra. Run: BE BP-III - Genset Structure

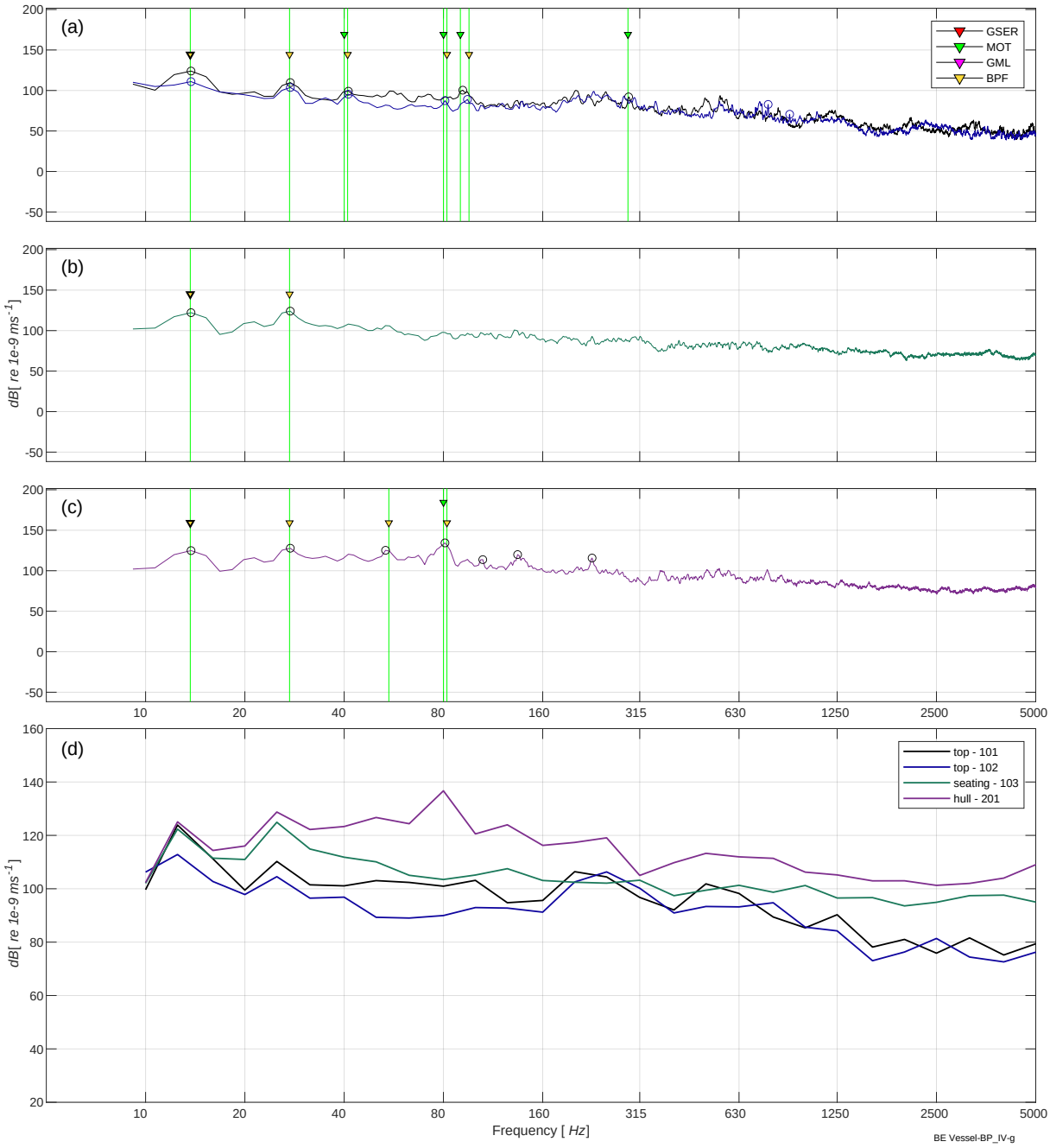


Figure D-38: Structural velocity narrow-band spectra (a) above the resilient mount, (b) on the seating, (c) on the hull and the respective (d) third-octave band spectra. Run: BE BP-IV - Genset Structure

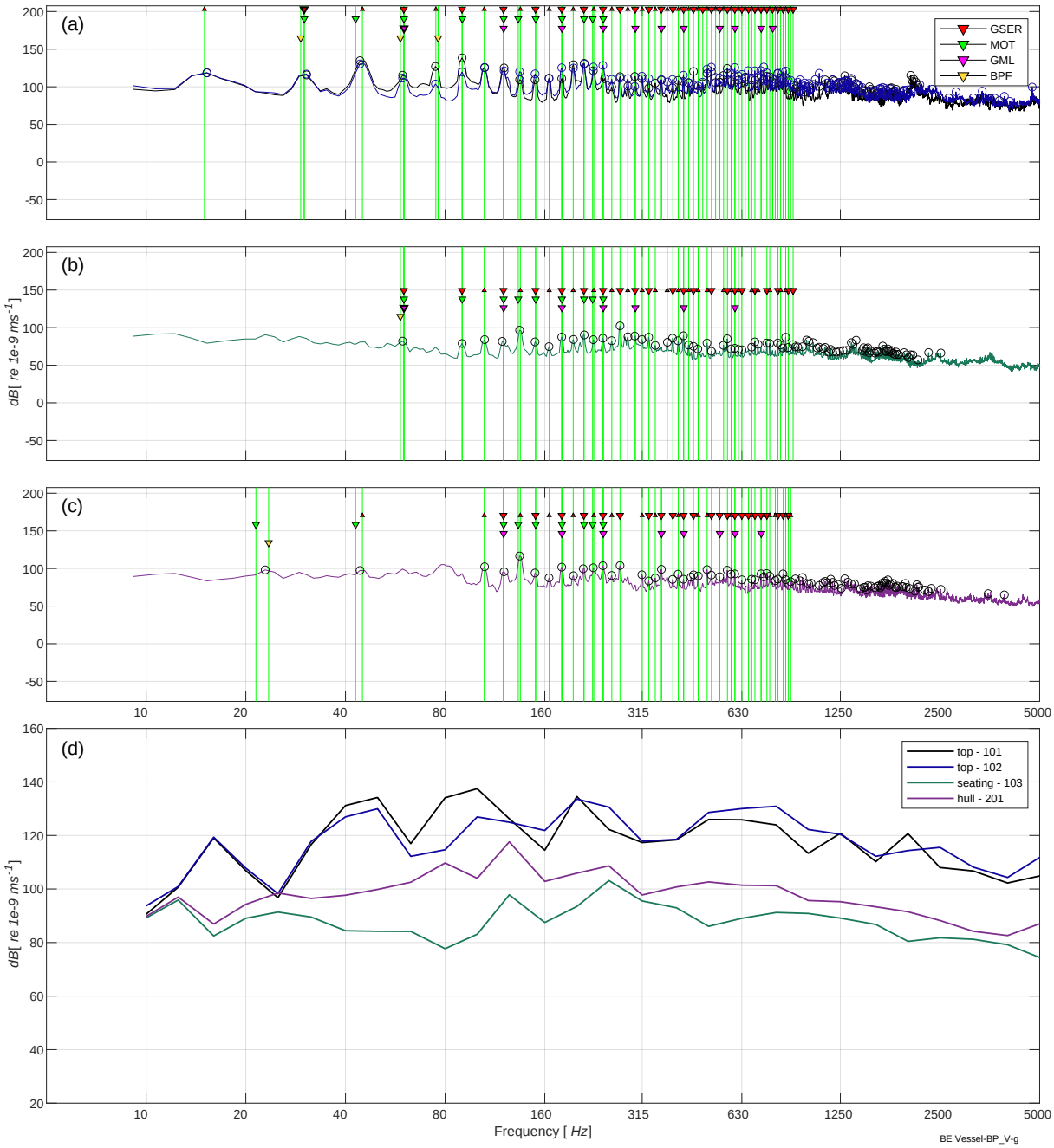


Figure D-39: Structural velocity narrow-band spectra (a) above the resilient mount, (b) on the seating, (c) on the hull and the respective (d) third-octave band spectra. Run: BE BP-V - Genset Structure

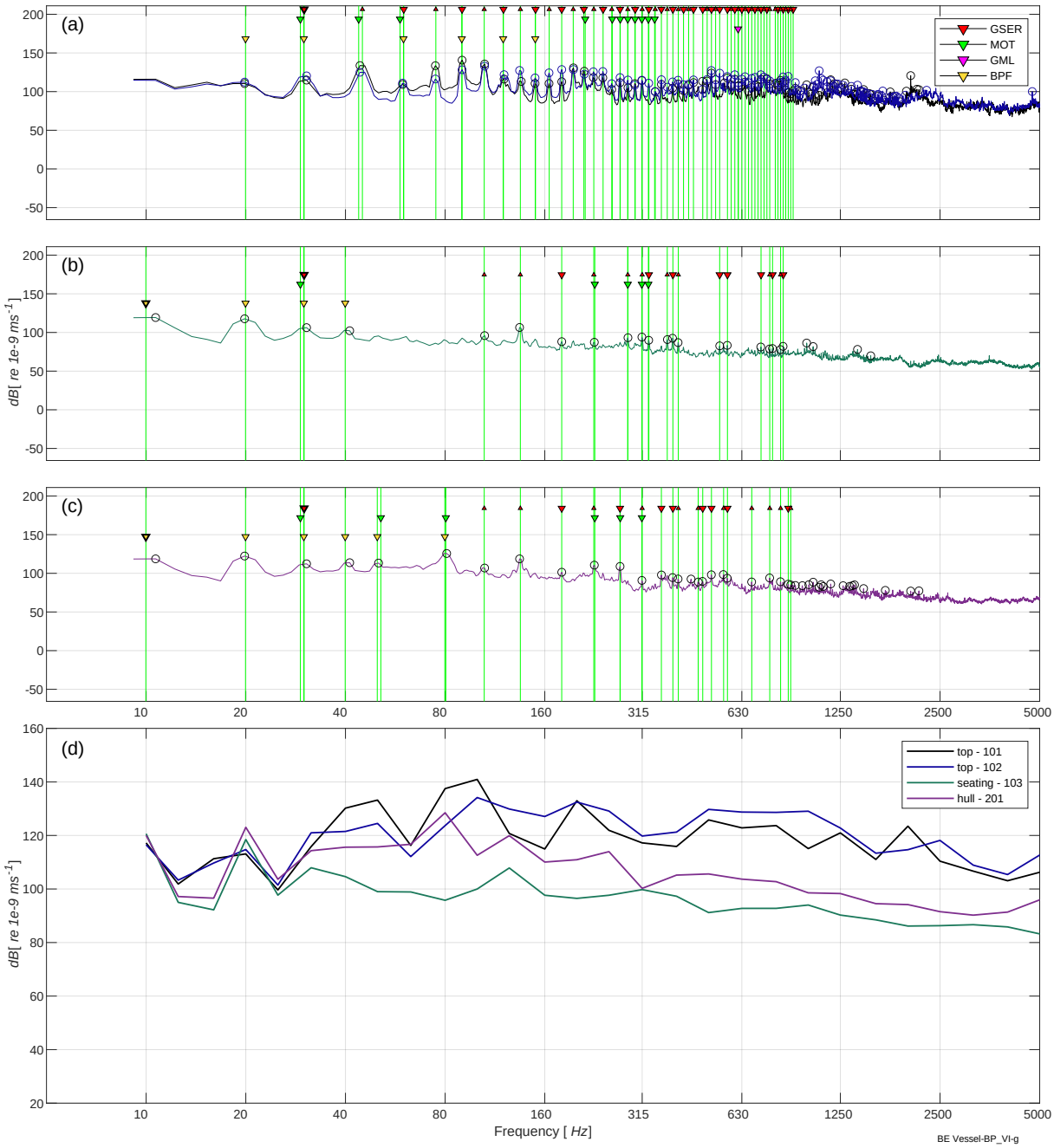


Figure D-40: Structural velocity narrow-band spectra (a) above the resilient mount, (b) on the seating, (c) on the hull and the respective (d) third-octave band spectra. Run: BE BP-VI - Genset Structure

D.9 DM Vessel - Structure-borne Noise - Engine Structure - Baseline Stationary (BS)

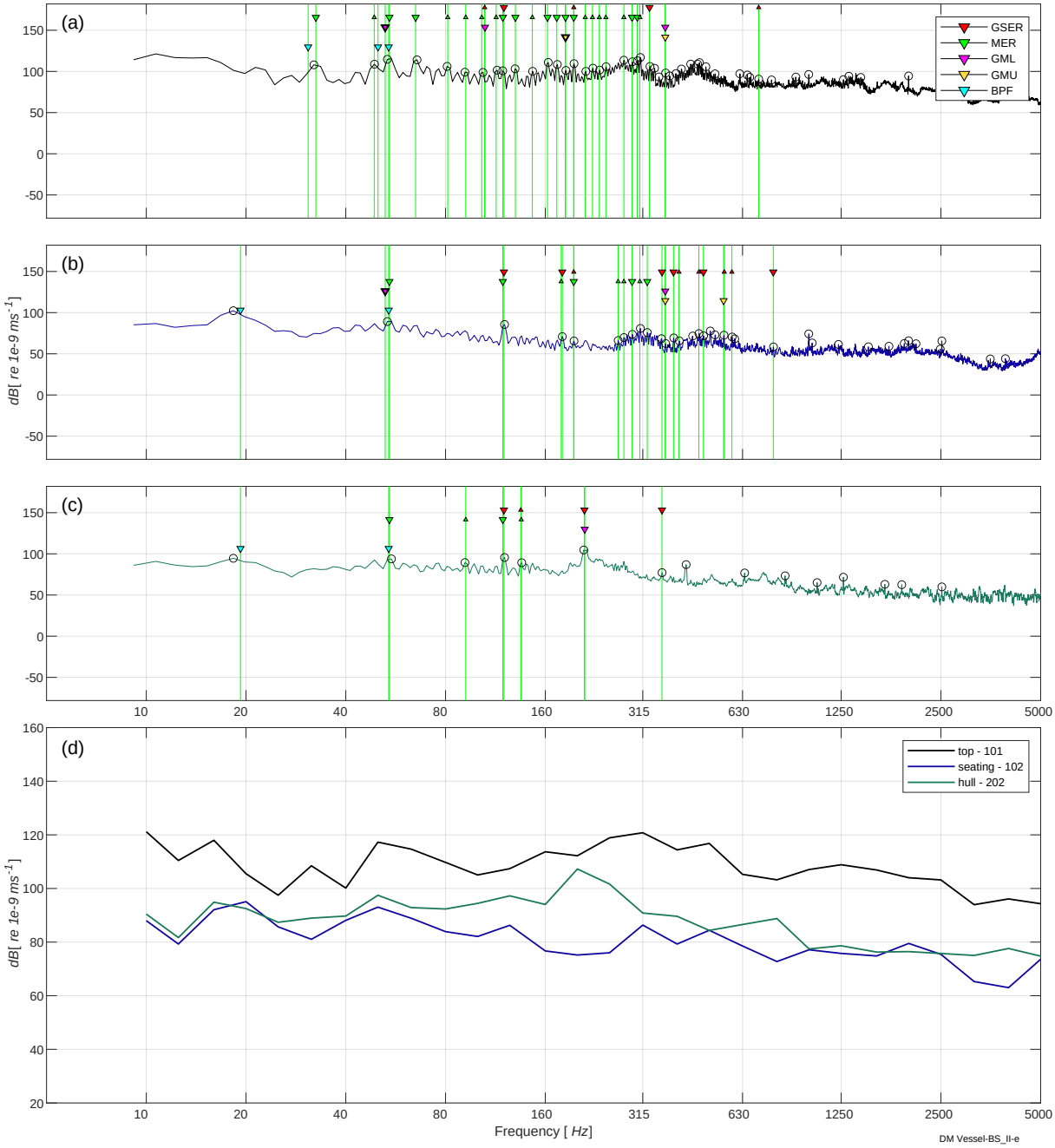


Figure D-41: Structural velocity narrow-band spectra (a) above the resilient mount, (b) on the seating, (c) on the hull and the respective (d) third-octave band spectra. Run: DM BS-II - Engine Structure

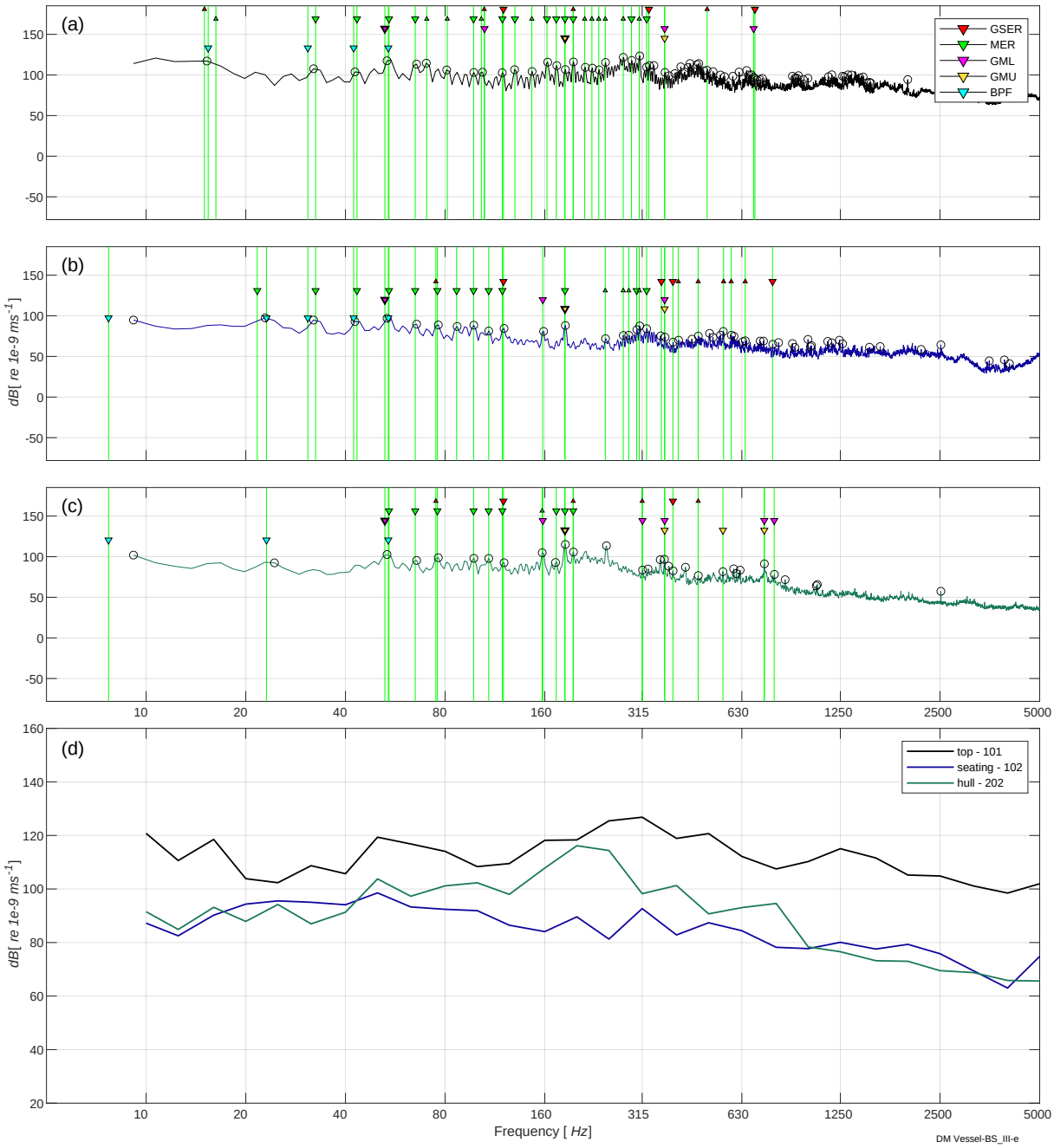


Figure D-42: Structural velocity narrow-band spectra (a) above the resilient mount, (b) on the seating, (c) on the hull and the respective (d) third-octave band spectra. Run: DM BS-III - Engine Structure

D.10 DM Vessel - Structure-borne Noise - Engine Structure - Straight Travel (ST)

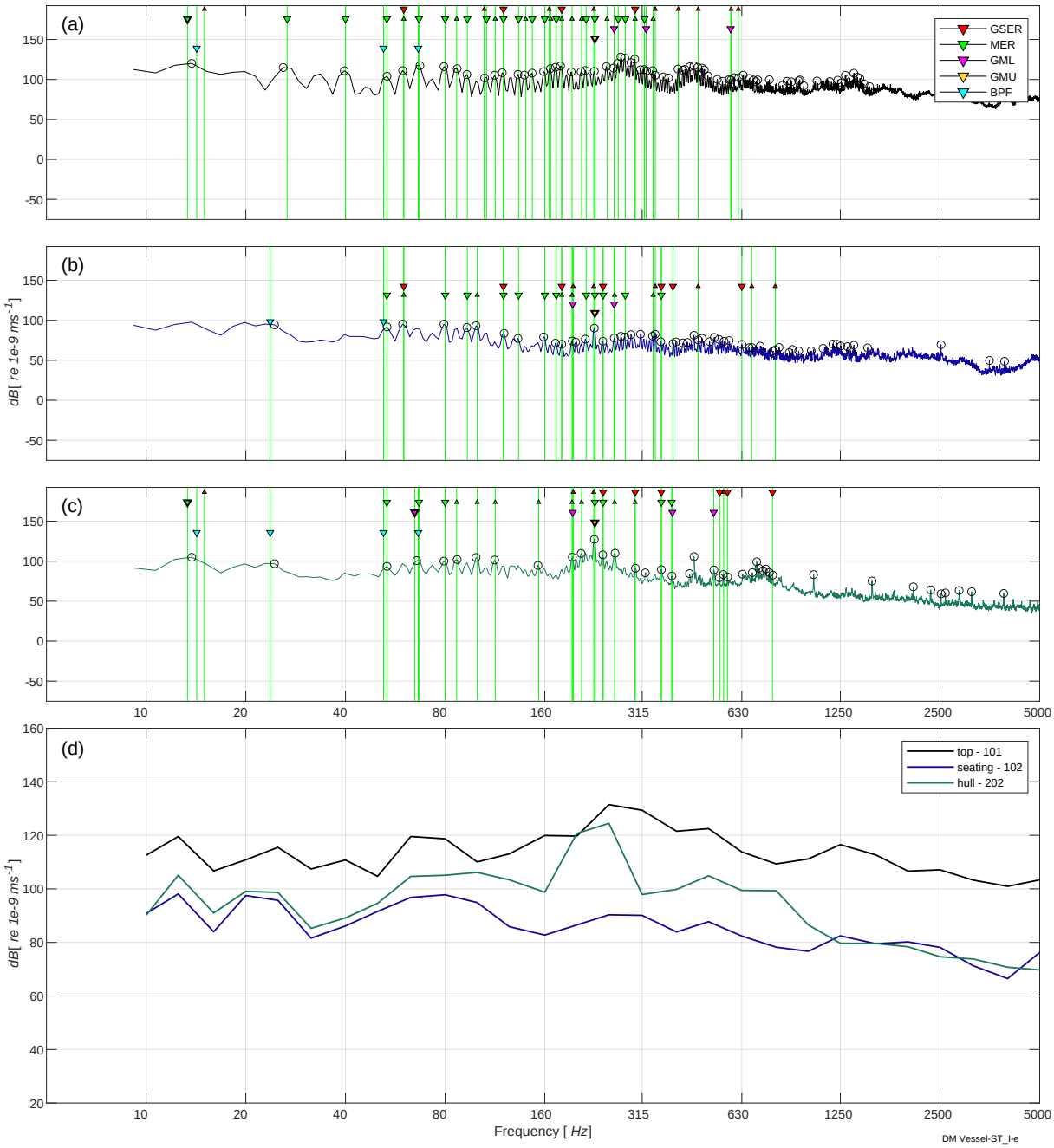


Figure D-43: Structural velocity narrow-band spectra (a) above the resilient mount, (b) on the seating, (c) on the hull and the respective (d) third-octave band spectra. Run: DM ST-I - Engine Structure

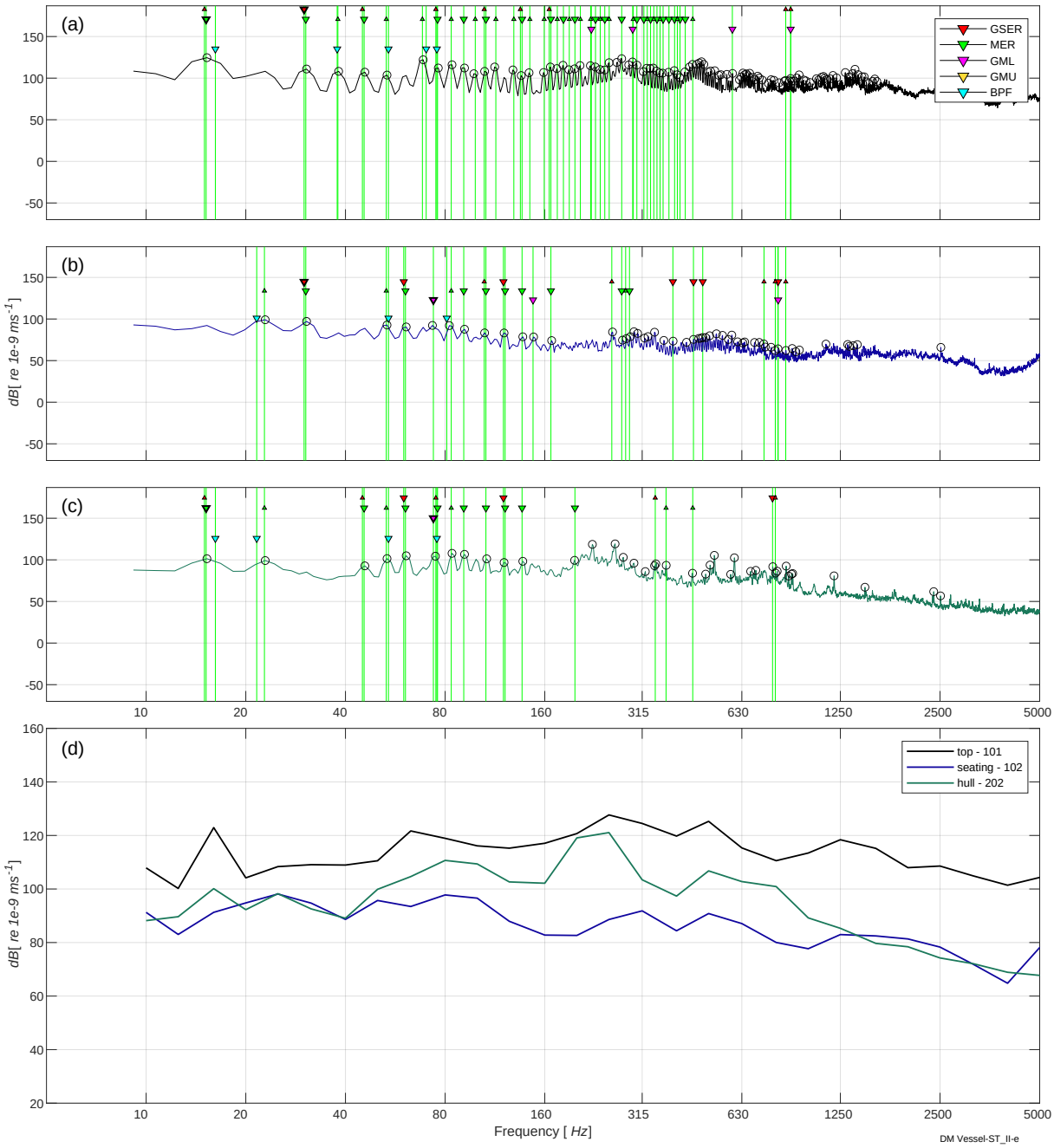


Figure D-44: Structural velocity narrow-band spectra (a) above the resilient mount, (b) on the seating, (c) on the hull and the respective (d) third-octave band spectra. Run: DM ST-II - Engine Structure

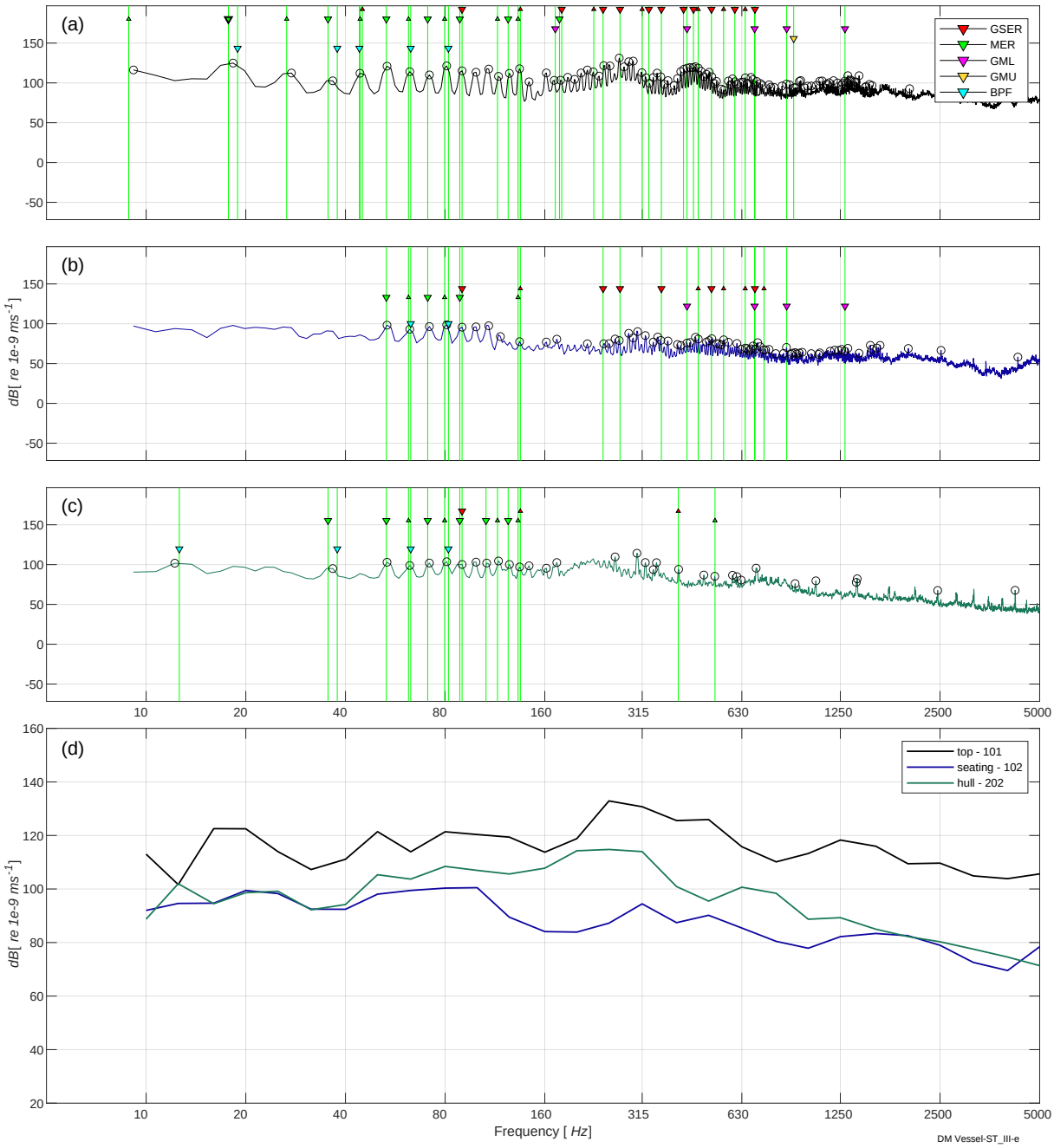


Figure D-45: Structural velocity narrow-band spectra (a) above the resilient mount, (b) on the seating, (c) on the hull and the respective (d) third-octave band spectra. Run: DM ST-III - Engine Structure

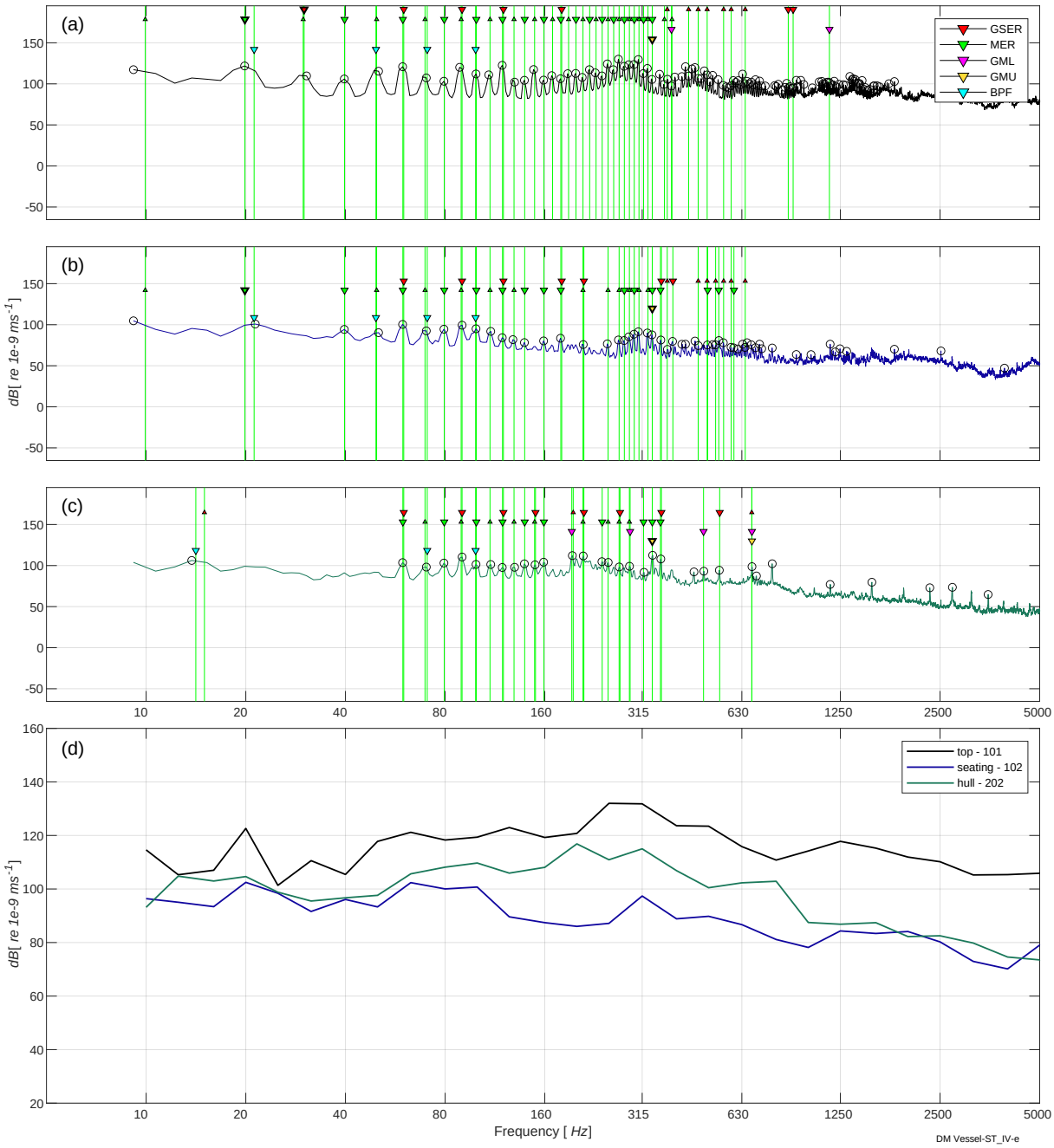


Figure D-46: Structural velocity narrow-band spectra (a) above the resilient mount, (b) on the seating, (c) on the hull and the respective (d) third-octave band spectra. Run: DM ST-IV - Engine Structure

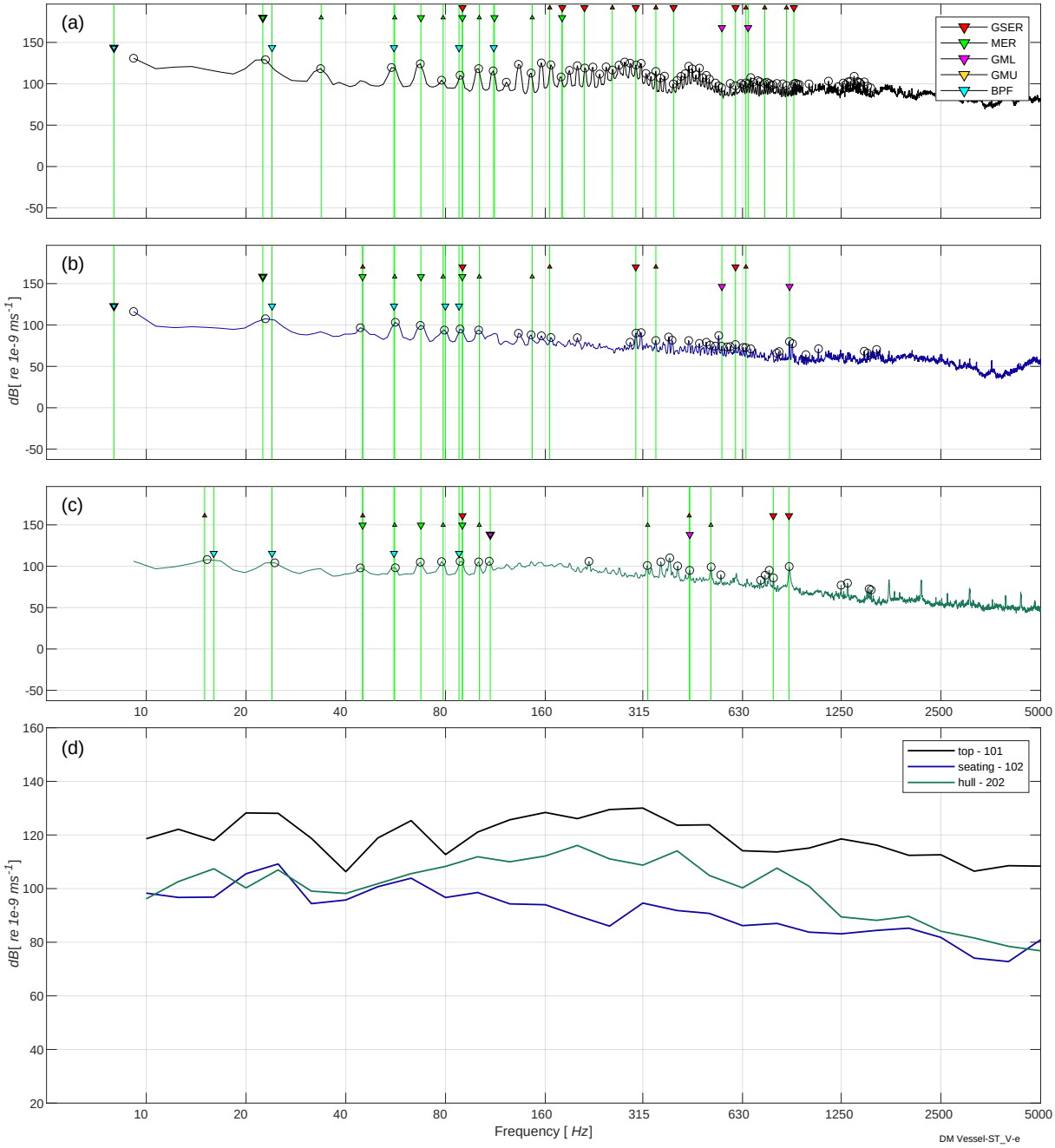


Figure D-47: Structural velocity narrow-band spectra (a) above the resilient mount, (b) on the seating, (c) on the hull and the respective (d) third-octave band spectra. Run: DM ST-V - Engine Structure

D.11 DM Vessel - Structure-borne Noise - Engine Structure - Bollard Pull (BP)

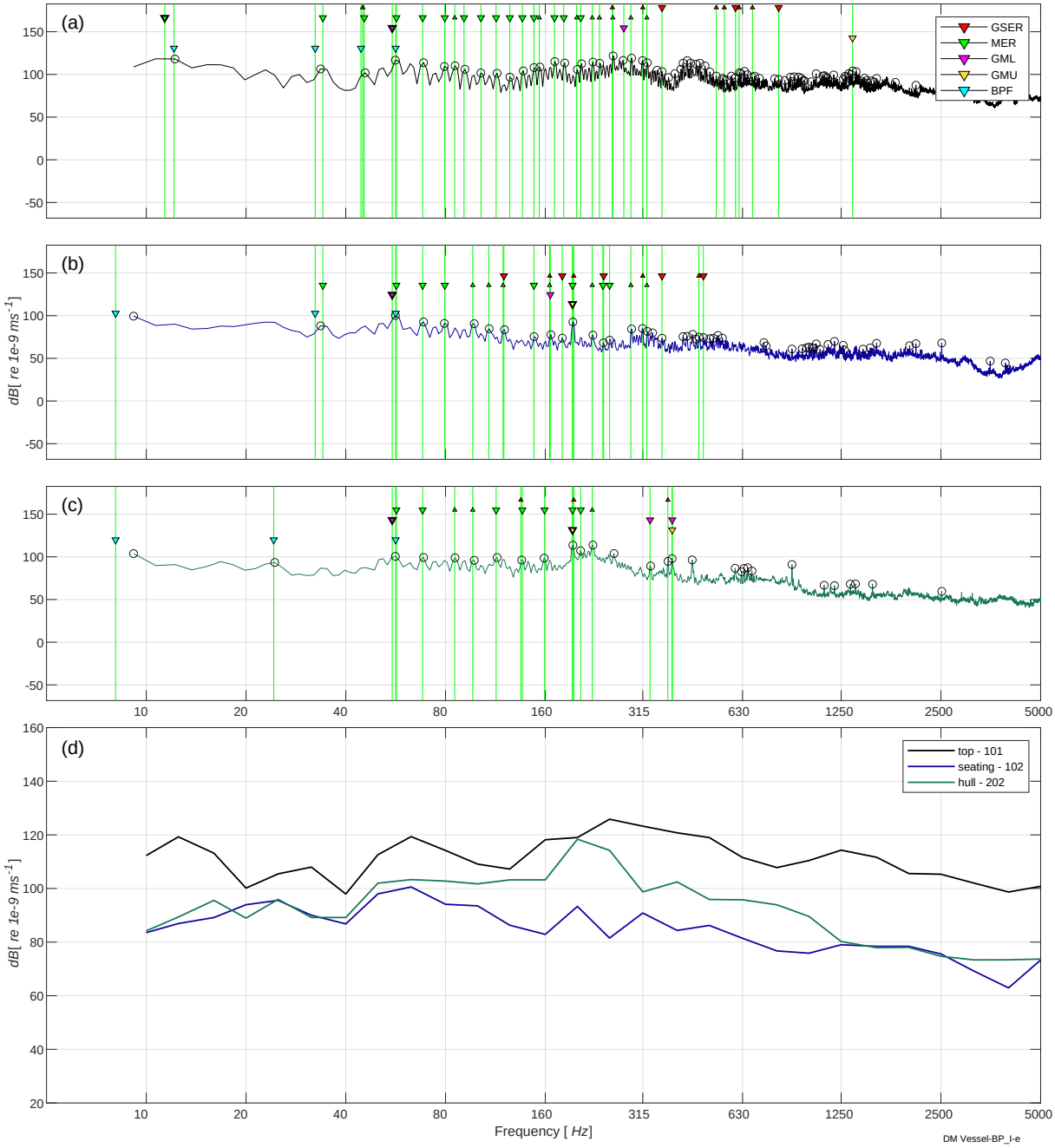


Figure D-48: Structural velocity narrow-band spectra (a) above the resilient mount, (b) on the seating, (c) on the hull and the respective (d) third-octave band spectra. Run: DM BP-I - Engine Structure

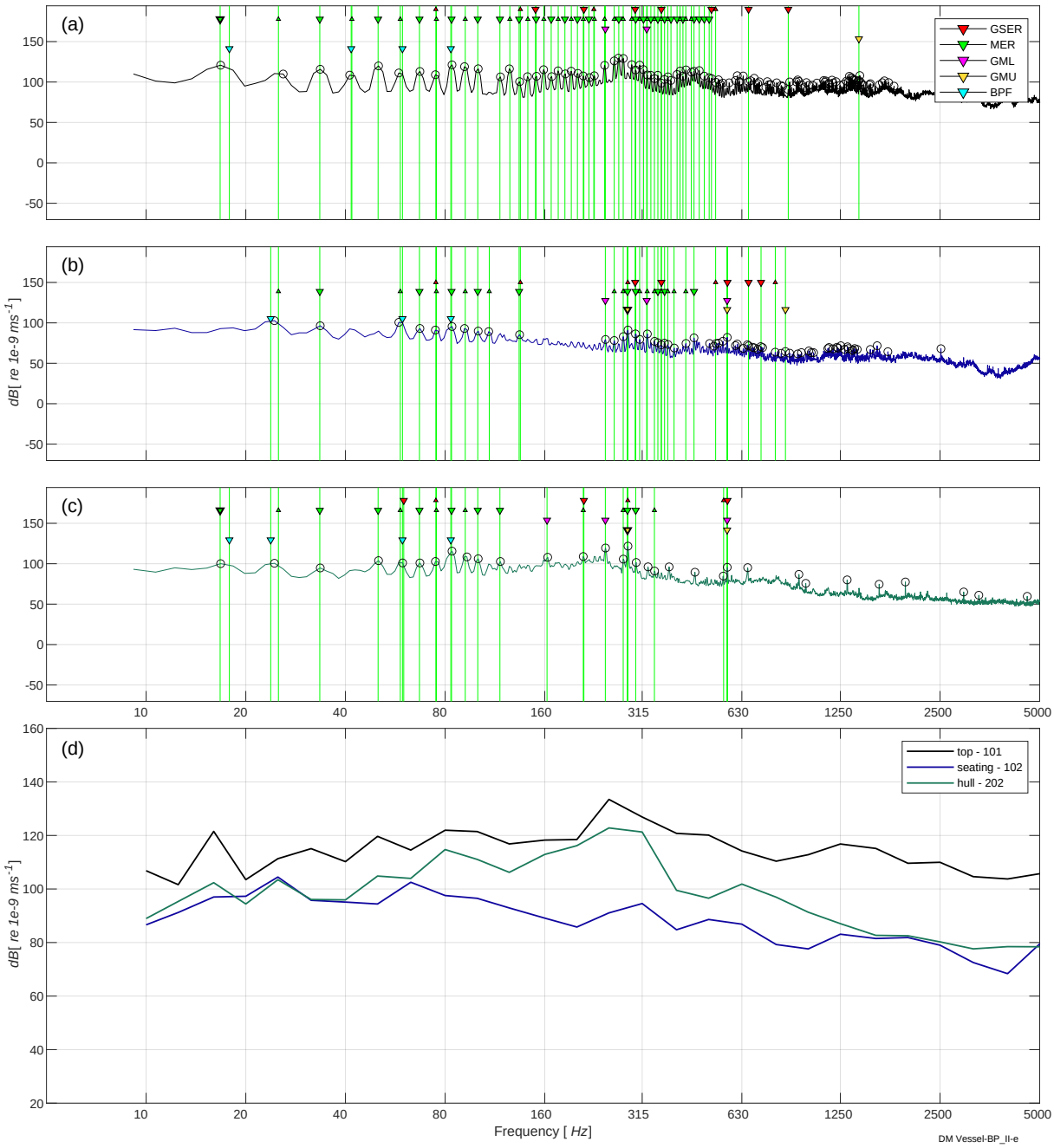


Figure D-49: Structural velocity narrow-band spectra (a) above the resilient mount, (b) on the seating, (c) on the hull and the respective (d) third-octave band spectra. Run: DM BP-II - Engine Structure

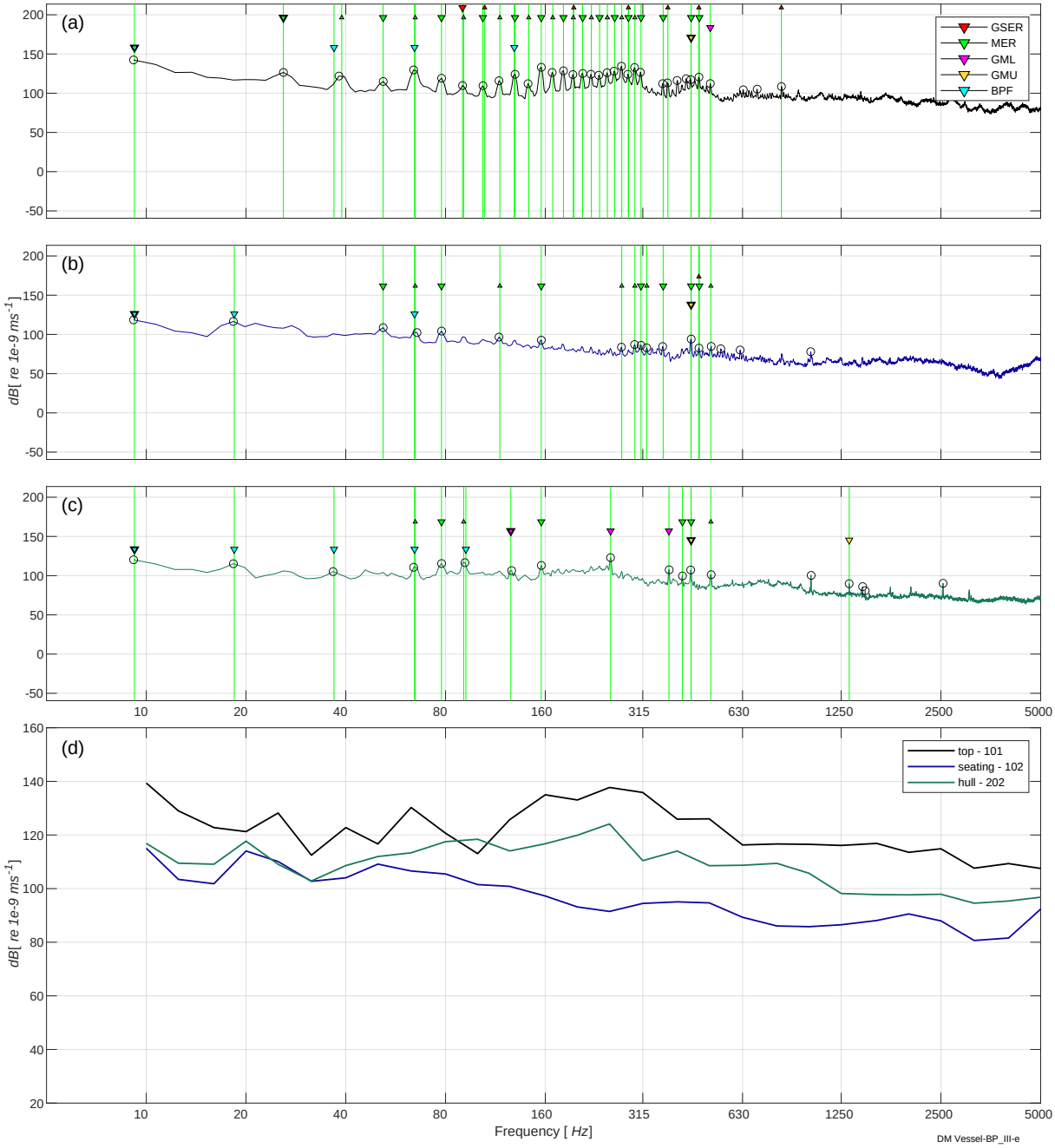


Figure D-50: Structural velocity narrow-band spectra (a) above the resilient mount, (b) on the seating, (c) on the hull and the respective (d) third-octave band spectra. Run: DM BP-III - Engine Structure

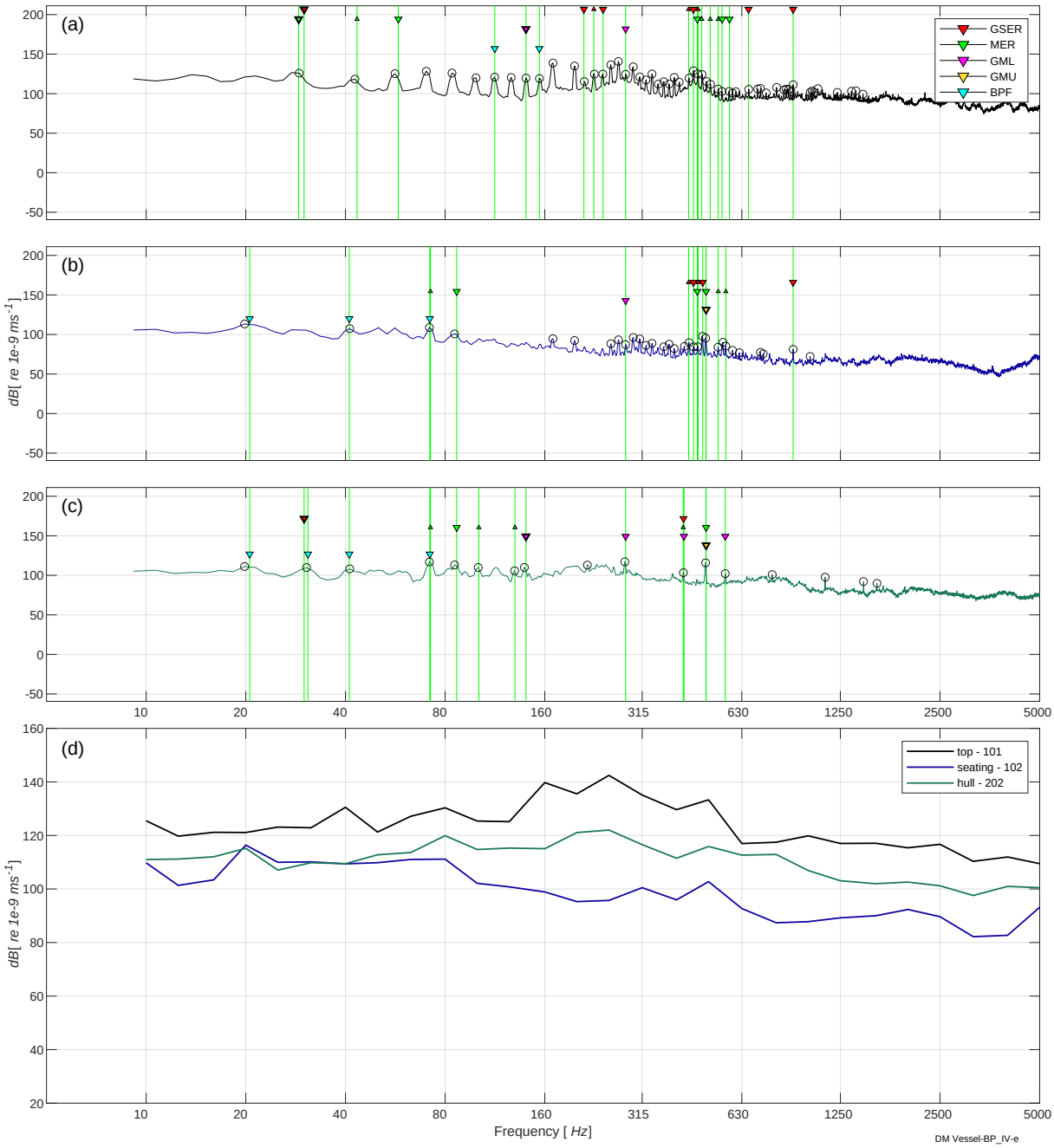


Figure D-51: Structural velocity narrow-band spectra (a) above the resilient mount, (b) on the seating, (c) on the hull and the respective (d) third-octave band spectra. Run: DM BP-IV - Engine Structure

D.12 DM Vessel - Structure-borne Noise - Drive Structure - Baseline Stationary (BS)

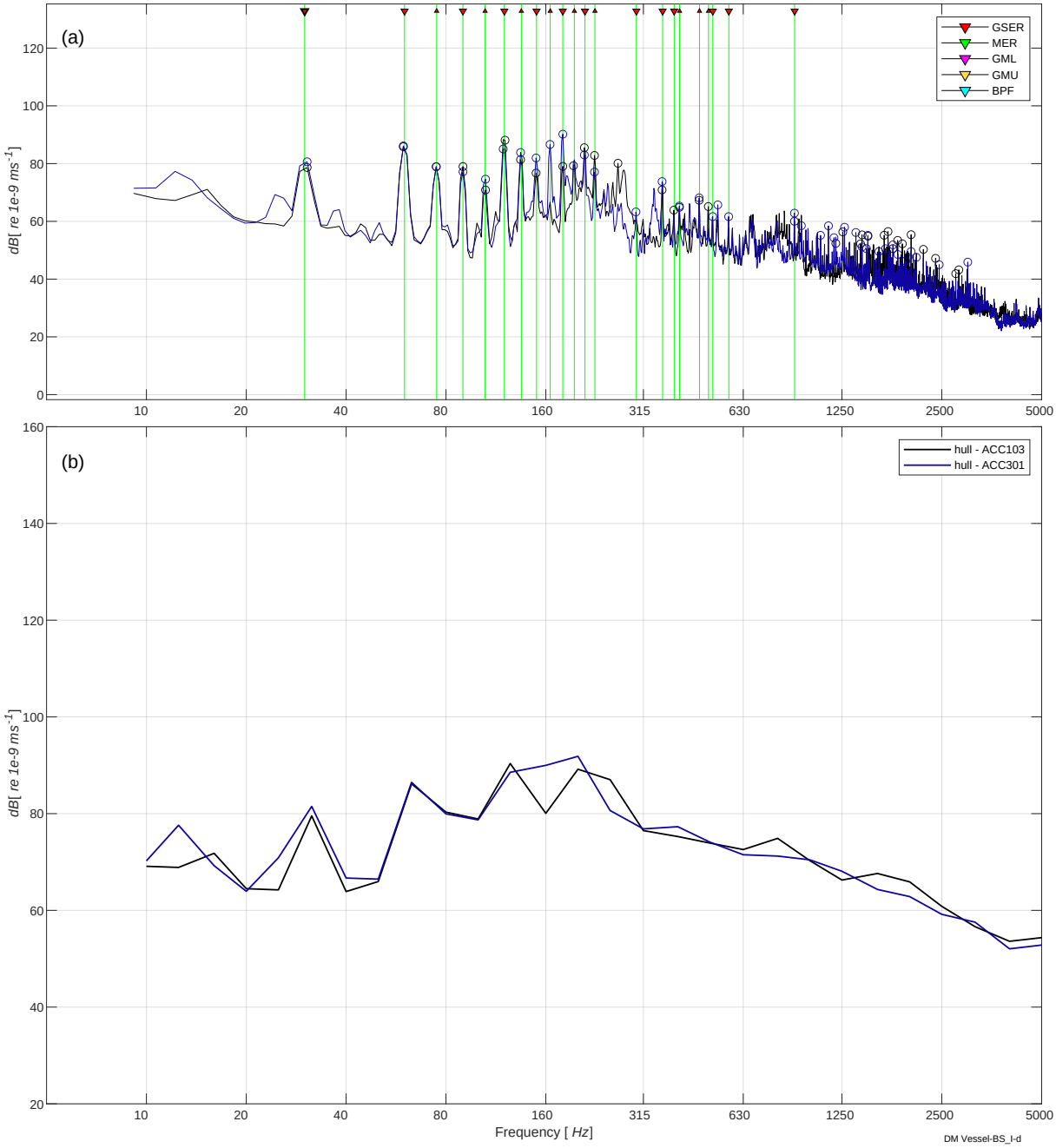


Figure D-52: Structural velocity narrow-band spectra (a) on the seating, (b) on the hull and the respective (c) third-octave band spectra. Run: DM BS-I - Drive Structure

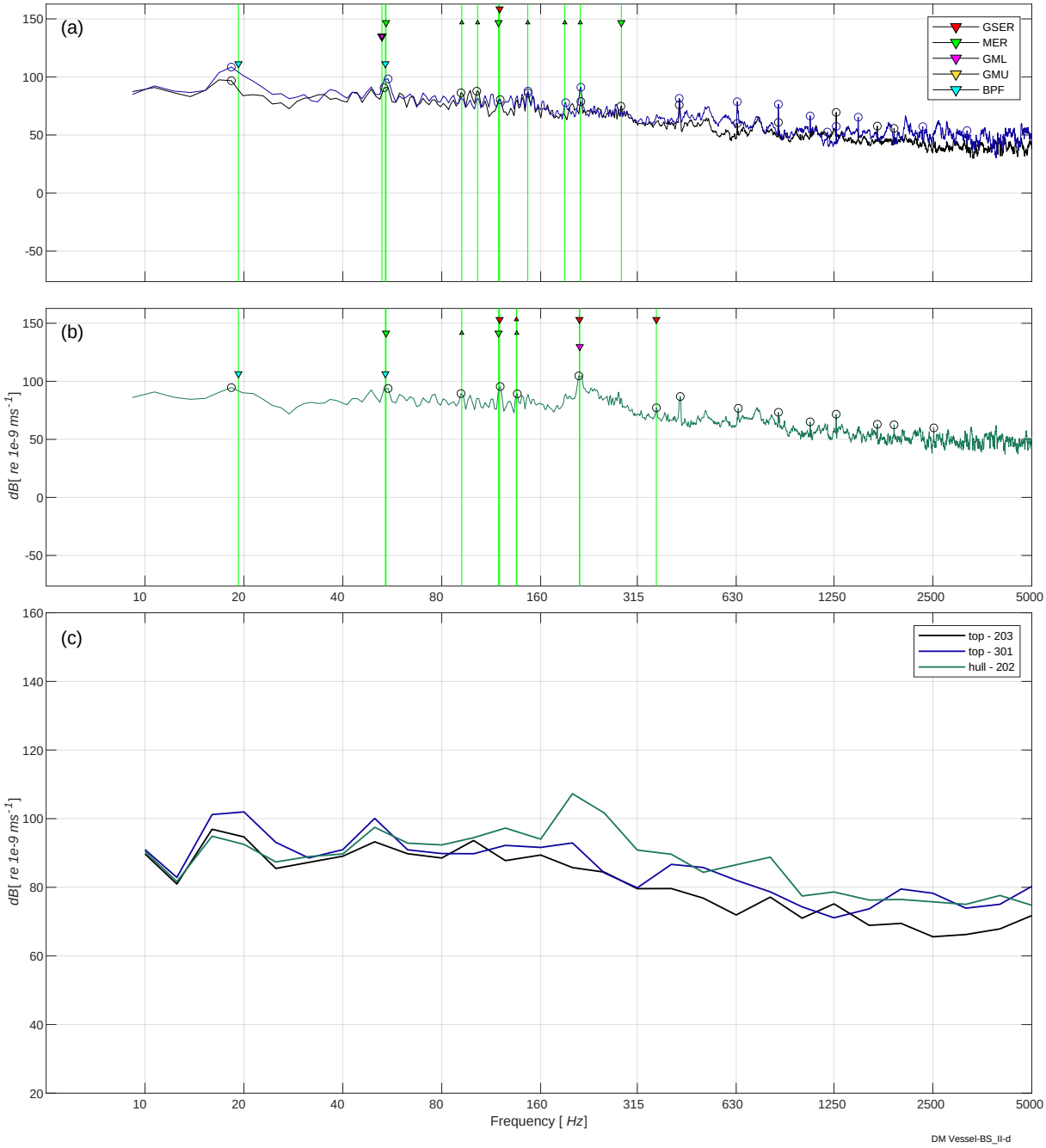


Figure D-53: Structural velocity narrow-band spectra (a) on the seating, (b) on the hull and the respective (c) third-octave band spectra. Run: DM BS-II - Drive Structure

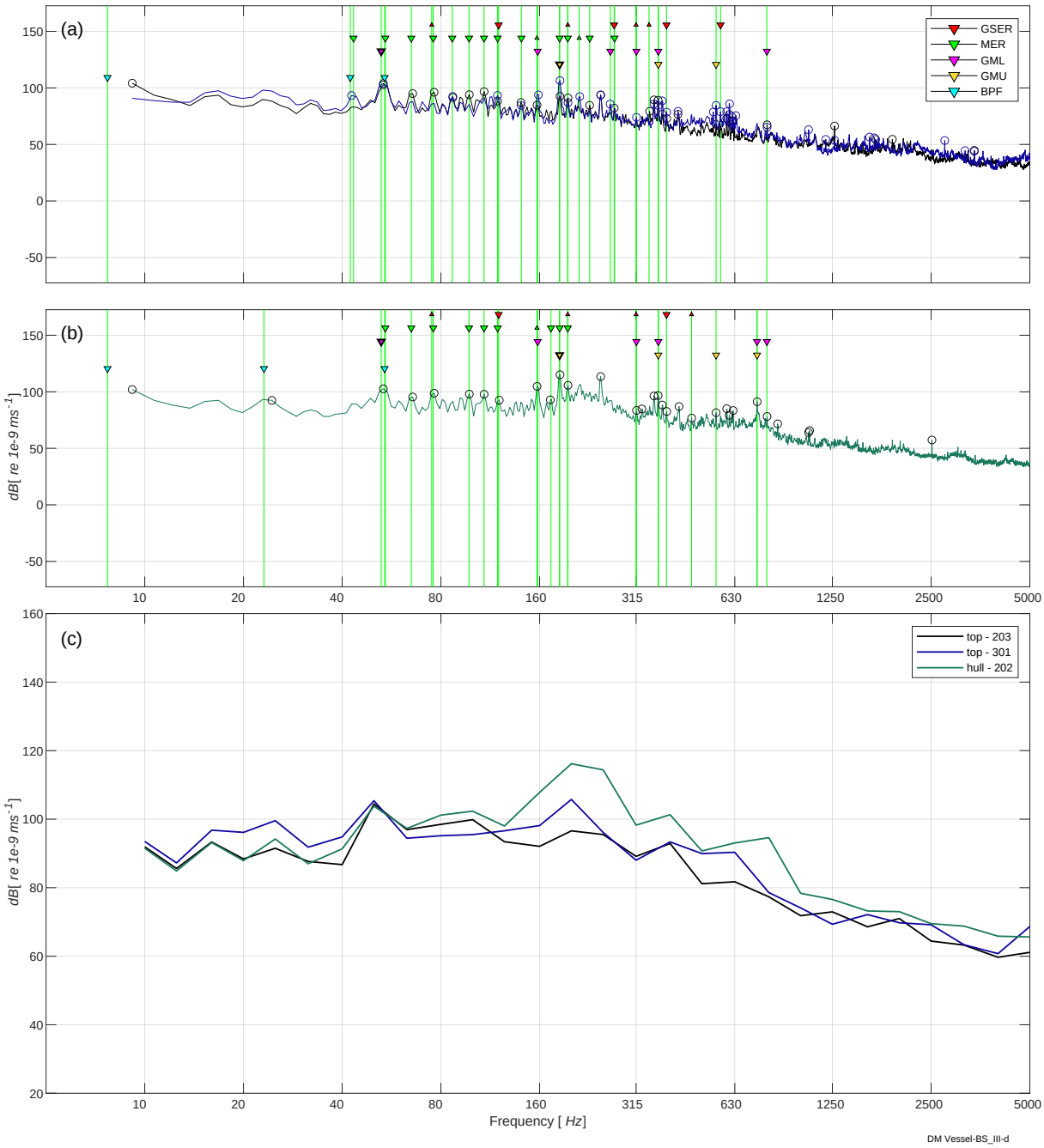


Figure D-54: Structural velocity narrow-band spectra (a) on the seating, (b) on the hull and the respective (c) third-octave band spectra. Run: DM BS-III - Drive Structure

D.13 DM Vessel - Structure-borne Noise - Drive Structure - Straight Travel (ST)

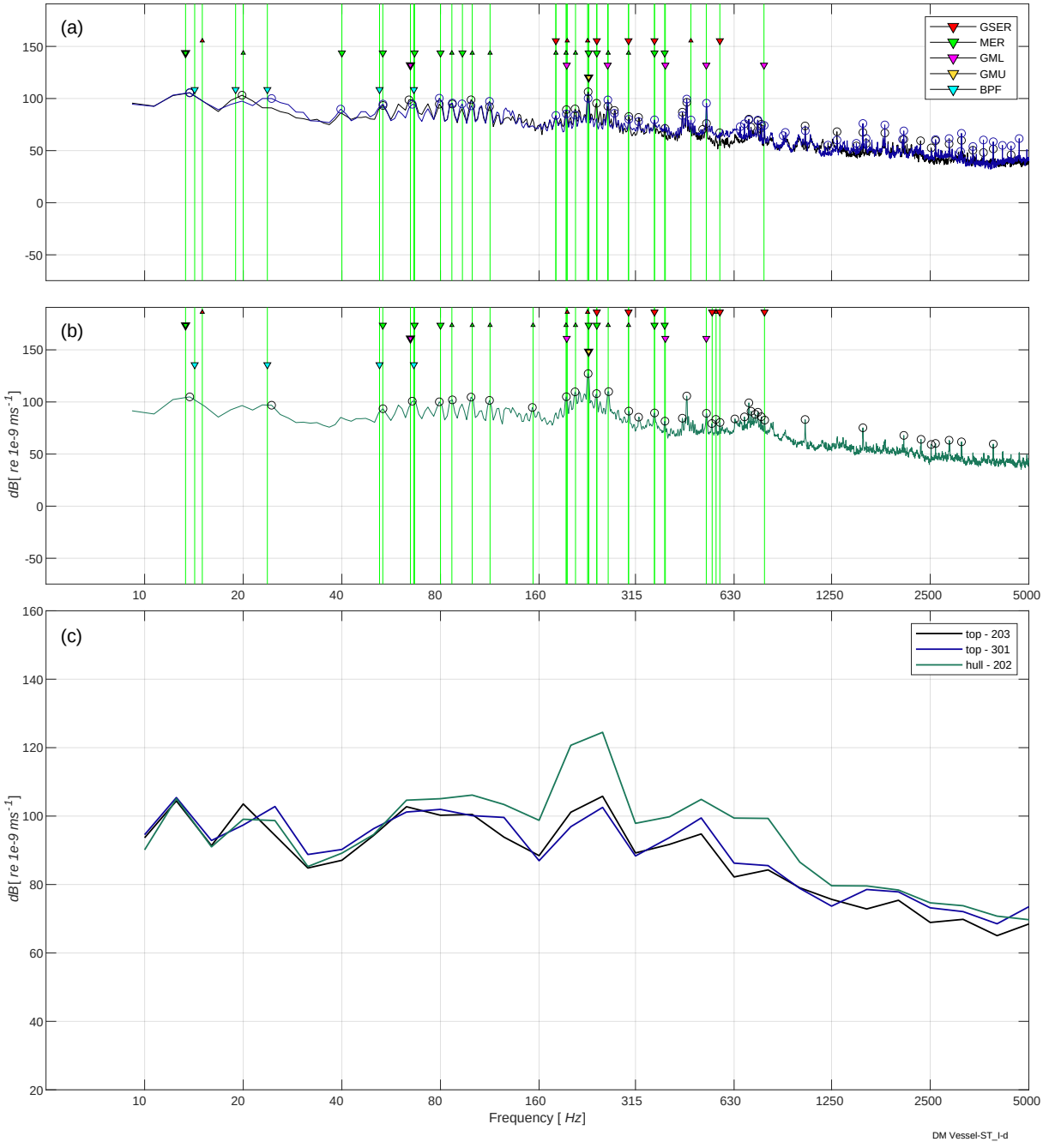


Figure D-55: Structural velocity narrow-band spectra (a) on the seating, (b) on the hull and the respective (c) third-octave band spectra. Run: DM ST-I - Drive Structure

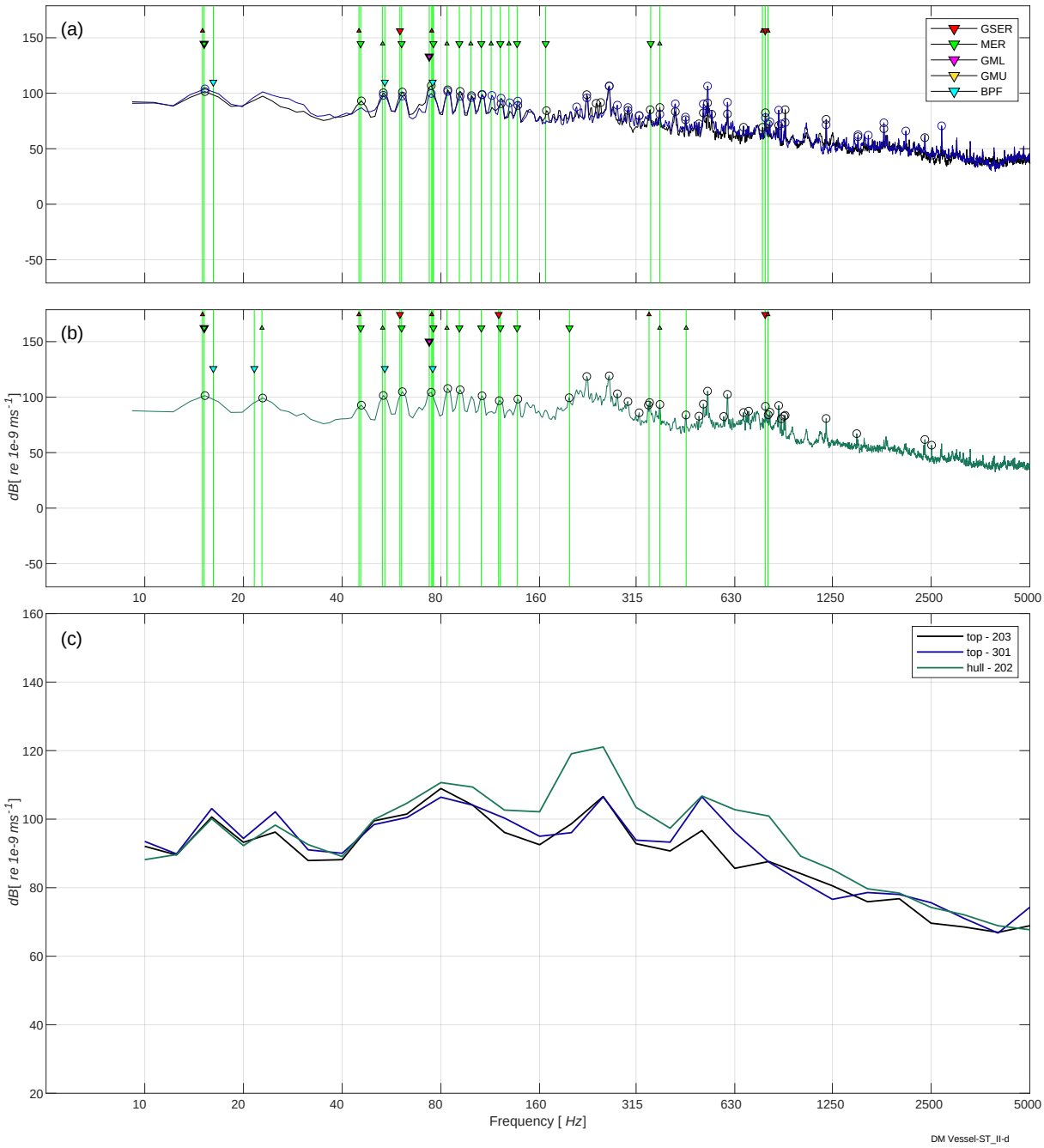


Figure D-56: Structural velocity narrow-band spectra (a) on the seating, (b) on the hull and the respective (c) third-octave band spectra. Run: DM ST-II - Drive Structure

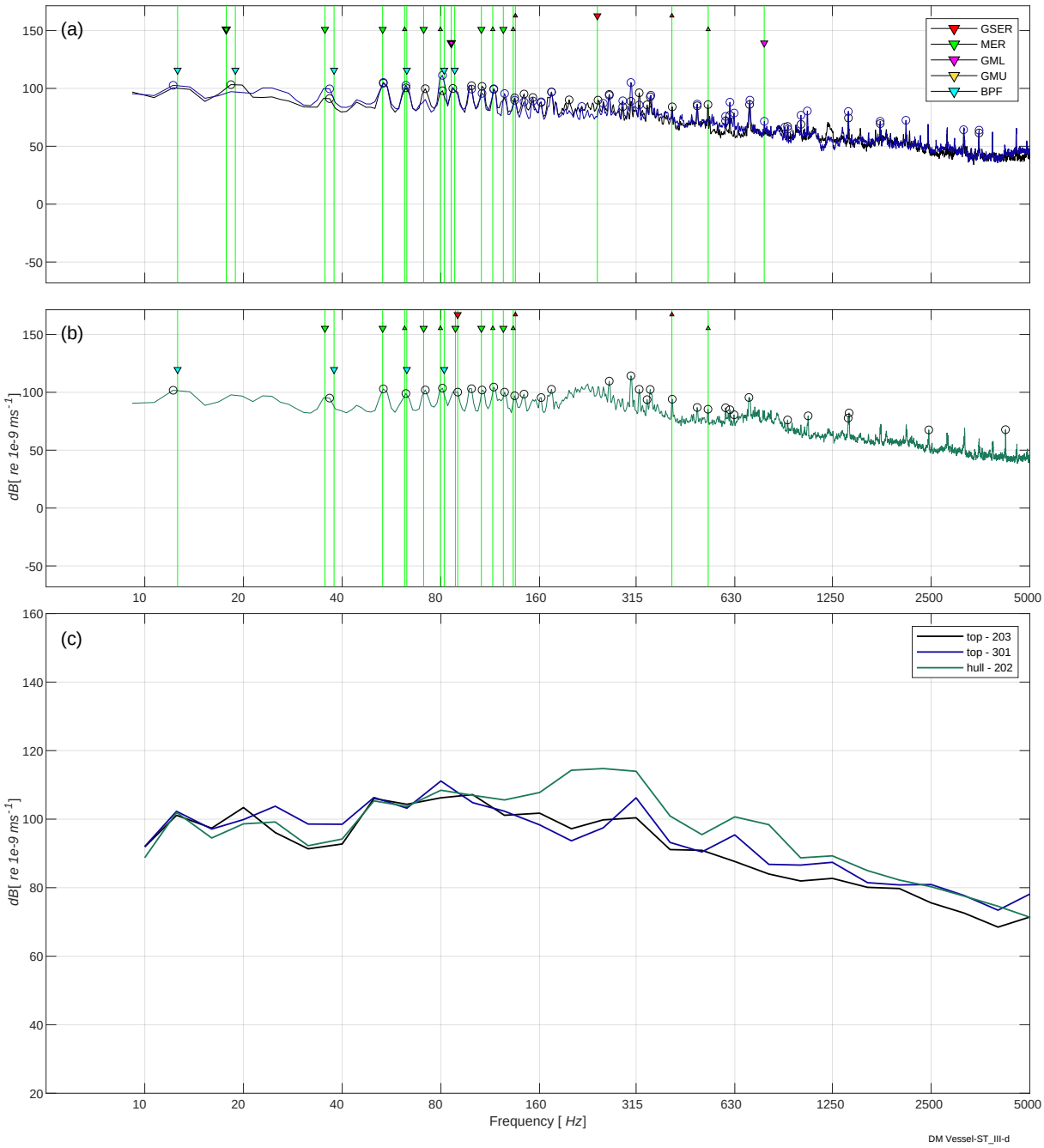


Figure D-57: Structural velocity narrow-band spectra (a) on the seating, (b) on the hull and the respective (c) third-octave band spectra. Run: DM ST-III - Drive Structure

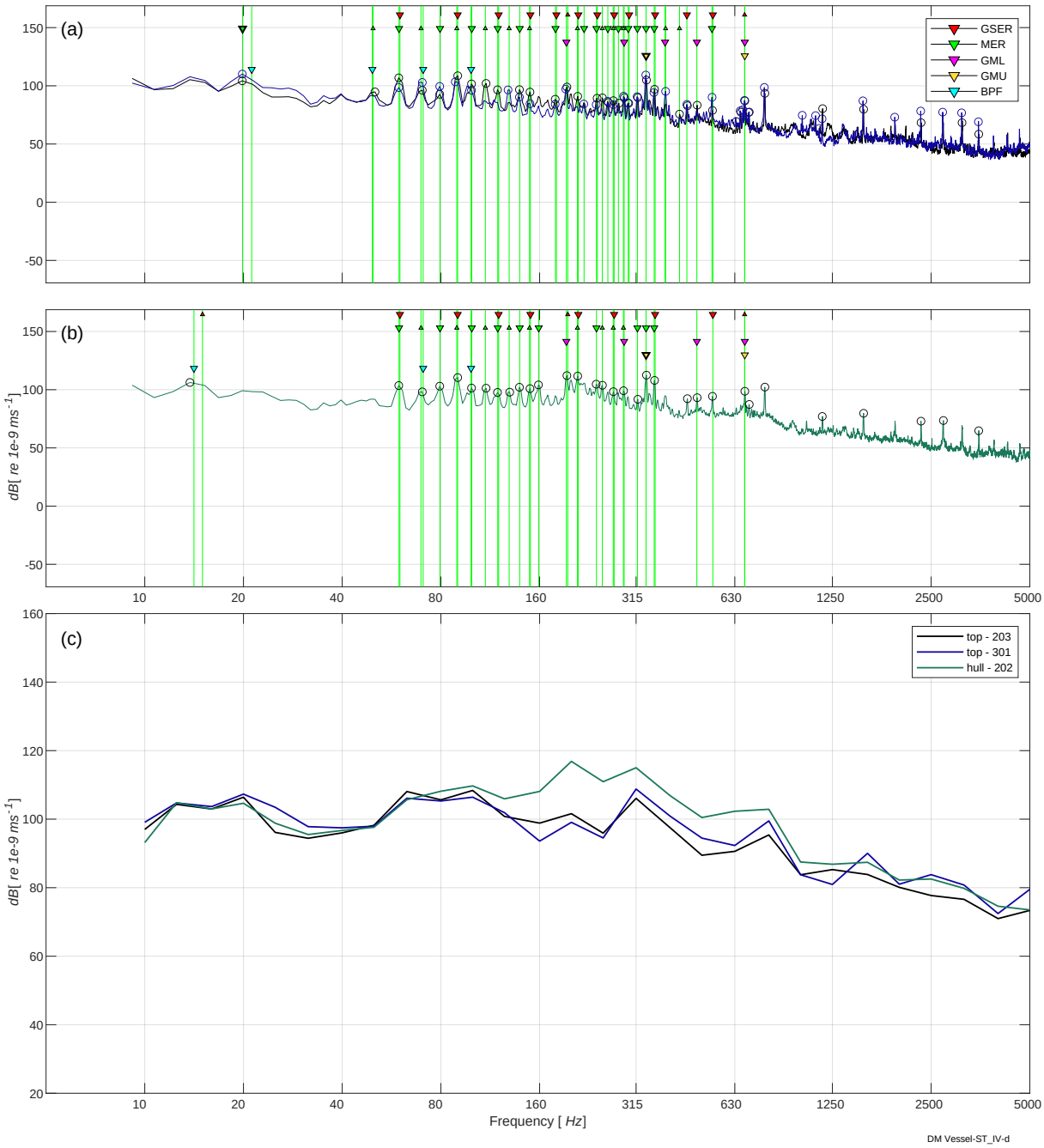


Figure D-58: Structural velocity narrow-band spectra (a) on the seating, (b) on the hull and the respective (c) third-octave band spectra. Run: DM ST-IV - Drive Structure

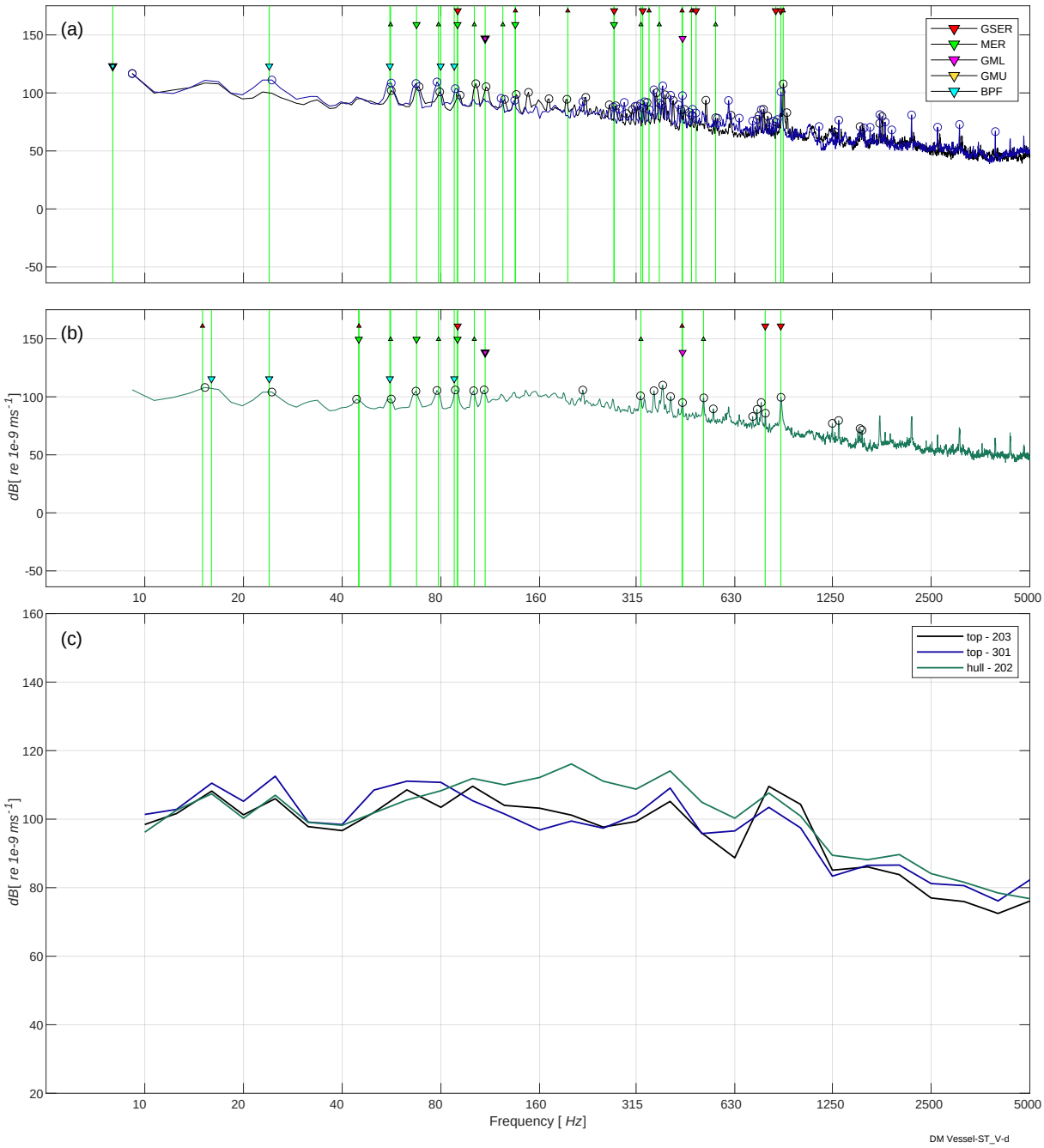


Figure D-59: Structural velocity narrow-band spectra (a) on the seating, (b) on the hull and the respective (c) third-octave band spectra. Run: DM ST-V - Drive Structure

D.14 DM Vessel - Structure-borne Noise - Drive Structure - Bollard Pull (BP)

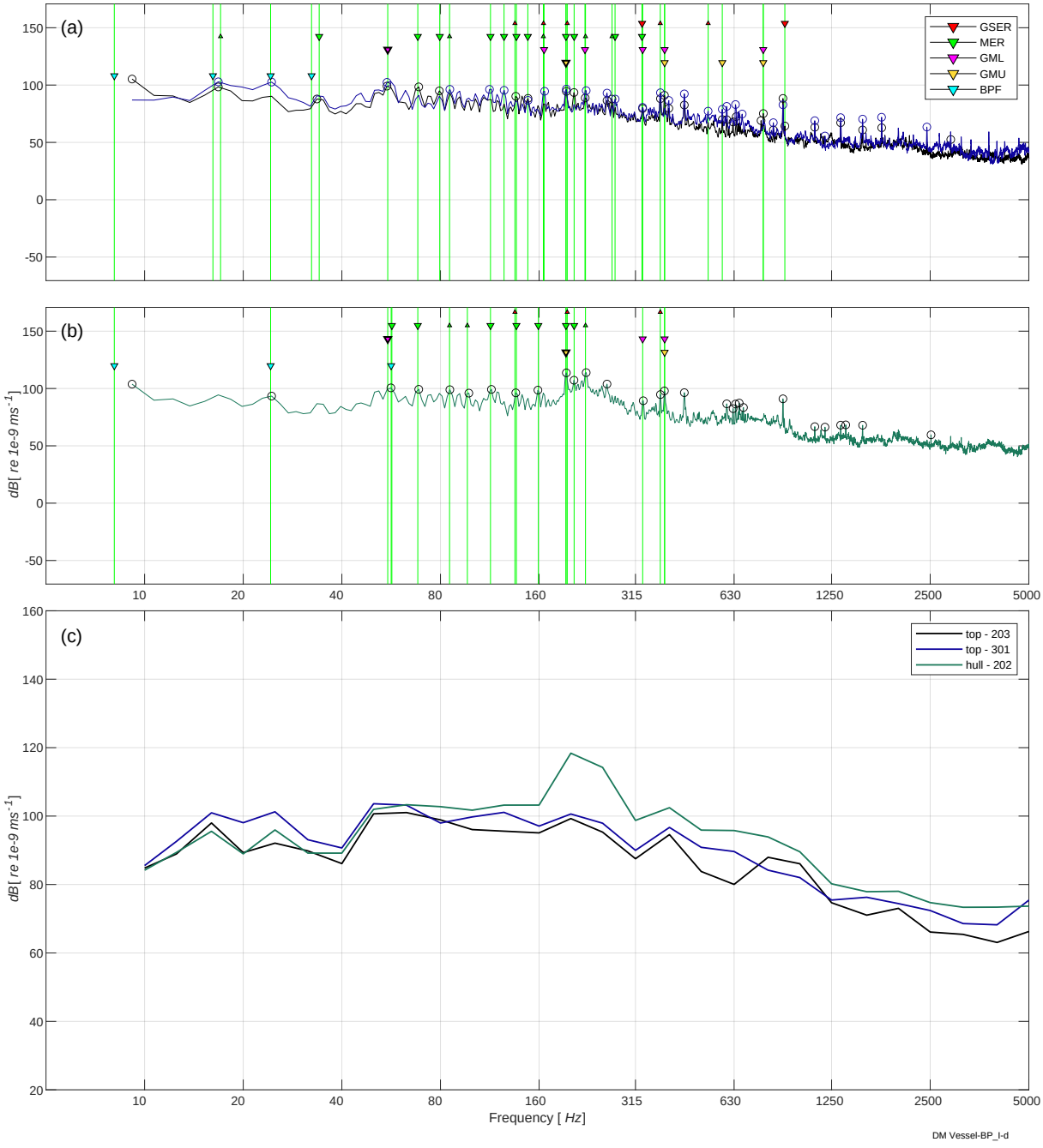


Figure D-60: Structural velocity narrow-band spectra (a) on the seating, (b) on the hull and the respective (c) third-octave band spectra. Run: DM BP-I - Drive Structure

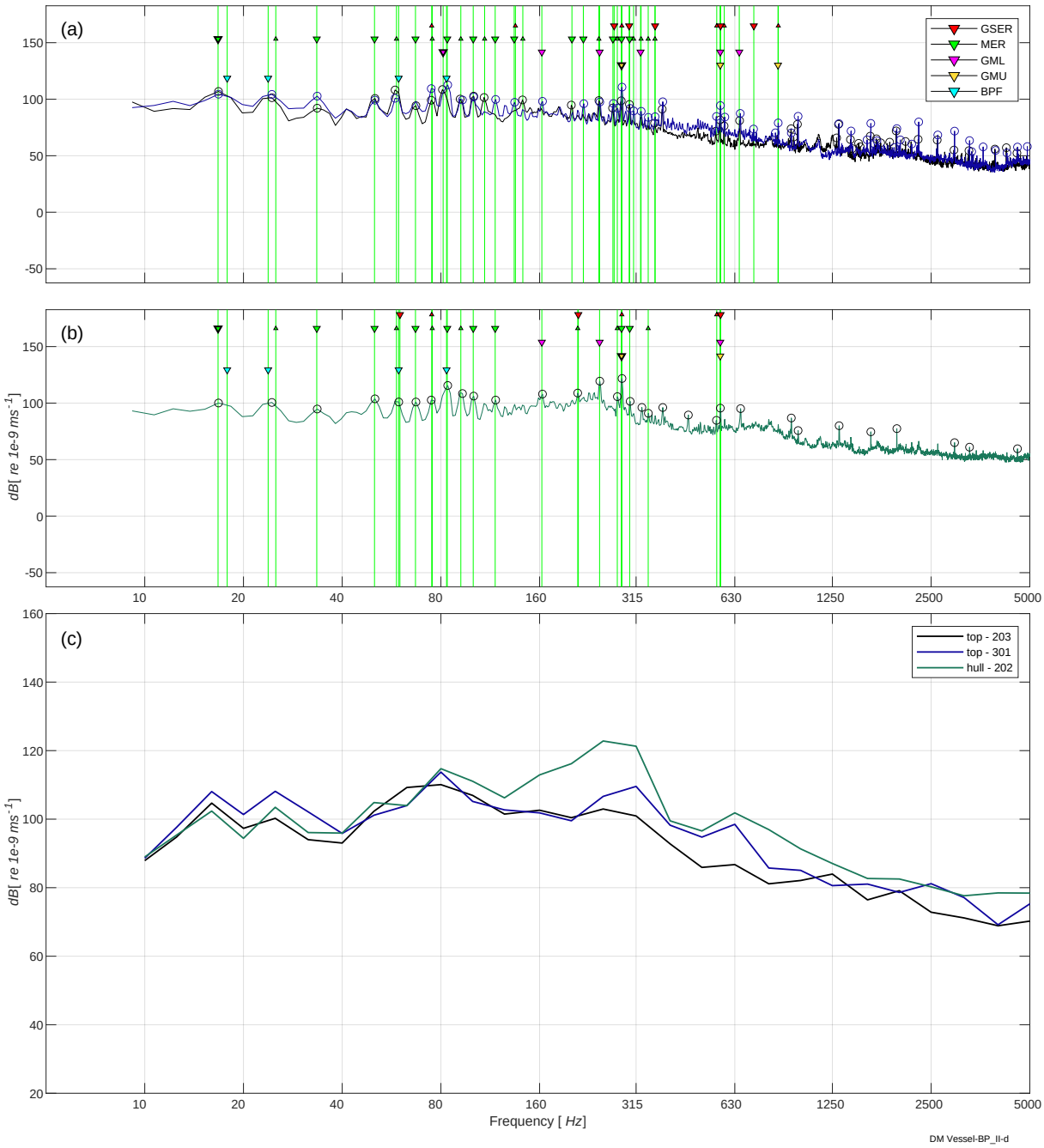


Figure D-61: Structural velocity narrow-band spectra (a) on the seating, (b) on the hull and the respective (c) third-octave band spectra. Run: DM BP-II - Drive Structure

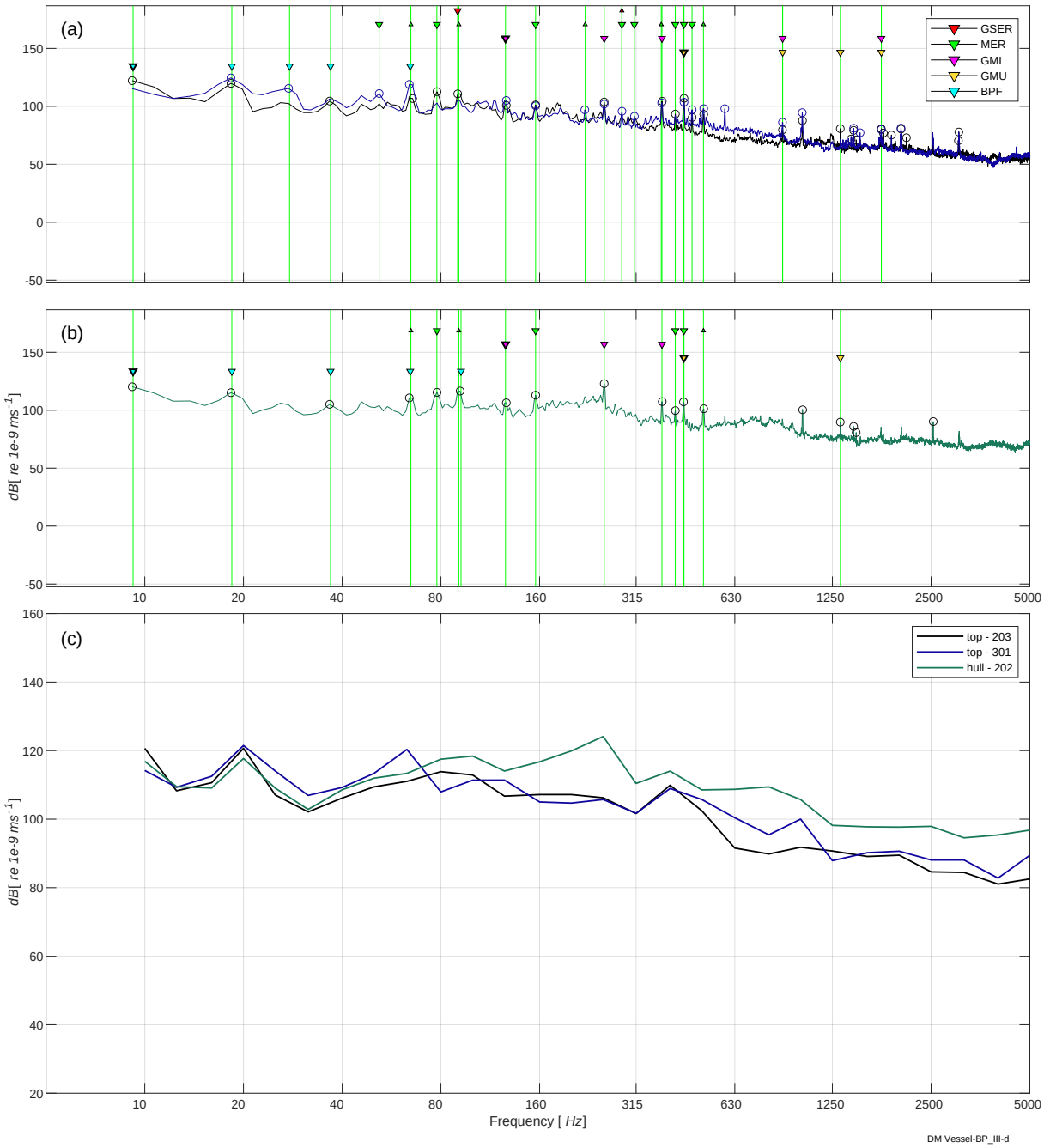


Figure D-62: Structural velocity narrow-band spectra (a) on the seating, (b) on the hull and the respective (c) third-octave band spectra. Run: DM BP-III - Drive Structure

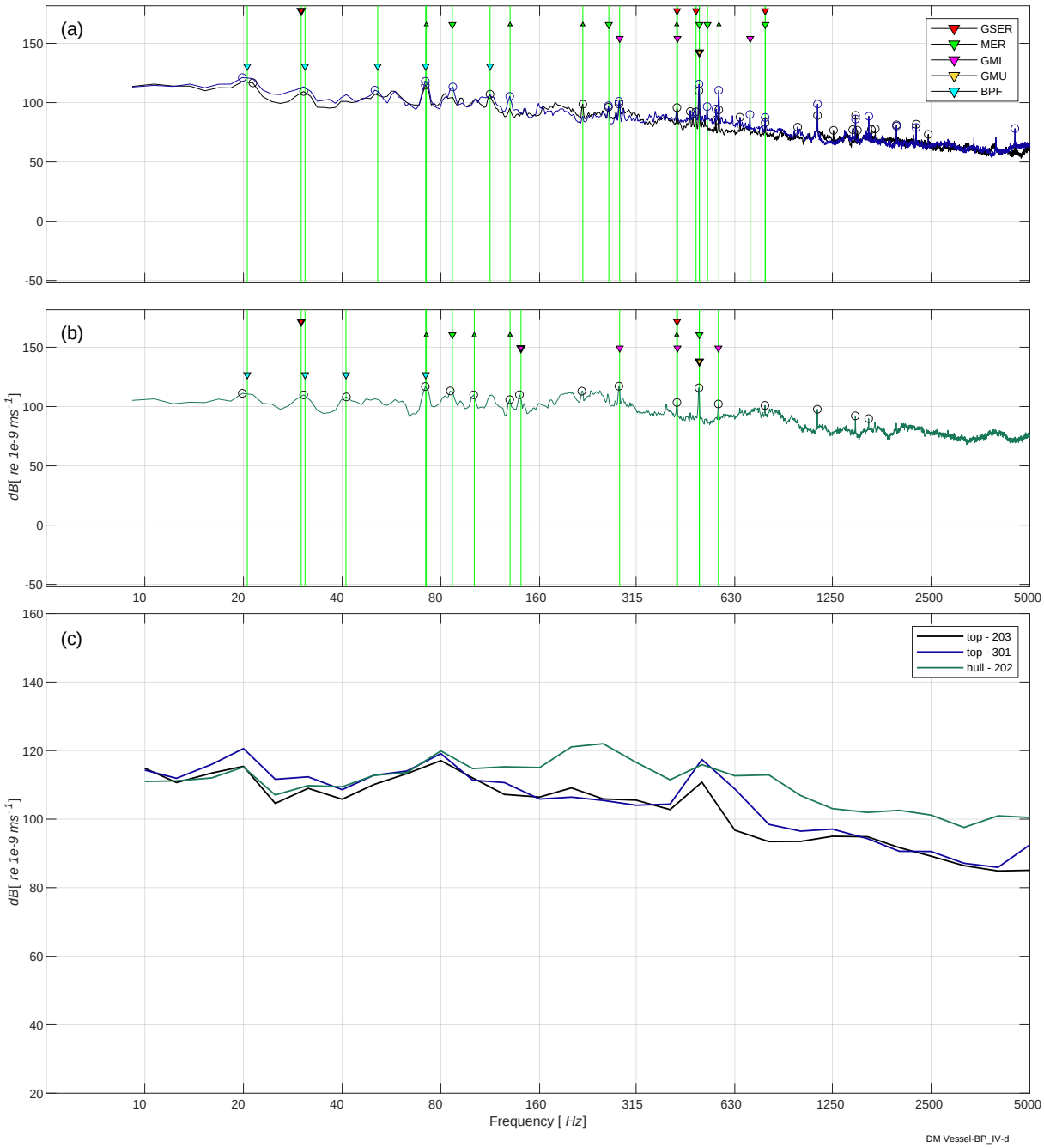


Figure D-63: Structural velocity narrow-band spectra (a) on the seating, (b) on the hull and the respective (c) third-octave band spectra. Run: DM BP-IV - Drive Structure

D.15 DM Vessel - Structure-borne Noise - Genset Structure - Baseline Stationary (BS)

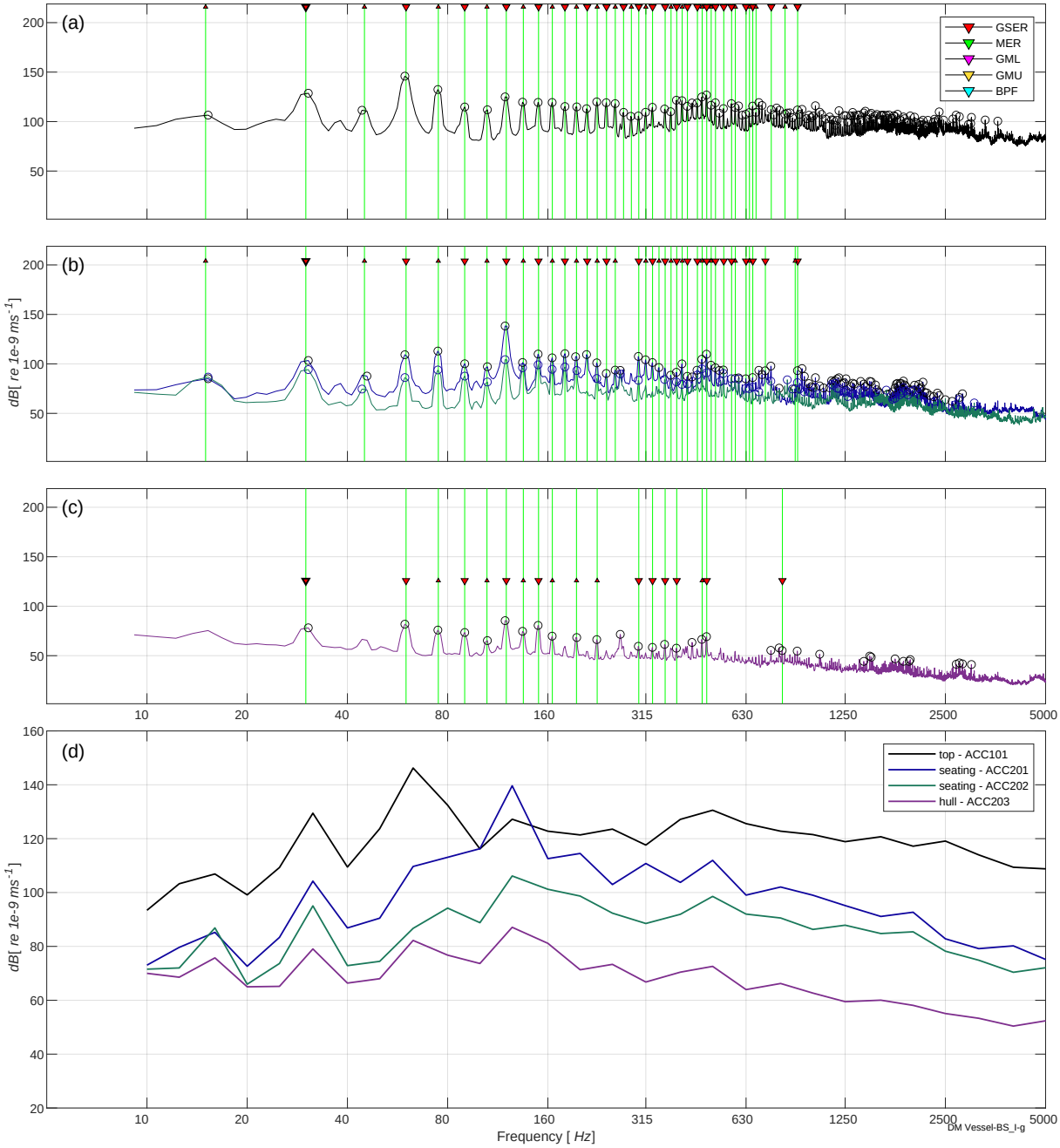


Figure D-64: Structural velocity narrow-band spectra (a) above the resilient mount, (b) on the seating, (c) on the hull and the respective (d) third-octave band spectra. Run: DM BS-I - Genset Structure

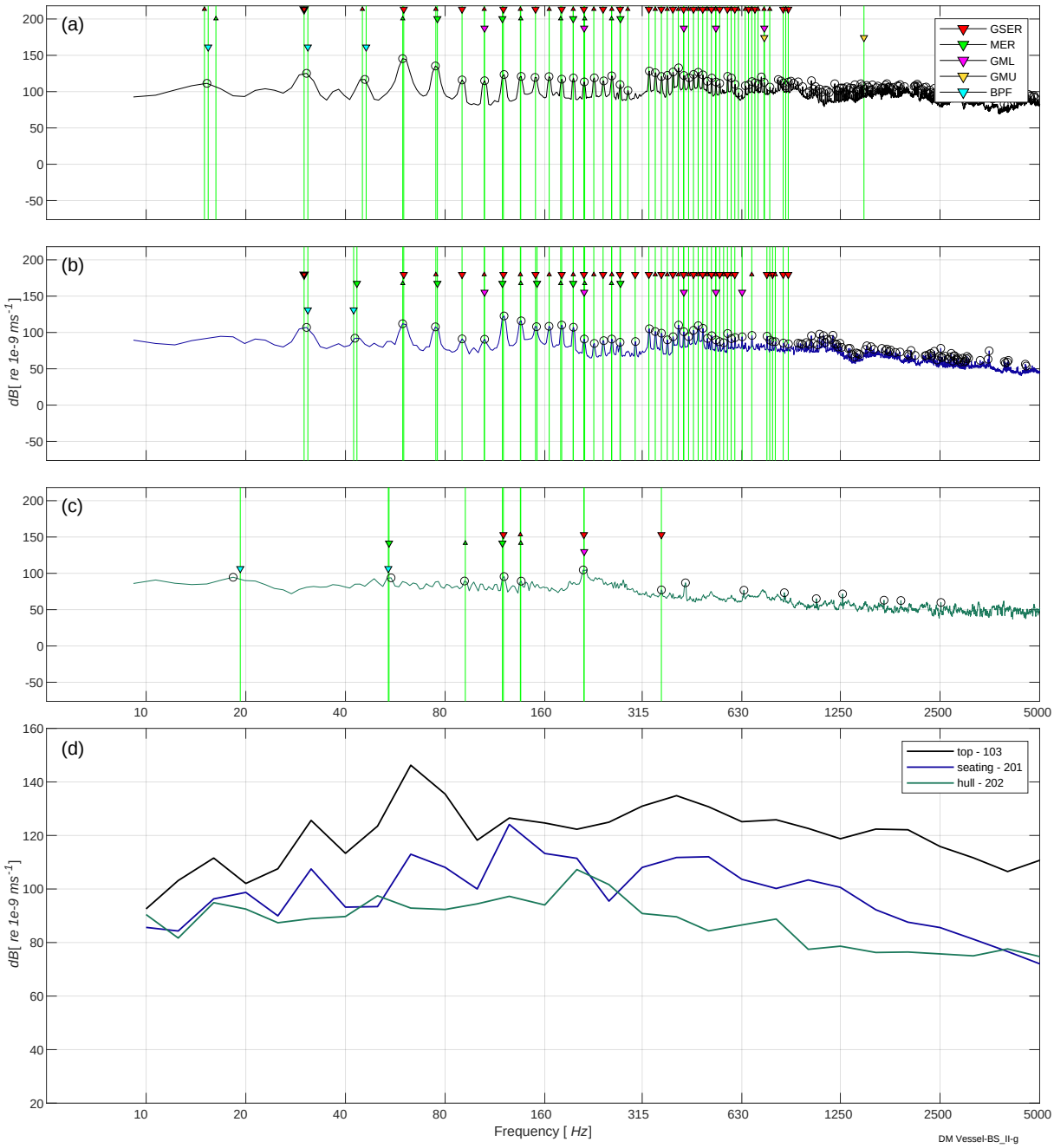


Figure D-65: Structural velocity narrow-band spectra (a) above the resilient mount, (b) on the seating, (c) on the hull and the respective (d) third-octave band spectra. Run: DM BS-II - Genset Structure

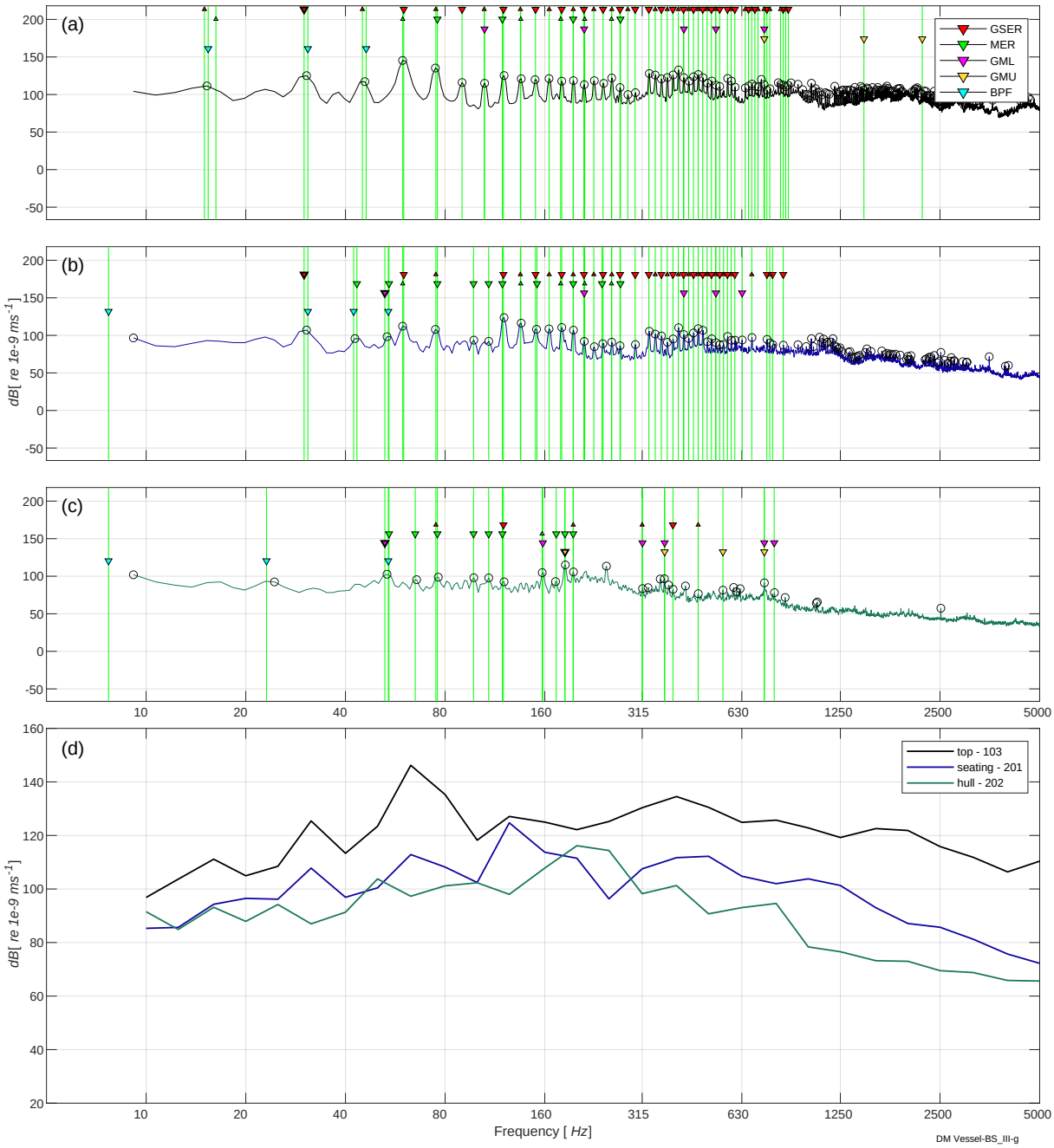


Figure D-66: Structural velocity narrow-band spectra (a) above the resilient mount, (b) on the seating, (c) on the hull and the respective (d) third-octave band spectra. Run: DM BS-III - Genset Structure

D.16 DM Vessel - Structure-borne Noise - Genset Structure - Straight Travel (ST)

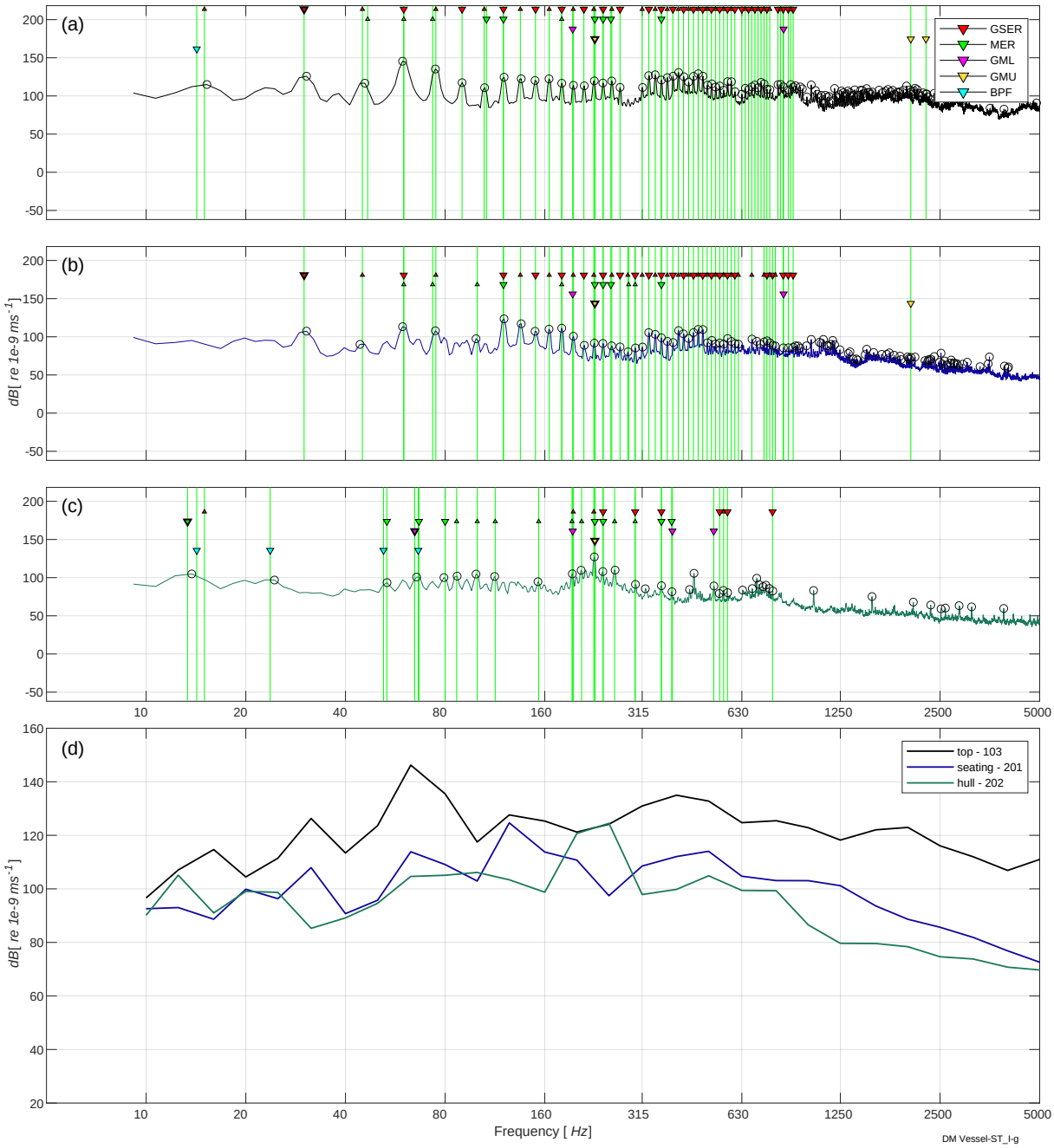


Figure D-67: Structural velocity narrow-band spectra (a) above the resilient mount, (b) on the seating, (c) on the hull and the respective (d) third-octave band spectra. Run: DM ST-I - Genset Structure

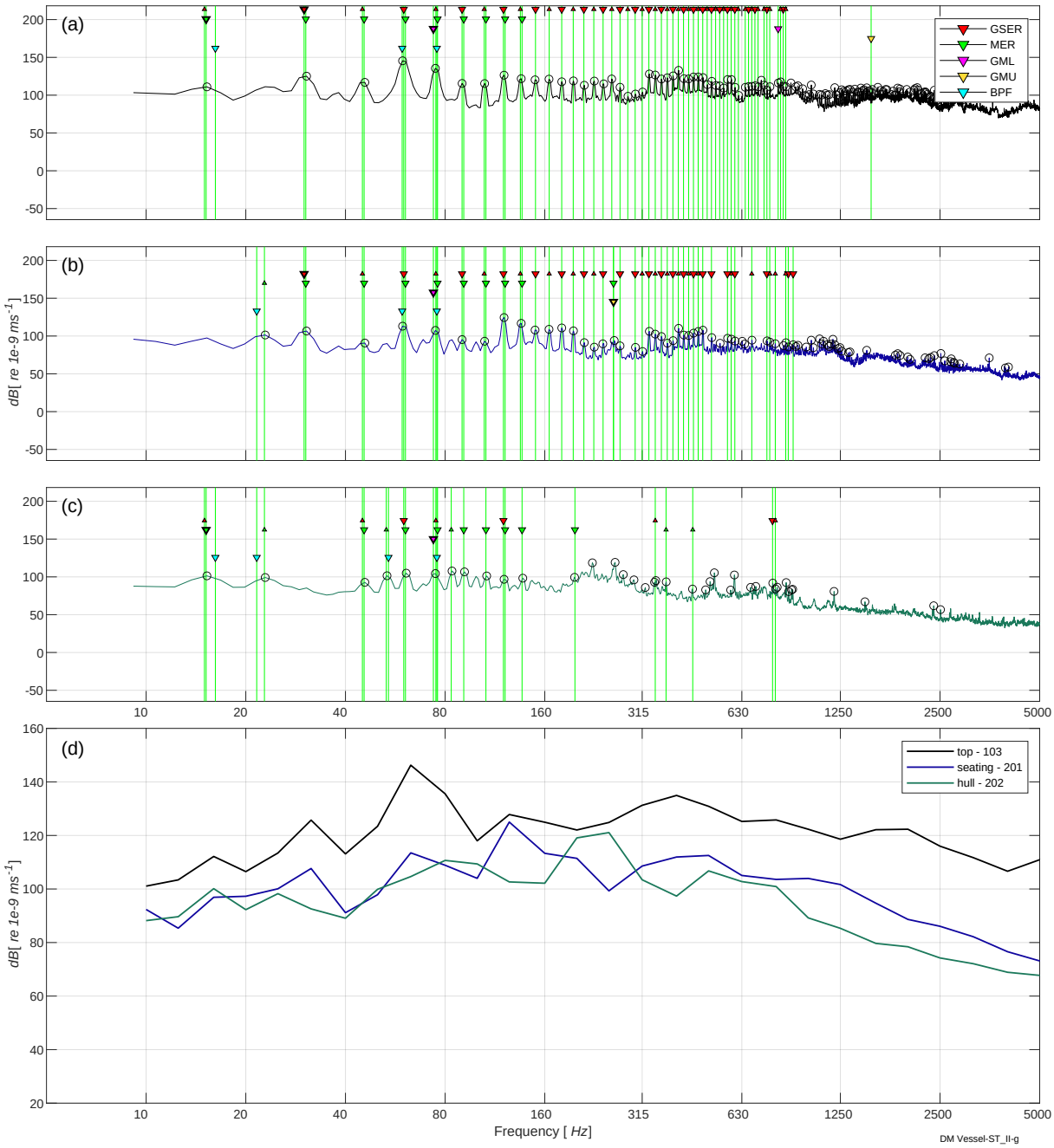


Figure D-68: Structural velocity narrow-band spectra (a) above the resilient mount, (b) on the seating, (c) on the hull and the respective (d) third-octave band spectra. Run: DM ST-II - Genset Structure

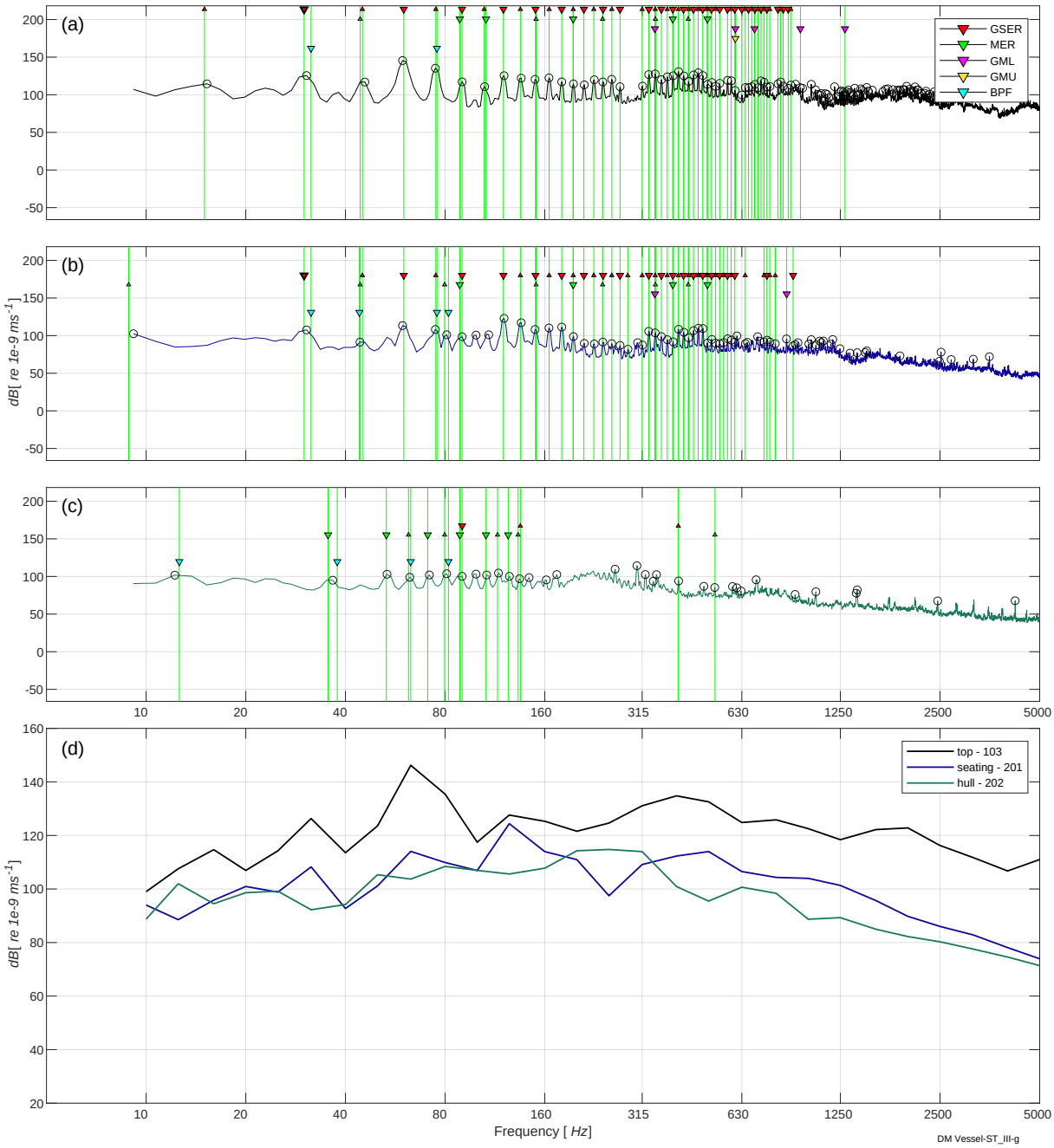


Figure D-69: Structural velocity narrow-band spectra (a) above the resilient mount, (b) on the seating, (c) on the hull and the respective (d) third-octave band spectra. Run: DM ST-III - Genset Structure

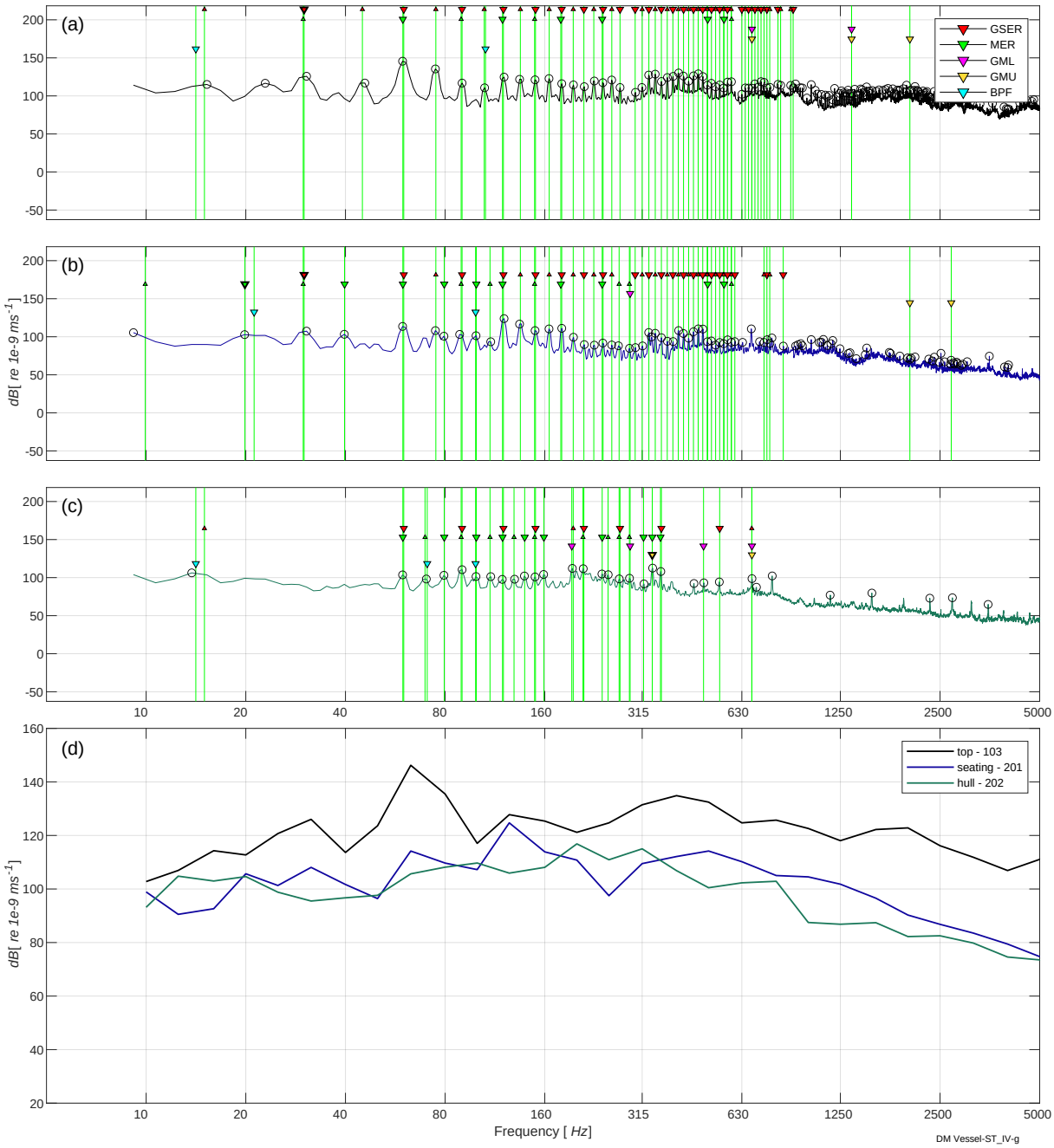


Figure D-70: Structural velocity narrow-band spectra (a) above the resilient mount, (b) on the seating, (c) on the hull and the respective (d) third-octave band spectra. Run: DM ST-IV - Genset Structure

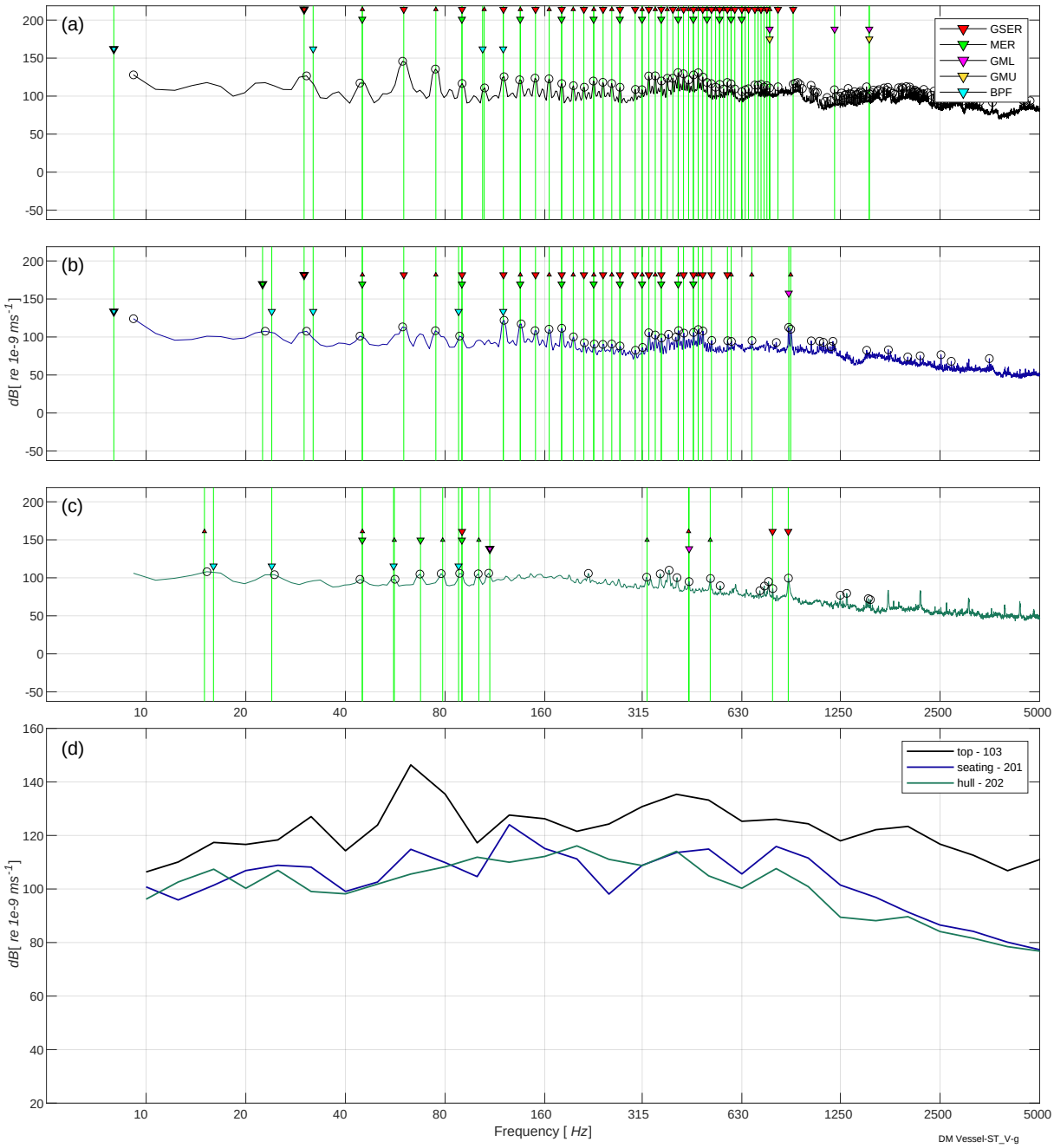


Figure D-71: Structural velocity narrow-band spectra (a) above the resilient mount, (b) on the seating, (c) on the hull and the respective (d) third-octave band spectra. Run: DM ST-V - Genset Structure

D.17 DM Vessel - Structure-borne Noise - Genset Structure - Bollard Pull (BP)

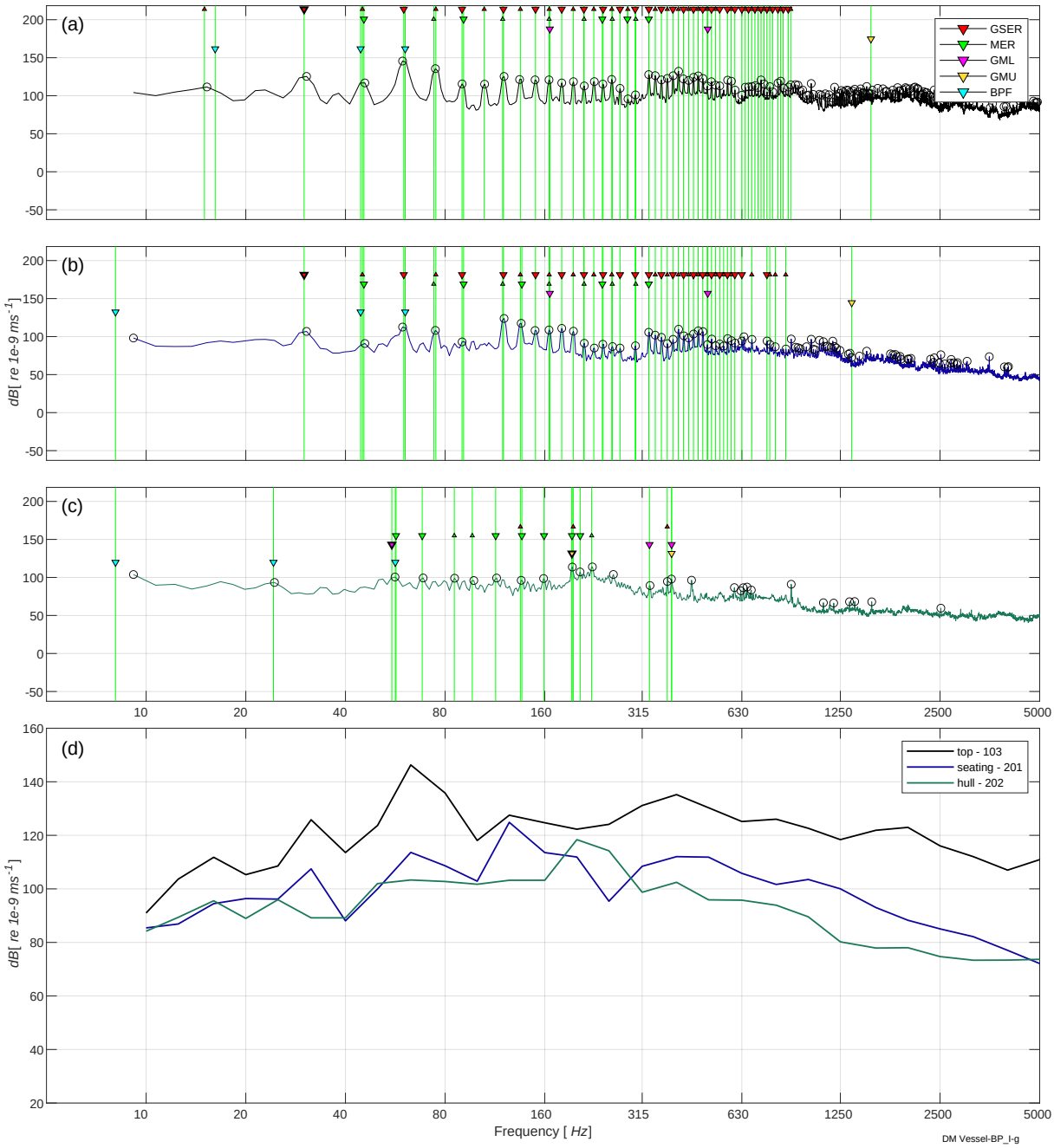


Figure D-72: Structural velocity narrow-band spectra (a) above the resilient mount, (b) on the seating, (c) on the hull and the respective (d) third-octave band spectra. Run: DM BP-I - Genset Structure

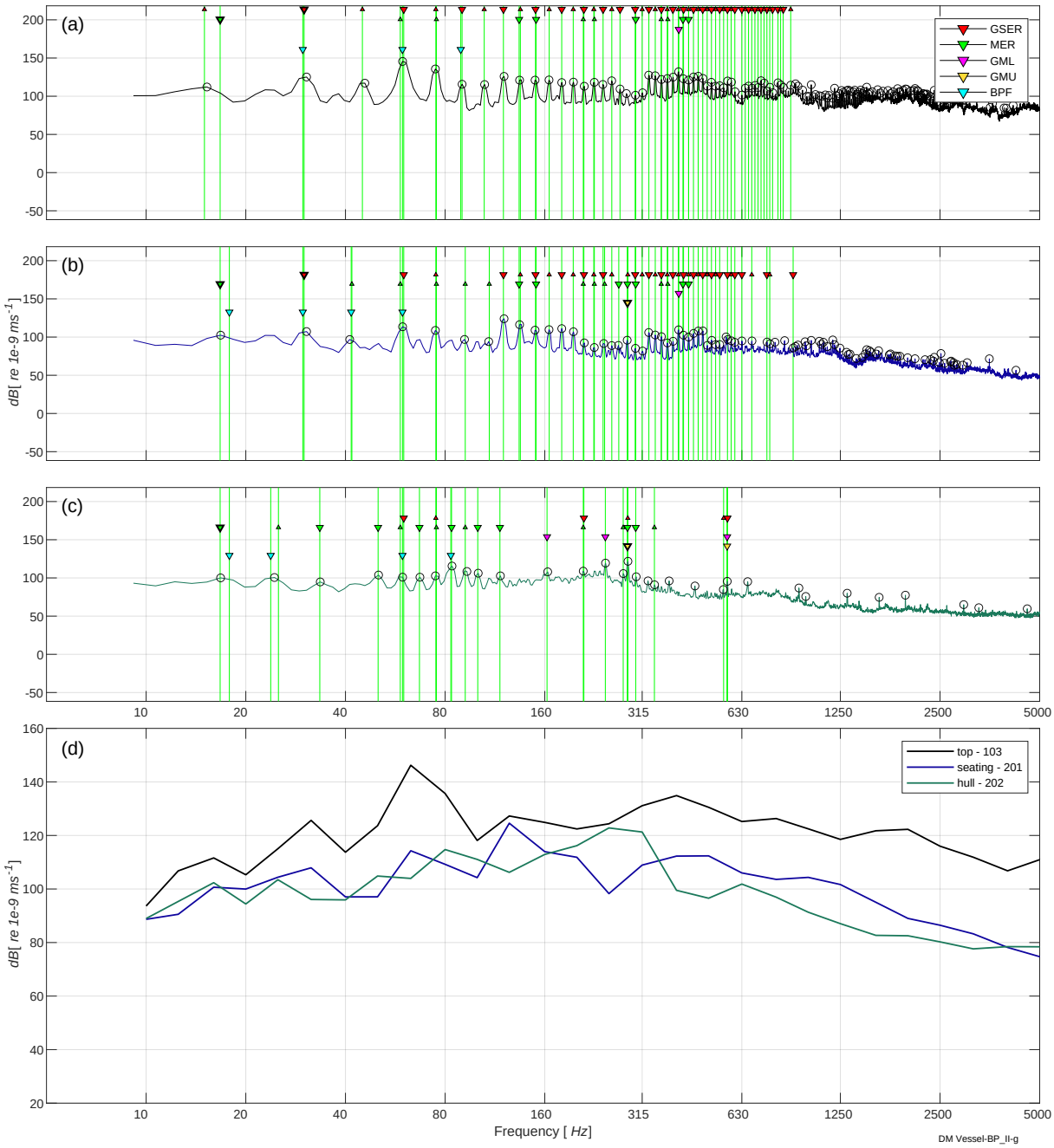


Figure D-73: Structural velocity narrow-band spectra (a) above the resilient mount, (b) on the seating, (c) on the hull and the respective (d) third-octave band spectra. Run: DM BP-II - Genset Structure

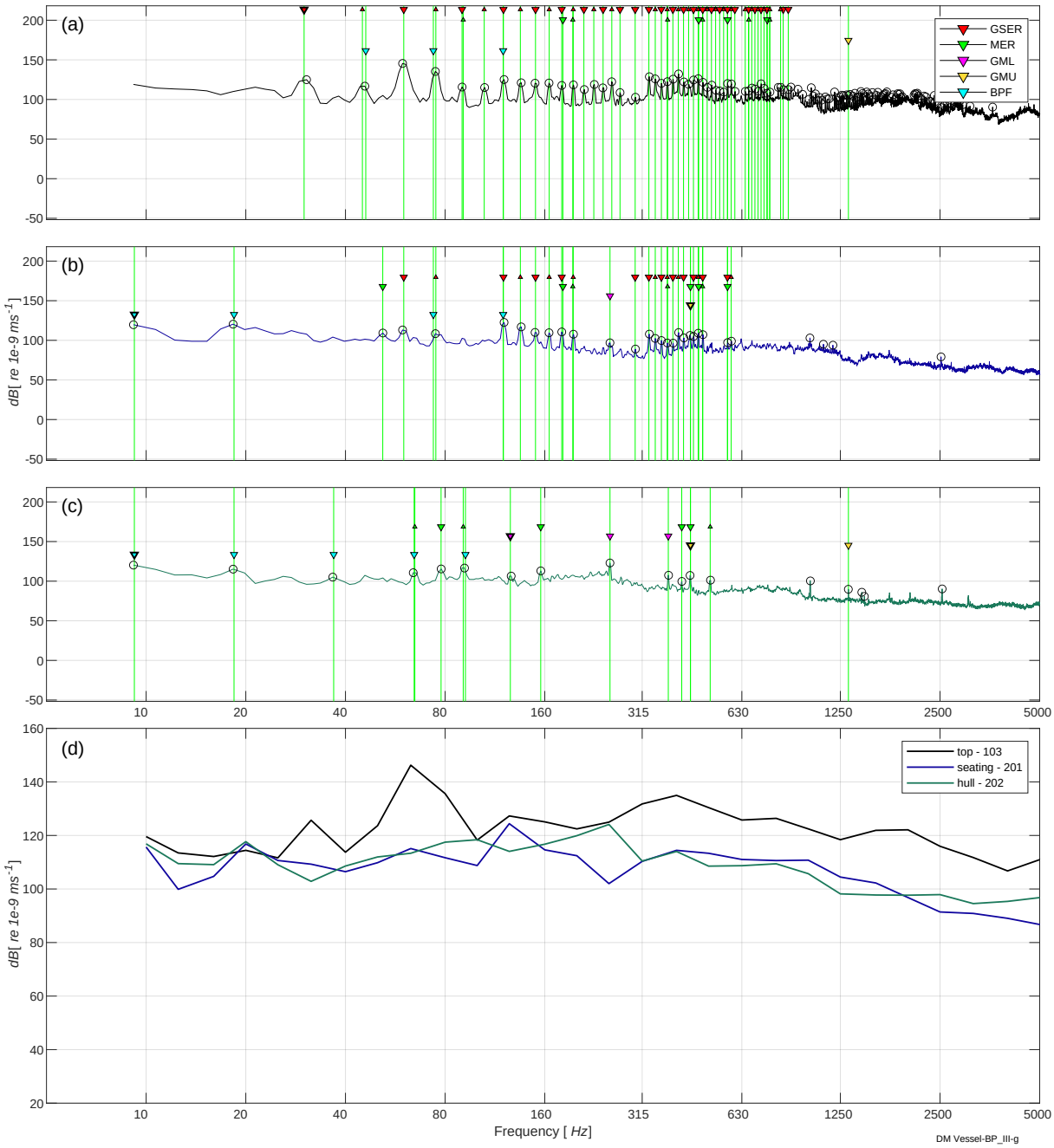


Figure D-74: Structural velocity narrow-band spectra (a) above the resilient mount, (b) on the seating, (c) on the hull and the respective (d) third-octave band spectra. Run: DM BP-III - Genset Structure

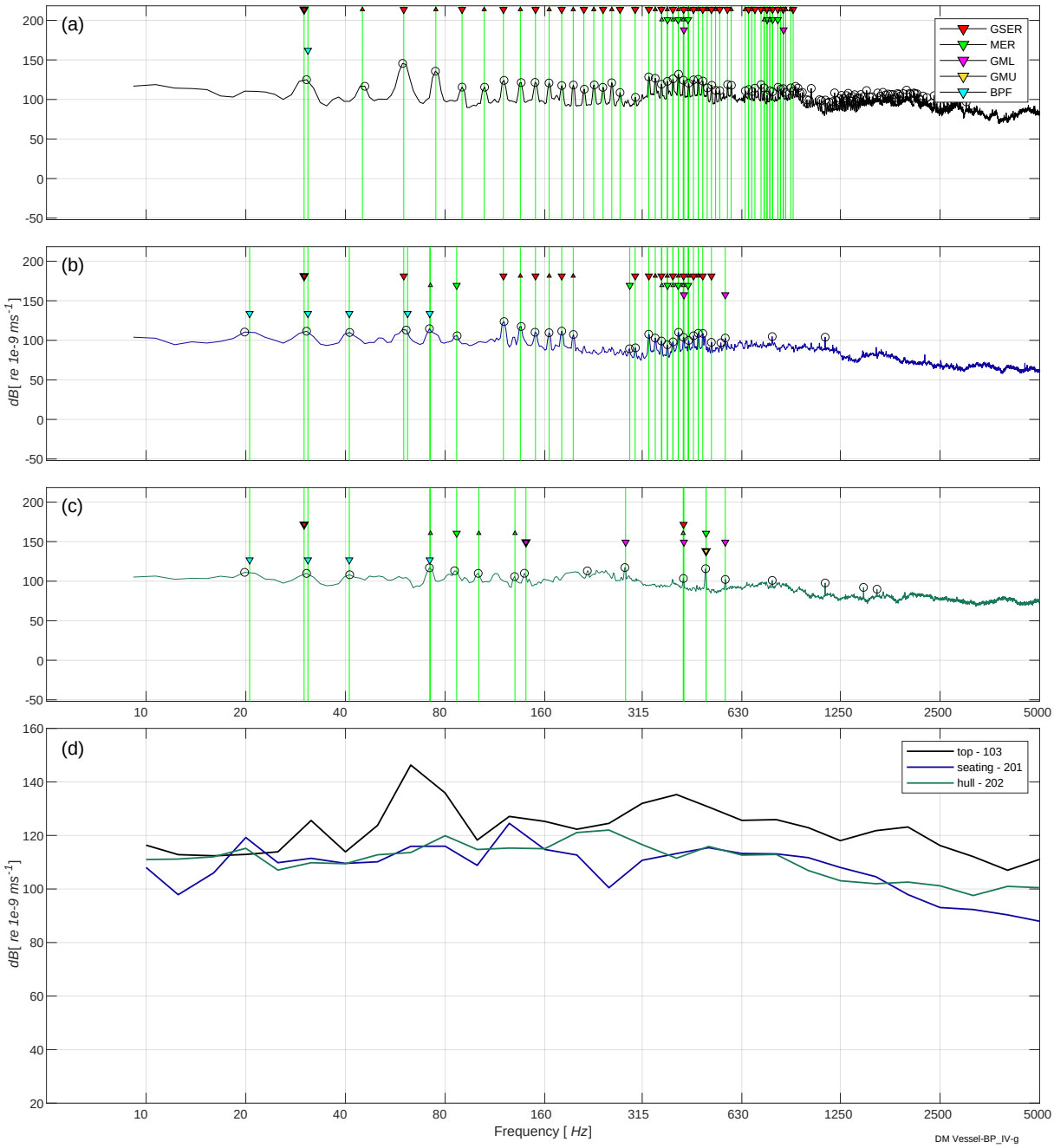


Figure D-75: Structural velocity narrow-band spectra (a) above the resilient mount, (b) on the seating, (c) on the hull and the respective (d) third-octave band spectra. Run: DM BP-IV - Genset Structure

Appendix E. Machinery Noise Generation, Transmission, and Radiation

This section presents results from a study aimed at characterizing the structure-borne (SBN) and airborne (ABN) noise generated by onboard machinery relative to the total URN signature of the vessels during sea trials. The contributions through the two transmission paths are calculated using the procedures shown in the Sections 3.5.3.2 and 3.5.3.3. The sections below compare the measured broadband URN source levels with the relevant contributions from structure- and airborne noise generated by the main propulsive items (engines, gensets, and drives).

As explained in Sections 3.5.3.2 and 3.5.3.3, the analysis for SBN contributions is restricted to RNL levels, and for ABN contributions to MSL levels due to limitations in the available dataset. Nonetheless, the analysis produces a quantitative analysis of the contributions, with meaningful insights into the composition of the machinery contributions to the overall URN.

E.1 Baseline Stationary

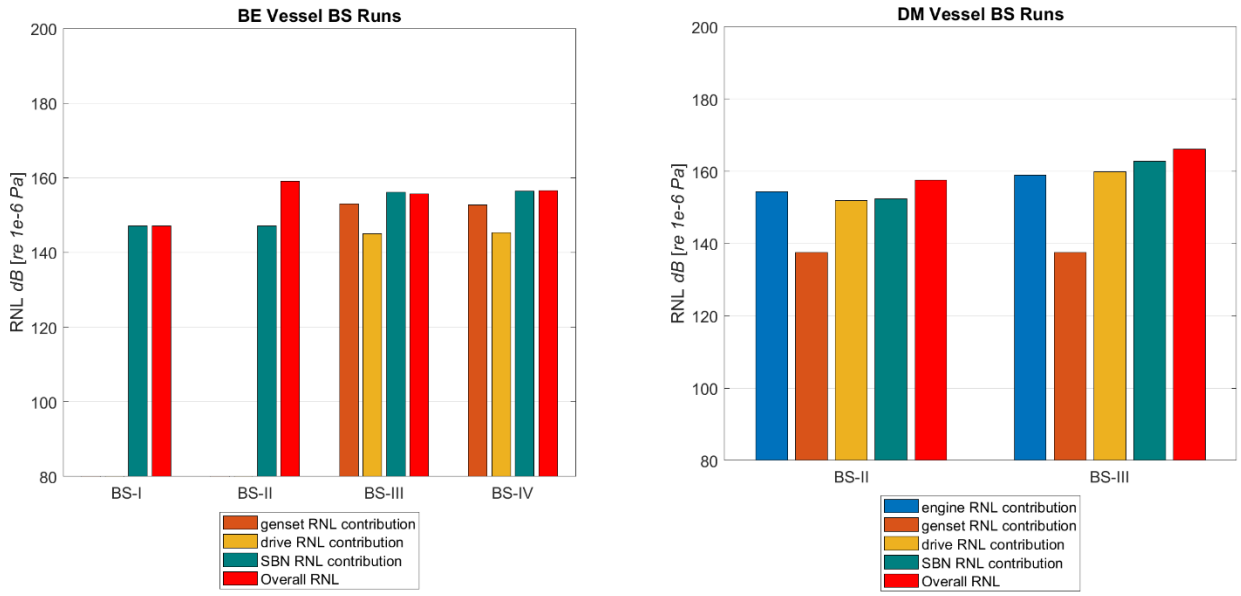


Figure E-1: Structure-borne noise sources contributions to the broadband *RNL* levels for the baseline stationary (BS) measurements. The left plot is for the BE tug, the right for the DM tug. "SBN *RNL* contributions" refers to the overall SBN contributions from all sources, including sources other than the one explicitly identified in the plot.

The composition of structure-borne noise during baseline stationary is shown in Figure E-1. The results show that:

- The BE vessel RNL composition (left in the figure) has two distinct groups. During runs on battery power, drive and gear meshing noise are major contributors to the overall RNL levels (BS-I and BS-II). Genset SBN noise contributes majorly to the overall SBN contribution in the gensets-only runs (BS-III and BS-IV)

- The DM vessel RNL composition (right in the figure) shows the influence of the drives clutching in, as shown by the difference in BS-II and BS-III. During this loiter condition, the main engines and auxiliary genset contribute significantly to the overall RNL levels. Although the clutch is partially engaged in BS-II, SBN contributions for the drives are lower compared to when they are fully engaged (BS-III), suggesting that the influence of gear meshing noise is negligible in this condition. Drives (and gear meshing noise) become dominant sources of noise when the clutch is fully engaged in BS-III condition. Genset SBN noise contributions to the overall RNL levels in this case are negligible when compared to the ones from the main engine and drives

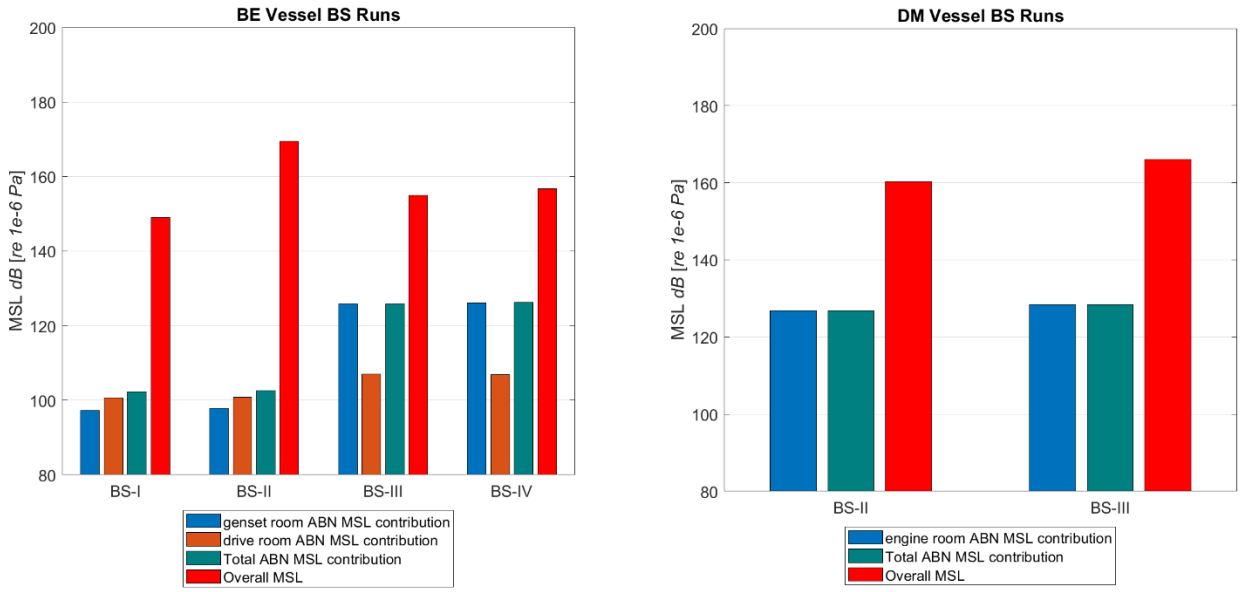


Figure E-2: Airborne noise contributions to the broadband MSL levels for the baseline stationary (BS) measurements. The left plot is for the BE tug, the right for the DM tug. "Total ABN MSL contributions" refers to the overall ABN contributions from the sources identified

Figure E-2 shows the ABN contributions to the MSL levels radiated from the BE tug (left) and DM tug (right). It is clear that ABN contributions in both cases are not significant to the overall MSL levels, with usual contribution levels $30dB$ below the overall levels.

E.2 Straight Run

Figure E-3 shows the SBN contribution of the main propulsive machinery to the overall RNL levels. The following can be stated:

- ST runs in battery mode for the BE tug (left-top plot in the figure) shows that the overall contributions from SBN levels to RNL levels from onboard sources can be explained mostly by gear meshing noise from the drive. However, as speed goes up (ST-BATT-II and higher), the overall SBN contributions are ~20 dB lower than the overall levels. This, for ST-BATT-II is explained by the fact that the SBN contributions calculated with the methodology shown in Section 3.5.3.2 do not take fully into account gear meshing noise generated by the lower gear in the propulsor and radiated directly from the underwater azimuthing propeller and nozzle assembly. As speed increases (ST-BATT-III and above), propeller hydrodynamic noise becomes increasingly dominant

- Similarly, ST runs in genset mode for the BE tug (left-top plot in the figure) shows similar trends related to the presence of increasing propeller noise masking SBN noise contributions from onboard machinery. The genset, in this case, is also contributing to the overall RNL noise, increasing the overall SBN contribution to the radiated underwater noise. The genset contributions do not vary with increasing speed, as the SBN input to the structure by the genset is constant regardless of the load

- For the DM vessel throughout the ST runs, the SBN contributions from main engines and gear meshing noise originating from drives dominate the signature. Notably, gear meshing appears to become the dominant source of URN at higher speeds. Overall, structure-borne noise from major propulsive machinery items is responsible for most of the URN radiated from the vessel

Figure E-4 shows the ABN contributions to the overall MSL levels during ST runs. For both BE and DM vessels, ABN contribution to the overall URN levels is insignificant, with >30 dB difference between overall ABN contributions to the total MSL levels.

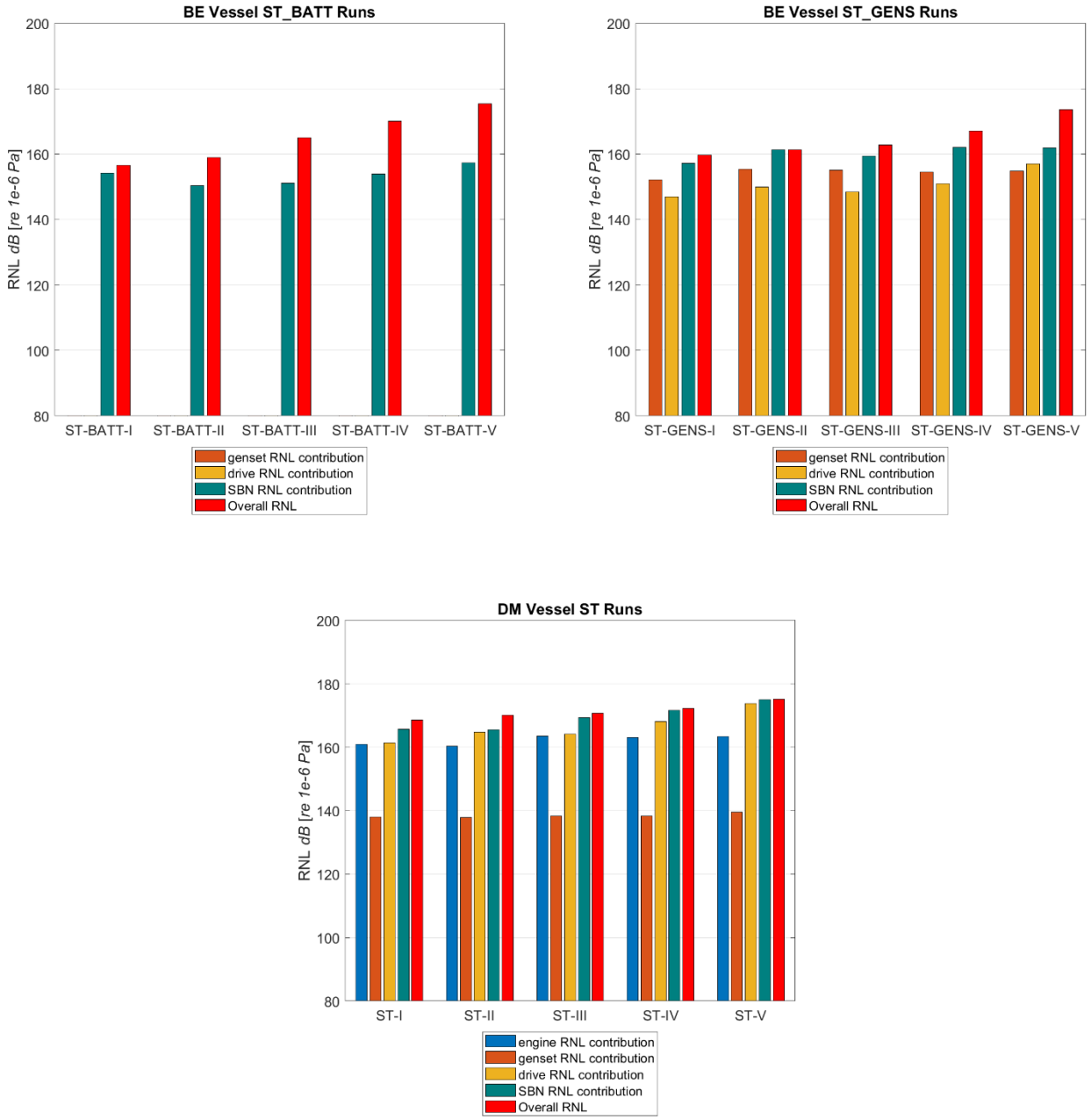


Figure E-3: Structure-borne noise sources contributions to the broadband RNL levels for straight travel (ST) runs. The left-top plot is for the BE tug in battery mode, the right-top for the BE tug in genset mode and the bottom plot for the DM tug. "SBN RNL contributions" refers to the overall SBN contributions from all sources, including sources other than the one explicitly identified in the plot.

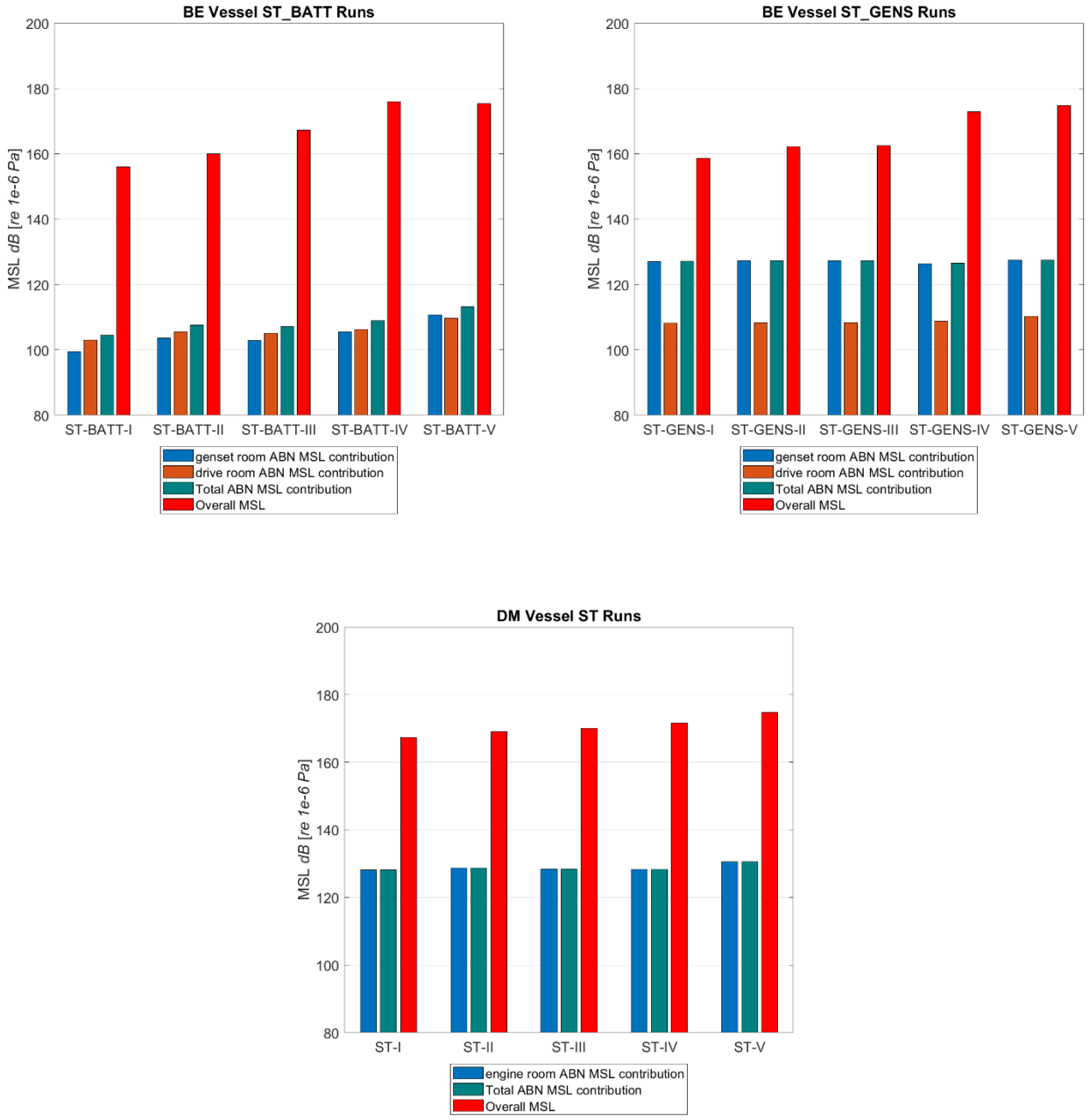


Figure E-4: Airborne noise contributions to the broadband MSL levels for the straight travel (ST) measurements. The left plot is for the BE tug, the right for the DM tug. "Total ABN MSL contributions" refers to the overall ABN contributions from the sources identified in the plots.

E.3 Bollard Pull

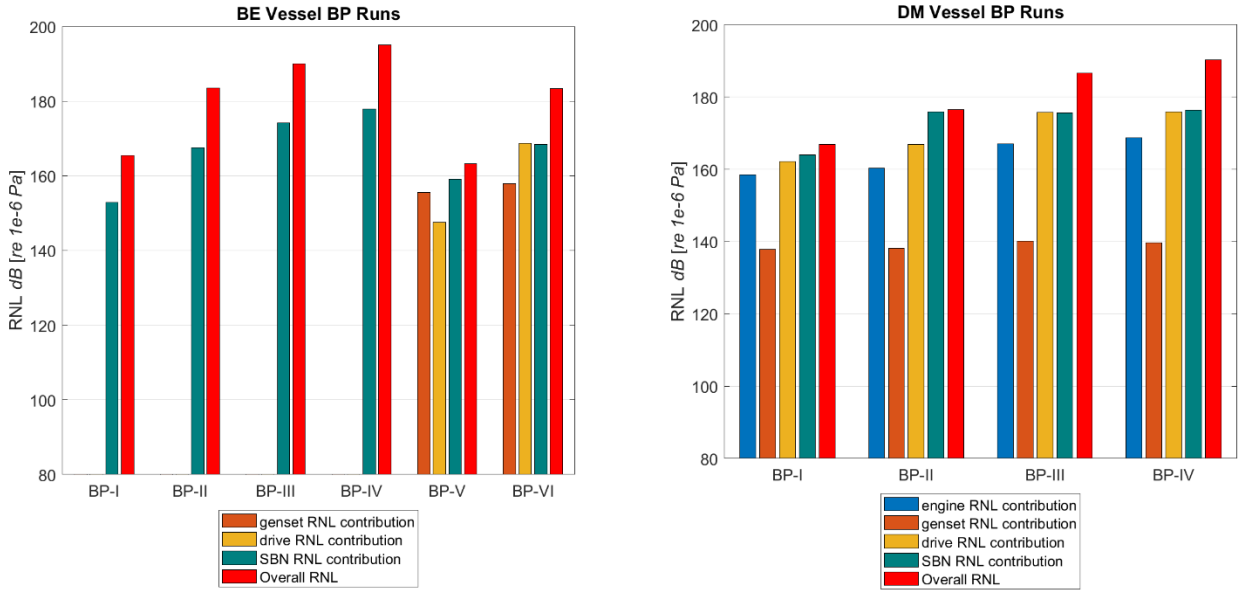


Figure E-5: Structure-borne noise sources contributions to the broadband RNL levels for bollard pull (BP) runs. The left plot is for the BE tug, the right for the DM tug. "SBN RNL contributions" refers to the overall SBN contributions from all sources, including sources other than the one explicitly identified in the plot.

Figure E-5 shows the contributions to the overall *RNL* levels from SBN generated by onboard machinery during bollard pull (BP). The following findings are reported:

- For the BE vessel, during bollard pull, SBN noise contributions to the overall *RNL* levels are primarily from the gear-meshing noise during battery-only operations (BP-I to BP-III, plot on the left in Figure E-5), and a combination of gear meshing noise and genset during BP-IV to BP-V, plot on the left in Figure E-5. However, SBN contributions are not dominating the overall *RNL* signature, due to the presence of heavy hydrodynamic and cavitation noise contributions from the propellers

- In contrast, *RNL* levels radiated during BP runs on the DM tug appear to be dominated by SBN noise from machinery at low power (BP-I and BP-II, right plot on Figure E-5), and by the propeller as the power increases (BP-III and BP-IV, right plot on Figure E-5)

As illustrated by Figure E-6, airborne noise contributions are again negligible to the overall URN signature from both DM and BE tugs during BP operations.

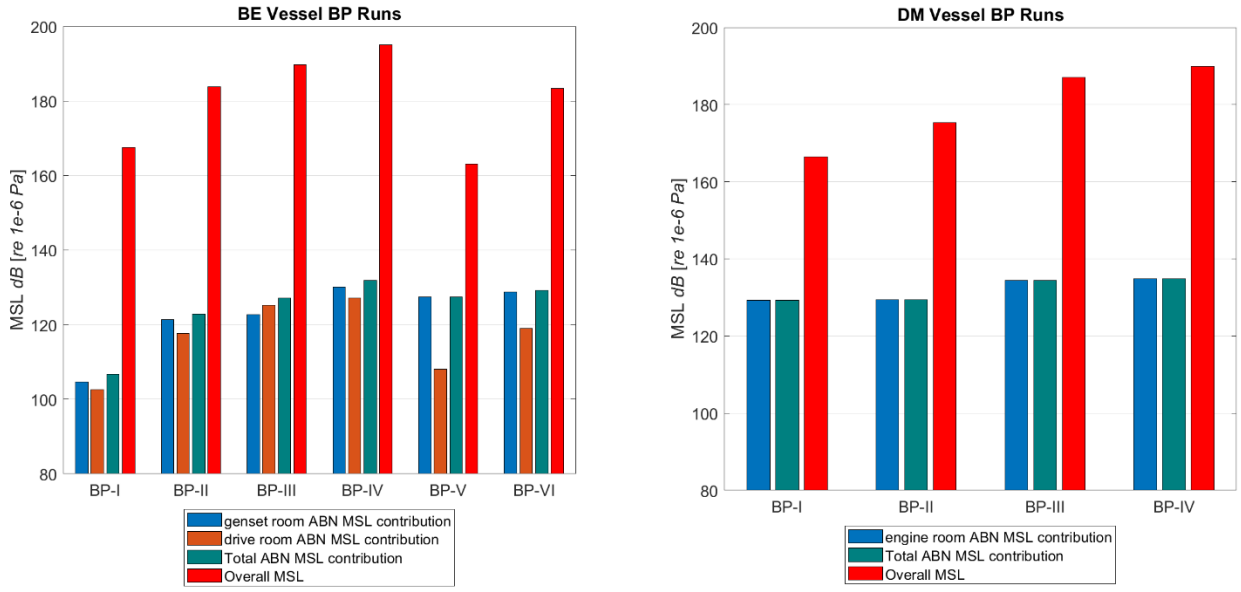


Figure E-6: Airborne noise contributions to the broadband MSL levels for the Bollard Pull (BP) measurements. The left plot is for the BE tug, the right for the DM tug. "Total ABN MSL contributions" refers to the overall ABN contributions from the sources identified in the plots.